A phase equilibrium modelling investigation of the consequences of entrainment of components of the source on the crystallisation of mantle-derived magmas in the upper crust, with specific relevance to the petrogenesis of chromitite layers in the Rustenburg Layered Suite of the Bushveld Complex, South Africa

By Tahnee Otto

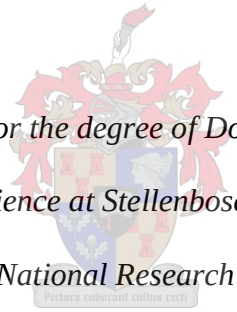

Dissertation presented for the degree of Doctor of Philosophy in the Faculty of Science at Stellenbosch University.

The financial assistance of the National Research Foundation (NRF) towards this research is hereby acknowledged. Opinions expressed and conclusions arrived at, are those of the author and are not necessarily to be attributed to the NRF.

Supervisor: Professor Gary Stevens, Stellenbosch University (South Africa)

Co-supervisors: Professor Jean-François Moyen, Université de Saint-Etienne (France)

Dr Matthew J. Mayne, Stellenbosch University (South Africa)

March 2023

Stellenbosch University https://scholar.sun.ac.za

DECLARATION

By submitting this dissertation electronically, I declare that the entirety of the work contained therein is my own, original work, that I am the sole author thereof (save to the extent explicitly otherwise stated), that reproduction and publication thereof by Stellenbosch University will not infringe any third party rights and that I have not previously in its entirety or in part submitted it for obtaining any qualification. This dissertation includes one original paper accepted for publication in a peer-reviewed journal and two unpublished publications. The development and writing of the papers (published and unpublished) were the principal responsibility of myself and, for each of the cases where this is not the case, a declaration is included in the dissertation indicating the nature and extent of the contributions of co-authors.

Date: March 2023

Copyright © 2023 Stellenbosch University

All rights reserved

Stellenbosch University https://scholar.sun.ac.za

ABSTRACT

Thermodynamic modelling techniques offer several advantages over experimental studies in investigations of the partial melting of mafic and ultramafic rocks under upper mantle conditions, but may not be as reliable as experimental studies in accurately predicting rock behaviour. The two main thermodynamic datasets that are in common use for such thermodynamic investigations have different levels of coverage. The Berman (1988) dataset is utilised by the MELTS family of software (Asimow & Ghiorso, 1998; Ghiorso & Sack, 1995; Ghiorso et al., 2002), and along with routines for handling activity-composition relations for solid and liquid solution phases, is embedded within the software. In contrast, the Holland & Powell (2011) dataset is used by a wide range of different software with different computational strategies. Activity-composition relations are handled by published models that are selectable and transparent. One of the programs using the Holland & Powell (2011) dataset, Rcrust (Mayne et al., 2016), has been developed to allow modelling of phase stabilities with changing bulk composition, which makes it particularly powerful for studying processes involving fractionation. In this study, the results of sets of experiments on ultramafic and mafic compositions under upper mantle conditions were compared with outputs from MELTS and Rcrust. Differences between the modelling and experimental results were quantified, and the Holland & Powell (2011) dataset combined with appropriately selected activity-composition models produced the best match with experimental results when melt fraction, melt composition, and the assemblage of coexisting phases were considered. The results demonstrate that modelling is a viable alternative to experimental techniques in investigating melting of the upper mantle. Thermodynamic modelling was used to map the envelope of uncertainty that exists around experimental results due to often unavoidable experimental pitfalls, and demonstrated that factoring in these uncertainties produced a better fit between modelling and experimental results. Next, this study developed a thermodynamic modelling methodology to investigate the stoichiometry of the melting reactions in an eclogite and peridotite as a function of pressure, temperature, and bulk compositional change due to melt loss. Pressure-temperature regions where the partial melting reactions produce peritectic crystals that increased in abundance with melt were identified. The entrainment of these crystals to the magma on segregation produces distinct shifts in the chemistry of the extracted magmas, for both sources. The results illustrate that variable amounts of peritectic crystal entrainment represents a previously unrecognised source of compositional heterogeneity in

Stellenbosch University https://scholar.sun.ac.za

basaltic and intermediate magmas. The modelled results highlight how peritectic crystal entrainment may be a principal mechanism for creating the magmas that produce layered mafic and ultramafic complexes, because the entrained phases react with melt on ascent to produce magmas with a high crystal load once they reach the upper crust. During the partial melting of peridotite, the most common entrainable peritectic mineral is orthopyroxene, which is Cr_2O_3-bearing. On ascent, entrained peritectic orthopyroxene reacts to form olivine and chromite, and such magmas will enter high-level magma chambers as a melt-olivine-chromite slurry. Density segregation on intrusion allows the formation of magmatic layering if the magma body has appropriate geometry. Thus, these results provide an explanation for the presence of chromitite seams in layered mafic complexes, as well as average bulk rock Cr_2O_3 contents well above mantle values in some layered intrusions, such as the Bushveld Complex. Chromitite layers are a consequence of peritectic orthopyroxene entrainment and do not require any complex phase equilibrium magma chamber processes.

Keywords: thermodynamic modelling, Rcrust, partial melting, upper mantle studies, peritectic minerals, mineral entrainment, chromite, Rustenburg Layered Suite, Bushveld Complex, Cr-paradox

Stellenbosch University https://scholar.sun.ac.za

OPSOMMING

Termodinamiese modelleringstegnieke bied verskeie voordele bo eksperimentele studies in ondersoeke van die gedeeltelike smelting van mafiese en ultra-mafiese gesteentes onder boonste manteltoestande, maar is dalk nie so betroubaar soos eksperimentele studies om gesteentegedrag akkuraat te voorspel nie. Die twee hoof termodinamiese datastelle wat algemeen gebruik word vir sulke termodinamiese ondersoeke, het verskillende vlakke van dekking. Die Berman (1988) datastel word gebruik deur die MELTS-familie van sagteware (Asimow & Ghiorso, 1998; Ghiorso & Sack, 1995; Ghiorso et al., 2002), en saam met roetines vir die hantering van aktiwiteit-samestelling-verhoudings vir vaste en vloeibare oplossingsfases, is in die sagteware ingebed. Daarteenoor word die Holland & Powell (2011) datastel gebruik deur 'n wye reeks verskillende sagteware met verskillende berekeningstrategieë. Aktiwiteit-samestelling verhoudings word hanteer deur gepubliseerde modelle wat selekteerbaar en deursigtig is. Een van die programme wat die Holland & Powell (2011) datastel gebruik, Rcrust (Mayne et al., 2016), is ontwikkel om modellering van fasestabiliteite met veranderende massasamestelling moontlik te maak, wat dit besonder geskik maak vir die bestudering van prosesse wat fraksionering behels. In hierdie studie is die resultate van stelle eksperimente op ultra-mafiese en mafiese samestellings onder boonste manteltoestande vergelyk met uitsette van pMELTS en Rcrust. Verskille tussen die modellering en eksperimentele resultate is gekwantifiseer, en die Holland & Powell (2011) datastel gekombineer met toepaslik geselekteerde aktiwiteit-samestelling modelle het die beste vergelyking met eksperimentele resultate gelewer wanneer smeltfraksie, smeltsamestelling en die samestelling van saambestaande fases in ag geneem is. Die resultate toon dat modellering 'n lewensvatbare alternatief vir eksperimentele tegnieke is om die smelting van die boonste mantel te ondersoek. Termodinamiese modellering is gebruik om die omhulsel van onsekerheid wat bestaan rondom eksperimentele resultate as gevolg van dikwels onvermydelike eksperimentele slaggate te karteer, en het getoon dat die inrekening van hierdie onsekerhede 'n beter passing tussen modellering en eksperimentele resultate tot gevolg gehad het. Vervolgens het hierdie studie 'n termodinamiese modelleringsmetodologie ontwikkel om die stoïgiometrie van die smeltreaksies in 'n eklogiet en peridotiet te ondersoek as 'n funksie van druk, temperatuur en massasamestellingsverandering as gevolg van smeltverlies. Druk-temperatuur streke waar die gedeeltelike smeltreaksies peritetiese kristalle produseer wat in oorvloed met smelt toegeneem het, is geïdentifiseer. Die meevoer van hierdie kristalle na die magma tydens

Stellenbosch University https://scholar.sun.ac.za

segregasie veroorsaak duidelike verskuiwings in die chemie van die onttrekde magmas, vir beide bronne. Die resultate illustreer dat veranderlike hoeveelhede peritetiese kristal-meevoer 'n voorheen onerkende bron van komposisionele heterogeniteit in basaltiese en intermediêre magmas verteenwoordig. Die gemodelleerde resultate beklemtoon hoe peritetiese kristal-meevoer 'n hoofmeganisme kan wees vir die skep van die magma wat gelaagde mafiese en ultra-mafiese komplekse produseer, omdat die meegesleurde fases met smelt reageer op styging om magmas met 'n hoë kristallading te produseer sodra hulle die boonste kors bereik. Tydens die gedeeltelike smelting van peridotiet is die mees algemene meevoerbare peritetiese mineraal ortopirokseen, wat Cr_2O_3-draend is. Met opstyg reageer meegesleurde peritetiese ortopirokseen om olivien en chromiet te vorm, en sulke magmas sal hoëvlak magmakamers binnegaan as 'n smelt-olivien-chromiet suspensie. Digtheid segregasie op indringing laat die vorming van magmatiese lae toe as die magma liggaam toepaslike geometrie het. Hierdie resultate verskaf dus 'n verduideliking vir die teenwoordigheid van chromietnate in gelaagde mafiese komplekse, sowel as gemiddelde grootmaatgesteentes Cr_2O_3-inhoud ver bo mantelwaardes in sommige gelaagde indringings, soos die Bosveld Kompleks. Chromitietlae is 'n gevolg van peritektiese ortopirokseen meevoer en vereis geen komplekse fase ewewig magma kamerprosesse nie.

Sleutelwoorde: termodinamiese modellering, Rcrust, gedeeltelike smelting, boonste mantelstudies, peritetiese minerale, minerale meevoer, chromiet, Rustenburg Layered Suite, Bosveld Kompleks, Cr-paradoks

Stellenbosch University https://scholar.sun.ac.za

ACKNOWLEDGEMENTS

Firstly, I would like to say a massive thank you to my main supervisor, Professor Gary Stevens. I cannot thank you enough for all you have taught me, your guidance, time, effort, patience, and support. Your input into my development as a scientist and researcher is unprecedented, and I appreciate all the advice and every word of encouragement that helped me get to the point where I am now. Thanks for always being available for 'just a quick chat about xyz', for telling me that my questions are not silly, and for reminding me to always look at the bigger picture. Another big thank you to my co-supervisors, Professor Jean-François Moyen and Dr Matthew Mayne. Matt – thank you for teaching me the ways of thermodynamic modelling and Rcrust and for our discussions about the research and future career plans. Being able to talk to you about your recent experiences has massively shaped the way I approach and think about things. Our 'arguments' about thermodynamic modelling has taught me a lot and will certainly be useful for my defence. Jeff – thank you for your insights into this project and your attention to detail. Your ability to always think about aspects that I have not considered has been tremendously helpful, and our long discussions about the work has played a big role in the development of the research. Also thank you for hosting me in Saint Etienne in 2019 and Clermont-Ferrand in 2022. I look forward to more successful South African – French collaborations. To all my supervisors, thank you for your reviews, suggestions, and comments on the work presented in this thesis, abstracts submitted to conferences, and conference presentations. Your role in the development of this project, especially considering the changes that had to be made due to COVID-19, has been paramount to the success of this research. Also thank you for always providing me with letters and forms needed for applications or the equivalent. Your continuous support in all my endeavours are gratefully acknowledged.

Thank you to the academic and administrative staff of the Earth Science Department at Stellenbosch University, particularly Alex Kisters, Gillian Strydom, and George Olivier, as well as Angélique Chanut from Laboratoire Magmas et Volcans at the University of Clermont Auvergne. Also thank you to the staff from the Central Analytics Facility labs, namely Madelaine Frazenberg, Mareli Grobbelaar-Moolman and Riana Rossouw, for all the analyses done on my behalf and teaching me how to use the analytical techniques….I apologise in advance that you may just have to show me how to do some things again. Thank you to Professor John Clemens for a few important chats and your contribution towards one of the manuscripts that form a part of this thesis. Thank you to Professor Daan Nel at the Centre for

Stellenbosch University https://scholar.sun.ac.za

Statistical Consultation for your assistance in analysing some global datasets. Thank you to Rose Richards for hiring me at Stellenbosch University Writing Lab – I am sure that helping others with their writing has greatly improved my own.

To my mother, Arnoline Taute, thank you for encouraging me to make the move to start a PhD and your undying support along the way. Your words of encouragement and love during the highs and the lows meant so much to me, even from afar. Thank you to my father, Jacques Otto, for your continuous support and your financial contributions towards me completing this degree. I may not have become a medical doctor as you had hoped, but a doctor (hopefully) none-the-less. A special thank you to my partner, Shane Teek, for your undying support. You have been my number one fan, but have also had to be there for the blood, sweat, and many tears that went into this project. Thank you for every bit of love and encouragement. I would not have gotten here without you – you are a continuous inspiration for me, every day. Thank you to Anna Durrheim for your role in getting me to end up in Stellenbosch and for many evenings of chats and wine that was needed through it all. To all the friends and family that contributed along the way, thank you to each and every one of you. The list would become rather exhaustive, but in particular, thank you to Chani van den Heever, Janet Otto, and Kae and Alan Teek. Your various contributions mean the world to me. Thank you to Tanisha Schultz for being my first friend in the department (although it may have been forced) as well as for teaching me the important basics of experimental petrology and some analytical techniques when I arrived; thank you to Helena Fest for cruising around with me in France and buying me last minute bus tickets, not to mention many a cappuccino; and thank you to Marcel, Steve and Mariana for being great company in Badplaas. Thank you to Andy Clark for informing us about a relatively cheap UPS – finishing up this thesis without a Wi-Fi connection during load shedding would have been rather extended and painful. Also thank you to Luna and Archie for comforting me during the hard times and for keeping me company into the late hours of the night or early hours of the morning.

Last, but not least, thank you to Stellenbosch University for hosting me for the past few years. The financial assistance of the National Research Foundation (NRF) towards this research is hereby acknowledged. Opinions expressed and conclusions arrived at, are those of the author and are not necessarily to be attributed to the NRF. Funding by the South African Research Chairs Initiative (SARChI) to G. Stevens, as well as other funds provided by G. Stevens, is gratefully acknowledged. Funding by the French Embassy of South Africa to T Otto, and funding from the BuCoMO International Research Project (IRP) by the French Centre for Scientific Research (CNRS) and the NRF, is also acknowledged with appreciation.

Stellenbosch University https://scholar.sun.ac.za

TABLE OF CONTENTS

Stellenbosch University https://scholar.sun.ac.za

LIST OF FIGURES

Stellenbosch University https://scholar.sun.ac.za

Stellenbosch University https://scholar.sun.ac.za

Chapter 4

Stellenbosch University https://scholar.sun.ac.za

Chapter 5

Stellenbosch University https://scholar.sun.ac.za

Figure 5-7 Plot showing the cumulative phase abundance produced upon a peritectic clinopyroxene entrained magma extracted from an eclogitic source being emplaced at 3 kbar and undergoing cooling from emplacement temperature to 1048 °C.

Stellenbosch University https://scholar.sun.ac.za

LIST OF TABLES

Stellenbosch University https://scholar.sun.ac.za

LIST OF ABBREVIATIONS, UNITS & NOMENCLATURE

ABBREVIATIONS

BC	Bushveld Complex
BG	Brits Graben
BIF	Banded Iron Formation
BuCoMO	Building Continents - From Mantle to Ore
B1	Bushveld parental magma 1
B2	Bushveld parental magma 2
B3	Bushveld parental magma 3
Chr	Chromite
CNRS	French Centre for Scientific Research
Cpx	Clinopyroxene
CRF	Crocodile River Fault
CZ	Critical Zone
EDS	Energy-Dispersive X-ray Spectroscopy
ES	Extract subsystem
Exp.	Experimental
Fsp	Feldspar
FS	Full system
Gt	Garnet
Ilm	Ilmenite
IRP	International Research Project
LCZ	Lower Critical Zone
LG	Lower Group chromitites
LG-FW	Lower Group Footwall
LMI(s)	Layered Mafic Intrusion(s)
LZ	Lower Zone
L21	Layer 21
MFootwall	Merensky Reef footwall
MG	Middle Group chromitites
MML	Main Magnetite Layer
MZ	Main Zone
NRF	National Research Foundation

Stellenbosch University https://scholar.sun.ac.za

Ol	Olivine
Opx	Orthopyroxene
PGE	Platinum Group Elements
Plag	Plagioclase
PM	Pyroxenite Marker
P-T	Pressure-Temperature
P-T-X/P-T-composition	Pressure-Temperature-Composition
RLS	Rustenburg Layered Suite
RS	Reactive subsystem
SARChI	South African Research Chairs Initiative
SCLM	Sub-continental lithospheric mantle
Sp	Spinel
SF	Steelpoort Fault
TML	Thabazimbi-Murchison Lineament
UCZ	Upper Critical Zone
UG	Upper Group chromitites
UZ	Upper Zone
WDS	Wavelength-Dispersive Spectroscopy
WF	Wonderkop Fault

UNITS

atm	Atmosphere
cm	centimetre
cm^3	centimetre cubed (volume)
dG	delta Gibbs energy
dm	decimetre
F	Fraction
f	Fugacity
Ga	Billion
GPa	Gigapascal
g/cm^3	grams per centimetre cubed (density)
ka	kiloannum
kbar	kilobar
km	kilometres

Stellenbosch University https://scholar.sun.ac.za

km^3	kilometres cubed (volume)
m	metres
mm	millimetres
mol.%	molar percentage
ppb	parts per billion
ppm	parts per million
vol.%	volume percentage
wt.%	weight percentage
°C	Degrees Celsius
μm	micrometre

NOMENCLATURE

a-x	activity-composition
AgPd	Silver-palladium
Al_2O_3	Aluminium oxide
An%	Anorthite percentage of feldspar as Ca/(Ca+Na)*100 by mol.%
CaO	Calcium oxide
C-CO	Graphite - CO_2 buffer
C-COH	Graphite - H_2O buffer
Cr_2O_3	Chromic oxide
fCO_2	Carbon dioxide fugacity
C1	Cbar1 plagioclase
Fe^{2+}	Iron (II)
Fe^{3+}	Iron (III)
FeO_t	Total iron as FeO + 0.89981*Fe_2O_3 by wt.%
Fe_2O_3	Iron(III) oxide
fH_2O	Water fugacity
fO_2	Oxygen fugacity
HGP	Holland, Green & Powell (2018)
HGPH	Holland, Green & Powell (2018); Heinrich & Connolly (2022)
HP*x*-eos	**E**quation **o**f **s**tate for phase compositional variation (***x***) founded on the **H**olland & **P**owell internally-consistent dataset.
K_2O	Potassium oxide

Stellenbosch University https://scholar.sun.ac.za

MgO	Magnesium oxide
Mg#	Magnesium number as Mg/(Fe + Mg)*100 by mol.%
MnO	Manganese(II) oxide
Na_2O	Sodium Oxide
NKCFMASTOCr	Na_2O–K_2O–CaO–FeO–MgO–Al_2O_3–SiO_2–TiO_2–Fe_2O_3–Cr_2O_3
NKCFMASTCr	Na_2O–K_2O–CaO–FeO–MgO–Al_2O_3–SiO_2–TiO_2–Cr_2O_3
NiO	Nickel oxide
NNO	Nickel-nickel oxide buffer
P_2O_5	Phosphorus pentoxide
Q*asm*	Quality of the match between predicted & observed assemblage
r-MELTS	rhyolite-MELTS
Sensu stricto	Narrow/strict sense
SiO_2	Silicon Dioxide
$^{87}Sr/^{86}Sr$	Strontium initial ratios
TH	Tomlinson & Holland (2021)
TiO_2	Titanium Oxide
T_P	Potential Temperature
$T^{30\ kbar}$	Temperature at 30 kbar
WPH	White, Powell, Holland & Worley (2000)
x_i	an increment in the vector direction x
y_i	an increment in the vector direction y

Stellenbosch University https://scholar.sun.ac.za

CHAPTER 1

Introduction

An important industrial element, chromium (Cr) has been used in a range of applications since its discovery, such as alloy metal fabrication, in the chemical industry, textiles, leather, ceramics, and more (Jacobs et al., 2005; Papp, 1990). Although there are several well-known Cr-based minerals, the concentration of Cr hosted in each mineral may vary depending on the character of the mineral and its origin, and may be unique to a deposit or locality. Chromite, an oxide mineral belonging to the spinel group, is the only commercially recoverable source of Cr (Mosier et al., 2012). A complex mineral with a range of compositions ($[(Mg,Fe^{2+})(Al,Cr,Fe^{3+})_2O_4]$; Figure 1-1), chromite (or chromian spinel) contains various proportions of Cr, iron (Fe), aluminium (Al) and magnesium (Mg), where the chromic oxide (Cr_2O_3) content can range from 7–64% (Jacobs et al., 2005; Thayer, 1973). Possibly also containing minor elements such as manganese (Mn), titanium (Ti), zinc (Zn), cobalt (Co) and nickel (Ni), chromite plays an important role in the understanding of crustal and mantle petrogenesis (e.g. Dick & Bullen, 1984; Irvine, 1965, 1967), as is discussed later.

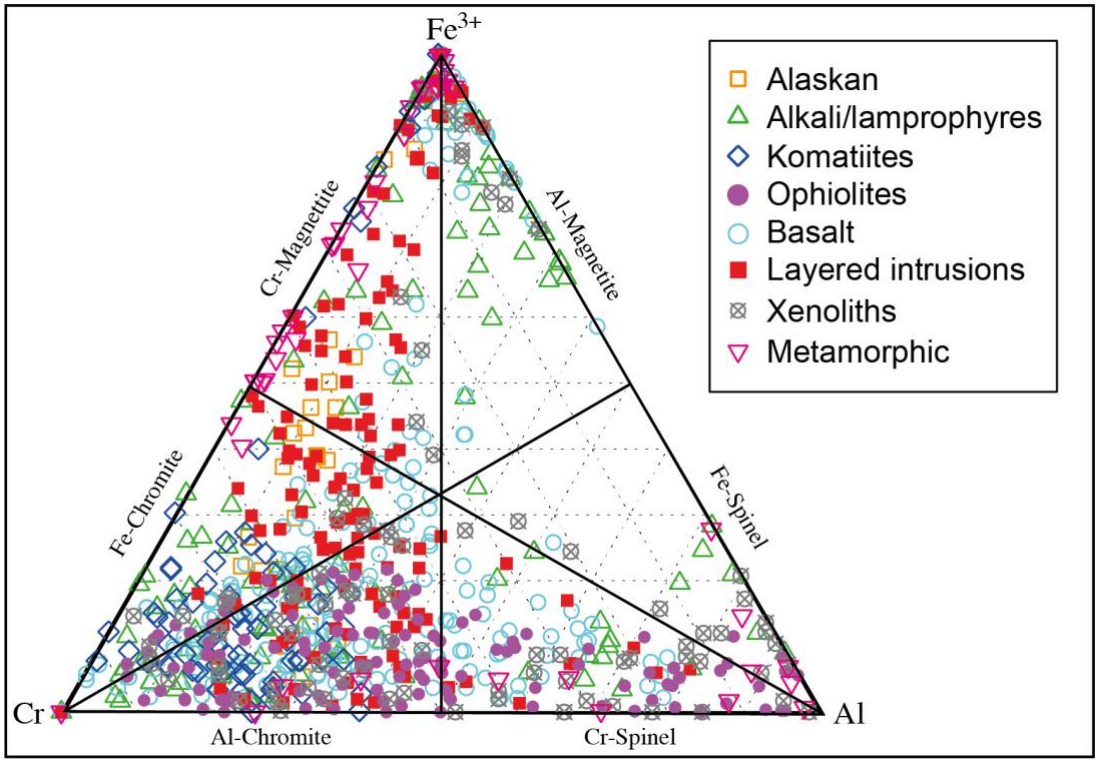

Figure 1-1. Cr-Al-Fe^{3+} ternary plot (after Stevens, 1944) displaying the compositions of 21 644 terrestrial spinels from mafic and ultramafic rocks, in subcategories (adapted from Barnes & Roeder, 2000).

Fundamentally distinguished by their continental or oceanic setting of formation and the associated degree of tectonic instability, concentrated chromite deposits are generally classed as podiform deposits or stratiform deposits (Mosier et al., 2012; Stowe, 1994; Wilson

Stellenbosch University https://scholar.sun.ac.za

& Anhaeusser, 1998). Located in mid-ocean ridge, intra- and supra-subduction zone environments (Zhou et al., 2014), podiform-type deposits occur as a variety of high-Cr or high-Al chromite bodies in ultramafic rocks (dunite, peridotite, or serpentinite) associated with ophiolites (Mosier et al., 2012). In stable continental settings, layered mafic intrusions (LMIs) host stratiform-type deposits of commonly high-Fe chromite bodies occurring as horizontal to sub-horizontal seams and layers (Stowe, 1994; Wilson & Anhaeusser, 1998). Igneous cumulate rocks containing ≥ 60 vol.% chromite are classified as chromitites, which may also contain minor plagioclase, pyroxenes, and/or olivine (Mosier et al., 2012). Chromitites may occur as pods and lenses, layers or bands, schlieren, dikes, or irregular bodies (Aria & Miura, 2014), and are regularly referred to on the basis of their thickness; massive bodies are generally centimetres to metres in thickness, and seams, stringers and other smaller bodies are millimetres to centimetres in thickness.

The majority of the world's chromite resources occur as stratiform deposits, accounting for 90% of the world's chrome reserves (Kleynhans et al., 2012). However, due the broad occurrence and nature of obducted mantle and crustal sequences along continental margins, investigations of ophiolites and podiform chromitites have provided unrivalled information on various mantle processes and dynamics (Aria & Miura, 2014). As a result, the conceptualisation of deep-seated magmatic evolution along mid-ocean ridges, such as the melting of peridotite due to mantle convection driven decompression, is well established (Kushiro, 2001; Langmuir et al., 1977). However, in continental settings and at subduction zones, the circumstances surrounding mantle melting and the details of the melting conditions and reactions are less well constrained (e.g. Long et al., 2019; Stern, 2002). Partial melting in the subcontinental mantle produces a broad range of mafic to intermediate magmas that intrude the continental crust in a variety of tectonic settings, such as continental arcs (Arculus, 1994), as well as rift zones with associated flood basalts (Turner & Hawkesworth, 1995; White & McKenzie, 1989) or bimodal volcanism (Mazzarini et al., 2004). Since the partial melting process cannot be observed directly, the current understanding of the possible sources that may undergo partial melting in the sub-continental lithospheric mantle (SCLM), as well as the composition of melts in the source prior to magmatic differentiation, is largely based on experimental studies using rare mantle xenoliths exhumed during the eruption of mantle-derived magmas (e.g. Jacob, 2004; Mathias et al., 1970). These investigations have provided some useful insights into the partial melting reactions of SCLM sources, and the uplift and erosion of LMIs have provided access to informative field observations about processes such as cooling and crystallisation of mantle magmas in magma chambers (Winter, 2010). However,

Stellenbosch University https://scholar.sun.ac.za

the mantle sources and source magma compositions involved in the formation of LMIs remain a debated issue, particularly due to the often monomineralic layered nature of the rocks, and importantly, the presence of massive chromitites.

The mantle signature of chromite is highlighted by fact that primary chromite deposits are limited to ultramafic and mafic igneous rocks and closely related anorthositic rocks (Jacobs et al., 2005; Papp & Lipin, 2006). Stable under a range of conditions, chromite is almost always associated with olivine, both being early-stage crystallisation phases in basaltic melts. The chromite crystals are generally small, however, and occur in low abundances (Roeder, 1994), largely because Cr has very limited solubility in mafic melts (Hill & Roeder, 1974; Roeder & Reynolds, 1971) and occurs as a trace element in the mantle, with abundances of 2645 ppm in proposed Primitive Mantle compositions (Lyubetskaya & Korenaga, 2006). As a result, numerous studies have been dedicated to investigating the chemistry of chromian spinels and their environments of formation; chromite compositions have been shown to be dependent on a complex interplay of the composition of its parental magma and mantle source, oxygen fugacity (fO_2), and the conditions of its crystallisation and cooling (e.g. Arai, 1992; Dick & Bullen, 1984; Fisk & Bence, 1980; Hill & Roeder, 1974; Irvine, 1965, 1967; Jaques & Green, 1980; Murck & Campbell, 1986; Roeder & Reynolds, 1991; Sack, 1982; Ulmer, 1969). The composition of the parental magma, which is dependent on the extent of depletion of the mantle source rock, is important, because the composition of the chromite depends on that of the melt with which it equilibrates. In other words, changes in the melt chemistry due the crystallisation of olivine, pyroxenes (which removes Cr from the melt) and plagioclase, will be reflected in the chromite composition (Roeder, 1994). The chemistry of chromian spinels can thus offer important petrogenetic information on primitive magmas, such as source fertility, and magma mingling and mixing (Kamenetsky et al., 2001, and references therein).

Considering the complex relationship between the melt from which the chromite crystallised, the conditions of its formation, and the composition of the chromite, as well as the constraints of the partitioning of Cr into melts produced during partial melting in the mantle, numerous models have been developed that attempt to explain the formation and nucleation of chromite in abundances great enough to produce chromitites within crustal magma chambers. The major challenge, however, remains the fact that the crystallisation of chromite only, or in large abundances, is difficult to explain from a phase equilibrium perspective. Although chromite and olivine regularly share the role of near-liquidus co-crystallising phases during cooling of mantle-derived magmas at crustal pressures, the expansion of the olivine stability field with decreasing pressure will ensure that these magmas become saturated in olivine

Stellenbosch University https://scholar.sun.ac.za

(±chromite), but not chromite alone (Latypov et al., 2018; Roeder, 1994). Nevertheless, the saturation of mantle-derived magmas purely in chromite became the entrenched requirement, and has been proposed to occur in the crustal magma chamber due to a number of mechanisms (e.g. Cawthorn, 2011; Ferreira Filho & Araujo, 2009; Latypov et al., 2018; Naldrett et al., 2009, 2012; Scoon & Costin, 2018). This paradigm has been disputed, however, with the development of several theories emphasising the importance of crystal-rich slurries (e.g. Eales & Costin, 2012; Lesher et al., 2019; Maier & Barnes, 2008; Mungall et al., 2016; Voordouw et al., 2009; Yao et al., 2021). These slurries are suggested to be comprised of chromite crystals alone, or mostly silicate phases with minor chromite. Crystal slurry models are slowly increasing in popularity due the growing consensus that magma chambers are almost entirely composed of crystal-rich mushes with minor amounts of interstitial liquid (e.g. Bachmann & Huber, 2019; Cashman et al., 2017). Formed through the amalgamation of numerous intrusions in the crust, such mushy reservoirs contain only small pockets of melt that exist briefly before coalescing and erupting at the Earth's surface (e.g. Edmonds et al., 2019; Sparks et al., 2019). For LMIs, such models propose their formation from a pile of arbitrarily-emplaced sills, with sequential pulses of crystal-magma slurries invading the pre-existing cumulates (e.g. Bédard et al., 1988; Hepworth et al., 2020; Mungall et al., 2016; Robb & Mungall, 2020; Wall et al., 2018; Yao et al., 2021).

A summary of many of the different theories proposed for chromite formation is displayed in Table 1-1, and are simplified into broad subcategories of (1)-(6) described below; the individual works should be consulted for more detail. The dominant processes suggested for producing chromite-saturated magmas have been divided here into four main themes of models, namely (1) magma mixing, (2) pressure fluctuations, (3) fO_2 increases, or (4) other mechanisms. Similarly, models involving crystal-slurries are divided based on whether the slurries are suggested to form (5) in the shallow-level magma chamber, or (6) are brought to the shallow-level chamber from a staging/lower chamber. With no current consensus on whether the formation of massive chromitites and thinner chromitites are attributed to the same processes and mechanisms, Table 1-1 reports postulations for both.

Many of the theories in Table 1-1 have been modelled and developed around well-known LMIs with great manifestations of chromite, such as the Great Dyke (e.g. Wilson, 1982), the Muscox Intrusion (e.g. Smith, 1962), the Stillwater Complex (e.g. Jackson, 1961) and the R(h)um Layered Suite (e.g. O'Driscoll et al., 2009, 2010). In particular, the Rustenburg Layered Suite (RLS) of Bushveld Complex (BC) in South Africa is a known host of giant reserves of a number of ores, being the world's largest host of Cr (Eales & Cawthorn, 1996)

Stellenbosch University https://scholar.sun.ac.za

with 74–80% of the world's viable chromite reserves (Glastonbury et al., 2010). As a result, the RLS is one of the most well-known and studied layered intrusions on Earth, with a number of chromitite models of formation based on data collected from the suite (e.g. Eales, 2000; Latypov et al., 2017b; Maier et al., 2012; Mondal & Mathez, 2007; Naldrett et al., 2012), displayed in cyan in Table 1-1. Numerous authors have published extensive and detailed descriptions of the 2.055 Ga BC and its world-class ore deposits (e.g. Cawthorn & Walraven, 1998; Eales & Cawthorn, 1996; von Gruenewaldt et al., 1985), with a brief summary of the complex and details as pertinent to this study provided here.

The Rustenburg Layered Suite of the Bushveld Complex

The RLS is the mafic-ultramafic component of the BC (Figure 1-2) and is the world's largest layered intrusion, spanning 350 km north to south and over 500 km east to west, with an estimated volume of 370 000–600 000 km^3 (Cawthorn & Walraven, 1998). The approximate 6.5–9 km thick RLS was emplaced in less than 100 ka (Zeh et al., 2015), and outcrops as five arcuate limbs/lobes, displaying variation in both lithology and thickness that can be observed along strike of individual limbs and between different limbs (Scoon & Teigler, 1994). The RLS is subdivided based on the lithological changes into five major zones (Figure 1-3a), yet strict definitions of these stratigraphic subdivisions are subjective depending on the characteristics favoured, be it field, geochemical or isotopic (Kruger, 1991; Mitchell & Scoon, 1991).

The first stage of development of the RLS is considered to be represented by the Marginal Zone and the Lower Zone (LZ). The variably thick Marginal Zone is an unlayered, heterogenous zone underlying most of the suite, characterised mainly by norites as well as minor pyroxenites and olivine-rich cumulates (Naldrett et al., 2012). The overlying LZ displays distinct variation in lateral thickness and composition across the RLS limbs. Modal data from the LZ in the western limb show intricate interlayering of olivine- and orthopyroxene-rich rocks, comprising of uniform harzburgite and orthopyroxenite layers alternating with thin dunite cumulates (Cameron, 1978), and a single layer of norite (~90 cm) present midway up the sequence (Maier et al., 2012). Minor amounts of plagioclase, clinopyroxene and other minerals, such as chromite (with no economic significance at < 1% modal), is present in most LZ samples.

Overlying the LZ is the Critical Zone (CZ), hosting several economically important chromitites (Figure 1-3b). Most cyclic units in the CZ are characterised by basal chromitite layers overlain by a repetitive sequence of cumulates changing vertically along the subsection (Cameron, 1982). The CZ contains 14 such major chromitites, with a total of 21 named

Stellenbosch University https://scholar.sun.ac.za

Chromite saturation of liquid				Crystal slurries	
(1) Magma Mixing	(2) Pressure Change	(3) fO_2 increase	(4) Other	(5) Formed in chamber	(6) Brought into chamber
Mixing of granitic melts/crustal rocks with the resident magma in the chamber	*Pressure increase due to deformation of the magma chamber*	*Chemical/physical processes: diffusion of H_2; loss of gases (diffusion); release of pressure*	*Addition of water, water vapour, water-rich fluid, interstitial melt, reactive fluid, or volatiles*	*Gravitationally unstable mush & kinetic sieving*	*Separation of phases due to gravity settling*
Irvine (1975) Schoenberg et al. (1999) Horan et al. (2001) Kinnaird et al. (2002) Marques et al. (2003) Nex (2004) Spandler et al. (2005) Kottke-Levin et al. (2009)	Cameron (1977, 1980, 1982)	Cameron & Desborough (1969) Ulmer (1969)	Ford et al. (1972) Nicholson & Mathez (1991) Armitage (1992) Prendergast (2008) Azar (2010) Boudreau (2008, 2016) Mathez & Kinzler (2017) Veksler & Hou (2020) Marsh et al. (2021)	Lee (1981) Maier & Barnes (2008) Maier et al. (2012)	Eales (2000, 2001) Eales & Costin (2012) Cawthorn (2003)
Mixing of differentiated resident melt with primitive magma	*Pressure increase: nucleation, ascent & expansion of gas bubbles*	*Assimilation of carbonate-rich host rocks*	*Magma is saturated/becomes saturated in chromite upon emplacement**		*Separation of phases due to kinetic sieving*
Wilson (1982) Irvine (1977) Eales et al. (1986) Campbell & Murck (1993) Scoon & Teigler (1994) Ferreira Filho & Araujo (2009) Naldrett et al. (2009) Latypov et al. (2013, (2015, 2017a)	Klemm et al. (1982) Lipin (1993)	Ferreira Filho & Araujo (2009)	Naldrett et al. (2012) Chistyakova et al. (2015) Yudovskaya et al. (2015) Latypov et al. (2017b) Mukherjee et al. (2017) Kaufmann et al. (2019) Hasch & Latypov (2021)		Mondal & Mathez (2007) Mungall et al. (2016)
Mixing of ultramafic magma with anorthositic magma	*Pressure decrease during magma transportation to crustal chamber*	*Assimilation of adjacent supracrustal rocks, possibly BIF*	*Infiltration of intercumulus melt thorough a compacting layered unit of cumulus crystals*		*Assimilation of wall-rock: magma injected as crystal mush*
Irvine et al. (1983) Irvine & Sharpe (1986)	Latypov et al. (2018)	Rollinson (1997)	Nikolaev et al. (2020)		Yao et al. (2021)
Mixing of ultramafic magma with a liquid derived from partial melting of plagioclase-rich cumulates	*Pressure increase: emplacement of a new magma pulse*		*Downwards percolation of emplaced melt into crystal mush*		*Partial melting, physical transport & dynamic upgrading of magnetite grains*
Eales et al. (1988) Mitchell & Scoon (2007)	Cawthorn (2005, 2011)		O'Driscoll et al. (2009, 2010) Leuthold et al. (2015) Sampson (1932)		Lesher et al. (2017, 2019)
	*Pressure increase**		*Re-melting of pre-existing rocks*		*Sill-like injections of chromite-only slurries*
	McDonald (1967) Loferski et al. (1990)		Scoon & Costin (2018) Veksler et al. (2018)		Voordouw et al. (2009)
			Sill-like injections of magma into crystal mush		
			Maghdour-Mashhour et al. (2021)		
			Earthquakes & associated shock waves		
			Cawthorn (2015)		

Table 1-1. A summary of the proposed theories for the formation of massive and smaller chromites bodies as found in LMIs and other deposits. Entries are colour coded according to the LMI/chromitite deposit the model was proposed for: Dark grey: Bacuri Complex; Red: Blackbird Chromite Deposit; Cyan: Bushveld Complex; Light grey: Ipueira-Medrado Sill; Dark green: Monchegorsk Intrusion; Brown: R(h)um Intrusion; Light green: Stillwater Complex; Magenta: Zimbabwe Craton deposits; Purple: Multiple; Orange: Experimental. *No exact cause or mechanism suggested. BIF: Banded Iron Formation.

Stellenbosch University https://scholar.sun.ac.za

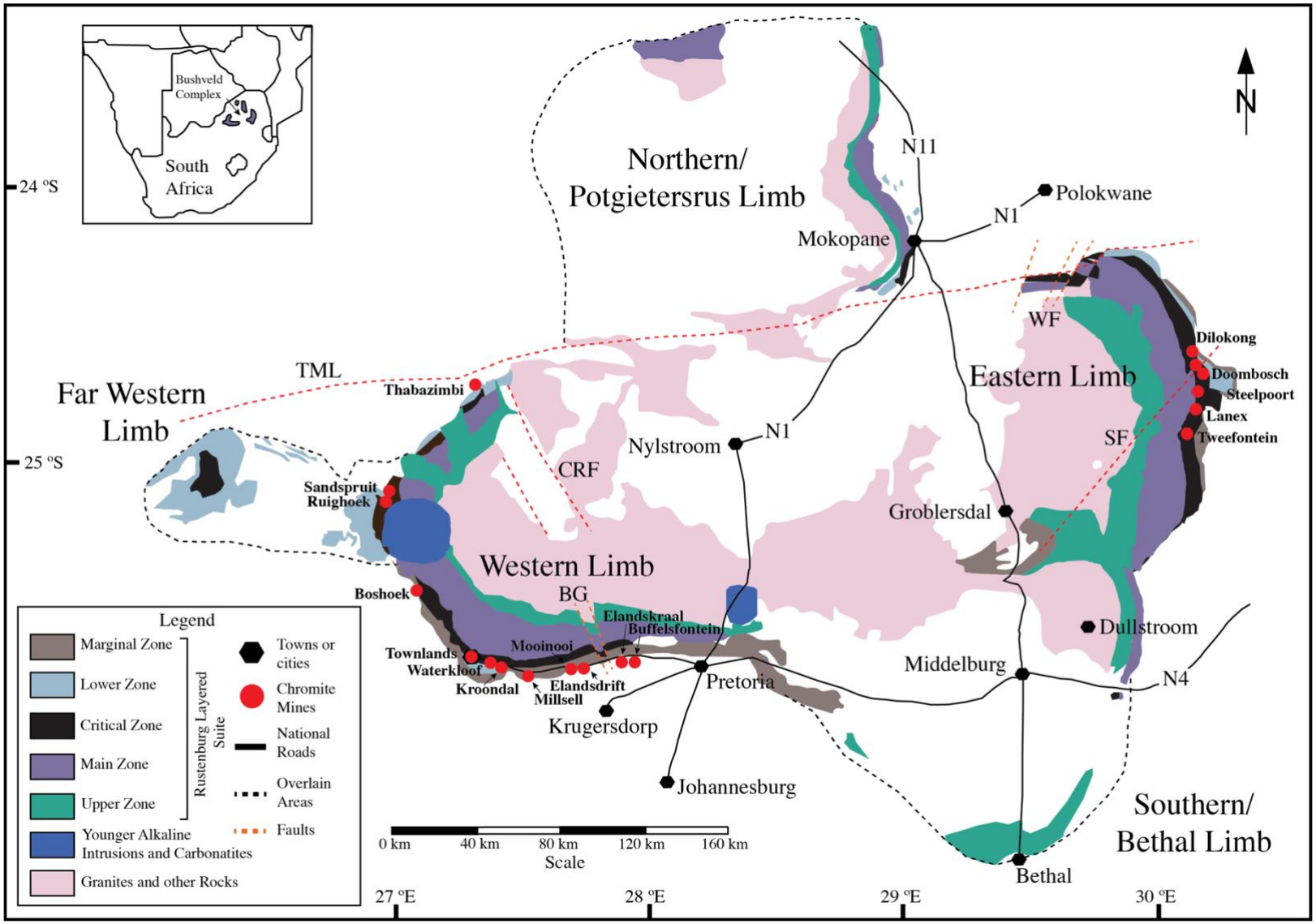

Figure 1-2. Simplified geological map of the Bushveld Complex, South Africa. Adapted from multiple sources (Bachmann et al., 2019; Maier et al., 2012; Mungall et al., 2016). TML: Thabazimbi-Murchison lineament; CRF: Crocodile River fault; BG: Brits Graben; SF: Steelpoort fault; WF*:* Wonderkop Fault.

Stellenbosch University https://scholar.sun.ac.za

horizons divided into three major groups: the Lower Group (LG), Middle Group (MG), and Upper Group (UG) chromitites (Cousins & Feringa, 1964; Mondal & Mathez, 2007; Schürmann et al., 1998; Scoon & Michell, 2018; Scoon & Teigler, 1994). A laterally continuous anorthosite layer (1–3 m thick) in the eastern and western limbs divides the CZ into a lower and upper sequence (Maier et al., 2012). Contacts between seams and host rocks are sharp, but major chromitites are frequently observed cutting down through sections of the underlying cumulates (Latypov et al., 2017b).

One of the most laterally persistent zones in the RLS, the overlying Main Zone (MZ) is > 2 km thick and made up almost entirely of plagioclase and two pyroxenes (Cawthorn et al., 2015), displaying a clear absence of cumulous chromite and olivine. Although less distinctively layered than the CZ, compositional layering is still observable in MZ gabbronorites and norites (occasional minor anorthosites). Lastly, the well-layered Upper Zone (UZ; 1–2 km thick) lies discordantly above the MZ, defined by the appearance of cumulus magnetite. Layers display sharp lower contacts, but upper contacts are often gradational (Maier et al., 2012). The UZ is divided into three subzones based on changes in the cumulous mineralogy: Subzones A and B have cyclic layers of magnetitite, gabbronorite and anorthosite, with the appearance of olivine marking the beginning of Subzone B. The addition of cumulous apatite delineates Subzone C, comprising of cyclic units of iron oxide (with granular ilmenite) and ferrodiorites.

Chromitites in the Critical Zone

The ultramafic Lower Critical Zone (LCZ) comprises nine major chromitites (LG1-7 and MG0-2a,b,c) alternating with layers of orthopyroxenite (Eales & Cawthorn, 1996). Harzburgites are interlayered with the orthopyroxenite in two intervals along the sequence (Maier et al., 2012), with minor disseminated chromite present in nearly all rocks. The Upper Critical Zone (UCZ) displays eight cycles of partial or complete sequences of orthopyroxenite through norite to anorthosite (Eales & Cawthorn, 1996), and generally contains the MG3, MG3a, MG4, MG4a, and UG1-2 (including the UG3 and UG3a in some areas). Although characteristic of LG cycles, the other groups do not always display basal chromitites. For example, the MG2 chromitite appears at the top of an orthopyroxenite layer, and the MG3 and UG1 layers are hosted completely in anorthositic rocks, with no associated orthopyroxene (Latypov et al., 2017b).

Several reefs enriched with platinum-group elements (PGEs) occur between UG1 and the base of the MZ. Amongst UG2, the Psuedoreefs, Merensky Reef, Bastard Reef, and

Stellenbosch University https://scholar.sun.ac.za

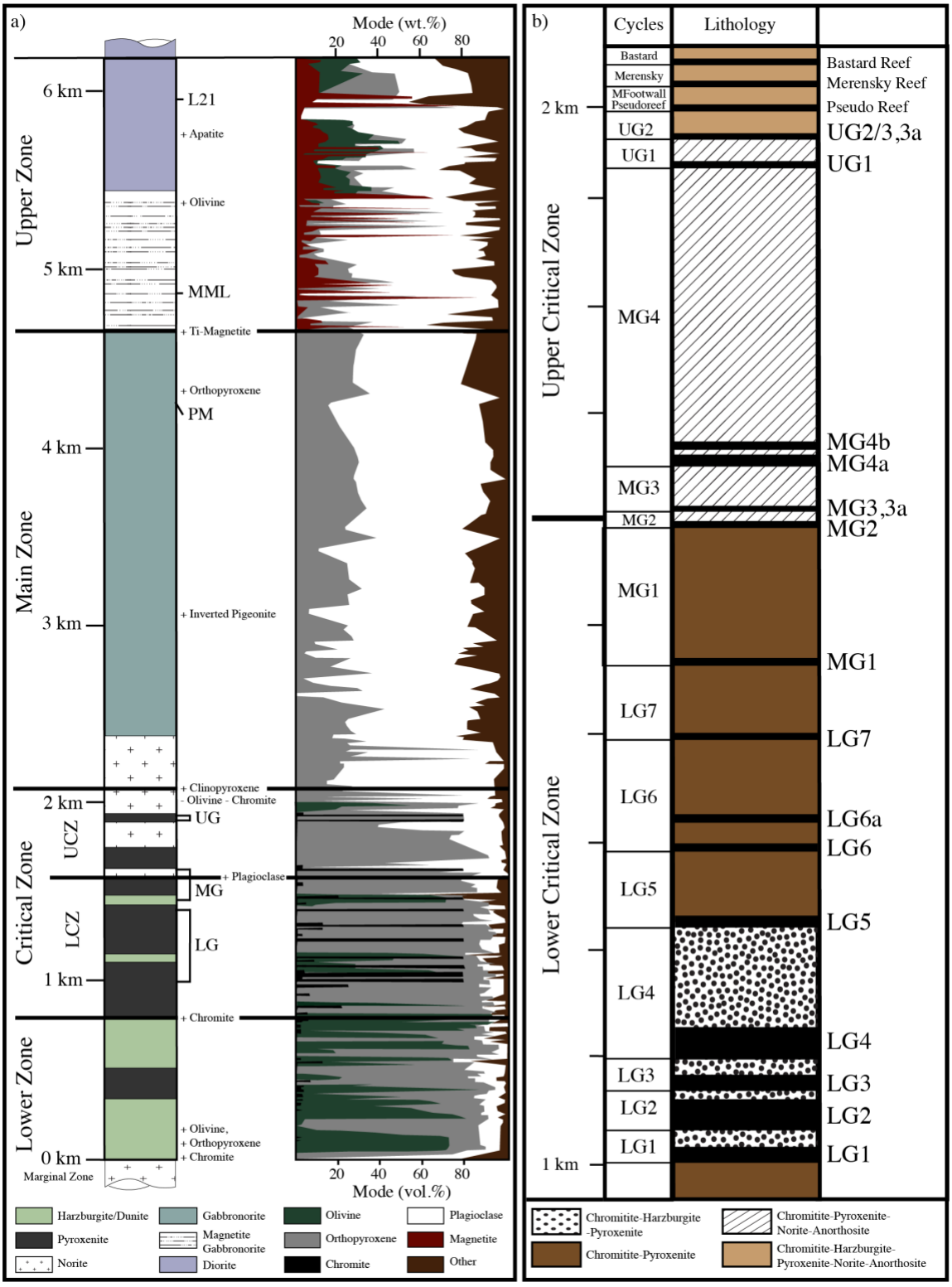

Figure 1-3. a) Generalised stratigraphic column of the western limb of the Rustenburg Layered Suite with modal proportions of minerals; adapted from Maier et al. (2012) with additional data from Scoon & Teigler (1994) and Yuan et al. (2017). Data from the Lower, Critical and Main Zones in modal vol.%; data from the Upper Zone in modal wt.%. LCZ: Lower Critical Zone; UCZ: Upper Critical Zone; LG: Lower Group chromitites; MG: Middle Group chromitites; UG: Upper Group chromitites; PM: Pyroxenite Marker; MML: Main Magnetite Layer; L21: Layer 21. b) Generalised stratigraphic column of the Critical Zone indicating major chromitite layers and lithology. Adapted from Scoon & Mitchell (2018). LG-FW: Lower Group Footwall; MFootwall: Merensky Reef Footwall.

Stellenbosch University https://scholar.sun.ac.za

Platreef, mining is restricted to Merensky and UG2 (Barnes & Maier, 2002). Cyclic variations in the reefs display thin layers of harzburgite, orthopyroxenite, anorthosite, and norite, as well as chromitites that are not included in the Cousins & Feringa (1964) nomenclature.

All named chromitite seams are not observed throughout the entire RLS and the occurrence of the seams varies between the different limbs, as well as between different segments within individual limbs (Naldrett et al., 2011). The majority of major chromitites (1 dm to 2 m in thickness) have, however, been traced along strike for distances ranging from 100–400 km in the western and eastern limbs (Schürmann et al., 1998), and generally cut down through several metres of the underlying cumulates (Latypov et al., 2017b). Main seams generally do not occur as single layers, and are accompanied by subsidiary chromitite leaders (10–60 cm thick) in the hanging- or footwall, that may be segregated from the main layer by orthopyroxenites of a few decimetres to metres in thickness (Latypov et al., 2017b). Leader chromitites are less laterally continuous and may bifurcate, terminate, or merge with main seams on various scales (Maier et al., 2012).

Chromitite layers typically contain chromite grains of < 50 μm to > 2 mm in size that exceed half of the mineral assemblage. The chromitites frequently develop a poikilitic texture, with very fine-grained chromite chadacrysts enclosed by oikocrysts of plagioclase or pyroxene (Kinnaird et al., 2002), and may display densely packed domains towards the centre of seams, bracketed by zones of more diffuse chromite (von Gruenewaldt et al., 1986). Accessory minerals include clinopyroxene, chlorite, biotite, phlogopite, quartz, talc, carbonates, and sulfides (Kinnaird et al., 2002). Additionally, small, isolated lenses or wisps of chromitite commonly occur parallel to the layers of the LZ and CZ, being only a few centimetres in thickness (Eales & Costin, 2012).

Textural and compositional variation can also be observed across individual chromite seams (Maier & Barnes, 2012), similarly observed between major and leader chromitites, which may show variation in major elements, trace elements, and PGE contents (Latypov et al., 2017b; Naldrett et al., 2011). Throughout the RLS, the chromitites display a decrease in Cr_2O_3 content moving upwards in the sequence (approximately 46–43%; Kinnaird et al., 2002), with gangue mineral contents increasing progressively with height (> 40% in UG chromitites; Maier & Barnes, 1999). Interstitial minerals change throughout the LG (orthopyroxene), MG (orthopyroxene and plagioclase) and UG (plagioclase and minor orthopyroxene) chromitites (Kinnaird et al., 2002). Elongated, narrow-tailed autoliths and xenoliths of anorthosite and pyroxenite may be present in chromitite layers, and may concentrate at specific levels in the

Stellenbosch University https://scholar.sun.ac.za

seams – other observations note chromitites enclosing such xenoliths, whilst retaining their original thickness (Maier et al., 2012).

The formation of the Rustenburg Layered Suite

As is the commonly accepted theory for many LMIs, the RLS is considered to have formed as a result of multiple magma injections (e.g. Cameron, 1978; Cawthorn, 1996; Hamilton, 1977; Kruger, 2005; Wager & Brown, 1968), interpreted on the basis of changes in crystallisation sequences, as well as cumulous compositional reversals and changes in isotopic ratio (Figure 1-4). Such data has been extensively published by a number of authors, ranging across the RLS limbs (e.g. Cameron, 1980; Eales & Cawthorn, 1996; Eales et al., 1990; Mitchell, 1986, 1990; Teigler, 1990; Teigler & Eales, 1996; Yuan et al., 2017). The observed vertical variations have highly influenced the interpretation of probable compositions of proposed RLS parental magmas and their manner of emplacement. Currently, general consensus surrounds Kruger's (2005) model, suggesting lateral expansion of the RLS chamber by successive injections of magma of various compositions and volume.

Evidently, understanding the nature, composition/s, and source/s of the parental magmas of the cumulate rocks and ores of the RLS form a great challenge. Without consideration of these aspects, interpretation of the formation of the suite is rather unfeasible. Consequently, a number of authors have put forward estimations of RLS parental magma compositions, with the earliest estimations by Lombard (1934), Willemse, (1959), Wager & Brown (1968), Hamilton (1977), and Frick (1987). Subsequent works (Cawthorn et al., 1981; Davies et al., 1980; Davies & Tredoux, 1985; Harmer & Sharpe, 1985; Sharpe, 1981, 1984, 1985; Sharpe & Hulbert, 1985) brought about major advances in the identification of different RLS lineages (Eales, 2002), with the experimental work of Cawthorn & Davies (1983), which investigated melts that could reproduce the crystallisation sequence of the lower parts of the suite, concluding that the melts of Willemse (1959), Wager & Brown (1968), as well as komatiitic melts, are not appropriate in composition.

The constraints from the work of Cawthorn & Davies (1983) were best met by the composition of Davies et al. (1980), representing a quench-textured micropyroxenite sill (Table 1-2, column 2). Systematic sampling and analyses of marginal contact zones and sills in the western and eastern limbs of the RLS, and the grouping of these estimations based on composition and stratigraphic division, gave way to the proposed parental Bushveld 1 (B1) magma for the LZ and LCZ, compositionally similar to Mg-rich basaltic andesite, followed by the Bushveld 2 (B2) magma for the UCZ, and the Bushveld 3 (B3) magma for the Main Zone,

Stellenbosch University https://scholar.sun.ac.za

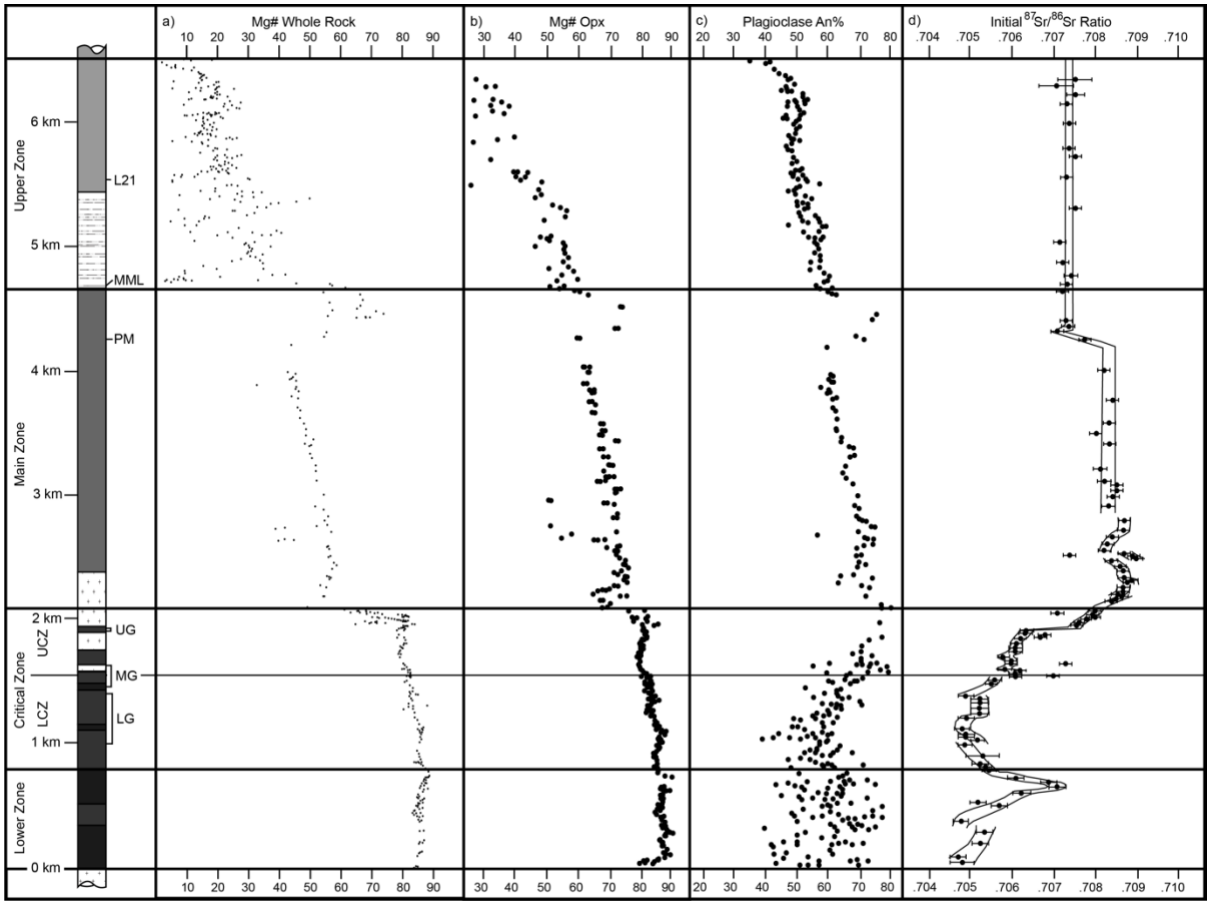

Figure 1-4. Geochemical stratigraphy of the Rustenburg Layered Suite, displaying a) Whole-rock Mg#. b) Orthopyroxene Mg#. c) Anorthite percent (An%) in plagioclase. d) $^{87}Sr/^{86}Sr$ initial ratios. Data compiled from Eales et al. (1990), Eales & Cawthorn (1996), Mitchell (1986, 1990; Main Zone), and Yuan et al. (2017). LCZ: Lower Critical Zone; UCZ: Upper Critical Zone; LG: Lower Group chromitites; MG: Middle Group chromitites; UG: Upper Group chromitites; PM: Pyroxenite Marker; MML: Main Magnetite Layer; L21: Layer 21.

which is compositionally similar to tholeiitic basalt. These B1-B3 magmas were originally defined by Sharpe (1981) and expanded by subsequent works (Davies & Tredoux, 1985; Harmer & Sharpe, 1985; Sharpe, 1984; Sharpe & Hulbert, 1985). The Bushveld 4 magma was proposed by Hatton (1988), suggesting that the LZ and LCZ originated from different parental magmas. Davies & Cawthorn (1984) postulated the introduction of another discrete magma at the level of the Pyroxenite Marker (Figure 1-3a), resulting in the formation of the UZ due to magma mixing. In the years following, numerous additional estimations have been postulated for specific zones of the suite or as bulk magmas for the entire suite (e.g. Barnes & Maier, 2002; Barnes et al., 2010; Cawthorn, 2006; Curl, 2001; Eales & Cawthorn, 1996; Eales & Costin, 2012; Godel et al., 2011; Maier et al., 2000; VanTongeren & Mathez, 2013; VanTongeren et al., 2010; Yang et al., 2019). Details of several of the proposed parental magmas are displayed in Table 1-2.

Stellenbosch University https://scholar.sun.ac.za

	1	2	3	4	5	6	7	8	9	10	11	12	13	14
SiO_2	50.55	55.52	56.2	56.02	56.74	55.74	48.47	50.35	50.79	51.61	52.54	51.33	50.20	49.79
TiO_2	0.66	0.36	0.33	0.34	0.36	0.34	0.33	0.66	0.76	0.89	0.19	0.37	0.9	0.82
Al_2O_3	15.23	12.70	11.4	11.46	13.06	11.82	5.64	16.23	15.70	15.36	17.06	16.14	19.5	15.82
Fe_2O_3	-	0.80	0.86	0.88	-	0.95	1.91	1.04	1.14	1.09	0.66	0.95	0.9	1.18
FeO	-	8.05	8.63	8.77	-	9.54	10.38	10.42	11.40	10.86	6.62	9.50	9.0	11.83
FeO_t	11.01	-	-		9.34	-	-	-	-	-	-	-	-	
MnO	0.23	0.09	0.18	0.18	0.18	0.18	-	0.19	0.19	0.19	0.15	0.18	0.15	0.19
MgO	8.30	12.40	13.1	12.95	9.06	11.85	27.31	7.09	6.91	6.73	8.07	7.69	6.7	6.14
CaO	11.30	6.94	6.44	6.67	6.89	6.50	4.13	11.40	10.70	10.11	12.03	11.25	9.8	10.93
Na_2O	2.24	2.01	1.75	1.68	1.89	1.63	0.89	2.28	1.94	2.66	2.35	1.91	2.6	2.97
K_2O	0.19	1.03	0.90	0.80	1.12	0.98	0.2	0.16	0.25	0.27	0.24	0.28	0.36	0.25
P_2O_5	0.12	0.10	-	0.07	0.09	0.08	-	0.13	0.16	0.22	0.02	0.03	-	0.07
Cr_2O_3	0.009	0.14	-	0.18	0.07	0.14	0.52	0.03	0.03	0.05	0.08	0.06	-	0.02
Cr (ppm)	67	970	-	1240	486	965	3557	197	201	373	547	408	-	111
Mg#	0.571	0.716	0.713	0.707	0.631	0.709	0.799	0.527	0.543	0.503	0.666	0.618	0.549	0.459

Table 1-2. Compositions/analyses of proposed primitive Rustenburg Layered Suite magmas. Adapted from Eales (2002) and Cawthorn (2006). All analysis recalculated to anhydrous conditions. FeO:Fe_2O_3 =10:1 (wt.%) or as is reported. Cr ppm numbers were recalculated to Cr_2O_3 and vice versa, except for Hatton (1998), and Sharpe & Hulbert (1985). (-) indicates unreported values.

1. Fine-grained gabbronorite (Wager & Brown, 1968)
2. Putative Lower Zone magma (Davies et al., 1980).
3. Putative Lower Zone B1-type magma (Hatton, 1988).
4. B1-type of Sharpe & Hulbert (1985).
5. Lower Zone and Lower Critical Zone parental magma (Maier et al., 2000)
6. Lower Zone and Lower Critical Zone B1 magma of Barnes et al. (2010).
7. Marginal, Lower and Critical Zone source: crustally contaminated komatiite (Eales & Costin, 2012) including 0.18 wt.% NiO.
8. Average of four B2-type quenched rocks of Harmer & Sharpe (1985) including 0.03 wt.% NiO.
9. Upper Critical Zone B2 magma of Barnes et al. (2010).
10. Tholeiitic basalt suite (Davies & Tredoux, 1985).
11. B3-type magma from Harmer & Sharpe (1985) and Hatton & Sharpe (1989). Includes 0.02 wt.% NiO.
12. Main Zone B3 magma of Barnes et al. (2010).
13. Theoretically derived B4 magma of Hatton (1988), proposed as parental to the Main Zone.
14. Magma proposed as parental to Upper Zone by Davies & Cawthorn (1984).

The reader is encouraged to consult Eales (2002) for a comprehensive discussion of the caveats (Mg#s, Sr-isotopic ratio, incompatible element data, cumulous mineral parageneses) surrounding many of the suggested magmas; although popular in the literature, the B1–B3 magmas have been met with criticism on various fronts due to some anomalies observed when compared with the RLS cumulate rocks. A large amount of scrutiny stems from the B1 magma's inability to yield olivine at assumed emplacement pressures (Eales & Costin, 2012). Such a magma cannot produce sequences of harzburgites and dunites as observed in the LZ and LCZ. Kruger (2005) criticised the notion of B2 and B3 magmas of the same lineage, pointing to a change in whole rock and isotopic compositions upwards in the sequence as evidence of two evolutionary stages with five magmas. Such constraints associated with the B1–B3 magmas question the true relationship of the sampled marginal rocks and sills with the

Stellenbosch University https://scholar.sun.ac.za

RLS, suggesting that these rocks may not be indicative of parental magmas. As is evident, the characteristics of the suggested parental magmas have long been debated and remain so, ensuing continuous scrutiny in the efforts to develop a magmatic model with widespread acceptance.

The 'Chrome-paradox'

The undefined nature of RLS parental magmas further convolute the controversial topic of the origin of the massive chromitites in the RLS. Already complicated by the discrepancy between Cr_2O_3 averages in RLS cumulates and the low solubility of Cr in mafic magmas (Figure 1-4), a glaring caveat of the majority of the suggested parental magmas are their low concentrations of Cr_2O_3, except for the magma proposed by Eales & Costin (2012) (Table 1-2, column 7). As was presented by Eales (2000), averages of Cr_2O_3 in the LZ cumulates (0.76%) and CZ cumulates (1.71% in the LCZ; 0.88% in the UCZ) results in a weighted average of 1.07% Cr_2O_3 throughout the LZ and CZ. Thus, it is difficult to reconcile the low abundances of Cr_2O_3 in suggested B1-type melts and even lower abundances in B2-type melts, with the abundance of Cr_2O_3 in the lower parts of the RLS. Additionally, considering the isotopic variation throughout the suite as is observed in Figure 1-4d, and the generally accepted involvement of several magma batches in forming the RLS, this suggests that these magma batches must remain distinct from new batches as they crystallise in order to preserve their isotopic variation. Simply put, multiple magma batches of great volume would have been required to account for the amount of Cr present in the LZ and CZ, and each with their own isotopic character. No evidence exists for the intrusion of such massive volumes of magma (Eales & Costin, 2012), and the various explanations that have been put forward (e.g. Naldrett et al., 2012) are hard to reconcile with the geological record. This 'Chrome-paradox' (e.g. Eales, 2000; Kruger, 2005; Figure 1-5) is considered one of the greatest limitations of proposed RLS parental magmas and proposed models for chromitite formation.

Whilst many of the models presented for chromite formation (Table 1-1) have been questioned on various grounds (e.g. Eales, 2000; Eales & Costin, 2012; Maier et al., 2013; Maier & Barnes, 2008; Mondal & Mathez, 2007; Mungall et al., 2016), with their strengths and limitations discussed comprehensively by Latypov et al. (2017b), the majority of the scientific community have remained focussed on the mechanisms that may result in chromite saturation or the formation of chromite crystals in the magma. Consequently, a fundamental aspect that has been overlooked in most of the proposed models is the host of the Cr. Although the solubility of Cr in mafic melts remain a constraint, there are several mineral phases that are

Stellenbosch University https://scholar.sun.ac.za

stable under upper mantle conditions, such as garnet and orthopyroxene, that can host high amounts of Cr (e.g. Jean & Shervais, 2017; Wood et al., 2013). It is thus pertinent to gain an understanding of the fundamental behaviour of Cr during partial melting in the mantle, which may provide clues as to how mantle-hosted Cr travels to crustal magma chambers in concentrations needed to form massive chromitites. In other words, what if Cr is transferred from the mantle to the crust not in the melt phase, but in a mantle mineral phase that is capable of hosting a much greater concentration of Cr than mafic melt is able to achieve?

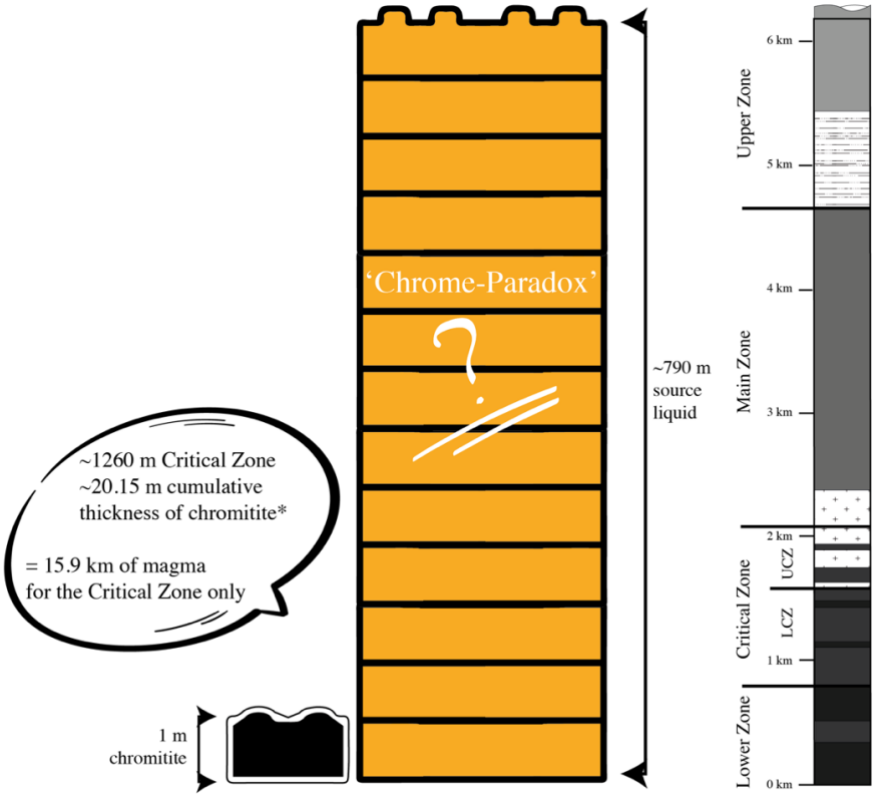

Figure 1-5. A schematic illustrating the concept of the 'Chrome-paradox'. a) Mass balance shows that if 1 metre of chromitite is to contain 68% Cr_2O_3 (4.5 g/cm^3 density; Eales, 2000), this would require ~790 metres of source liquid containing 0.15% Cr_2O_3 (2.57 g/cm^3 density; Eales, 2000). If we consider the cumulative thickness of the chromitites in the CZ of the RLS as reported by Eales (2000), calculations show that 15.9 kilometres of magma is needed to form the CZ alone, which is far beyond the approximate 1.26 kilometres thickness of the CZ as observed in the western limb of the RLS.

Peritectic crystal entrainment: a phase equilibrium modelling approach

From the range of experimental insights gathered for partial melting processes in the crust, the concept of peritectic phase formation is well-established, particularly the importance of source peritectic assemblage entrainment in shaping granitic magma chemistry (e.g. Chappell et al., 1987; Clemens et al., 2011; Stevens et al., 2007). In the upper mantle, mafic to intermediate magmas that have separated from their sources have major element chemistries dictated by the composition of the source rock, the degree to which partial melting has occurred, and the mineral assemblage of the residuum. Importantly, during the incongruent

Stellenbosch University https://scholar.sun.ac.za

mantle melting process, the formation of small amounts of peritectic phases have been identified at a variety of melt fractions, with new crystal formation dependant on the composition of the source, as well as the Pressure-Temperature (P-T) conditions (e.g. Grove et al., 2013; Niu, 1997; Tomlinson & Kamber, 2021). In light of the entrainment of solid xenoliths of mantle material to mantle-derived magmas, the entrainment of some or all of the new peritectic crystals to the magma during separation from the source is highly probable, as the crystals form in and are suspended in the melt (Erdmann et al., 2012). Additionally, considering the known impact of the entrainment of source components on the nature of the magmas in the continental crust, mantle-derived partial melts that have entrained peritectic phases during extraction from the source may explain some the compositional variation observed for mafic to intermediate rocks on a planetary scale, which has not been investigated previously. Moreover, depending on the nature of the peritectic phase and the abundance of the phase produced, it is important to consider what effect peritectic phase entrainment may have on the overall budget of Cr in mantle-derived partial melts, if any. The possible implications of the abovementioned can only be established via investigations into the stoichiometry of the partial melting reactions in the SCLM; however, the hinderance of studying mantle melting processes in that it cannot be observed directly, remains problematic.

Having previously relied heavily on experimental studies for insights, the caveats associated with experimental results, its tedious nature, and limitation to small snapshots of Pressure-Temperature-Compositional (P-T-X) space, has emphasised the need to explore alternative forms of investigation into upper mantle partial melting processes. With the recent expansion of the available thermodynamic datasets (e.g. Holland & Powell, 2011) and models for the behaviour of solid-solution and liquid-solution phases (e.g. Ghiorso et al., 2002; Holland et al., 2018) to upper mantle conditions (≤ 60 kbar in volatile-free systems), thermodynamic modelling is a welcomed alternative for studying partial melting processes and dynamics in the upper mantle, already being an established form of investigation for crustal processes for several decades (Figure 1-6). The development of one such modelling front-end, Rcrust (Mayne et al., 2016), allows investigations of assemblages evolving in an open system, i.e. it has the ability to simulate magma extractions. This capability makes Rcrust ideally suited to study the effects that may result from the entrainment of peritectic phases in mantle-derived melts, should the stoichiometry of the melting reactions point to the production of peritectic phase/s for a given ultramafic or mafic bulk composition.

Stellenbosch University https://scholar.sun.ac.za

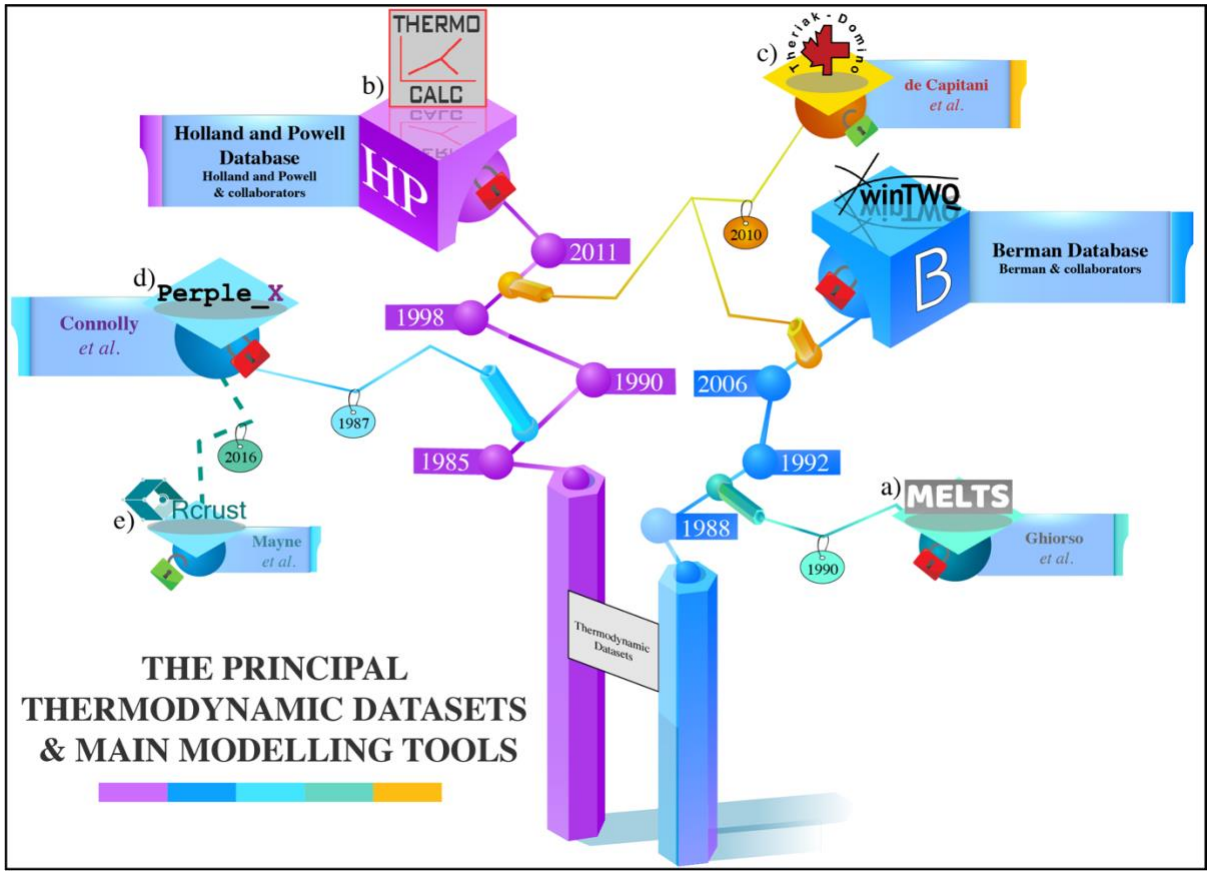

Figure 1-6. Summary of the principle thermodynamic datasets and main modelling software available for investigating crustal and mantle processes, adapted from Lanari (2021). The dates in blue or purple indicate when the associated thermodynamic dataset was updated. The dates illustrated as a tag-like feature indicate the start of the associated software's development. The locks indicate open (green) or closed (red) software. a) The MELTS family (Asimow & Ghiorso, 1998; Ghiorso et al., 2002; Ghiorso & Sack, 1995) follow a Gibbs free energy minimisation approach using the dataset of Berman (1988) and embedded activity-composition (*a-x*) models. b) The calculation strategy of THERMOCALC (Powell et al., 1998; Powell & Holland, 1988) solves for reaction boundaries where dG=0 using the Holland & Powell (2011) dataset, with several options of *a-x* models depending on the bulk composition under investigation. c) Theriak/Domino (de Capitani & Petrakakis, 2010) and d) Perple_X (Connolly, 2005; Connolly & Kerrick, 1987) uses Gibbs free energy minimisation techniques with any dataset and *a-x* models that are appropriately formatted for the software. Generally, the Holland & Powell (2011) dataset is used. e) Rcrust (Mayne et al., 2016, 2019) also uses Gibbs free energy minimisation techniques inherited from Perple_X, where its path-dependant iterations allow investigations into compositional change. Rcrust can use any dataset and *a-x* models that have been appropriately formatted for Perple_X.

Aims of this study

This work aims to thermodynamically constrain the stoichiometry of partial melting reactions in typical upper mantle source rocks in order to identify the areas of peritectic phase formation during the partial melting process, and investigate the extent to which the entrainment of these peritectic phases may alter the resulting magma chemistries. The crystallisation sequence of the resultant magmas at crustal pressures are considered, and this is finally applied to the formation of the lower parts of the Bushveld Complex in South Africa, particularly the formation of the economically important chromitite seams in the Critical Zone of the Rustenburg Layered Suite. The initial stage of the project includes investigating two modelling

Stellenbosch University https://scholar.sun.ac.za

programs that are appropriate for use under upper mantle conditions to analyse how accurately these software can reproduce results from partial melting experimental investigations of mantle sources. Once the most appropriate software is identified – in this case, Rcrust – the partial melting reactions of an eclogitic and peridotitic source are modelled from 15–30 kbar, and areas of peritectic phase formation are identified along isobaric and adiabatic decompression paths. The entrainment of the peritectic phases are modelled by simulating extractions of melt plus peritectic phases (i.e. magma), and extractions of melt only along the same temperature or pressure-temperature paths. Analyses of the extracted melt and magma chemistries compared to global basalt data show that peritectic crystal entrained magmas fall within the denser array and larger scatter of basaltic rock compositions found in continental tectonic environments. This suggests that peritectic crystal entrainment may play a large role in the compositional diversity observed for basaltic rocks worldwide, and how mechanisms such as fractionation mirror the compositional diversity produced in the source. The influence of peritectic entrained crystals is then investigated in the context of LMIs, in particular the Rustenburg Layered Suite of the Bushveld Complex. At shallow crustal conditions, emplacement simulations of peritectic crystal entrained magmas derived from a peridotitic source show the equilibration of the entrained pyroxene with the melt during magma ascent, which allow the formation of peritectic olivine and chromite. Emplacement as sills sees the immediate formation of chromite and dunite layers when assuming density separation, and continued cooling can produce orthopyroxene, clinopyroxene, and plagioclase. This crystallisation sequence can thus produce a range of ferromagnesian and anorthositic layered silicate rocks as is observed in the lower parts of the Rustenburg Layered Suite, including the chromitite layers – the presence of which remains a highly debated topic.

Thesis Structure

In the next chapter of this thesis, the different available modelling software, thermodynamic datasets, and activity-composition (*a*-*x*) models for thermodynamic modelling in the upper mantle are discussed, providing some of the important details as is relevant to this study. Then, the advantages and disadvantages of both experimental techniques and thermodynamic modelling methodologies are noted. Most importantly, thermodynamic modelling using Rcrust software and the Holland & Powell (2011) dataset is established as suitable for the investigation of partial melting reactions occurring in upper mantle source rocks, as compared to outputs from another thermodynamic modelling bundle, and in relation to experimental studies. This opens up a wide range of possibilities for investigating reactions in the upper mantle, including

Stellenbosch University https://scholar.sun.ac.za

magma extractions, in a thermodynamically constrained way. Subchapter 2.2 presents additional work done in determining the suitability of Rcrust modelling for investigating upper mantle source bulk compositions, by considering the outputs of the same thermodynamic dataset with different modelling software for the same source composition. Subchapter 2.3 successfully investigates and expands the applicability of Rcrust modelling to include crustal conditions, conducted as a precursor for magma emplacement simulations performed in Chapter 4.

Chapter 3 discusses how Rcrust software was used to investigate the stoichiometry of partial melting reactions in the upper mantle using a representative eclogitic and peridotitic source from Premier mine in South Africa, resulting in the identification of areas of peritectic mineral formation as part of the incongruent melting reaction. This production of peritectic phases with the melt and the entrainment of these new phases to the magma (i.e. melt plus crystals) upon segregation form the source has profound effects on the composition of the magma as compared to the compositions of extracts of pure melt (i.e. batch melting or dynamic partial melting). The capability of Rcrust to model mineral phase extractions and melt extractions allowed the investigation of the resultant bulk compositions formed via peritectic phase entrainment to the melt, and the outputs point to important fundamental aspects of observed global basalt compositional variations that have previously been overlooked.

In considering the significant effects of the entrainment of peritectic phases to mantle-derived melts on the bulk composition of the magma, Chapter 4 presents an alternative theory for the formation of massive chromitites as found in LMIs such as the RLS. By showing that the entrainment of Cr-bearing peritectic phases can completely alter the budget of Cr in the magma during ascent and upon emplacement at crustal conditions, as well as producing igneous cumulates that broadly match those of the lower portions of the RLS as described earlier, a simple, alternative model is proposed that can produce the massive chromitite seams and general igneous stratigraphy of the lower RLS. Chapter 5 serves as the Conclusion of this research project, followed by the Addenda, which provide and describe the supplemetary files for each chapter, where applicable.

Stellenbosch University https://scholar.sun.ac.za

References

1. Arai, S. 1992. Chemistry of chromian spinel in volcanic rocks as a potential guide to magma chemistry. *Mineralogical Magazine,* 56:17–184.
2. Arai, S. and Miura, M. 2016. Formation and modification of chromitites in the mantle. *Lithos,* 264:277–295.
3. Armitage, G.J. 1992. The petrogenesis of potholes in the UG2 chromitite layer, Crocodile River Mine, Western Bushveld Complex. Unpublished doctoral dissertation. Pietermaritzburg: University of Natal.
4. Asimow, P.D. and Ghiorso, M.S. 1998. Algorithmic modifications extending MELTS to calculate subsolidus phase relations. *American Mineralogist,* 83:1127–1132.
5. Azar, B. 2010. The Blackbird chromite deposit, James Bay lowlands of Ontario, Canada: Implications for chromitite genesis in ultramafic conduits and open magmatic systems. Unpublished master's thesis. Toronto: University of Toronto.
6. Bachmann, O. and Huber, C. 2019. The inner workings of crustal distillation columns; the physical mechanisms and rates controlling phase separation in silicic magma reservoirs. *Journal of Petrology,* 60:318.
7. Bachmann, K., Menzel, P., Tolosana-Degado, R., Schmidt, C., Hill, M. and Gutzmer, J. 2019. Multivariate geochemical classification of chromitite layers in the Bushveld Complex, South Africa. *Applied Geochemistry,* 103:106–117.
8. Barnes, S.-J. and Maier, W.D. 2002. Platinum-group elements and microstructures of normal Merensky Reef from Impala platinum mines, Bushveld Complex. *Journal of Petrology,* 43:103–128.
9. Barnes, S.J. and Roeder, P.L. The Range of Spinel Compositions in Terrestrial Mafic and Ultramafic Rocks. *Journal of Petrology,* 42(12):2279–2302.
10. Barnes, S.-J., Maier, W.D. and Curl, E.A. 2010. Composition of the Marginal Rocks and Sills of the Rustenburg Layered Suite, Bushveld Complex, South Africa: Implications for the formation of the Platinum-Group Element Deposits. *Economic Geology,* 105:1491–1511.
11. Bédard, J.H., Sparks, R.S.J., Renner, R., Cheadle, M.J. and Hallworth, M.A. Peridotite sills and metasomatic gabbros in the Eastern Layered Series of the Rhum complex. *Journal of the Geological Society of London,* 145:207–224.

Stellenbosch University https://scholar.sun.ac.za

12. Berman, R.G. 1988. Internally-consistent thermodynamic data for minerals in the system Na_2O-K_2O-CaO-MgO-FeO-Fe_2O_3-Al_2O_3-SiO_2-TiO_2-H_2O-CO_2. *Journal of Petrology*, 29(2):445–522.
13. Boudreau, A.E. 2008. Modeling the Merensky Reef, Bushveld Complex, Republic of South Africa. *Contributions to Mineralogy and Petrology*, 156:431–437.
14. Boudreau, A.E. 2016. The Stillwater Complex, Montana - Overview and the significance of volatiles. *Mineralogical Magazine*, 80(4):585–637.
15. Cameron, E.N. 1977. Chromite in the central sector of the eastern Bushveld Complex, South Africa. *American Mineralogist*, 62:1082–1096.
16. Cameron, E.N. 1978. The Lower Zone of the eastern Bushveld Complex in the Olifants River trough. *Journal of Petrology*, 19:437–462.
17. Cameron, E.N. 1980. Evolution of the lower critical zone, central sector, eastern Bushveld Complex. *Economic Geology*, 75:845–871.
18. Cameron, E.N. 1982. The Upper Critical Zone of the eastern Bushveld Complex—precursor of the Merensky Reef. *Economic Geology*, 77:1307–1327.
19. Cameron, E.C., Desborough, G.A. 1969. Occurrence and characteristics of chromite deposits - Eastern Bushveld Complex, South Africa. *Economic Geology Monographs*, 4:23–40.
20. Cashman, K.V., Sparks, R.S.J. and Blundy, J.D. 2017. Vertically extensive and unstable magmatic systems: a unified view of igneous processes. *Science*, 355:eaag3055.
21. Cawthorn, R.G (ed.). 1996. *Layered Igneous Rocks*. Amsterdam: Elsevier Science. 580.
22. Cawthorn, R.G. 2003. Genesis of magmatic oxide deposits – a view from the Bushveld Complex. *Norges Geologiske Undersokelse Special Publication*, 9:11–21
23. Cawthorn, R.G. 2005. Pressure fluctuations and the formation of the PGE-rich Merensky and chromitite reefs, Bushveld Complex. *Mineralium Deposita*, 40:231–235.
24. Cawthorn, R.G. 2006. Cr and Sr: keys to parental magmas and processes in the Bushveld Complex, South Africa. *Lithos*, 95:381–398.
25. Cawthorn, R.G. 2011. Geological interpretations from the PGE distribution in the Bushveld Merensky and UG2 chromitite reefs. *Journal of the South African Institute of Mining and Metallurgy*, 111:67–79.
26. Cawthorn, R.G. 2015. Bushveld Complex, in B. Charlier, O. Namur, R. Latypov and C. Tegner (eds.). *Layered Intrusions*. Springer Nature. 517–587.

Stellenbosch University https://scholar.sun.ac.za

27. Cawthorn, R.G. and Davies, G. 1983. Experimental data at 3 kbars pressure on parental magma to the Bushveld Complex. *Contributions to Mineralogy and Petrology*, 83:128–135.
28. Cawthorn, R.G. and Walraven, F. 1998. Emplacement and crystallization time for the Bushveld Complex. *Journal of Petrology*, 39:1669–1687.
29. Cawthorn, R.G., Davies, G., Clubley-Armstrong, A. and McCarthy, T.S. 1981. Sills associated with the Bushveld Complex, South Africa. *Lithos*, 14:1–15.
30. Cawthorn R.G., Eales, H.V., Walraven, F., Uken, R. and Watkeys, M.K. 2009. The Bushveld Complex, in M.R. Johnson, C.R. Anhauesser and R.J. Thomas (eds.). *Geology of South Africa.* Reprinted Edition. Johannesburg: Geological Society of South Africa. Pretoria: Council for Geoscience. 261–281.
31. Cawthorn, R.G., Lundgaard, K.L., Tegner, C. and Wilson, J.R. 2016. Lateral variations in plagioclase compositions, Main Zone, Bushveld Complex, South Africa: Evidence for slow mixing of magmas in basinal structures. *Mineralogical Magazine*, 80:213–225.
32. Campbell, I.H. and Murck, B.W. 1993. Petrology of the G and H chromitite zones in the Mountain View area of the Stillwater Complex, Montana. *Journal of Petrology*, 34:291–316.
33. Chistyakova, S., Latypov, R.M. and Zaccarini, F. 2015. Chromitite dykes in the Monchegorsk layered intrusion, Russia: in situ crystallization from chromite-saturated magma flowing in conduits. *Journal of Petrology*, 56:2395–2424.
34. Cousins, C.A. and Feringa, G. 1964. The chromite deposits of the western belt of the Bushveld Complex, in S.H. Haughton (ed.). *The Geology of Some Ore Deposits in Southern Africa.* Volume II. Johannesburg: Geological Society of South Africa. 183–202.
35. Curl, E.A. 2001. Parental magmas of the Bushveld Complex, South Africa: Unpublished doctoral dissertation, Melbourne: Monash University.
36. Davies, G. and Tredoux, M. 1985. The platinum-group element and gold contents of the marginal rocks and sills of the Bushveld Complex. *Economic Geology*, 80(4):838–848.
37. Davies, G., Cawthorn, R.G., Barton, J.M. and Morton, M. 1980. Parental magma to the Bushveld Complex. *Nature*, 287:33–35.
38. de Capitani, C. and Petrakakis, K. 2010. The computation of equilibrium assemblage diagrams with Theriak/Domino software. *American Mineralogist*, 95:1006–1016.

Stellenbosch University https://scholar.sun.ac.za

39. Dick, H.J.B. and Bullen, T. 1984. Chromian spinel as a petrogenetic indicator in abyssal and alpine type peridotites and spatially associated lavas. *Contributions to Mineralogy and Petrology*, 86:54–76.

40. Eales, H.V. 2000. Implications of the chromium budget of the Western Limb of the Bushveld Complex. *South African Journal of Geology*, 103:141–150.

41. Eales, H.V. 2002. Caveats in defining the magmas parental to the mafic rocks of the Bushveld Complex, and the manner of their emplacement: review and commentary. *Mineralogical Magazine*, 66:815–832.

42. Eales, H.V. and Cawthorn, R.G. 1996. The Bushveld Complex. *Developments in Petrology* 15:181–229.

43. Eales, H.V. and Costin, G. 2012. Crustally Contaminated Komatiite: Primary Source of the Chromitites and Marginal, Lower, and Critical Zone Magmas in a Staging Chamber Beneath the Bushveld Complex. *Economic Geology*, 107:645–665.

44. Eales, H.V., De Klerk, W.J. and Teigler, B. 1990. Evidence for magma mixing processes within the critical and lower zones of the northwestern Bushveld Complex, South Africa. *Chemical Geology*, 88:261–278.

45. Eales, H.V., Field, M., De Klerk, W.J. and Scoon, R.N. 1988. Regional trends of chemical variation and thermal erosion in the Upper Critical zone, western Bushveld Complex. *Mineralogical Magazine*, 52:63–79.

46. Eales, H.V., Marsh, J.S., Mitchell, A.A., de Klerk, W.J. and Kruger, F.J. 1986. Some geochemical constraints upon models for the crystallization of the upper critical zone—main zone interval, Northwestern Bushveld Complex. *Mineralogical Magazine*, 50:567–582.

47. Edmonds, M., Cashman, K.V., Holness, M. and Jackson, M. 2019. Architecture and dynamics of magma reservoirs. *Philosophical Transactions of the Royal Society A*, 377:20180298.

48. Engelbrecht, J.P. 1990. The Marico Hypabyssal Suite and the Marginal Zone of the Bushveld Complex in the Marico district, western Transvaal, South Africa. *South African Journal of Geology*, 93:318–328.

49. Erdmann, S., Scaillet, B. and Kellett, D.A. 2012. Textures of Peritectic Crystals as Guides to Reactive Minerals in Magmatic Systems: New Insights from Melting Experiments. *Journal of Petrology*, 53(11):2231–2258.

50. Ferreira Filho, C.F. and Araujo, S.M. 2009. Review of Brazilian chromite deposits associated with layered intrusions: Geological and petrological constraints for the origin

Stellenbosch University https://scholar.sun.ac.za

of stratiform chromitites. *Transactions of the Institution of Mining and Metallurgy, Section B: Applied Earth Science*, 118:86–100.

51. Fisk, M.R. and Bence, A.E. 1980. Experimental crystallization of chrome spinel in FAMOUS basalt 527-1-1. *Earth and Planetary Science Letters*, 48:111–123.
52. Ford, C.E., Biggar, G.M., Humphries, D.J., Wilson, G., Dixon, D. and O'Hara, M.J. 1972. Role of water in the evolution of the lunar crust; an experimental study of sample 14310; an indication of lunar calc-alkaline volcanism. Proceedings of the Third Lunar Science Conference, *Geochimica et Cosmochimica Acta*, 3(1):207–229.
53. Ghiorso, M.S. and Sack, R.O. 1995. Chemical mass transfer in magmatic processes, IV. A revised and internally consistent thermodynamic model for the interpolation and extrapolation of liquid-solid equilibria in magmatic systems at elevated temperatures and pressures. *Contributions to Mineralogy and Petrology*, 119:197–212.
54. Ghiorso, M.S., Hirschmann, M.M., Reiners, P.W. and Kress, V.C.III. 2002. The pMELTS: A revision of MELTS for improved calculation of phase relations and major element partitioning related to partial melting of the mantle to 3 GPa. *Geochemistry Geophysics Geosystems*, 3(5).
55. Glastonbury, R.I., van der Merwe, W., Beukes, J.P., van Zyl, P.G., Lachmann, G., Steenkamp, C.J.H., Dawson, N.F. and Stewart, H.M. 2010. Cr(VI) generation during sample preparation of solid samples – A chromite ore case study. *Water SA*, 36(1):105–110.
56. Godel, B., Barnes, S.-J. and Maier, W.D. 2011. Parental magma composition inferred from *in situ* trace elements in cumulus and intercumulus silicate minerals: example from the Lower and Lower Critical Zones of the Bushveld Complex (South Africa). *Lithos*, 125:537–552.
57. Grove, T.L., Holbig, E.S., Barr, J.A., Till, C.B., and Krawczynski, M.J. 2013. Melts of garnet lherzolite: experiments, models and comparison to melts of pyroxenite and carbonated lherzolite. *Contributions to Mineralogy and Petrology*, 166:887–910.
58. Guertin, J., Jacobs, J.A. and Avakian, C. P. 2005. *Chromium(VI) Handbook*. 1st edition. Florida: CRC Press.
59. Harmer, R.E. and Sharpe, M.R. 1985. Field relations and strontium isotope systematics of the marginal rocks of the eastern Bushveld Complex. *Economic Geology*, 80:813–837.
60. Hasch, M. and Latypov, R. 2021. Too large to be seen: Regional structures in Lower and Middle Group chromitites of the Bushveld Complex, South Africa. *Ore Geology Reviews*, 139:104520.

Stellenbosch University https://scholar.sun.ac.za

61. Hatton, C.J. 1988. Densities and liquidus temperatures of Bushveld parental magmas as constraints on the formation of the Merensky Reef in the Bushveld Complex, South Africa, in M.D. Prendergast and M.J. Jones (eds.). *Magmatic Sulphides: the Zimbabwe Volume*. London: Institution of Mining and Metallurgy. 87–93.

62. Hill, R. and Roeder, P. 1974. The crystallization of spinel from basaltic liquid as a function of oxygen fugacity. *The Journal of Geology*, 82:709–729.

63. Holland, T.J.B. and Powell, R. 2011. An improved and extended internally consistent thermodynamic dataset for phases of petrological interest, involving a new equation of state for solids. *Journal of Metamorphic Geology*, 29:333–383.

64. Horan, M.F., Morgan, J.W., Walker, R.J. and Cooper, R.W. 2001. Re-Os isotopic constraints on magma mixing in the peridotite zone of the Stillwater Complex, Montana, USA. *Contributions to Mineralogy and Petrology*, 141:446–457.

65. Irvine, T.N. 1967. Chromian spinel as a petrogenetic indicator. Part 1. Theory. *Canadian Journal of Earth Sciences*, 2:648–671.

66. Irvine, T.N. 1967. Chromian spinel as a petrogenetic indicator. Part 2. Petrologic applications. *Canadian Journal of Earth Sciences*, 4:71–103.

67. Irvine, T.N. 1975. Crystallization sequences in the Muskox intrusion and other layered intrusions—II. Origin of chromitite layers and similar deposits of other magmatic ores. *Geochimica et Cosmochimica Acta*, 39:991–1020.

68. Irvine, T.N. 1977. Origin of chromitite layers in the Muskox intrusion and other layered intrusions: a new interpretation. *Geology*, 5:273–277.

69. Irvine, T.N. and Sharpe, M.R. 1986. Magma mixing and the origin of stratiform oxide ore zones in the Bushveld and Stillwater Complexes. In: Gallagher, M.J., Ixer, R.A., Neary, C.R. and Pritchard, H.M. (eds) *Metallogeny of Basic and Ultrabasic Rocks*. Institution of Mining and Metallurgy, 183-198.

70. Irvine, T.N., Keith, D.W. and Todd, S.G. 1983. The J-M platinum–palladium reef of the Stillwater Complex, Montana: II. Origin by double-diffusive convective magma mixing and implications for the Bushveld Complex. *Economic Geology*, 78:1287–1334.

71. Jackson, E.D. 1961. Primary textures and mineral associations in the ultramafic zone of the Stillwater complex, Montana. *Geological Survey Professional Paper 358*, https://doi.org/10.3133/pp358.

72. Jaques, A.L. and Green, D.H. 1980. Anhydrous melting of peridotite at 0-15 kb pressure and the genesis of tholeiitic basalts. *Contributions to Mineralogy and Petrology*, 73:28–310.

Stellenbosch University https://scholar.sun.ac.za

73. Jean, M.M. and Shervais, J.W. 2017. The distribution of fluid mobile and other incompatible trace elements in orthopyroxene from mantle wedge peridotites. *Chemical Geology*, 457:118–130.

74. Kamenetsky, V.S., Crawford, A.J. and Meffre, S. 2001. Factors controlling chemistry of magmatic spinel: an empirical study of associated olivine, Cr-spinel and melt inclusions from primitive rocks**.** *Journal of Petrology,* 42:655–671.

75. Kaufmann, F.E.D., Hoffmann, M.C., Bachmann, K., Veksler, I.V., Trumbull, R.B. and Hecht, L. 2019. Variations in composition, texture, and platinum group element mineralization in the Lower Group and Middle Group chromitites of the northwestern Bushveld Complex, South Africa. *Economic Geology,* 114(3):569–590.

76. Kinnaird, J.A., Kruger, F.J., Nex, P.A.M. and Cawthorn, R.G. 2002. Chromite formation-a key to understanding processes of platinum enrichment. *Transactions of the Institution of Mining and Metallurgy,* 11:B23–B35.

77. Klemm, D.D., Snethlage, R., Dehm, R.M., Henckel, J. and Schmidt-Thome, R. 1982. The Formation of Chromite and Titanomagnetite Deposits Within the Bushveld Igneous Complex, in G.C. Amstutz, A.EI. Goresy, G. Frenzel, C. Kluth, G. Moh, A. Wauschkuhn and R.A. Zimmermann (eds.). *Ore Genesis. Special Publication of the Society for Geology Applied to Mineral Deposits*. Berlin: Springer-Verlag. 351–370.

78. Kleynhans, E.L.J., Beukes, J.P., Van Zyl, P.G., Kestens, P.H.I. and Langa, J.M. 2012. Unique challenges of clay binders in a pelletised chromite pre-reduction process. *Minerals Engineering* 34, 55e62.

79. Kottke-Levin, J., Tredoux, M. and Grab, P.-J. 2009. An investigation of the geochemistry of the Middle Group of the eastern Bushveld Complex, South Africa Part 1—the chromitite layers. *Transactions of the Institution of Mining and Metallurgy Section B: Applied Earth Science,* 118:111–130.

80. Kruger, F. 1994. The Sr-isotopic stratigraphy of the western Bushveld Complex. *South African Journal of Geology,* 97:393–398.

81. Kruger, F. 2005. Filling the Bushveld Complex magma chamber: Lateral expansion, roof and floor interaction, magmatic unconformities, and the formation of giant chromitite, PGE and Ti–V-magnetite deposits. *Mineralium Deposita,* 40:451–472.

82. Kushiro, I. 2001. Partial Melting Experiments on Peridotite and Origin of Mid-Ocean Ridge Basalt. *Annual Review of Earth and Planetary Sciences,* 29(1):71–107.

83. Lanari, P. 2021. Part 1: Overview of thermodynamic databases. Phase Equilibrium Modeling: approaches and pitfalls. 10 May 2021. Online Workshop.

Stellenbosch University https://scholar.sun.ac.za

84. Langmuir, C.H., Bender, J.F., Bence, A.E., Hanson, G.N. and Taylor, S.R. 1977. Petrogenesis of basalts from the FAMOUS area: Mid-Atlantic Ridge. *Earth and Planetary Science Letters*, 36(1):133–156.

85. Latypov, R., Chistyakova, S., Barnes, S.J. and Hunt, E.J. 2017a. Origin of Platinum Deposits in Layered Intrusions by *In Situ* Crystallization: Evidence from Undercutting Merensky Reef of the Bushveld Complex. *Journal of Petrology*, 58(4):715–761.

86. Latypov, R., Chistyakova, S. and Mukherjee, R. 2017b. A Novel Hypothesis for Origin of Massive Chromitites in the Bushveld Igneous Complex. *Journal of Petrology*, 58:1899–1940.

87. Latypov, R., Chistyakova, S., Page, A. and Hornsey, R. 2015. Field Evidence for the *In Situ* Crystallization of the Merensky Reef. *Journal of Petrology*, 56(12):2341–2372.

88. Latypov, R., Costin, G., Chistyakova, S., Hunt, E.J., Mukherjee, R. and Naldrett, T. 2018. Platinum-bearing chromite layers are caused by pressure reduction during magma ascent. *Nature Communications*, 9:462.

89. Latypov, R., O'Dricoll, B. and Lavrenchuk, A. 2013. Towards a model for the in-situ origin of PGE reefs in layered intrusions: insights from chromitite seams of the Rum Eastern Layered Intrusion, Scotland. *Contributions to Mineralogy and Petrology*, 166(1):309–327.

90. Lee, C.A. 1981. Post-deposition structures in the Bushveld Complex mafic sequence. *Journal of the Geological Society*, 138(3):327–341.

91. Lesher, C.M. 2017. Roles of xenomelts, xenoliths, xenocrysts, xenovolatiles, residues, and skarns and the genesis, transport, and localization of magmatic Fe-Ni-Cu-PGE sulfides and chromite. *Ore Geology Reviews*, 90:465–484.

92. Lesher, C.M., Carson, H.J.E. and Houl´e, M.G. 2019. Genesis of chromite deposits by dynamic upgrading of Fe ± Ti oxide xenocrysts. *Geology*, 47(3):207–210.

93. Leuthold, J., Blundy, J.D. and Brooker, R.A. 2015. Experimental petrology constraints on the recycling of mafic cumulate: a focus on Cr-spinel from the Rum Eastern Layered Intrusion, Scotland. Contributions to Mineralogy and Petrology 170:12.

94. Lipin, B.R. 1993. Pressure increases, the formation of chromite seams, and the development of the ultramafic series in the Stillwater Complex, Montana. *Journal of Petrology*, 34:955–976.

95. Loferski, P.J., Lipin, B.R. and Cooper, R.W. 1990. Petrology of chromite-bearing rocks from the lowermost cyclic units in the Stillwater Complex, Montana, *U.S. Geological Survey Bulletin*, 1674-E.

Stellenbosch University https://scholar.sun.ac.za

96. Lyubetskaya, T. and Korenaga, J. 2006. Chemical composition of Earth's primitive mantle and its variance: 1. Method and results. *Journal of Geophysical Research*, 112:B03211.

97. Maghdour-Mashhour, R., Hayes, B., Bolhar, R. and Ueckermann, H. 2021. Sill intrusion into pyroxenitic mush and the development of the Lower-Upper Critical Zone boundary of the Bushveld Complex: implications for the origin of stratiform anorthosites an chromitites in layered intrusions. *Journal of Petrology*, 62(1):egaa090.

98. Maier, W.D. and Barnes, S.-J. 1999. Platinum-group elements in silicate rocks of the Lower, Critical, and Main zones at Union Section, western Bushveld Complex. *Journal of Petrology*, 40:1647–1671.

99. Maier, W.D., Arndt, N.T. and Curl, E.A. 2000. Progressive crustal contamination of the Bushveld Complex: evidence from Nd isotopic analyses of the cumulate rocks. *Contributions to Mineralogy and Petrology*, 140:316–327.

100. Maier, W.D. and Barnes, S.-J. 2008. Platinum-group elements in the UG1 and UG2 chromitites, and the Bastard Reef, at Impala platinum mine, western Bushveld Complex, South Africa: evidence for late magmatic cumulate instability and reef constitution. *South African Journal of Geology*, 111:159–176.

101. Maier, W.D., Barnes, S.-J. and Groves, D.L. 2012. The Bushveld Complex, South Africa: formation of platinum-palladium, chrome- and vanadium-rich layers via hydrodynamic sorting of a mobilized cumulate slurry in a large, relatively slowly cooling, subsiding magma chamber. *Mineralium Deposita*, 48:1–56.

102. Marques, J.C., Ferreira Filho, C.F., Carlson, R.W. and Pimentel, M.M. 2003. Re–Os and Sm–Nd isotope systematics and trace elements geochemistry constraints for the origin of the chromite deposits of the Ipueira–Medrado sill, Bahia, Brazil. *Journal of Petrology*, 44:659–678.

103. Mathez, E.A. and Kinzler, R.J. 2017. Metasomatic Chromitite Seams in the Bushveld and Rum Layered intrusions. *Elements*, 13(6):397–402.

104. Mayne, M.J, Moyen, J.-F., Stevens, G. and Kaislaniemi, L. 2016. Rcrust: a tool for calculating path-dependent open system processes and application to melt loss. *Journal of Metamorphic Petrology*, 34(7):663–682.

105. Mayne, M.J, Stevens, G., Moyen, J.-F. and Johnson, T. 2019. Performing process-oriented investigations involving mass transfer using Rcrust: a new phase equilibrium modelling tool, in V. Janoušek, B. Bonin, W.J. Collins, F. Farina and P. Bowden (eds.).

Stellenbosch University https://scholar.sun.ac.za

Post-Archean Granitic Rocks: Petrogenetic Processes and Tectonic Environments. Bath: Geological Society of London Special Publications 491. 209–221.

106. Mazzarini, F., Corti, G., Manetti, P. and Innocenti, F. 2004. Strain rate and bimodal volcanism in the continental rift: Debre Zeyt volcanic field, northern MER, Ethiopia. *Journal of African Earth Sciences*, 39(3–5):415–420.
107. McDonald, J.A. 1967. Evolution of part of the lower critical zone, farm ruighoek, Western Bushveld. *Journal of Petrology*, 8(2):165–209.
108. Mitchell, A.A. 1986. The petrology, mineralogy and geochemistry of the Main Zone of the Bushveld Complex at Rustenburg Platinum Mine, Union Section. Unpublished doctoral dissertation. Grahamstown: Rhodes University.
109. Mitchell, A.A. 1990. The stratigraphy, petrography and mineralogy of the Main Zone of the northwestern Bushveld Complex. *South African Journal of Geology*, 93:818–831.
110. Mitchell, A.A. and Scoon, R.N. 2007. The Merensky reef at Winnaarshoek, eastern Bushveld Complex: A primary magmatic hypothesis based on a wide reef facies. *Economic Geology*, 102:971–1009.
111. Mondal, S.K. and Mathez, E.A. 2007. Origin of the UG2 chromitite layer, Bushveld Complex. *Journal of Petrology*, 48:495–510.
112. Mosier, D.L., Singer, D.A., Moring, B.C. and Galloway, J.P. 2012. Podiform chromite deposits - database and grade and tonnage models. *United States Geological Survey Scientific Investigations Report 2012*, 5157.
113. Mukherjee, R., Latypov, R. and Balakrishna, A. 2017. An intrusive origin of some UG-1 chromitite layers in the Bushveld Igneous Complex, South Africa: insights from field relationships. *Ore Geology Reviews*, 90:94–109.
114. Mungall, J.E., Kamo, S.L. and McQuade, S. 2016. U–Pb geochronology documents out-of-sequence emplacement of ultramafic layers in the Bushveld Igneous Complex of South Africa. *Nature Communications*, 7:13385.
115. Murck, B.W. and Campbell, I.H. 1986. The effects of temperature, oxygen fugacity and melt composition on the behaviour of chromium in basic and ultrabasic melts. *Geochimica et Cosmochimica Acta*, 50:1871–1887.
116. Naldrett, A.J., Kinnaird, J.A., Wilson, A., Yudovskaya, M. and Chunnett, G. 2012. The origin of chromitites and related PGE mineralization in the Bushveld Complex: new mineralogical and petrological constraints. *Mineralium Deposita*, 47:209–232.
117. Naldrett, A.J., Kinnaird, J.A., Wilson, A., Yudovskaya, M., McQuade, S., Chunnett, G. and Stanley, C. 2009. Chromite composition and PGE content of Bushveld chromitites:

Stellenbosch University https://scholar.sun.ac.za

Part 1—the Lower and Middle Groups. *Transactions of the Institution of Mining and Metallurgy Section B*: *Applied Earth Science*, 118:131–161.

118. Nex, P.A.M. 2004. Formation of bifurcating chromitite layers of the UG1 in the Bushveld Igneous Complex, an analogy with sand volcanoes. *Journal of Geology Society of London*, 161:903–909.
119. Nicholson, D.M. and Mathez, E.A. 1991. Petrogenesis of the Merensky Reef in the Rustenburg section of the Bushveld Complex. *Contributions to Mineralogy and Petrology*, 107:293–309.
120. Nikolaev, G.S., Ariskin, A.A. and Barmina, G.S. 2020. SPINMELT-2.0: Simulation of spinel-melt equilibrium in basaltic systems under pressures up to 15 kbar: III. The effects of major components in the melt on the chrome-spinel stability and a possible solution of the problem of origin of chromitites. *Geochemistry International*, 58:1–10.
121. O'Driscoll, B., Donaldson, C.H., Daly, J.S. and Emeleus, C.H. 2009. The roles of melt infiltration and cumulate assimilation in the formation of a Cr-spinel seam in the Rum Eastern Layered Intrusion, NW Scotland. *Lithos*, 111:6–20.
122. O'Driscoll, B., Emeleus, C.H., Donaldson, C.H. and Daly, J.S. 2010. Cr-spinel seam petrogenesis in the Rum Layered Suite, NW Scotland: Cumulate assimilation and *in situ* crystallization in a deforming crystal mush. *Journal of Petrology*, 51:1171–1201.
123. Papp, J.F. 1990. Chromium. United States Geological Survey (USGS). Available: http://images.library.wisc.edu/EcoNatRes/EFacs2/MineralsYearBk/MinYB1990v1/reference/econatres.minyb1990v1.jpapp.pdf [2022, August 21].
124. Prendergast, M.D. 2008. Archean komatiitic sill-hosted chromite deposits in the Zimbabwe craton. Economic *Geology*, 103:981–1004.
125. Powell, R. and Holland, T.J.B. 1988. An internally consistent dataset with uncertainties and correlations: 3. Applications to geobarometry, worked examples and a computer program. *Journal of Metamorphic Petrology*, 6(2):173–204.
126. Powell, R., Holland, T.J.B. and Worley, B. 1998. Calculating phase diagrams involving solid solutions via non-linear equations, with examples using THERMOCALC. *Journal of Metamorphic Geology*, 16:577–588.
127. Robb, S.J. and Mungall, J.E. 2020. Testing emplacement models for the Rustenburg Layered Suite of the Bushveld Complex with numerical heat flow models and plagioclase geospeedometry. *Earth and Planetary Science Letters*, 534:116084.
128. Roeder, P.L. and Reynolds, I. 1991. Crystallization of chromite and chromium solubility in basaltic melts. *Journal of Petrology*, 32:909–934.

Stellenbosch University https://scholar.sun.ac.za

129. Rollinson, H. 1997. The Archean komatiite-related Inyala Chromitite, southern Zimbabwe. *Economic Geology*, 92(1):98–107.

130. Sack, R.O. 1982. Spinels as petrogenetic indicators: activity–composition relations at low pressures. *Contributions to Mineralogy and Petrology*, 79:169–186.

131. Sampson, E. 1932. Magmatic chromite deposits in Southern Africa. *Economic Geology*, 27:113–144.

132. Schoenberg, R., Kruger, F.J., Nägler, T.F., Meisel, T. and Kramers, J.D. 1999. PGE enrichment in chromitite layers and the Merensky reef of the western Bushveld Complex; a Re-Os and Rb-Sr isotope study. *Earth and Planetary Science Letters*, 172:49–64.

133. Scoon, R.N. and Costin, G. 2018. Chemistry, morphology and origin of magmatic-reaction chromite stringers associated with anorthosite in the Upper Critical Zone at Winnaarshoek, Eastern Limb of the Bushveld Complex. *Journal of Petrology*, 59(8):1551–1578.

134. Scoon, R.N. and Teigler, B. 1994. Platinum-group element mineralization in the Critical Zone of the Western Bushveld Complex: I. Sulfide poor chromitites below the UG-2. *Economic Geology*, 89:1094–1121.

135. Schürmann, L.W., Grabe, P-J. and Steenkamp, C.J. 1998. Chromium, in M.G.C. Wilson and C.R. Anhaeusser (eds.). *The Mineral Resources of South Africa*. Handbook 16. Cape Town: Council for Geosciences. 90–105.

136. Sharpe, M.R. 1981. The chronology of magma influxes to the eastern compartment of the Bushveld Complex, as exemplified by its marginal border group. *Journal of the Geological Society of London*, 138:307–326.

137. Sharpe, M.R. and Hulbert, L.J. 1985. Ultramafic sills beneath the Eastern Bushveld Complex. *Economic Geology*, 80:849–71.

138. Smith, C.H. 1962. Notes on the Muskox intrusion, Coppermine River area, District of Mackenzie. *Geological Survey of Canada Paper*, 61–25.

139. Spandler, C., Mavrogenes, J. and Arculus, R. 2005. Origin of chromitites in layered intrusions: Evidence from chromite-hosted melt inclusions from the Stillwater Complex. *Geology*, 33:893–896.

140. Sparks, R.S.J., Annen, C., Blundy, J.D., Cashman, K.V., Rust, A.C. and Jackson, M.D. 2019. Formation and dynamics of magma reservoirs. *Philosophical Transactions of the Royal Society A*, 377:20180019.

141. Stevens, R.E. 1944. Composition of some chromites of the Western Hemisphere. *American Mineralogist*, 29(1–2):1–34.

Stellenbosch University https://scholar.sun.ac.za

142. Stowe, C.W. 1994. Compositions and Tectonic Settings of Chromite Deposits through Time. *Economic Geology*, 89:528–546.

143. Teigler, B. 1990. Mineralogy, petrology and geochemistry of the Lower and Lower Critical zones, northwestern Bushveld Complex: Unpublished doctoral dissertation, Grahamstown: Rhodes University.

144. Thayer, T.P. 1973. Chromium, in D.A. Brobst and W.P. Pratt (eds.). *United States Mineral Resources, United States Geological Survey Professional Paper 820*. Washington: U.S. Government Printing Office. 111–121.

145. Turner, S. and Hawkesworth, C. 1995. The nature of the sub-continental mantle: constraints from the major-element composition of continental flood basalts. *Chemical Geology*, 120(3–4):295–314.

146. Ulmer, G.C. 1969. Experimental investigations of chromite spinels. In: Wilson, H.D.B. (ed.) Magmatic Ore Deposits. *Economic Geology Monograph*, 4:114–131.

147. VanTongeren, J.A. and Mathez, E.A. 2013. Incoming magma composition and style of recharge below the Pyroxenite Marker, eastern Bushveld Complex, South Africa. *Journal of Petrology*, 54:1585–1605.

148. VanTongeren, J.A., Mathez, E.A. and Kelemen, P.B. 2010. A felsic end to Bushveld differentiation. *Journal of Petrology*, 51:1891–1912.

149. Veksler, I.V. and Hou, T. 2020. Experimental study on the effects of H_2O upon crystallization in the Lower and Critical Zones of the Bushveld Complex with an emphasis on chromitite formation. *Contributions to Mineralogy and Petrology*, 175(9):1–17.

150. Veksler, I.V., Sedunova, A.P., Darin, A.V., Anosova, M.O., Reid, D.L., Kaufmann, F.E., Hecht, L. and Trumbull, R.B. 2018. Chemical and textural re-equilibration in the UG2 chromitite layer of the Bushveld Complex, South Africa. *Journal of Petrology*, 59(6):1193–1216.

151. Von Gruenewaldt, G. 1973. The Main and Upper Zones of the Bushveld Complex in the Rossenekal area, Eastern Transvaal. *Transactions of the Geological Society of South Africa*, 76:207–227.

152. Von Gruenewaldt, G., Hatton, C.J., Merkle, R.K.W. and Gain, S.B. 1986. Platinum-group element-chromitite associations in the Bushveld Complex. *Economic Geology*, 81:1067–1079.

153. Von Gruenewaldt, G., Sharpe, M.R. and Hatton, C.J. 1985. The Bushveld Complex: Introduction and Review. *Economic Geology*, 80:803–812.

Stellenbosch University https://scholar.sun.ac.za

154. Voordouw, R., Gutzmer, J. and Beukes, N.J. 2009. Intrusive origin for upper group (UG1, UG2) stratiform chromitite seams in the Dwars River area, Bushveld Complex, South Africa. *Mineralogy and Petrology*, 97:75–94.

155. Wall, C.J., Scoates, J.S., Weiss, D., Friedman, R.M., Amini, M. and Meurer, W.P. 2018. The Stillwater Complex: integrating zircon geochronological and geochemical constraints on the age, emplacement history and crystallization of a large, open-system layered intrusion. *Journal of Petrology*, 59:153–190.

156. Wilson, A.H. 1982. The Geology of the Great 'Dyke', Zimbabwe: The Ultramafic Rocks. *Journal of Petrology*, 23:240–292.

157. Wilson, M.G.C. and Anhaeusser, C.R. 1998. *The Mineral Resources of South Africa: Handbook 16.* Cape Town: Council for Geoscience.

158. Winter, J.D.N. 2010. *Principles of Igneous and Metamorphic Petrology.* New York: Prentice Hall. 222.

159. Wood, B.J., Kiseeva, E.S. and Matzen, A.K. 2013. Garnet in the Earth's Mantle. *Elements*, 9:421–426.

160. Yang, S.-H., Maier, W.D., Godel, B., Barnes, S.-J., Hanski, E. and O'Brien, H. 2019. Parental Magma Composition of the Main Zone of the Bushveld Complex: Evidence from *in situ* LA-ICP-MS Trace Element Analysis of Silicate Minerals in the Cumulate Rocks. *Journal of Petrology*, 60(2):359–392.

161. Yao, Z., Mungall, J.A. and Jenkins, C.M. 2021. The Rustenburg Layered Suite formed as a stack of mush with transient magma chambers. *Nature Communications*, 12:505.

162. Yuan, Q., Namur, O., Fischer, L.A., Roberts, R.J., Lü, X. and Charlier, B. 2017. Pulses of Plagioclase-laden Magmas and Stratigraphic Evolution in the Upper Zone of the Bushveld Complex, South Africa. *Journal of Petrology*, 58:1619–1644.

163. Yudovskaya, M.A., Naldrett, A.J., Woolfe, J.A.S., Costin, G. and Kinnaird, J. 2015. Reverse compositional zoning in the Uitkomst chromitites as an indication of crystallisation in a magmatic conduit. *Journal of Petrology*, 56:2373–2394.

164. Zeh, A., Ovtacharova, M., Wilson, A.H. and Schaltegger, U. 2015. The Bushveld Complex was emplaced and cooled in less than one million years - results of zirconology, and geotectonic implications. *Earth and Planetary Science Letters*, 418:103–114.

Stellenbosch University https://scholar.sun.ac.za

CHAPTER 2

PRESENTATION OF RESEARCH PAPER 1

PHASE EQUILIBRIUM MODELLING OF UPPER MANTLE PARTIAL MELTING: A COMPARISON BETWEEN DIFFERENT MODELLING METHODOLOGIES AND EXPERIMENTAL RESULTS

This paper, first authored by Tahnee Otto, is accepted for publication by *Lithos* and is currently in production.

The following aspects of the research were done independently by Tahnee Otto while receiving standard supervision by her supervisors Professor Gary Stevens, Professor Jean-François Moyen, and Dr Matthew J Mayne: (i) conducting thermodynamic modelling; (ii) generation of the figures; (iii) writing of the manuscript.

Stellenbosch University https://scholar.sun.ac.za

Phase equilibrium modelling of partial melting in the upper mantle: A comparison between different modelling methodologies and experimental results

Tahnee Otto, Gary Stevens, Matthew Jason Mayne, Jean-François Moyen

Abstract

Recent advances in thermodynamic modelling now allow phase equilibrium studies of partial melting in mafic and ultramafic sources under upper mantle conditions. This potentially offers several advantages over experimental investigations, including the fact that capsule-sample interactions are avoided, there is no uncertainty over the volatile content of the charge, the process is much faster, and open system behaviour can be investigated with relative ease. Two different thermodynamic datasets are in common use for phase equilibrium investigations of mantle rocks, compiled alongside a range of constantly evolving phase solution models. This study compares the results of published experimental studies on partial melting in the upper mantle with phase equilibrium modelling results from the popular pMELTS software (Ghiorso et al., 2002), which uses an embedded dataset from Berman (1988), and with results from the Rcrust software (Mayne et al., 2016), which uses the dataset of Holland & Powell (2011). The aim of this comparative study is to investigate the suitability of each combination of software specific calculation routines, thermodynamic datasets and phase solution models to provide a viable alternative to conventional experimental techniques when studying magma genesis from the upper mantle. The main points of interest are how the phase assemblages, proportions, and compositions predicted by the modelling compare with those produced in the experiments. The set of experimental results used for comparison includes both peridotitic and eclogitic compositions, investigated over a pressure range of 1.0–3.0 GPa and a temperature range of 1165–1950 ºC. The results indicate that software using the Holland & Powell (2011) dataset and appropriately selected phase solution models provides the best match with experimental results in terms of melt volume, melt composition and the assemblage of coexisting phases produced during partial melting under upper mantle conditions.

Keywords: phase equilibrium modeling; thermodynamic modeling tools; experimental petrology; partial melting; upper mantle; SCLM

Stellenbosch University https://scholar.sun.ac.za

Highlights

- Experimental results are compared with thermodynamic modelling calculations.
- The two thermodynamic datasets yield different results, notably for melt production.
- The use of the Holland & Powell (2011) dataset best matches experimental results.
- Thermodynamic modelling is a viable method to analyse upper mantle partial melting.

1. Introduction

Understanding the mechanisms of partial melting in the upper mantle is essential to understanding energy and mass transfer between the mantle and the crust. Experimental studies have provided insight into the partial melting behaviour of a range of possible mantle source compositions that may produce mafic to intermediate magmas (e.g. Baker & Stolper, 1994; Ito & Kennedy, 1973; Kushiro, 2001 and references therein; Takahashi et al., 1993). However, as detailed in a subsequent section of the manuscript, conducting partial melting experiments at pressures and temperatures relevant to even the uppermost mantle is difficult for a variety of reasons, principally because the temperature range of interest is above the melting point of gold, a common capsule material used in experiments. Consequently, capsules consisting of platinum group elements must be used and these all alloy with iron (e.g. Brugier et al., 2015; Merrill & Wyllie, 1973), resulting in the common usage of graphite inner capsules or liners (e.g. Falloon et al., 1988; Wang et al., 2020). The result is that the effective bulk composition in such experiments may be different from the intended composition, particularly with regards to volatile content, fugacity (f) of volatile content, Fe content and Mg# (e.g. Médard et al., 2008; Merrill & Wyllie, 1973). Thermodynamic modelling does not have these problems, but does have problems with the availability of suitable experimental data on the thermodynamic properties of minerals. This may result in imperfect and incomplete thermodynamic datasets and activity-composition (a-x) models for solid and liquid solution phases, which are thus inadequate to express the complexity of solid solution behaviour in minerals, particularly at mantle pressures where a range of pressure sensitive substitutions become important in micas, pyroxenes and amphiboles (e.g. Holland et al., 2018).

Recently, thermodynamic modelling has been expanded to enable phase equilibrium studies of partial melting in mafic and ultramafic sources (Ghiorso et al., 2002; Holland et al., 2018; Tomlinson & Holland, 2021) under upper mantle pressure-temperature (P-T) conditions using a variety of different software (e.g. Connolly & Kerrick, 1987; de Capitani & Petrakakis, 2010; Ghiorso et al., 2002; Powell & Holland, 1988; Riel et al., 2022) that utilise at least two different thermodynamic datasets i.e. Berman (1998) and Holland & Powell (2011).

Stellenbosch University https://scholar.sun.ac.za

Additionally, methodologies and software have also been developed to investigate open system behaviour, such as melt loss (e.g. Mayne et al., 2016; Xiang & Connolly, 2022) or magma movements (Bohrson et al., 2014). These developments have evolved phase equilibrium modelling into a useful and powerful tool for igneous rock studies, providing several crucial advantages over experimental studies, such as the ability to conduct investigations much faster with greater P-T resolution on any composition of the investigators choice (within the limits of modelling capabilities), and the ability to simulate open system processes. These techniques could be very beneficial to advancing understanding of mantle melting, if phase equilibrium approaches can be shown to be sufficiently accurate.

Underpinning all thermodynamic modelling applications are thermodynamic datasets of liquid and solid species, including databases of standard-state properties as well as sets of *a-x* models that define the variation in thermodynamic properties of liquid and solid solution phases. Table 2-1 provides a summary of some of the software/front-ends that are available for modelling upper mantle behaviour, and their calculation strategies. The next section of the manuscript expands on these details by discussing the available thermodynamic datasets and *a-x* models applicable to the software.

Software/Front-end	Calculation Strategy
THERMOCALC[1]	Solving for reaction boundaries where dG = 0
Theriak/Domino[2]	Gibbs free energy minimisation
Perple_X[3]	Gibbs free energy minimisation
Rcrust[4]	Gibbs free energy minimisation inherited from Perple_X. Path-dependant iterations allow compositional change
MELTS Family[5]	Gibbs free energy minimisation with P-T input, or minimisation of other energies

Table 2-1. Calculation strategies of some of the thermodynamic modelling software/front-ends available for conducting investigations under upper mantle conditions.
[1]Powell & Holland (1988); Powell et al. (1998).
[2]de Capitani & Brown (1987); de Capitani & Petrakakis (2010).
[3]Connolly (2005, 2009); Connolly & Kerrick (1987).
[4]Mayne et al. (2016; 2019).
[5]Asimow & Ghiorso (1998); Ghiorso & Sack (1995); Ghiorso et al. (2002).

The complexity that exists with different modelling approaches, different thermodynamic datasets and different *a-x* models, as well as the uncertainties introduced by the fact that some experiments may not be “on composition” (i.e. the true effective bulk composition deviates from that reported), means that comparisons involving one set of experiments with one modelling exercise might miss crucial discrepancies and do not test how

Stellenbosch University https://scholar.sun.ac.za

well a particular modelling platform replicates experimental data within upper mantle P-T-composition ranges. This study aims to address this by comparing the results of a range of partial melting experiments on ultramafic and mafic compositions under P-T conditions appropriate to the subcontinental lithospheric mantle (SCLM), with the results from phase equilibrium modelling conducted with multiple software packages. Additionally, thermodynamic modelling is used to produce an envelope of uncertainty around the experimental results that considers the uncertainties in Fe, H_2O and CO_2 content that are inherent to the experimental design. By comparing the outputs produced via modelling exercises utilising pMELTS (Ghiorso et al., 2002) using the embedded thermodynamic dataset from Berman (1988), and Rcrust (Mayne et al., 2016), which performs minimisation using Perple_X in the thermodynamic dataset of Holland & Powell (2011), with the results of experimental studies of selected eclogitic and peridotitic bulk compositions, extended evaluation of the performance of these modelling tools across a range of temperatures at 1.0–3.0 GPa can be performed. Comparative investigations not only contribute to the improvement of the individual tools, but also provide insights into the variation that may be observed when using different software bundles, ultimately aiding in the selection of the appropriate modelling platform when considering upper mantle P-T-X conditions for investigation. Details of how the modelling was conducted are provided in the methodology section, and the outputs are reported in Addendum A.

2. Thermodynamic Modelling under upper mantle conditions – the available tools

The ongoing expansion of phase equilibrium modelling as a tool to understand metamorphic and igneous processes has produced a range of different applications (Lanari & Duesterhoeft, 2019). This section does not attempt a comprehensive review of all of the available options for conducting modelling at upper mantle P-T conditions (see Riel et al., 2022; Xiang & Connolly, 2022), rather the work focusses on the differences in modelling strategies and/or the thermodynamic datasets used in some of the commonly utilised applications, so that the non-specialist reader can understand why the same phase equilibria modelling exercise may produce different results when processed through different applications.

2.1. MELTS Family

MELTS is a thermodynamic software, solution model, and dataset package designed to facilitate thermodynamic modelling of phase relations during melting and crystallisation in

Stellenbosch University https://scholar.sun.ac.za

magmatic systems (Asimow & Ghiorso, 1998; Ghiorso & Sack, 1995). The original MELTS package was primarily developed for fractional crystallisation processes in systems of basic composition (Ghiorso & Sack, 1995), having since expanded to have the widest uptake of all the thermodynamic modelling packages in the Igneous Petrology community (Smith & Asimow, 2005), particularly for mantle studies. Designed principally for forward modelling of igneous processes using a constrained energy minimisation approach (Hirschmann et al., 1998a), MELTS utilises embedded thermodynamic *a-x* models of solid and liquid phases alongside energy optimisation techniques that are dependent on the process under investigation. These techniques utilise iterative application of three different algorithms: estimates of stable phase identities and compositions; minimisation of applicable thermodynamic potential(s) subject to compositional constraints, whilst other variables remain constant; and metastability examinations of resultant computed phases in relation to possible miscibility gaps or additional phases excluded in initial phase assemblages (Hirschmann et al., 1998a). For MELTS, the standard-state properties of end-member mineral components are based on the internally-consistent dataset of Berman (1988), with several exceptions detailed by Sack & Ghiorso (1994) and references therein. The mixing properties for solid solutions are drawn from several works detailed in Hirschmann et al. (1998a).

The original MELTS bundle has been superseded by several versions with modifications to allow applicability over a range of applications. This includes the rhyolite-MELTS bundles (Gualda et al., 2012), which are used to investigate crystallisation in natural composition magmas (basalts to rhyolites) below 2.0 GPa. rhyolite-MELTS is available in three versions: (i) the original version, 1.0.2., which excludes CO_2-bearing systems; (ii) version 1.1.0., suitable for silicic systems that are CO_2-bearing (Ghiorso & Gualda, 2015); and (iii) version 1.2.0., suitable for mafic, intermediate and alkalic CO_2-bearing systems and for calculating mixed fluid saturation. Additionally, the pMELTS bundle (Ghiorso et al., 2002) is optimised for investigating anhydrous or nominally anhydrous (pHMELTS, Asimow et al., 2004) mantle bulk compositions such as peridotites and pyroxenites from 1.0–3.0 GPa and 1000–2500 ºC.

2.2. THERMOCALC

The software THERMOCALC performs thermodynamic calculations using a non-linear equation approach to solve mineral equilibria problems (Holland & Powell, 1998; Powell & Holland, 1990; Powell et al., 1998). The THERMOCALC application utilises an internally-consistent thermodynamic dataset to construct and solve chemical potential calculations, supplemented

Stellenbosch University https://scholar.sun.ac.za

by mass-balance or constraints on compositional variables where necessary, i.e. by solving for the points where the change in Gibbs free energy between two potential assemblages is zero, a reaction boundary is found. This allows the prediction of phase assemblages and phase compositions by utilising both forward and inverse calculation facilities, under user-specified conditions (Powell et al., 1998; Worley & Powell, 2002). THERMOCALC originated as a metamorphic petrology tool and evolved from the approach of constraining simple system grid topology as a means of understanding metamorphic reactions (Powell & Holland, 1988). The development of *a*-*x* models for melt (Holland & Powell, 2001) allowed the software to find substantial applicability in the study of partial melting of metamorphic rocks, and ultimately to the investigation of igneous processes (Holland et al., 2018; Jennings & Holland, 2015; Tomlinson & Holland, 2021).

The thermodynamic data underlying phase equilibria calculations in THERMOCALC is read in the form used by HP*x*-eos (White et al., 2007), which are thermodynamic solution models for geological phases, fluids, and silicate melts. The building blocks of an HP*x*-eos include a set of compositional end-members, as well as a set of *a*-*x* relations (Holland & Powell, 1996a, 1996b; Powell & Holland, 1993) which describe the end-member mixing thermodynamics. The most current sets of HP*x*-eos families are the Metapelite set (White et al., 2014), suitable for use below 1.5 GPa; the Metabasite set (Green et al., 2016), suitable for use below 2.0 GPa; and the Igneous set (Holland et al., 2018; Tomlinson & Holland, 2021), suitable for partial melting of basaltic to granitic melt compositions, allowing anhydrous (≤ 6.0 GPa) and hydrous (≤ 3.0 GPa) calculations. These HP*x*-eos families are built on the revised Holland & Powell (2011) dataset, which has undergone several updates from its previous versions (Holland & Powell, 1985, 1990, 1998).

Multiple thermodynamic modelling software have implemented the use of the HP*x*-eos families and the Holland & Powell (2011) dataset, including Perple_X (Connolly, 2005; Connolly & Kerrick, 1987) and Theriak/Domino (de Capitani & Brown, 1987; de Capitani & Petrakakis, 2010). As a result, THERMOCALC and such other programs should produce identical outputs for calculations involving the same thermodynamic dataset and *a*-*x* models, as has been shown to be the case (e.g. Connolly, 2007, 2021; Horváth, 2007). This application of the HP*x*-eos and Holland & Powell (2011) dataset requires regular updates across platforms, and routine benchmark comparisons provide quick insights into the correct implementation of such input data to other programs.

Stellenbosch University https://scholar.sun.ac.za

2.3. Theriak/Domino

Theriak/Domino is a software program collection that uses a linear programming strategy combined with a Gibbs free energy minimisation calculation method to conduct and produce a wide range of thermodynamic equilibrium calculations and illustrations, including thermodynamic functions of phases, phase diagrams, equilibrium assemblages, and pseudosections (de Capitani & Brown, 1987; de Capitani & Petrakakis, 2010). The equilibrium phase compositions and stable mineral assemblage for a bulk rock composition along a specified P-T path or set of P-T conditions is calculated using the Theriak program, and Domino is used for plotting a range of equilibrium assemblage diagrams (de Capitani & Petrakakis, 2010). Theriak/Domino has compatibility with the currently available thermodynamic datasets, and the capability of porting most THERMOCALC HP*x*-eos families, as mentioned above. An add-on to the Theriak/Domino software package, Theriak_D works as an interface to process thermodynamic data in a programming environment outside the Theriak/Domino package (Duesterhoeft & de Capitani, 2013).

2.4. Perple_X and derivatives of the program

The software package Perple_X is a modular collection of sub-programs created for the rapid computation of all types of phase diagrams, as well as performing general thermodynamic calculations (Connolly, 2005; Connolly & Kerrick, 1987). By utilising a calculation method based on minimisation of total Gibbs free energy of multiple phase configurations and pseudocompounds, Perple_X programs are able to calculate the most stable set of phase equilibria for an arbitrary chosen system (Connolly, 2005; Connolly & Petrini, 2002). The thermodynamic datasets and *a-x* models implemented in Perple_X can be selected from several compiled databases, as the software accepts thermodynamic data that has been suitably formatted for Perple_X from any source; as mentioned, the THERMOCALC HP*x*-eos families and Holland & Powell (2011) dataset are readily incorporated into Perple_X.

2.4.1. Rcrust

Rcrust is a phase equilibria modelling tool that utilises the Meemum function of Perple_X (Connolly, 2009) to calculate phase stabilities for a series of points, inheriting databases and *a-x* models from Perple_X (Mayne et al., 2016). The Rcrust calculation strategy applies path dependencies to allow bulk compositional change via processes of mass transfer. Importantly, Rcrust strategies allow the investigation of processes dependent on assemblages evolving throughout a given P-T-X space, as changes in bulk compositions are transferred across points. Prior to passing the information along, phases can be extracted or added depending on a broad

Stellenbosch University https://scholar.sun.ac.za

range of flexible trigger signals (e.g. mode of melt, melt viscosity, phase proportion, phase to melt ratio, etc), allowing open or closed systems. Mayne et al. (2019) describe the division of the full system (bulk rock composition) into a reactive subsystem and an extract subsystem, the former being the system on which phase equilibrium modelling is conducted and the latter representing the phases that have been removed from the residual system by phase extraction events. The development of Rcrust was primarily as a tool for the forward modelling of partial melting and magma generation in the crust, but the use of Perple_X formatted input data allows Rcrust to perform modelling across any P-T-X range that is compatible with the available thermodynamic datasets and *a-x* models (Mayne et al., 2019). Thus, if the P-T resolution in Rcrust is set to match the highest resolution attained by Perple_X gridded-minimisation, Rcrust and Perple_X modelled outputs will be identical if the same *a-x* models are utilised.

2.5. Experiments compared with thermodynamic modelling

Several recent studies have compared the results of experiments with the results of thermodynamic modelling of the same bulk composition for upper mantle conditions (e.g. García-Arias, 2020; Gervais & Trapy, 2021; Ghiorso et al., 2002; Hernández-Uribe et al., 2022; Hirschmann et al., 1998a; Holland et al., 2018; Jennings & Holland, 2015; Tomlinson & Holland, 2021; Tropper & Hauzenberger, 2015). In general, most studies have concluded that modelling compares favourably with experiments, but consistent issues within the different platforms are worth noting. Hirschmann et al. (1998a) have reported a systematic difference between the melt compositions predicted by MELTS relative to those of experiments investigating the partial melting of peridotite, with concentrations of SiO_2 initially underpredicted by 4–5 wt.%. This is also reflected by MELTS predicting systematically lower melt fractions relative to experimental observations, equivalent to an approximate 100 ºC offset (Hirschmann et al., 1998a). This has been improved with revisions to the pMELTS algorithm, such that the consistent underestimate in melt proportion is lower, equating to a temperature offset averaging 50 ºC, and overpredictions of melt SiO_2 values are reported as lowered to approximately 1% (Ghiorso et al., 2002). Additionally, improvement in calculated liquid MgO concentrations are also reported, although still between 1–4% higher, and attributed by Ghiorso et al. (2002) to the temperature offset. Other known problems of pMELTS predictions include, at low pressures, the addition of Cr-spinel to the assemblage that is not observed experimentally and the continued overstabilisation of clinopyroxene relative to melt, as well as the oversaturation of garnet with increasing pressure (Ghiorso et al., 2002).

Stellenbosch University https://scholar.sun.ac.za

Comparisons of melt fraction curves for partial melting of peridotite from THERMOCALC with experimental results generally display good agreement near the solidus (considering a range of different experimental results), but also display systematically underestimated melt fraction at high temperatures (~20 vol.%), which equates with a temperature offset of approximately 50 ºC (Jennings & Holland, 2015). Consequently, the melt compositions differ significantly from experiments at higher melt fractions, especially at higher pressure. The persistence of garnet (with underestimated Cr-content) and a small fraction of spinel with melt to higher temperatures was also noted (Jennings & Holland, 2015). Revisions by Holland et al. (2018) show improvement of the melt phase liquidus temperatures, as well as improved fitting of garnet compositions with P-T change and a new *a-x* model for spinel that eliminates its default appearance up to liquidus temperatures. Overestimations of orthopyroxene abundance was noted in the Holland et al. (2018) model, and subsequently expanded upon by Tomlinson & Holland (2021) through changes made to the structure of the melt model. Another known problem of the Igneous HP*x*-eos of THERMOCALC was the stability of a high-Ca orthopyroxene phase in various rock assemblages (Green, 2020). This has reportedly been eliminated from the orthopyroxene solution model in the *x*-eos bundle from 31-10-2020 (Green, 2022), and implementations of these changes to the Perple_X formatted phase solution models was confirmed as of 02-12-2020 (Connolly, 2022).

Regardless of the issues discussed above, the results of experiments and phase equilibrium modelling results cannot be expected to correlate perfectly. Each approach has its own advantages and pitfalls, and investigations utilising one or the other cannot be classified as more or less appropriate unless these inherent aspects are considered (White et al., 2011). The more serious pitfalls of both approaches, as relevant to studies of partial melting of mantle lithologies, are briefly considered below.

At P-T conditions above the melting point of gold, the required use of Pt or AgPd capsules in experimental studies introduces potential uncertainties in the degree to which the effective bulk composition matches the intended composition, and the degree to which the fluid state of experiments is known. Although experimental studies can handle the full chemical complexity of natural rocks, the uptake of Fe by Pt or Pd capsules is known to potentially change the bulk composition (Brugier et al., 2015 and references therein; Merrill & Wyllie, 1973). Pre-saturation of the capsule alloy with Fe and the use of graphite inner capsules (liners) are common strategies to counter this (e.g. Falloon et al., 1988; Grove, 1981; Shaw, 2018; Wang et al., 2020). However, the common use of graphite liners comes with its own set of problems, as it is probably impossible in most laboratories to conduct a partial melting

Stellenbosch University https://scholar.sun.ac.za

experiment without the inclusion of some unintended O_2 or H_2O into the capsule (Médard et al., 2008). This will result in reactions between H_2O, O_2, and C (in the liner) and may result in partial melting initially occurring in a fluid-saturated system. Whilst at very low melt fractions this may be undetectable, the resultant higher fH_2O and fCO_2 must affect melting behaviour even after the system has become fluid-absent. In addition, irrespective of the fO_2 conditions of starting material synthesis, experiments conducted with graphite liners are inevitably buffered to C-CO. Thus, capsule uptake of Fe and the existence of small amounts of unintended H_2O and CO_2 in experimental charges are a potential source of discrepancy between experimental results and modelling studies that are not often considered when the outputs of modelling studies are benchmarked against experiments. In this study, phase equilibrium modelling is used to attempt to constrain the envelope of uncertainty that these factors introduce into experimental results.

In contrast, for the various designs of piston-cylinder apparatus that form the mainstay of experimental studies under upper mantle P-T conditions, measurement and control of pressure and temperature represent a potential but largely insignificant source of error. It is possible to place the thermocouple within 0.5 mm of the capsule and to control temperature to ± 1 ºC. Capsules of large enough volume to contain graphite liners may experience temperature gradients, however when these are tested using multiple thermocouple arrangements these are found to be low (5–10 ºC across 0.8–1.0 cm capsules) (e.g. Baker & Stolper, 1994; Schilling & Wunder, 2004). Given the fact that pressure is generated hydraulically and transmitted to the capsule using a salt medium with negligible frictional losses if using the hot piston-out technique, the accuracy of the pressure gauge determines pressure uncertainty. For labs with a precision test gauge this is typically 0.1% of the measured value.

Additional experimental uncertainties revolve around the analysis of phase compositions, especially silicate glasses (quenched melts). Due to the need for a high degree of spatial resolution, the standard technique for analysing the major element compositions of phases in experimental run products is electron beam analysis, using EDS and/or WDS on an electron microprobe or scanning electron microscope. Regardless of the instrument details, the accelerating voltage (or beam energy) utilised during the analysis of silicate glass has a significant effect on the reported compositions, especially for glasses that are hydrous or have higher alkali contents (Humphreys et al., 2006; Morgan & London, 1996; Varshneya et al., 1966). In these cases, even the lowest energy beams that are viable will record a decrease in Na counts as a function of time under the beam. This is due to the migration of Na away from the analysis point, and this effect is exacerbated by the increased count-rate for immobile

Stellenbosch University https://scholar.sun.ac.za

components such as Si and Al, increasing their relative contributions (Morgan & London, 1996). Studies try to counter this problem by using defocused beams, but freezing the sample to approximate liquid nitrogen temperatures using a cryo-stage is the only truly effective way to counter the problem (Humphreys et al., 2006; Stevens et al., 1997), which is uncommon in experimental studies.

Moreover, some glasses with mafic and ultramafic compositions are hard to identify at low melt fractions due to extensive crystallisation upon quenching (Baker & Stolper, 1994; Cawthorn et al., 1973). The methods used to increase the efficacy of the analyses, such as diamond aggregates (Baker & Stolper, 1994; Falloon et al., 1999) or carbon spheres (Wasylenki et al., 1996), have their own pitfalls that need to be considered (Falloon et al., 1996; Wasylenki et al., 2003). For example, the pressures in the void spaces of diamond aggregates are initially low, possibly leading to the separation of liquids that are not in equilibrium with the system (Wasylenki et al., 2003). Comparatively, the use of carbon spheres segregate melt due to surface effects, and requires longer equilibrations runs (increasing Fe loss to the capsule; Pertermann & Hirschmann, 2003a). Both methods will likely result in some C-bearing gas species in the charge prior to melting.

In thermodynamic modelling, bulk compositions and fluid states are set, and analytical errors sensu stricto are non-existent. Nevertheless, the internal consistency of thermodynamic datasets are important in their perceived accuracy; internal consistency is dependent on the thermodynamic properties of pure phases and end-members in thermodynamic datasets, and their interactions with *a-x* models (Lanari & Duesterhoeft, 2019). These thermodynamic properties, together with the formulation of *a-x* models, can be a great source of systematic uncertainties (Berman, 1988; García-Arias, 2020; Holland & Powell, 2011; Powell, 1985; White et al., 2014). For example, the complexity of certain chemical components, such MnO, NiO and P_2O_5, currently inhibit the development of complete *a-x* models to describe the activity relations of mineral phases that incorporate these components (Gervais & Trapy, 2021). The omission of these components from thermodynamic datasets is likely to be an important source of error when modelling rock compositions where these components are important to the stability of one or more phases (e.g. Forshaw et al., 2019; García-Arias, 2020). Consequently, an important consideration of thermodynamic modelling is that these calculations are wholly dependent on the input thermodynamic data, and the outcomes remain a simplification of nature – even with extended chemical systems – only reporting approximations of phase behaviours that also do not consider any kinetics, such as crystal sizes,

Stellenbosch University https://scholar.sun.ac.za

crystal growth and nucleation, and diffusion, amongst others (García-Arias, 2020; White et al., 2011).

3. Methodology

Three sets of partial melting experiments (Table 2-2) were chosen for comparison with the thermodynamic modelling outcomes by means of phase assemblages, phase proportions, phase compositions, and phase-in/phase-out boundaries. The chosen studies represent compositions that include two peridotites and an eclogite: Experiments KLB-1 from the studies of Takahashi (1986) and Takahashi et al. (1993) and MM3 from Baker & Stolper (1994) and Hirschmann et al. (1998b) represent a fertile spinel lherzolite sourced from the Kilborne Hole crater, New Mexico; experiments G2 from the studies of Pertermann & Hirschmann (2003a, 2003b) represent an eclogite prepared from natural garnet and clinopyroxene sourced from the Münchberg Massif, Bavaria. Experiments KLB-1 consisted of 95 runs conducted from 1 atm to 14.0 GPa, however only the runs from 1.0–3.0 GPa are investigated in this study. Experiments MM3 consisted of 21 runs conducted at 1.0 GPa from 1250–1390 ºC, and only the experiments where phase proportions are reported were considered. Experiments G2 consisted of six runs from 1165–1375 ºC at 2.0 GPa, one run at 1325 ºC and 2.5 GPa, and 20 runs from 1300–1525 ºC at 3.0 GPa. Compositions of olivine, clinopyroxene, orthopyroxene, garnet, plagioclase, spinel, and glass/melt have been considered for the comparison. Where applicable, the reported experimental bulk compositions were modified to be NiO, P_2O_5, and MnO free due to an incomplete set of *a-x* models defining the compositional space.

The experimental studies have some limitations for the purpose of this study. For KLB-1, Takahashi et al. (1993) only report selected melt fractions at 1.5 GPa, and Takahashi (1986) only reports phase compositions at the P-T points of 1325 ºC and 1.0 GPa, and 1550 ºC and 3.0 GPa. For MM3, Baker & Stolper (1994) report phase compositions for all runs where proportions are noted, apart from 1310 ºC where only the liquid composition is reported. Hirschmann et al. (1998b) provide reanalysed compositions for some of the MM3 experiments, but report only the liquid compositions at 1250 ºC and 1260 ºC and no additional data. The experimental works on G2 report phase proportions (Pertermann & Hirschmann, 2003a) for the majority of the investigated P-T points, except at 2.0 GPa for experiments at 1165 ºC, 1185 ºC, and 1225 ºC. Consequently, comparisons between experimental results and thermodynamic modelling outputs were made where the relevant data was available. Additionally, where no phase proportions were reported, a sum of squared residuals mixing routine was used to calculate phase proportions from the compositional data where possible, and also to assess the

Stellenbosch University https://scholar.sun.ac.za

soundness of reported proportions, where these were provided; these results are reported in Addendum A.

Experimental Set	**KLB-1[1]**		**MM3[2]**		**G2[3]**	
Composition (wt.%)	Reported	Modified	Reported	Modified	Reported	Modified
SiO_2	44.48	44.65	45.50	45.67	50.05	50.13
TiO_2	0.16	0.16	0.11	0.11	1.97	1.97
Al_2O_3	3.59	3.60	3.98	3.99	15.76	15.79
Cr_2O_3	0.31	0.31	0.68	0.68	-	0.00
FeO_t	8.10	8.13	7.18	7.21	9.35	9.36
MnO	0.12	0.00	0.13	0.00	0.19	0.00
MgO	39.22	39.37	38.30	38.44	7.90	7.91
CaO	3.44	3.45	3.57	3.58	11.74	11.76
Na_2O	0.30	0.30	0.31	0.31	3.04	3.04
K_2O	0.02	0.02	-	0.00	0.03	0.03
P_2O_5	0.03	0.00	-	0.00	-	0.00
NiO	0.25	0.00	0.23	0.00	-	0.00
Sum	100.02	100.00	99.99	100.00	100.03	100.00
Pressure (GPa)	1.5–3.0		1.0		2.0–3.0	
Temperature (°C)	1325–1950		1270–1390		1165–1525	
Reported H_2O Content	Anhydrous		Anhydrous		Nominally anhydrous	
Reported fO_2	NNO		Below GCO (C-CO) buffer		Below C-CO buffer	
Reported Capsule Material	Graphite-lined/Re-foil lined Pt-Capsules		Graphite-lined Pt-Capsules		Graphite-lined Pt-Capsules	

Table 2-2. Details of the experimental sets investigated in this study. Modified analyses were normalised to be NiO, P_2O_5 and MnO free. All comparisons were based on FeO_{tot} values. (-) indicates no data available.
[1]Fertile spinel lherzolite from Takahashi (1986) and Takahashi et al. (1993).
[2]Fertile spinel lherzolite from Baker & Stolper (1994) and Hirschmann et al. (1998b).
[3]Bi-mineralic eclogite from Pertermann & Hirschmann (2003a, 2003b).

All of the studied experimental works make use of Pt-capsules with graphite liners to minimise the uptake of Fe to the capsule, and as the experiments are intended to be volatile free, the authors describe several strategies to avoid the absorption of H_2O by materials in the capsules. All three studies describe drying loaded but unsealed capsules (at 110 ºC and 300 ºC) for various timeframes before welding. Additionally, Baker & Stolper (1994) report including a layer of diamond powder in the capsules as a melt trap, similarly applied using carbon spheres for near solidus runs by Pertermann & Hirschmann (2003a, 2003b). Pertermann & Hirschmann (2003a, 2003b) also report packing capsules in a layer of Fe_2O_3 powder to reduce the influx of hydrogen to the experiments, a potential source of H_2O in the capsules.

In all of the studies, capsules were loaded and welded in an air environment, and therefore the development of CO_2 and CO from the reaction of air with the graphite liner is inevitable. Both H_2O and CO_2 lower the mafic and ultramafic rock solidi at upper mantle pressures. As a result, thermodynamic modelling was used to investigate the uncertainty that may accompany experimental results if small but realistic amounts H_2O or CO_2 were unintentionally included in the capsule. Similarly, the effects of the loss of Fe to the capsule were also investigated, the details of which are described below.

Stellenbosch University https://scholar.sun.ac.za

The thermodynamic modelling software utilised in the comparative study investigating closed system evolution includes pMELTS (mafic and ultramafic compositions) and Rcrust (ultramafic to intermediate compositions). The outcomes for all comparisons have been recorded in Addendum A. Firstly, runs were performed for each P-T point listed in the relevant experiments using the latest pMELTS (version 5.6.1.) bundle in the NKCFMASTOCr (Na_2O-K_2O-CaO-FeO-MgO-Al_2O_3-SiO_2-TiO_2-Fe_2O_3-Cr_2O_3) chemical system, embedded with the thermodynamic dataset from Berman (1988) with modifications detailed in Ghiorso et al. (2002), and *a-x* models included in the pMELTS calibration. The system was considered H_2O and CO_2 free, and the fO_2 was set along the C-COH buffer for the three source compositions. Phase assemblages, phase proportions, and phase compositions were recorded at the specific P-T conditions of each experiment performed in the experimental set within the range of 1.0–3.0 GPa. As pMELTS outputs FeO and Fe_2O_3, direct comparison to experimental results required recalculation to FeO_t.

Secondly, runs were performed for each P-T point listed in the relevant experiments in the NKCFMASTOCr chemical system using Rcrust version 2022-09-03, the 2022 revised hp634ver.dat thermodynamic data file from Perple_X, and the internally consistent dataset of Holland & Powell (2011). The following *a-x* models were used: Cpx(TH) for clinopyroxene, Gt(TH) for garnet, Opx(TH) for orthopyroxene, Sp(TH) for spinel, and melt(TH) for melt (Tomlinson & Holland, 2021), O(HGP) for olivine (Holland et al., 2018), Fsp(C1) for plagioclase and potassium-feldspar (Holland & Powell, 2003), and Ilm(WPH) for ilmenite (White et al., 2000). Adjustments made to *a-x* model parameters are listed in Addendum A. Similar volatile content and fO_2 constraints were applied as described for the pMELTS bundle; data was also recorded similarly.

Thirdly, the effects of Fe loss, and H_2O or CO_2 addition was modelled similar to that described above, with changes made to the reported bulk compositions of KLB-1 and MM3 assuming either a 10% decrease in the FeO_t content, or the inclusion of 0.05 wt.% H_2O, or 0.08 wt.% CO_2 in the capsule. These are upper realistic boundaries for water adsorbed to the charge and liner and CO_2 production by air included the capsule. Runs were performed using Rcrust in a similar manner as above, but using the 2020 revised hp633ver.dat thermodynamic data file from Perple_X, and the following *a-x* models: Cpx(HGP) for clinopyroxene, Gt(HGP) for garnet, O(HGP) for olivine, Opx(HGP) for orthopyroxene, and Sp(HGP) for spinel (Holland et al., 2018), melt(HGPH) for melt (Holland et al., 2018; Heinrich & Connolly, 2022), Fsp(C1) for plagioclase and potassium-feldspar (Holland & Powell, 2003), and Ilm(WPH) for ilmenite (White et al., 2000). The use of this set of *a-x* models is due to the ability of the selected melt

Stellenbosch University https://scholar.sun.ac.za

model to accommodate H_2O and CO_2. The adapted bulk compositions and results are reported in Addendum A.

Quantification of the differences between experimental results and modelling outputs for the reported experimental and modelled phase assemblages was achieved using the model quality factor Q*asm* (Lanari & Duesterhoeft, 2019), expressed as:

$$Q_{asm} = \frac{l}{k} \times 100 \quad (1)$$

where l is the number of matching phases between experimental results and modelled outputs and k is total number of phases present. Q*asm* is reported for each relevant P-T point listed in the experimental sets, and bulkQ*asm* is reported for all conditions combined. Percentage difference and relative difference was calculated where the relevant data was available in order to evaluate the match of predicted and experimental phase compositions. Percentage difference was calculated for each component in a phase as:

$$\%\ Difference = \frac{(m-e)\times 100}{e} \quad (2)$$

where m is the modelled value and e is the experimental value (García-Arias, 2020). This quantification was also used for phase proportions. Relative difference (or sum of residuals^2) was used to evaluate the goodness of fit between modelled and experimental compositions, calculated for each component in the phase as:

$$Sum\ of\ residuals^2 = \varepsilon(m-e)^2 \quad (3)$$

Relative differences of ≤ 4 (2^2 wt.% difference) suggests a good fit, ≥ 25 (5^2 wt.% difference) suggests a bad fit, and values of 4–25 suggest a reasonable fit.

4. Results

4.1. Comparison of relevant experimental results with thermodynamic modelling

The full set of thermodynamic modelling results from KLB-1, MM3, and G2 are reported in Addendum A.

4.1.1. KLB-1: Partial melting of peridotite under upper mantle conditions

Both the experiments and modelling agree in the presence of olivine, orthopyroxene, clinopyroxene, garnet, spinel and melt, with very similar Q*asms* displayed for Rcrust and pMELTS, as shown in Table 2-3. The phase assemblages from the experiments and modelled outcomes by pMELTS and Rcrust in this study at 1.5 and 3.0 GPa are illustrated in Figure 2-1, and comparisons between melt fraction (in wt.%) as a function of temperature at 1.5 and 3.0 GPa is illustrated in Figure 2-2.

Stellenbosch University https://scholar.sun.ac.za

Assemblage: Q*asm*		
Bulk Q*asm* in 33 experiments	Rcrust	pMELTS
	78.05	74.24

Compositions: Sum of residuals^2				
	1.0 GPa, 1325 ºC		3.0 GPa, 1550 ºC	
	Rcrust	pMELTS	Rcrust	pMELTS
Ol	0.47	0.01	3.35	6.32
Opx	11.26	3.52	1.10	9.14
Cpx	28.19	15.13	4.21	27.61
Sp	616.94	12.79	-	-
Gt	-	-	-	21.94
Melt	108.74	7.92	51.00	173.97

Table 2-3. Scoring of the modelled assemblages (bulkQ*asm*) and compositions (sum of residuals^2) from pMELTS and Rcrust in comparison with the experimental study on KLB-1 of Takahashi (1986) and Takahashi et al. (1993), where such data was available.

For the majority of the pressure range investigated, pMELTS predicts the position of the solidus at lower temperatures than the experiments, similarly at 1.0 and 1.5 GPa by Rcrust (Figure 2-1). In terms of the liquidus, the experimental study and Rcrust show reasonable agreement at 1.5 and 3.0 GPa, although the exhaustion of olivine is 50 ºC lower at higher pressure (Figure 2-1). In comparison, pMELTS predicts the liquidus to be at considerably lower temperatures at both low and high pressures, with the exhaustion of olivine predicted 200 ºC lower at 1.5 GPa due to a rapid increase in the melt fraction (Figures 2-1 & 2-2). As displayed in Figure 2-1, the spinel phase predicted by both modelling bundles persists to higher temperatures than observed in the experimental assemblages, but show good agreement with experiments at 1.0 GPa (Addendum A). At low and high pressures, pMELTS predict the presence of pyroxenes at higher temperatures than the experimental data, similarly by Rcrust at low pressure. At 3.0 GPa, the garnet phase predicted by Rcrust is exhausted at 50 ºC lower, whilst pMELTS delays garnet exhaustion by 50 ºC.

In terms of phase compositions (Table 2-3 & Addendum A), modelled melts shows bad agreement with experiments at 3.0 GPa. A great mismatch is displayed by pMELTS due to overestimated FeO (+94.91%), MgO (+28.10%), and Na_2O (+180.45%), and underestimated SiO_2 (-14.37%), Al_2O_3 (-35.33%), and CaO (-39.47%). However, the melts predicted by pMELTS at 1.0 GPa shows reasonable agreement with experiments. At high and low pressures, Rcrust predicts lower Al_2O_3 (-30.06% & -22.44%) and higher MgO (+89% & +30.40%) in the melt, and lower CaO (-25.25%) at 3.0 GPa. For the mineral phases, pMELTS and Rcrust are both in good agreement with the experimental data for the olivine composition at low pressure, but pMELTS shows only reasonable agreement at 3.0 GPa due to FeO values (+28.33%). For

Stellenbosch University https://scholar.sun.ac.za

orthopyroxene, both modelling bundles show good to reasonable agreement with experiments, but bad agreement for clinopyroxene is observed for Rcrust (+29.63% CaO & -37.46% Al_2O_3) and pMELTS (+47.16% CaO & -8.51% MgO) at 1.0 and 3.0 GPa, respectively. At high pressure, pMELTS shows reasonable agreement with experimental garnet compositions, apart from MgO (-11.96%), whilst Rcrust does not predict garnet above 1500 ºC. The spinel composition of pMELTS matches experimental results reasonably, apart from Cr_2O_3 (+16.57%) and Al_2O_3 values (-21.75%), with Rcrust displaying a bad match due to Al_2O_3 (-29.83%), MgO (-12.41%), and Cr_2O_3 (+133.29%).

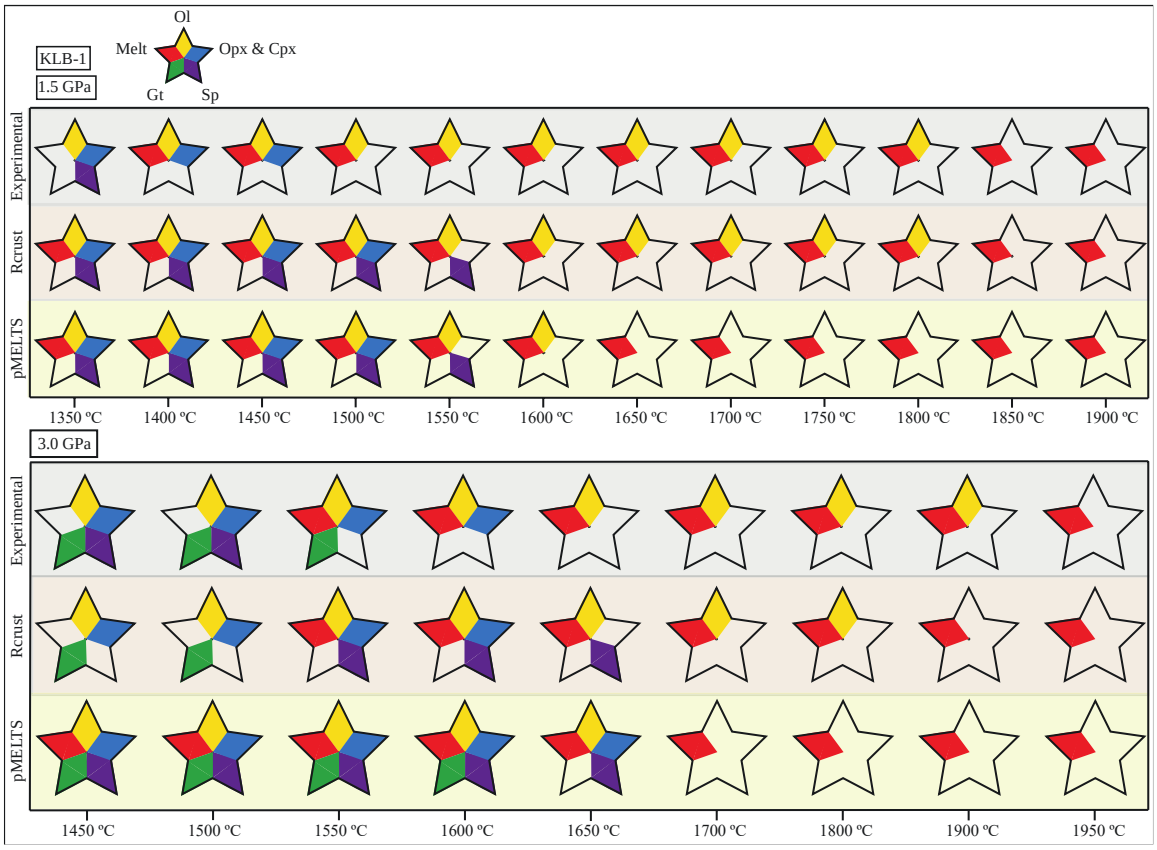

Figure 2-1. A comparison of the phase assemblages from the experimental study of Takahashi (1986) on composition KLB-1 with the modelled assemblages produced using pMELTS and Rcrust in this study. The results are at 1.5 and 3.0 GPa for the temperature values indicated. Note that at 1.5 GPa, both modelling outputs predict the solidus at lower temperatures, however, Rcrust and the experimental study are in good agreement for the position of the liquidus, whereas pMELTS predicts the liquidus at a much lower temperature. At 3.0 GPa, Rcrust and the experimental study are in good agreement for the position of both the solidus and liquidus, whilst pMELTS predicts both to be at considerably lower temperatures. Rcrust does not predict spinel below 1550 ºC at 3.0 GPa, and both sets of modelling outcomes predict spinel exhaustion at much higher temperatures, at both pressures.

Stellenbosch University https://scholar.sun.ac.za

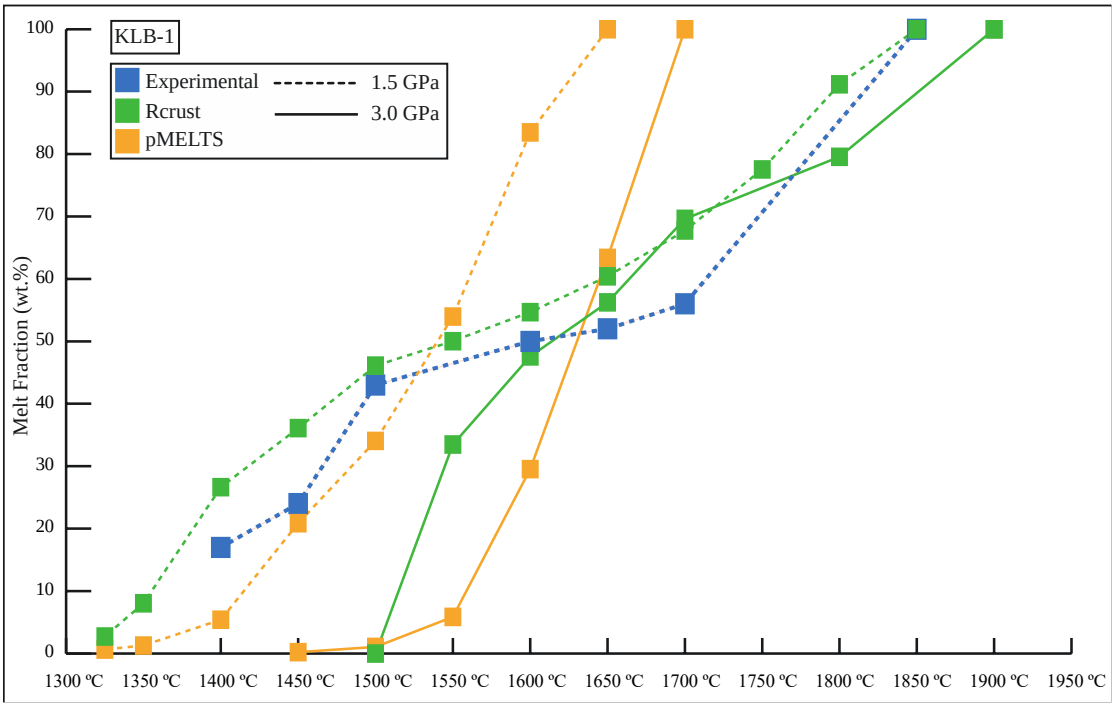

Figure 2-2. Modelled melt fractions at 1.5 GPa and 3.0 GPa from pMELTS and Rcrust as determined in this study, compared with melt fractions from the experimental study on KLB-1 of Takahashi et al. (1993) at 1.5 GPa (the only pressure that phase proportion information was reported in the experimental study within the pressure range of 1.0–3.0 GPa). At 1.5 GPa, pMELTS predicts the liquidus to be at much lower temperatures than the experiments, whereas there is excellent agreement between melt fraction (and consequently, olivine consumption) between Rcrust and the experiments. A similar melt-curve is displayed by pMELTS at 3.0 GPa, which is not the case for Rcrust predicted melt fractions.

4.1.2. MM3: Partial melting of peridotite under upper mantle conditions

Comparison of the MM3 experiments with the results from pMELTS have previously been conducted by Ghiorso et al. (2002), however, the comparison has been repeated here to analyse predicted peridotite partial melting behaviour in Rcrust at 1.0 GPa using a more detailed experimental dataset. In this study, both the experiments and modelling agree in the presence of olivine, orthopyroxene, clinopyroxene, spinel and melt, with Rcrust predicting 100% and pMELTS almost 95% of the assemblage, as is reported in Table 2-4. Comparisons between abundances of melt, clinopyroxene, orthopyroxene, olivine and spinel as a function of temperature at 1.0 GPa are illustrated in Figure 2-3. Figure 2-4 displays components from the experimental and modelled melt compositions as a function of increasing melt fraction (in wt.%) and increasing temperature.

Both pMELTS and Rcrust are in good agreement with experimental phase abundances (Figure 2-3), however, lower modelled melt fractions can be observed for pMELTS, and for Rcrust below 1310 ºC. Rcrust has an overall smaller percentage difference between experimental and Rcrust predicted melt abundances (14–42% versus 17–83% in pMELTS).

Stellenbosch University https://scholar.sun.ac.za

Most Rcrust and pMELTS predicted melt compositions (Addendum A, Table 2-4) show bad agreement with experimental results, yet pMELTS predicts the only good match at 1390 ºC.

Assemblage: Q*asm*

Bulk Q*asm* in 8 experiments	Rcrust	pMELTS
	100.00	94.87

Compositions: Sum of residuals^2

1.0 GPa	1250 ºC		1260 ºC		1270 ºC		1280 ºC		1300 ºC	
	Rcrust	pMELTS	Rcrust	pMELTS	Rcrust	pMELTS	Rcrust	pMELTS	Rcrust	pMELTS
Ol	-	-	-	-	0.48	0.55	0.06	0.07	0.83	0.96
Opx	-	-	-	-	7.23	6.44	9.48	3.86	7.38	4.96
Cpx	-	-	-	-	1.62	3.96	1.17	4.27	2.78	4.72
Sp	-	-	-	-	70.14	102.21	20.25	58.59	104.73	298.66
Melt	96.91	15.88	38.12	43.16	28.73	72.81	26.13	68.90	28.51	54.57

1.0 GPa	1310 ºC		1330 ºC		1350 ºC		1360 ºC		1390 ºC	
	Rcrust	pMELTS	Rcrust	pMELTS	Rcrust	pMELTS	Rcrust	pMELTS	Rcrust	pMELTS
Ol	-	-	0.60	0.91	0.94	1.27	0.82	1.10	1.33	1.59
Opx	-	-	9.48	2.96	7.50	2.71	5.25	3.62	4.56	5.56
Cpx	-	-	8.16	6.13	-	-	-	-	-	-
Sp	-	-	134.46	764.42	105.02	845.91	76.25	284.60	22.11	151.53
Melt	39.91	34.84	37.54	22.13	48.10	13.12	10.22	39.27	58.87	4.15

Table 2-4. Scoring of the modelled assemblages (bulkQ*asm*) and compositions (sum of residuals^2) from pMELTS and Rcrust in comparison with the experimental study on MM3 of Baker & Stolper (1994) and Hirschmann et al. (1998b), where such data was available.

When considering the composition of the melts (Figure 2-4), pMELTS predicted values as a function of melt fraction match well with experimental values for SiO_2 (at higher fractions), FeO, CaO and Na_2O, but under-and overpredicts Al_2O_3 values and overpredicts MgO. The proposed ~1% overestimate in melt SiO_2 reported by Ghiorso et al. (2002) is found to be ~ 2% for the majority of the melting range in this study. For Rcrust, FeO, CaO and Na_2O matches well with the experimental melts, whereas underpredictions of SiO_2, Al_2O_3 and MgO are observed. When considering the same components of melt with increasing temperature, the pMELTS values show pronounced differences from experimental data, particularly at lower melt fractions. Rcrust shows better overall agreement, but discrepancies are also obvious. For olivine, the modelled compositions (Addendum A) match well with experiments across the entire temperature range (Figure 2-3 & Table 2-4). Although clinopyroxene proportions are higher in modelled results, good to reasonable agreement can be seen in terms of its composition. Experimental orthopyroxene has mostly good matches with pMELTS proportions and compositions across the entire temperature range, and Rcrust values generally

Stellenbosch University https://scholar.sun.ac.za

agree reasonably with experiments. Although Rcrust and pMELTS shows good agreement in terms of spinel stability and proportions, the modelled compositions generally agree badly with experiments, except for Rcrust predictions at 1280 ºC and 1390 ºC.

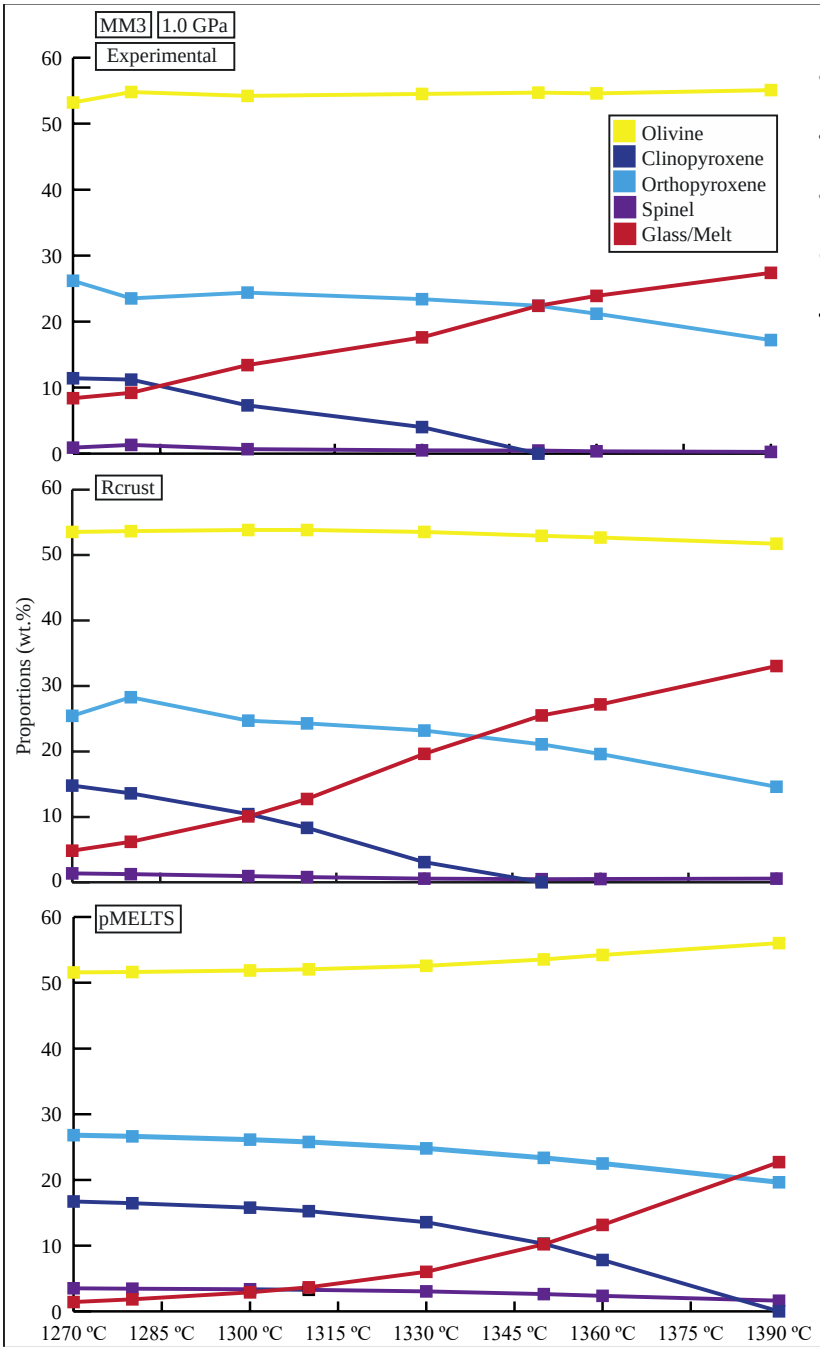

Figure 2-3. A comparison of melt (glass), olivine, clinopyroxene, orthopyroxene and spinel abundances at 1.0 GPa from the experimental study on MM3 of Baker & Stolper (1994) and Hirschmann et al. (1998b), with the calculated values from pMELTS and Rcrust as determined by this study. Compared to experiments, both Rcrust and pMELTS predict lower melt abundances at 1270 ºC, and the rate of increase in melt fraction predicted by pMELTS is slower than the experiments and Rcrust, displayed by the subsequent slower consumption of clinopyroxene. Rcrust and pMELTS outputs for olivine vary as temperature increases, showing overestimations of olivine abundance by pMELTS, and underestimations by Rcrust. Both modelling bundles predict very similar abundances and rates of orthopyroxene consumption.

Stellenbosch University https://scholar.sun.ac.za

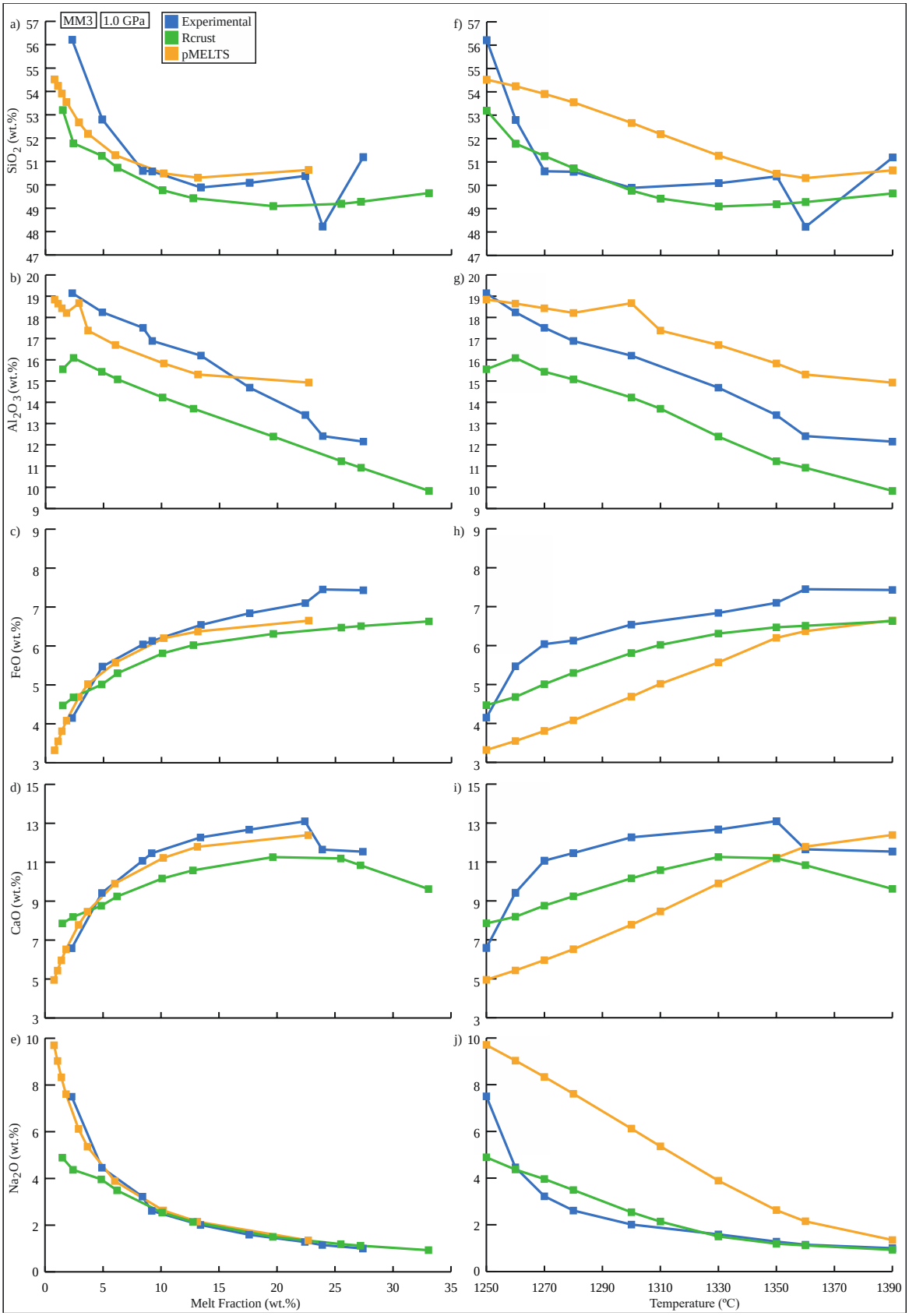

Figure 2-4. A comparison of selected components of melt compositions as the melt fraction (a-f) increases and as the temperature (g-l) increases at 1.0 GPa from the experimental study on MM3 of Baker & Stolper (1994) and Hirschmann et al. (1998b), with the calculated values from pMELTS and Rcrust as determined in this study. Both pMELTS and Rcrust show better agreement with experimental values along increasing melt fraction, although Rcrust shows better overall agreement along increasing temperature.

Stellenbosch University https://scholar.sun.ac.za

4.1.3. G2: Partial melting of eclogite under upper mantle conditions

Both the experiments and modelling agree in the presence of clinopyroxene, garnet, rutile, quartz, plagioclase and melt, with a higher Q*asm* for Rcrust as is reported in Table 2-5. Due to the limited phase proportion data reported in the experimental study at 2.0 GPa and only a single run at 2.5 GPa, Figure 2-5 displays comparisons between phase abundances as a function of temperature at 3.0 GPa only. Figure 2-6 displays components from the experimental and modelled melt compositions as a function of increasing melt fraction (in wt.%) and increasing temperature.

In Figure 2-5, the appearance and proportions of rutile and quartz in the Rcrust modelled assemblage match the experimental results, although all are greater in proportion; pMELTS does not predict rutile or quartz as part of the assemblage. Although both bundles predict larger abundances of garnet, its exhaustion occurs at the same temperature in the experiments and Rcrust, whereas for pMELTS, it fluctuates consistently around an approximate 32–35 wt.% across the P-T range considered, and its exhaustion will thus occur at significantly higher temperatures. In Rcrust calculations, clinopyroxene disappears at a lower temperature than in the experiments, with the opposite observed for pMELTS. Rcrust predicts a slightly faster increase in melt fraction, whereas pMELTS predicts the liquidus to be at much higher temperatures, resulting in a much slower increase in the melt fraction and consequently delaying the exhaustion of garnet and clinopyroxene (Figure 2-6).

Considering phase compositions (Table 2-5 & Addendum A), at 2.0 GPa, the Rcrust melt compositions show good agreement with experiments, except for the bad fit of the melt composition at 1250 ºC. pMELTS displays a bad fit with the experimental melts at all temperatures at 2.0 GPa. Experimental and Rcrust plagioclase compositions at 1250 ºC agree badly, with mismatches for Al_2O_3 (+27.85%) and CaO (+27.04%); pMELTS does not predict any plagioclase here. At 2.5–3.0 GPa, compositional comparisons could be made for clinopyroxene, garnet, and melt, except for the 1300 ºC run at 3.0 GPa, where no melt was detected in the experiments or Rcrust calculations. Clinopyroxene and garnet compositions predicted by pMELTS show reasonable agreement with experiments, whereas Rcrust displays bad to good agreement with experimental clinopyroxene, and bad agreement with garnet below 1375 ºC at 3.0 GPa. As displayed in Figure 2-6, the comparisons of pMELTS melt compositions with experimental melts at 3.0 GPa show bad agreement, mainly due to SiO_2 (+47 to 230%), Al_2O_3 (-17 to 28%), FeO (-21 to 71%), MgO (-53 to 61%), and CaO (-23.8 to 62%). For Rcrust calculations, bad matches with melt are due to FeO (-33.92 to 60%) and TiO_2 (+56 to 68%), however at lower pressure and above 1365 ºC at 3.0 GPa, melt compositions

Stellenbosch University https://scholar.sun.ac.za

show better matches, ranging from reasonable to good (Table 2-5 & Figure 2-6).

Assemblage: Q*asm*

Bulk Q*asm* in 21 experiments	Rcrust	pMELTS
	87.65	72.29

Compositions: Sum of residuals^2

	2.0 GPa						2.5 GPa		3.0 GPa	
	1250 ºC		1325 ºC		1375 ºC		1325 ºC		1275 ºC	
	Rcrust	pMELTS	Rcrust	pMELTS	Rcrust	pMELTS	Rcrust	pMELTS	Rcrust	pMELTS
Cpx	11.16	14.5	17.93	11.70	21.44	12.77	26.93	15.14	10.04	7.10
Gt	13.58	8.28	9.36	4.18	-	-	20.55	7.70	36.74	6.83
Plag	64.93	-	-	-	-	-	-	-	-	-
Melt	63.34	288.20	3.79	69.15	4.43	28.55	16.06	90.46	-	105.05

	3.0 GPa									
	1300 ºC		1315 ºC		1325 ºC		1335 ºC		1350 ºC	
	Rcrust	pMELTS	Rcrust	pMELTS	Rcrust	pMELTS	Rcrust	pMELTS	Rcrust	pMELTS
Cpx	6.33	17.57	4.58	10.57	5.44	17.84	10.69	18.31	12.43	16.68
Gt	38.72	11.49	36.34	12.36	37.94	12.88	37.33	14.68	32.47	12.87
Melt	-	-	-	305.83	53.06	239.81	43.99	236.43	28.67	211.89

	3.0 GPa									
	1365 ºC		1375 ºC		1400 ºC		1425 ºC		1450 ºC	
	Rcrust	pMELTS	Rcrust	pMELTS	Rcrust	pMELTS	Rcrust	pMELTS	Rcrust	pMELTS
Cpx	24.49	21.27	26.55	16.52	30.81	17.13	30.63	15.91	34.57	16.91
Gt	29.08	13.93	27.84	14.95	22.73	14.82	14.28	10.38	10.74	10.66
Melt	23.85	184.24	18.47	148.28	19.10	164.44	12.05	140.14	4.43	125.76

	3.0 GPa					
	1450 ºC		1475 ºC		1500 ºC	
	Rcrust	pMELTS	Rcrust	pMELTS	Rcrust	pMELTS
Cpx	34.57	16.91	39.58	21.14	-	19.02
Gt	10.74	10.66	15.08	15.88	-	-
Melt	4.43	125.76	3.85	92.61	1.96	92.56

Table 2-5. Scoring of the modelled assemblages (bulkQ*asm*) and compositions (sum of residuals^2) from pMELTS and Rcrust in comparison with the experimental study on G2 from Pertermann & Hirschmann (2003a, 2003b), where such data was available.

Stellenbosch University https://scholar.sun.ac.za

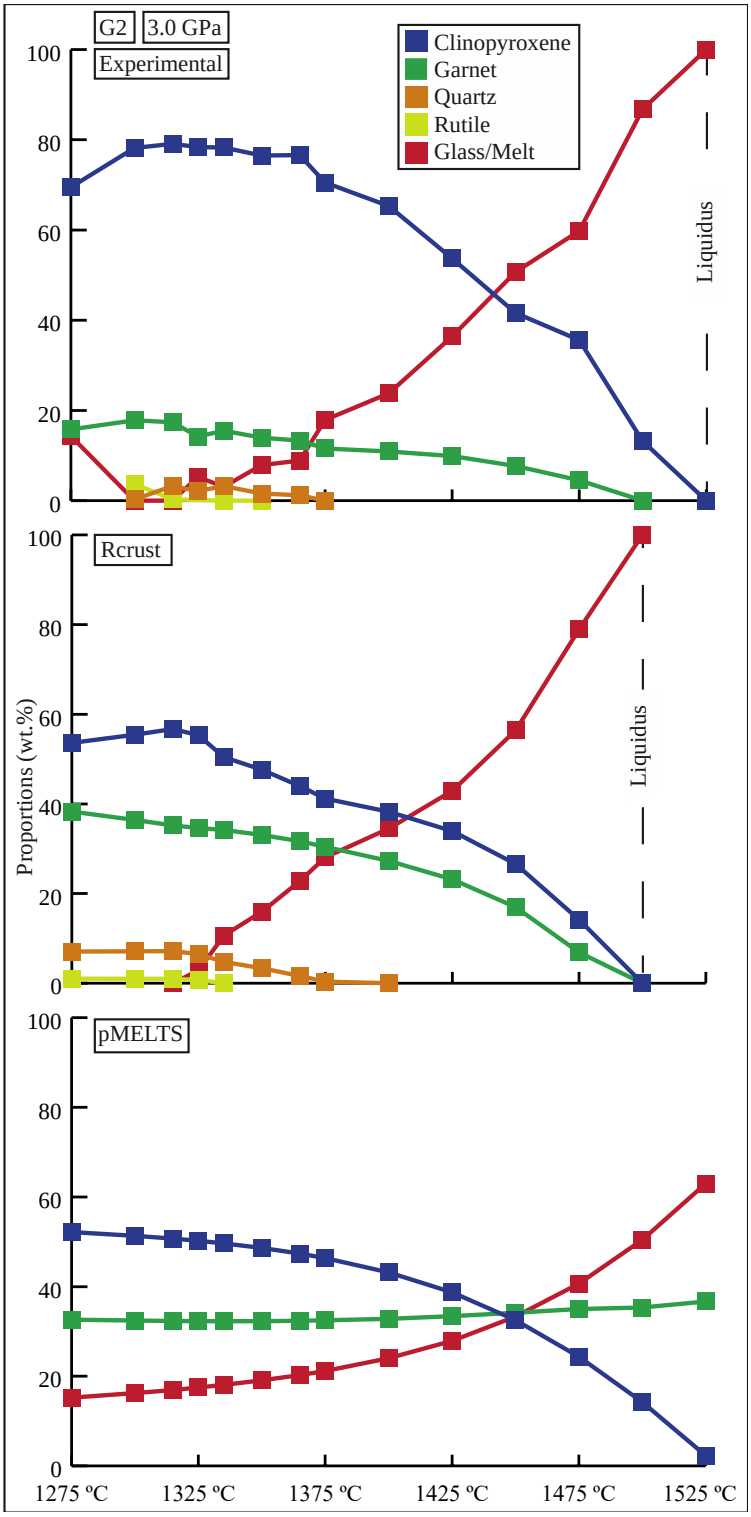

Figure 2-5. A comparison of melt (glass), clinopyroxene, garnet, quartz and rutile abundances at 3.0 GPa from the experimental study on G2 of Pertermann & Hirschmann (2003a), with the calculated values from pMELTS and Rcrust as determined by this study. pMELTS predicts the liquidus to be at much higher temperatures than the experiments, whilst there is good agreement between the curve of the melt fraction predicted by Rcrust and the experiments. This is similarly observed for rutile and quartz (although greater phase abundances are predicted by Rcrust), which was not predicted by pMELTS. This lack of quartz results in the pMELTS system not predicting the reactions between garnet and quartz seen in the experiments and in Rcrust, hence the different abundance curves observed for pMELTS and the exhaustion of garnet at higher temperatures. Rcrust predicts the exhaustion of clinopyroxene at lower temperatures than the experiments, whereas pMELTS predicts this at higher temperatures.

Stellenbosch University https://scholar.sun.ac.za

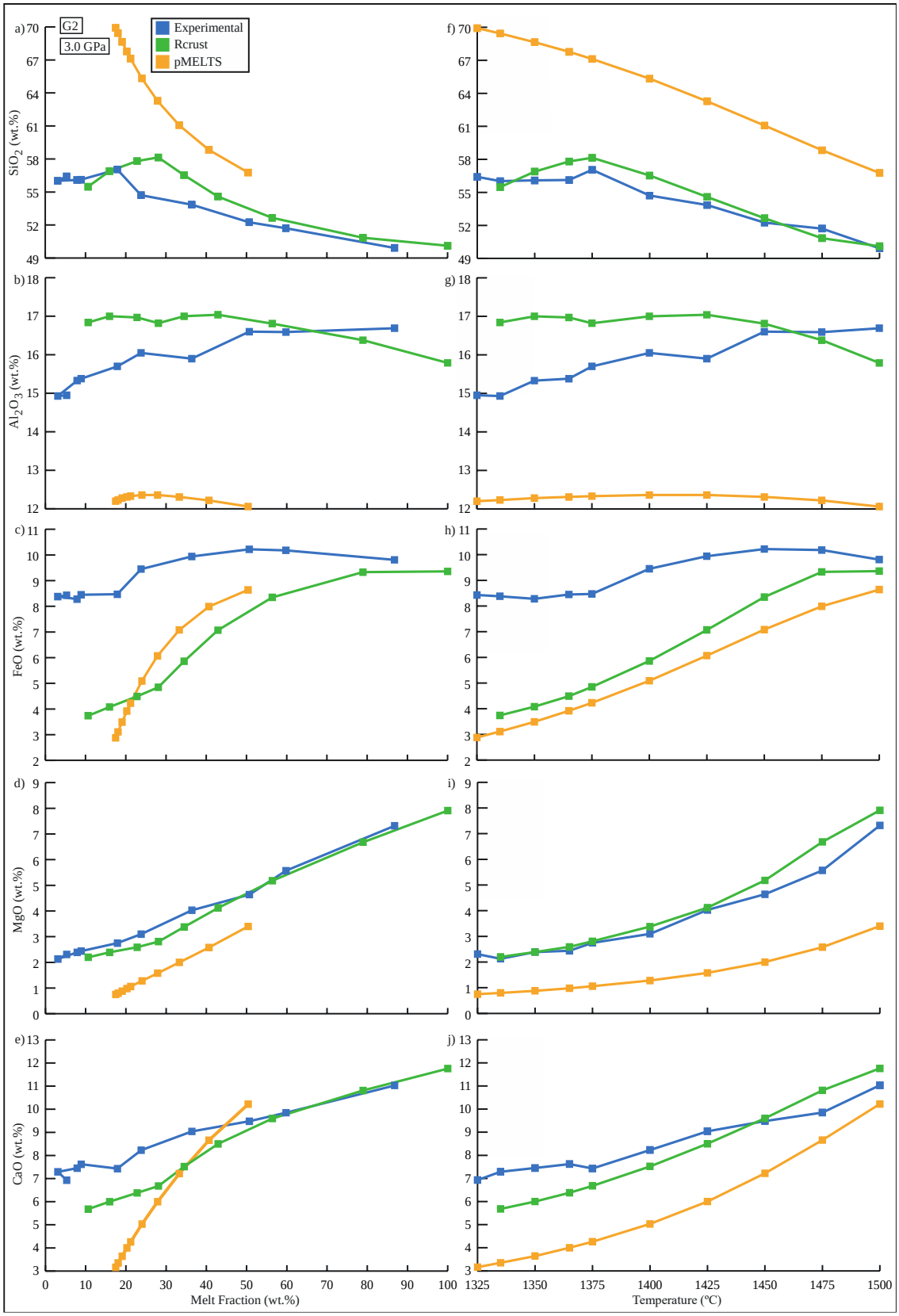

Figure 2-6. A comparison of selected components of melt compositions as the melt fraction (a-e) increases and as the temperature (f-j) increases at 3.0 GPa from the experimental study on G2 from Pertermann & Hirschmann (2003a, 2003b) with the calculated values from Rcrust and pMELTS as determined in this study. Rcrust predicted melt compositions range from bad to good in terms of agreement with experimental melt compositions, depending on the component. As discussed in-text, pMELTS indicates significantly lower values for several of the melt phase components, showing bad agreement with experimental melts in terms of melt fraction and temperature.

Stellenbosch University https://scholar.sun.ac.za

4.2. Uncertainty surrounding experimental results

The full set of thermodynamic modelling results from investigating unintended changes to reported bulk compositions from experimental studies are available in Addendum A. For the purpose of this comparison, particularly in terms of the location of the solidi, the modelling has been extended to 1000 ºC, which is beyond the temperature range of the experimental studies.

From the KLB-1 and MM3 results displayed in Figure 2-7, it is mainly H_2O addition that causes significant changes in predicted phase assemblages and proportions (Addendum A), where the resultant inhibition or stabilisation of several phases across the P-T range investigated may result in a better or worse match with the experimental assemblages reported. As is expected, H_2O addition also lowers the solidus quite significantly (> 230 ºC), which conversely may be shifted by Fe loss to higher temperatures above 2.0 GPa (Addendum A). The shift in the solidi caused by H_2O incorporation results in the increase of the melt fraction of up to 4.7% for KLB-1 and 3.6 wt.% for MM3, whereas this increase is less prominent for CO_2 (up to 1.2 wt.% increase). Fe loss may result in small variations in olivine, pyroxene, and melt proportions, similarly for clinopyroxene and melt due to CO_2 formation. Compared to experimental data, H_2O and CO_2 addition also decreases the percentage difference of olivine and melt proportions for KLB-1, similarly for MM3 proportions of olivine, clinopyroxene, and melt, and orthopyroxene at higher temperature. This improvement in predicted abundances is much more prominent for H_2O than CO_2. Changes in the compositions of the phases are reported in Addendum A.

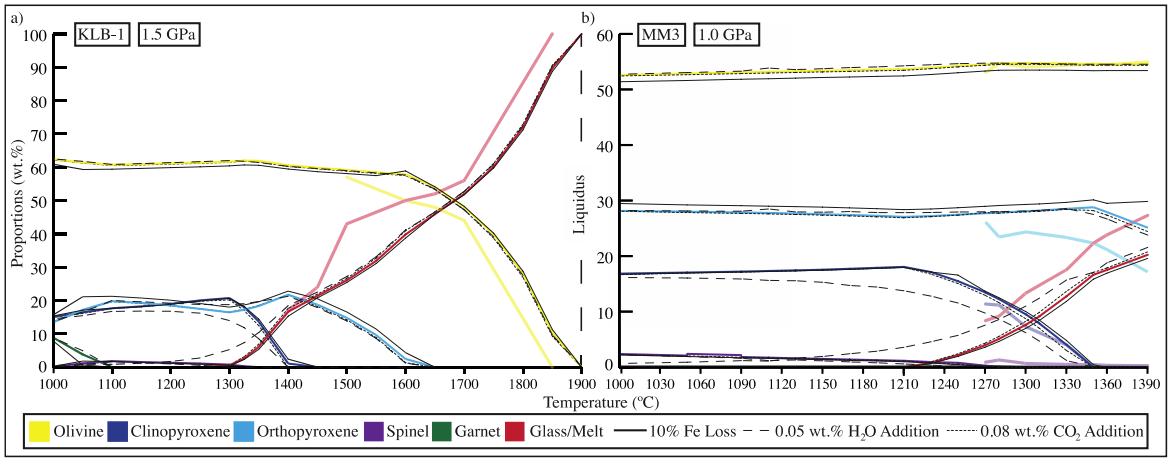

Figure 2-7. A comparison of changes in phase abundances with increasing temperature as a result of minor amounts of Fe loss to the capsule and the incorporation of very small amounts of H_2O or CO_2 to the capsule. Phase proportions reported by the experimental studies are included in faded colouring. a) Adjustment modelling of the 1.5 GPa experiments on KLB-1 of Takahashi (1986) and Takahashi et al. (1993), extended down to 1000 ºC. b) Adjustment modelling of the 1.0 GPa experiments on MM3 of Baker & Stolper (1994) and Hirschmann et al. (1998b), extended down to 1000 ºC. H_2O addition of 0.05 wt.% results in the extensive lowering of the solidus and decrease in clinopyroxene abundance. An increase in the melt fraction can be observed distinctly below 1500 ºC for both compositions.

Stellenbosch University https://scholar.sun.ac.za

5. Discussion

Several general observations can be drawn from the results presented in the previous section. It is important to reiterate that quantitative comparison between experimental and modelled results are extremely unlikely to produce outputs that match perfectly, because of the uncertainties inherent to both sets of findings, as discussed earlier. For upper mantle studies, previously conducted comparative works acknowledge and may briefly discuss these uncertainties (e.g. García-Arias, 2020; Gervais & Trapy, 2021; Ghiorso et al., 2002), but do not attempt quantitative comparison of the effects that well-known causes of experimental uncertainties may have on phase stability and composition. Using thermodynamic modelling and reasonable estimates of Fe loss and H_2O or CO_2 addition, a potential envelope of uncertainty around the experimental results has been defined (Figure 2-7). Changes in fO_2 have not been considered, as the use of graphite liners in all the experimental studies considered here limits the fO_2 to C-CO. The results indicate that a modelled Fe loss of 10% shows little variance in phase proportions and compositions (Figure 2-7). The incorporation of a small amount of CO_2 (0.08 wt.%) has a similarly small effect on the results, but these effects will be more prominent at higher pressure conditions. The addition of 0.05 wt.% H_2O shows a significant shift of the solidus to lower temperatures for both compositions. At any given temperature above the solidus, melt volumes are significantly increased and the abundance of clinopyroxene decreased. These results support two observations: Firstly, although the experimental investigations utilised in this study do not appear to be severely affected by Fe loss and CO_2 formation, unintended H_2O may have been incorporated into the capsules (Figure 2-7), which is not considered by Takahashi (1986) to be significant for KLB-1 below 1700 ºC, and is noted by Hirschmann et al. (1998b) for MM3 as ≤ 0.4 wt.% at higher temperatures only. Secondly, even with the modelled effects of added H_2O and CO_2, or a loss of Fe, differences in the modelling and the experimental melt abundances are still evident. Although this could suggest that the incorporated H_2O may exceed what is modelled and/or reported, this seems unlikely due to the discrepancy of the clinopyroxene abundance when compared to experimental results at the current modelled H_2O weight fraction. Rather, the uncertainties in thermodynamic modelling input data appear to play a larger role in this discrepancy. This has two implications: 1) Experiments considered as ‘anhydrous’ or ‘volatile free’ may unintentionally propagate uncertainties into thermodynamic datasets, which are calibrated using experimental phase equilibria and calorimetric data, and in some cases, data of natural mineral partitioning; but (2) does not render all such experimental data as ultimately unreliable

Stellenbosch University https://scholar.sun.ac.za

for comparisons with modelling at anhydrous conditions, as inherent uncertainties in the thermodynamic input files and calculation strategies cannot be ignored and identified otherwise. Thus, the suggestion of Ghiorso et al. (2002) that a portion of the offset of pMELTS predicted melt fraction of peridotite partial melting is due to 'phantom' volatile incorporation in piston cylinder experiments, which causes an increase in the melt abundance, is reasonable (Addendum A), but this does not surpass the inaccuracies still prevalent in thermodynamic modelling input data or calculation strategies.

Evaluations on the performance of the selected modelling tools to investigate partial melting across a range of temperatures at 1.0–3.0 GPa show that the Rcrust bundle displays good to excellent agreement with experimental phase assemblages (Figure 2-1; bulk Q*asm* of 78–100%) and proportions (Figures 2-2, 2-3, 2-5; Addendum A), and predict compositions that mostly agree reasonably with experiments (Tables 2-3 to 2-5; Addendum A), with the most notable discrepancies being spinel, garnet, and melt. The outputs from pMELTS show good to excellent agreement with experimentally determined phase assemblages (bulk Q*asm* of 72-95%) under SCLM conditions, however, greater overall discrepancies can be noted for phase proportions (Figures 2-2, 2-3, 2-5; Addendum A) as well as for compositions of spinel, melt, and the 3.0 GPa clinopyroxene of KLB-1 (Tables 2-3 to 2-5; Addendum A). These discrepancies are more pronounced for the eclogitic composition (Figures 2-5, 2-6; Table 2-5).

When considering closed system interactions, the properties of any one phase cannot change without an equal exchange in the accompanying phases, as is evident by the interchanges observed in phase assemblages, compositions, and proportions. Many of the observed discrepancies between experimental studies and thermodynamic calculations can thus be reconciled by considering the effects of predicted phase behaviours on these properties. For the partial melting of eclogite, pMELTS fails to predict the stabilisation of the ilmenite and quartz phases (Figure 2-5, Addendum A), with a smooth evolution of melt fraction increase accompanied by a mirrored decrease in the clinopyroxene as the only phase contributing towards melt formation. For the MM3 comparison of Ghiorso et al. (2002), the authors note the stabilisation of clinopyroxene at the expense of melt, however, the converse is displayed for the eclogite, where clinopyroxene abundances are 17.32 wt.% lower, whilst melt is only 0.91 wt.% higher. This is likely due to due to the observation of the supersaturation of garnet displayed by pMELTS at higher temperature (Ghiorso et al., 2002). The observed smoothed increase in melt fraction is less obvious for KLB-1 in Figure 2-2, but a prominent feature of the comparison is that the system reaches the liquidus at 200 ºC lower than the experiments at 1.5 GPa, although melt abundances remain lower than the experiments until ~1550 ºC. Distinct

Stellenbosch University https://scholar.sun.ac.za

inflection points in the temperature-melt fraction trends of pMELTS are visible at 1400 ºC and 1550 ºC, and because no other inflections occur, the melt fraction increases rapidly and is mirrored by the consumption of olivine (Addendum A). As a result, major overall discrepancies of the melt phase compositions (Tables 2-3 to 2-5) in terms of temperature (as noted in Section 2.4 and by Ghiorso et al., 2002) and eclogitic melt fractions (Figures 2-4, 2-6) are observed at high and low pressures (Table 2-4). Of note is that pMELTS calculations of olivine and clinopyroxene compositions (sans KLB-1 at 3.0 GPa) show reasonable to good agreement with experiments, fitting slightly better at low pressures for the peridotites (Tables 2-3, 2-4) and at higher temperatures at 3.0 GPa for the eclogite (Table 2-5) than Rcrust predicted compositions. It thus appears that although pMELTS is generally effective at phase assemblage predictions and compositions of specific phases, particularly for peridotite partial melting, the predicted melt fraction has a strong temperature dependence (Figures 2-2, 2-4, 2-6). This influences the proportions and compositions of several phases, although this is less obvious at lower P-T conditions such as those investigated for MM3. Ultimately, melt compositions predicted by pMELTS for the eclogite may vary noticeably from experimental results because of the overstabilisation of melt relative to clinopyroxene or olivine, which are subsequently exhausted from the system more quickly. Ghiorso et al. (2002) note unsatisfactory results for pMELTS predictions of peridotite partial melting from 3.0–7.0 GPa, but as is displayed here, this is also evident for more basaltic compositions from 2.0–3.0 GPa.

Overall, Rcrust predicted phase proportions display a comparable increase in melt fraction to that of the experiments (Figure 2-2, 2-3, 2-5), mostly displaying the sudden drops or increases in the phase proportions as melt volume increases, regardless of phases missing in the assemblage or differences in the predicted initial proportions of phases and their rates of consumption. For example, although the liquidus is displaced to 50 ºC higher in Figure 2-2 for KLB-1, the increase in melt fraction and subsequent rate of olivine consumption (Addendum A) predicted by Rcrust is comparable with the experimental study. For the eclogite, Rcrust predicts increased garnet and decreased clinopyroxene proportions as compared to the experiments (Figure 2-5). Clinopyroxene is consumed more rapidly, and due to its lower proportions, is exhausted at the same temperature as garnet. Conversely, because clinopyroxene has higher proportions in the experimental results, it is exhausted at a higher temperature due to its rate of consumption. Although this difference influences the melt proportion at lower temperatures, the curve of the melt fraction mostly follows that of the experiments and thus produce mostly similar melt compositions, apart from FeO content

Stellenbosch University https://scholar.sun.ac.za

(Figure 2-6). Similar behaviour can be noted in Figure 2-3, although melt components show notable variation from experimental results for peridotite partial melting.

It is clear that the discrepancies displayed by pMELTS and Rcrust compared to experimental results are likely as a result of differences in the thermodynamic datasets and formulation of the *a-x* models (particularly the melt *a-x* model), because the calculation strategy of the software are reported as similar (Table 2-1). The interactions of *a-x* models with the thermodynamic dataset should also be taken into consideration. The input data clearly result in notable variance across P-T-X space, but unfortunately, due to the embedded nature of these input components in the pMELTS software, this cannot be investigated in more detail. Similar discrepancies have been noted for where software utilise the same thermodynamic dataset and related *a-x* models, which may be a result of two important factors: The requirement of HP*x*-eos families to be formatted for use in Perple_X (and subsequently, Rcrust and others) mean that small oversights or mistakes, or even a delay in the formatting process can easily result in a mismatch in the predicted outcomes. The second factor is the calculation method of the software, where different strategies can cause mismatches due to user-specified parameters inherent to the strategy. For example, failing to identify assemblage tie-lines in THERMOCALC could exclude an entire assemblage field from the pseudosection, or not implementing the appropriate resolution in Perple_X (and Rcrust) would cause a failure to identify phases or even small assemblage fields. Evidently, thermodynamic input data or calculation strategies can have implications on the results produced by thermodynamic modelling when compared to experiments, not without taking into consideration the mismatches that may be as a result of experimental pitfalls, as is discussed earlier.

6. Conclusions

This comparative study supports two primary conclusions. Firstly, when compared with experimental results, the use of phase equilibrium modelling routines is a viable method for analysing the phase assemblages, proportions and compositions in ultramafic and mafic rock compositions under SCLM P-T conditions. This approach should be seen as complementary to experimental work, with several advantages such as being an extremely rapid form of investigation when compared to experimental studies, allowing greater P-T-X resolution and control over the incorporation of volatiles, as well as their fugacities. Secondly, Rcrust using Gibbs free energy minimisation from Perple_X, the internally consistent dataset of Holland & Powell (2011), and the *a-x* models of clinopyroxene, garnet, orthopyroxene, spinel, and melt (Tomlinson & Holland, 2021), olivine (Holland et al., 2018), feldspar (Holland & Powell,

Stellenbosch University https://scholar.sun.ac.za

2003), and ilmenite (White et al., 2000), generally mapped out melt production and compositions reliably at SCLM P-Ts, when compared with the experimental results. The software, *a-x* models and thermodynamic dataset are a good combination for studying petrogenic processes where the melt fraction changes significantly within the P-T-X range of this study, and for compositions that range from ultramafic to mafic. This, in combination with the capability of Rcrust to allow phase extraction and accommodate the resultant bulk compositional change, makes the Rcrust methodology presented here well-suited for the study of partial melting reactions in the upper mantle, including the effects of magma segregation.

Acknowledgements

The authors thank M. Garçia-Arias and an anonymous reviewer for their comments and suggestions that aided in the improvement of this manuscript. This work was supported by the South African National Research Foundation (NRF) through the South African Research Chairs Initiative (SARChI) awarded to G. Stevens, and the BuCoMO International Research Project (IRP) by the French Centre for Scientific Research (CNRS) and the NRF.

Stellenbosch University https://scholar.sun.ac.za

References

1. Asimow, P.D., Ghiorso, M.S., 1998. Algorithmic modifications extending MELTS to calculate subsolidus phase relations. American Mineralogist 83, 1127–1132.
2. Asimow, P.D., Dixon, J.E., Langmuir, C.H., 2004. A hydrous melting and fractionation model for mid-ocean ridge basalts: Application to the Mid-Atlantic Ridge near the Azores. Geochemistry, Geophysics, Geosystems 5, 1.
3. Baker, M.B., Stolper, E.M., 1994. Determining the composition of high-pressure mantle melts using diamond aggregates. Geochimica et Cosmochimica Acta 58, 2811–2827.
4. Berman, R.G., 1988. Internally-consistent thermodynamic data for minerals in the system Na_2O-K_2O-CaO-MgO-FeO-Fe_2O_3-Al_2O_3-SiO_2-TiO_2-H_2O-CO_2. Journal of Petrology 29, 445–522.
5. Bohrson, W.A., Spera, F.J., Ghiorso, M.S., Brown, G.A., Creamer, J.B., Mayfield, A., 2014. Thermodynamic model for energy-constrained open-system evolution of crustal magma bodies undergoing simultaneous recharge, assimilation and crystallization: the Magma chamber simulator. Journal of Petrology 55, 1685–1717.
6. Brugier, Y.-A., Alletti, M., Pichavant, M., 2015. Fe pre-enrichment: A new method to counteract iron loss in experiments on basaltic melts. American Mineralogist 100, 2106–2111.
7. Cawthorn, R.G., Ford, C.E., Biggar, G.M., Bravo, M.S., Clarke, D.B., 1973. Determination of the liquid composition in experimental samples: Discrepancies between microprobe analysis and other methods. Earth and Planetary Science Letters 21, l–5.
8. Connolly, J.A.D., 2005. Computation of phase equilibria by linear programming: A tool for geodynamic modeling and its application to subduction zone decarbonation. Earth and Planetary Science Letters 236, 524–541.
9. Connolly, J.A.D., 2007. Perple_X Comparisons [Online]. Available: https://www.perplex.ethz.ch/perplex_thermocalc_comparison.html [2022, November 4].
10. Connolly, J.A.D., 2009. The geodynamic equation of state: what and how. Geochemistry, Geophysics, Geosystems 10, 10.
11. Connolly, J.A.D., 2021. Index of/perplex/examples [Online]. Available: https://www.perplex.ethz.ch/perplex/examples/ [2022, November 10].
12. Connolly, J.A.D., 2022. Perple_X Updates [Online]. Available: https://hpxeosandthermocalc.org/2020/10/31/high-ca-opx-again/ [2021, May 13].

Stellenbosch University https://scholar.sun.ac.za

13. Connolly J.A.D., Kerrick, D.M., 1987. An algorithm and computer program for calculating composition phase diagrams. CALPHAD 11, 1–55.
14. Connolly J.A.D., Petrini, K., 2002. An automated strategy for calculation of phase diagram sections and retrieval of rock properties as a function of physical conditions. Journal of Metamorphic Geology 20, 697–708.
15. de Capitani, C., Brown, T.H., 1987. The computation of chemical equilibrium in complex systems containing non-ideal solutions. Geochimica et Cosmochimica Acta 51, 2639–2652.
16. de Capitani, C., Petrakakis, K., 2010. The computation of equilibrium assemblage diagrams with Theriak/Domino software. American Mineralogist 95, 1006–1016.
17. Duesterhoeft, E., de Capitani, C., 2013. Theriak_D: An add-on to implement equilibrium computations in geodynamic models. Geochemistry, Geophysics, Geosystems 14, 4962–4967.
18. Falloon, T.J., Green, D.H., Danyushevsky, L.V., Faul, U.H., 1999. Peridotite melting at 1.0 and 1.5 GPa: An experimental evaluation of techniques using diamond aggregates and mineral mixes for determination of near-solidus melts. Journal of Petrology 40, 1343–1375.
19. Falloon, T.J., Green, D.H., Hatton., C.J., Harris, K.L., 1988. Anhydrous Partial Melting of a Fertile and Depleted Peridotite from 2 to 30 kb and Application to Basalt Petrogenesis. Journal of Petrology 29, 1257–1282.
20. Falloon, T.J., Green, D.H., O'Neill, H.S.C., Ballhaus, C.G., 1996. Quest for low degree partial melts. Nature 381, 285.
21. Forshaw, J.B., Waters, D.J., Pattinson, D.R.M., Palin, R.M., Gopon, P., 2019. A comparison of observed and thermodynamically predicted phase equilibria and mineral compositions in mafic granulites. Journal of Metamorphic Geology 37, 15–179.
22. García-Arias, M., 2020. Consistency of the activity–composition models of Holland, Green, and Powell (2018) with experiments on natural and synthetic compositions: a comparative study. Journal of Metamorphic Geology 38, 993–1010.
23. Gervais, F., Trapy, P.-H., 2021. Testing solution models for phase equilibrium (forward) modeling of partial melting experiments. Contributions to Mineralogy and Petrology 167, 4.
24. Ghiorso, M.S., Hirschmann, M.M., Reiners, P.W., Kress, V.C.III., 2002. The pMELTS: A revision of MELTS for improved calculation of phase relations and major element

Stellenbosch University https://scholar.sun.ac.za

partitioning related to partial melting of the mantle to 3 GPa. Geochemistry, Geophysics, Geosystems 3, 1–36.

25. Ghiorso, M.S., Gualda, G.A.R., 2015. An H_2O–CO_2 mixed fluid saturation model compatible with rhyolite-MELTS. Contributions to Mineralogy and Petrology 169, 53.
26. Ghiorso, M.S., Sack, R.O., 1995. Chemical mass transfer in magmatic processes, IV. A revised and internally consistent thermodynamic model for the interpolation and extrapolation of liquid-solid equilibria in magmatic systems at elevated temperatures and pressures. Contributions to Mineralogy and Petrology 119, 197–212.
27. Green, E.C.R., 2020. High-Ca opx again [Online]. Available: https://hpxeosandthermocalc.org/2020/10/31/high-ca-opx-again/ [2021, May 13].
28. Green, E.C.R., 2022. The HPx-eos and THERMOCALC [Online]. Available: https://hpxeosandthermocalc.org/the-hpx-eos/the-hpx-eos-families/igneous-set/ [2022, Feb 8].
29. Green, E.C.R., White, R.W., Diener, J.F.A., Powell, R., Holland, T.J.B., Palin, R.M., 2016. Activity-composition relations for the calculation of partial melting equilibria in metabasic rocks. Journal of Metamorphic Geology 34, 845–869.
30. Grove, T.L., 1981. Use of FePt alloys to eliminate the iron loss problem in 1 atmosphere gas mixing experiments: theoretical and practical considerations. Contributions to Mineralogy and Petrology 78, 298–304.
31. Gualda, G.A.R., Ghiorso, M.S., Lemons, R.V., Carley, T.L., 2012. Rhyolite-MELTS: a Modified Calibration of MELTS Optimized for Silica-rich, Fluid-bearing Magmatic Systems. Journal of Petrology 53, 875–890.
32. Heinrich, C.A., Connolly, J.A.D., 2022. Physical transport of magmatic sulfides promotes copper enrichment in hydrothermal ore fluids. Geology 50, 1101–1105.
33. Hernández-Uribe, D., Spera, F.J., Bohrson, W.A., Heinonen, J.S., 2022. A comparative study of two-phase equilibria modeling tools: MORB equilibrium states at variable pressure and H_2O concentrations. American Mineralogist 107, 1789–1806.
34. Hirschmann, M.M., Ghiorso, M.S., Wasylenki, L.E., Asimow, P.D., Stolper, E.M., 1998a. Calculation of Peridotite Partial Melting from Thermodynamic Models of Minerals and Melts. I. Review of Methods and Comparison with Experiments. Journal of Petrology 39, 1091–1115.
35. Hirschmann, M.M., Baker, M.B., Stolper, E.M., 1998b. The effect of alkalis on the silica content of mantle-derived melts. Geochimica et Cosmochimica Acta 62, 883–902.

Stellenbosch University https://scholar.sun.ac.za

36. Holland, T.J.B., Powell, R., 1985. An internally consistent thermodynamic dataset with uncertainties and correlations: 2. Data and results. Journal of Metamorphic Geology 3, 343–370.
37. Holland, T.J.B., Powell, R., 1990. An enlarged and updated internally consistent thermodynamic dataset with uncertainties and correlations: the system Na_2O-K_2O-CaO-MgO-MnO-FeO-Fe_2O_3-Al_2O_3-SiO_2-TiO_2-C-H_2-O_2. Journal of Metamorphic Geology 8, 89–124.
38. Holland, T.J.B., Powell, R., 1996a. Thermodynamics of order–disorder in minerals 1: symmetric formalism applied to minerals of fixed composition. American Mineralogist 81, 1413–1424.
39. Holland, T.J.B., Powell, R., 1996b. Thermodynamics of order–disorder in minerals 2: symmetric formalism applied to solid solutions. American Mineralogist 81, 1425–1437.
40. Holland, T.J.B., Powell, R., 1998. An internally consistent thermodynamic data set for phases of petrological interest. Journal of Metamorphic Geology 16, 309–343.
41. Holland, T.J.B., Powell, R., 2001. Calculation of phase relations involving haplogranitic melts using an internally consistent thermodynamic dataset. Journal of Petrology 42, 673–683.
42. Holland, T.J.B., Powell, R., 2003. Activity-composition relations for phases in petrological calculations: an asymmetric multicomponent formulation. Contributions to Mineralogy and Petrology 145, 492–501.
43. Holland, T.J.B., Powell, R., 2011. An improved and extended internally consistent thermodynamic dataset for phases of petrological interest, involving a new equation of state for solids. Journal of Metamorphic Geology 29, 333–383.
44. Holland, T.J.B., Green, E.C.R., Powell, R., 2018. Melting of peridotites through to granites: A simple thermodynamic model in the system KNCFMASHTOCr. Journal of Petrology 59, 881–900.
45. Humphreys, M.C.S., Kearns, S.L., Blundy, J.D., 2006. SIMS investigation of electron-beam damage to hydrous, rhyolitic glasses: Implications for melt inclusion analysis. American Mineralogist 91, 667–679.
46. Horváth, P., 2007. P-T pseudosections in KFMASH, KMnFMASH, NCKFMASH and NCKMnFMASH systems: a case study from garnet-staurolite mica schist from the Alpine metamorphic basement of the Pannonian Basin (Hungary). Geologica Carpathica 58, 107–119.

Stellenbosch University https://scholar.sun.ac.za

47. Ito, K., Kennedy, G.C., 1973. The composition of liquids formed by partial melting of eclogites at high temperatures and pressures. Journal of Geology 82, 383–392.
48. Jennings, E.S., Holland, T.J.B., 2015. A simple thermodynamic model for melting of peridotite in the system NCFMASOCr. Journal of Petrology 56, 869–892.
49. Kushiro, I., 2001. Partial Melting Experiments on Peridotite and Origin of Mid-Ocean Ridge Basalt. Annual Review of Earth and Planetary Sciences 29, 71–107.
50. Lanari, P., Duesterhoeft, E., 2019. Modeling Metamorphic Rocks Using Equilibrium Thermodynamics and Internally Consistent Databases: Past Achievements, Problems and Perspectives. Journal of Petrology 60, 19–56.
51. Mayne, M., Moyen, J.-F., Stevens, G., Kaislaniemi, L., 2016. Rcrust: a tool for calculating path-dependent open system processes and application to melt loss. Journal of Metamorphic Petrology 34, 663–682.
52. Mayne, M., Stevens, G., Moyen, J.-F., Johnson, T., 2019. Performing process-oriented investigations involving mass transfer using Rcrust: a new phase equilibrium modelling tool, in: Janoušek, V., Bonin, B., Collins, W.J., Farina, F., Bowden, P. (Eds.), Post-Archean Granitic Rocks: Petrogenetic Processes and Tectonic Environments, Geological Society of London Special Publications 491, Bath, pp. 209–221.
53. Médard, E., McCammon, C.A., Barr, J.A., Grove, T.L., 2008. Oxygen fugacity, temperature reproducibility, and H_2O contents of nominally anhydrous piston-cylinder experiments using graphite capsules. American Mineralogist 93, 1838–1844.
54. Merrill, R.B., Wyllie, P.J., 1973. Absorption of iron by platinum capsules in high pressure rock melting experiments. American Mineralogist 58, 16–20.
55. Morgan, G.B.IV., London, D., 1996. Optimizing the electron microprobe analysis of hydrous alkali aluminosilicate glasses. American Mineralogist 81, 1176–1185.
56. Pertermann, M., Hirschmann, M.M., 2003a. Partial melting experiments on a MORB-like pyroxenite between 2 and 3 GPa: constraints on the presence of pyroxenite in basalt source regions from solidus location and melting rate. Journal of Geophysical Research: Solid Earth 108, 2125.
57. Pertermann, M., Hirschmann, M.M., 2003b. Anhydrous partial melting experiments on MORB-like eclogite: phase relations, phase compositions and mineral–melt partitioning of major elements at 2-3 GPa. Journal of Petrology 44, 2173–2201.
58. Powell, R., 1985. Geothermometry and geobarometry: a discussion. Journal of the Geological Society 142, 29–38.

Stellenbosch University https://scholar.sun.ac.za

59. Powell, R., Holland, T.J.B., 1988. An internally consistent dataset with uncertainties and correlations: 3. Applications to geobarometry, worked examples and a computer program. Journal of Metamorphic Petrology 6, 173–204.
60. Powell, R., Holland, T.J.B., 1990. Calculated mineral equilibria in the pelite system. KFMASH (K_2O–FeO–MgO–Al_2O_3–SiO_2–H_2O). American Mineralogist 75, 367–380.
61. Powell, R., Holland, T.J.B., 1993. On the formulation of simple mixing models for complex phases. American Mineralogist 78, 1174–1180.
62. Powell, R., Holland, T.J.B., Worley, B., 1998. Calculating phase diagrams involving solid solutions via non-linear equations, with examples using THERMOCALC. Journal of Metamorphic Geology 16, 577–588.
63. Riel, N., Kaus, B.J.P., Green, E.C.R., Berlie, N., 2022. MAGEMin, an Efficient Gibbs Energy Minimizer: Application to Igneous Systems. Geochemistry, Geophysics, Geosystems 23, e2022GC010427
64. Sack., R.O., Ghiorso, M.S., 1994. Thermodynamics of multi-component pyroxenes. 3. Calibration of $Fe^{2+}(Mg)_{-1}$, $TiAl_2(MgSi_2)_{-1}$, $TiFe^{3+}{}_2(MgSi_2)_{-1}$, $AlFe^{3+}(MgSi)_{-1}$, $NaAl(CaMg)_{-1}$, $Al_2(MgSi)_{-1}$ and $Ca(Mg)_{-1}$ exchange-reactions between pyroxenes and silicate melts. Contributions to Mineralogy and Petrology 118, 271–296.
65. Schilling, F., Wunder, B., 2004. Temperature distribution in piston-cylinder assemblies: Numerical simulations and laboratory experiments. European Journal of Mineralogy 16, 7–14.
66. Stevens, G., Clemens, J.D., Droop, T.R., 1997. Melt production during granulite-facies anatexis: experimental data from “primitive” metasedimentary protoliths. Contributions to Mineralogy and Petrology 128, 352–370.
67. Takahashi, E., 1986. Melting of a dry peridotite KLB-1 up to 14 GPa: implications on the origin of peridotitic upper mantle. Journal of Geophysical Research 91, 9367–9382.
68. Takahashi, E., Shimazaki, T., Tsuzaki, Y., Yoshida, H., 1993. Melting study of a peridotite KLB–1 to 6.5 GPa, and the origin of basaltic magmas. Philosophical Transactions: Physical Sciences and Engineering 342, 105–120.
69. Tomlinson, E.L., Holland, T.J.B., 2021. A Thermodynamic model for the subsolidus evolution and melting of peridotite. Journal of Petrology 62, egab012.
70. Tropper, P., Hauzenberger, C., 2015. How well do pseudosection calculations reproduce simple experiments using natural rocks: an example from high-P high-T granulites of the Bohemian Massif. Austrian Journal of Earth Sciences 108, 123–138.

Stellenbosch University https://scholar.sun.ac.za

71. Varshneya, A.K., Cooper, A.R., Cable, M., 1966. Changes in composition during electron microprobe analysis of K_2O-SrO-SiO_2 glass. Journal of Applied Physics 37, 2199–2202.
72. Wang, J., Xiaolin, X., Zhang, L., Takahashi, E., 2020. Element loss to platinum capsules in high-temperature-pressure experiments. American Mineralogist 105, 1593–1597.
73. Wasylenki, L.E., Baker, M.B., Hirschmann, H.H., Stolper, E.M., 1996. The effect of source depletion on equilibrium mantle melting. EOS Transactions, American Geophysical Union 77, F847.
74. Wasylenki, L.E., Baker, M.B., Kent, A.J.R., Stolper, E.M., 2003. Near-solidus Melting of the Shallow Upper Mantle: Partial Melting Experiments on Depleted Peridotite. Journal of Petrology 44, 1163–1191.
75. White, R.W., Powell, R., Holland, T.J.B., 2007. Progress relating to calculation of partial melting equilibria for metapelites. Journal of Metamorphic Petrology 25, 511–527.
76. White, R.W., Powell, R., Holland, T.J.B., Johnson, T.E., Green, E.C.R., 2014. New mineral activity-composition relations for thermodynamic calculations in metapelitic systems. Journal of Metamorphic Geology 32, 261–286.
77. White, R.W., Powell, R., Holland, T.J.B., Worley, B.A., 2000. The effect of TiO_2 and Fe_2O_3 on metapelitic assemblages at greenschist and amphibolite facies conditions: mineral equilibria calculations in the system K_2O–FeO–MgO–Al_2O_3–SiO_2–H_2O–TiO_2–Fe_2O_3. Journal of Metamorphic Geology 18, 497–512.
78. White, R.W., Stevens, G., Johnson, T.E., 2011. Is the Crucible Reproducible? Reconciling Melting Experiments with Thermodynamic Calculations. Elements 7, 241–246.
79. Worley, B.A., Powell, R., 2002. High-precision relative thermobarometry: theory and a worked example. Journal of Metamorphic Geology 18, 91–101.
80. Xiang, H., Connolly, J.A., 2022. GeoPS: An interactive visual computing tool for thermodynamic modelling of phase equilibria. Journal of Metamorphic Geology 40, 243–255.

Stellenbosch University https://scholar.sun.ac.za

SUBCHAPTER 2.2

A COMPARISON BETWEEN DIFFERENT THERMODYNAMIC MODELLING METHODOLOGIES: KLB-1 PSEUDOSECTION PRODUCED VIA THERMOCALC AND VIA RCRUST

As a precursor for the comparative study of Chapter 2, a pressure-temperature (P-T) pseudosection for KLB-1 (Takahashi, 1986, Takahashi et al., 1993) was generated using Rcrust. The KLB-1 bulk composition is regularly used as part of benchmarking exercises to investigate updates to the HP*x*-eos families (Holland et al., 2018; Tomlinson & Holland, 2021) and the Holland & Powell (2011) thermodynamic dataset, as well as to investigate the soundness of the formatting of these models for use in other software than THERMOCALC, such as Perple_X (and subsequently, Rcrust and others). Thus, the same results should be produced by different modelling platforms if appropriate care has been taken when setting grid resolution, and regardless of the differences in the calculation strategy used (Table 2-1).

Details of the Rcrust modelling methodology is discussed in detail in Chapter 2; it is assumed that the set of *a*-*x* models used in Rcrust corresponds to those used by Holland et al. (2018). A pseudosection was not produced in Rcrust using the Tomlinson & Holland (2021) *a*-*x* models, because their study did not provide a pseudosection of KLB-1 for comparison. A pseudosection was also not generated using pMELTS as it is not a functionality of the software.

Figure 2.2-1 displays the KLB-1 pseudosection produced via THERMOCALC to assess the performance of updates made to the models of the KNCFMASTOCr system (Holland et al., 2018), and the pseudosection produced via Rcrust in this study across a P-T range of 1–30 kbar (1.0–3.0 GPa) and 80–1700 ºC. The results show that the Rcrust pseudosection displays excellent agreement with the pseudosection produced in THERMOCALC. Rcrust, however, does not predict spinel below 1200 ºC at pressures lower than 7 kbar, whereas the presence of spinel at these conditions create an additional field in the THERMOCALC output. Spinel also persists to higher temperatures in the Rcrust output, stabilising two additional fields at low pressure. Additionally, the Gt + Cpx + Ol field extends to lower P-Ts compared to the pseudosection of Holland et al. (2018), stabilising another field of Gt + Cpx + Ol + Melt that not present in the THERMOCALC pseudosection. These minor differences in the predicted phase stabilities and fields may be due to several reasons, as discussed in detail Chapter 2. In summary, the results displayed in Figure 2.2-1 show that the pseudosection produced via Rcrust is greatly similar to the pseudosection produced in THERMOCALC for the same bulk composition, with both pseudosections displaying very similar topologies.

Stellenbosch University https://scholar.sun.ac.za

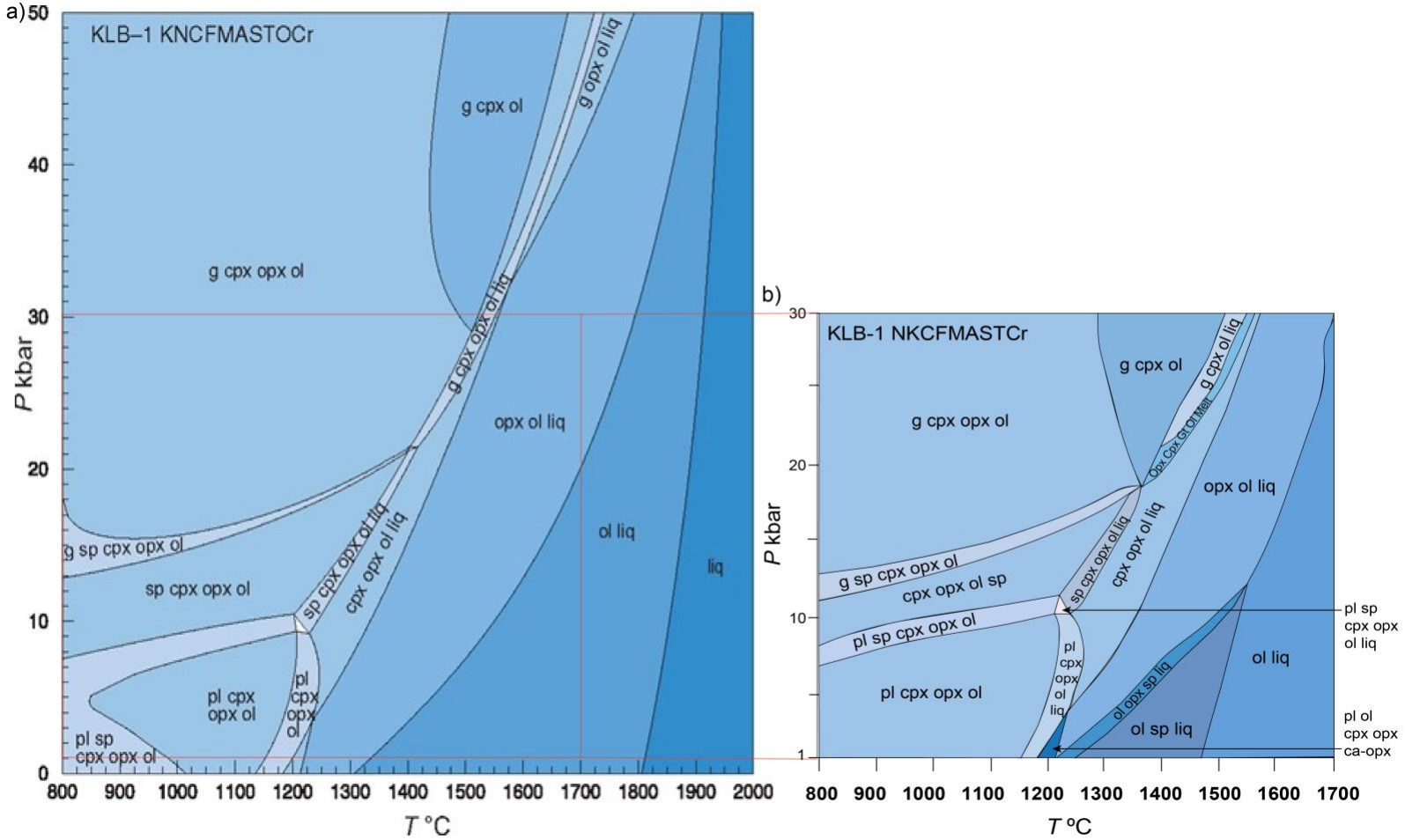

Figure 2.2-1. P-T pseudosections for KLB-1 in the KNCFMASTOCr system calculated using THERMOCALC (from Holland et al., 2018), and the KNCFMASTCr system using Rcrust (note, no fO_2 was set). Layout and phase reporting has been adapted to fit the Holland et al. (2018) pseudosection for ease of comparison. Phases: cpx: clinopyroxene; g: garnet; liq: melt; ol: olivine; opx: orthopyroxene; pl: plagioclase; sp: spinel; ca-opx: high-ca-opx. Compared to the Holland et al. (2018) pseudosection (1–30 kbar and 800–1700 ºC, outlined in red) for the same bulk rock composition calculated via THERMOCALC in (a), Rcrust predicts three additional stability fields in (b) across 1–30 kbar and 800–1700 ºC. For example, spinel does not appear at lower temperatures, but is present at higher temperatures, thus stabilising an additional field. Additionally, the Gt + Cpx + Ol field extends to lower temperatures and pressures compared to the outputs of Holland et al. (2018). It is assumed that Holland et al. (2018) used the set of *a-x* models corresponding to the Holland et al. (2018) *a-x* models used in Rcrust at the time of publication.

Stellenbosch University https://scholar.sun.ac.za

References

1. Holland, T.J.B., Green, E.C.R. and Powell, R. 2018. Melting of peridotites through to granites: A simple thermodynamic model in the system KNCFMASHTOCr. *Journal of Petrology*, 59:881–900.
2. Takahashi, E. 1986. Melting of a dry peridotite KLB-1 up to 14 GPa: implications on the origin of peridotitic upper mantle. *Journal of Geophysical Research*, 91:9367–9382.
3. Takahashi, E., Shimazaki, T., Tsuzaki, Y. and Yoshida, H. 1993. Melting study of a peridotite KLB–1 to 6.5 GPa, and the origin of basaltic magmas. *Philosophical Transactions: Physical Sciences and Engineering,* 342:105–120.
4. Tomlinson, E.L. and Holland, T.J.B. 2021. A Thermodynamic model for the subsolidus evolution and melting of peridotite. *Journal of Petrology,* 62(1):egab012.

Stellenbosch University https://scholar.sun.ac.za

SUBCHAPTER 2.3

A COMPARISON BETWEEN DIFFERENT THERMODYNAMIC MODELLING METHODOLOGIES AND EXPERIMENTAL RESULTS AT LOW PRESSURE: PARTIAL MELTING OF BASALT UNDER SHALLOW CRUSTAL CONDITIONS

Chapter 2 presents a comparative study of experimental results of different ultramafic to mafic bulk compositions with thermodynamic modelling outputs produced using Rcrust (Mayne et al., 2016) and pMELTS (Ghiorso et al., 2002). For analysing upper mantle source rocks, three sets of partial melting experiments were chosen for comparison with thermodynamic modelling outcomes by means of phase assemblages, phase and liquid proportions (wt.%), and phase-in/phase-out boundaries. Additionally, one set of crystallisation experiments (Table 2.3-1) was chosen for comparison which has not been discussed in Chapter 2, as the focus of this chapter centred on upper mantle sources and the effects of partial melting at upper mantle pressure-temperature (P-T) conditions. As thermodynamic modelling techniques are used to investigate crystallisation at crustal conditions at a later step in this project (Chapter 4), additional experimental-modelling comparisons were performed to analyse the modelled outcomes produced under crustal conditions, particularly phase crystallisation, and how this compares with experimental data at the same P-Ts. The chosen composition is that from experiments *Ar anhydrous* (Pertermann & Lundstrom, 2006), which represents a composition of least evolved basaltic andesite from a volcanic eruption at Arenal, Costa Rica. Details are displayed in Table 2.3-1.

***Ar anhydrous*[1]**				
Composition (wt.%)	**Reported**	**Modified**	**Details**	
SiO_2	54.3	54.35	Pressure (GPa)	0.5
TiO_2	0.60	0.60	Temperature (°C)	1100–1300
Al_2O_3	18.80	18.82	Reported H_2O Content	Nominally anhydrous
Cr_2O_3	-	0.00	Reported Oxygen Fugacity (fo_2)	Below C-CO buffer
FeO_t	8.50	8.51	Capsule Material	Graphite-Lined Pt-Capsules
MnO	-	0.00		
MgO	5.10	5.11		
CaO	9.00	9.01		
Na_2O	3.00	3.00		
K_2O	0.60	0.60		
Sum	99.9	100.00		

Table 2.3-1. Details of the low-pressure experimental set investigated in this study. Where applicable, modified analyses were recalculated to 100% NiO, P_2O_5 and MnO free, as these oxides are not considered in the comparisons due to an incomplete set of activity-composition models defining the compositional space. All comparisons were based on FeO_t values, and recalculation was performed where necessary. (-) indicates no data available. All details listed here were gathered from the experimental study.

[1]Basaltic andesite from Pertermann & Lundstrom (2006).

Stellenbosch University https://scholar.sun.ac.za

Methodology

Experiments *Ar anhydrous* consisted of 8 runs from 1100–1300 ºC at 0.5 GPa. All of the outcomes from the experimental runs were considered in the comparison, except for duplicates; here, the greater phase assemblage and its reported data was used. Thermodynamic modelling outcomes were investigated using phase assemblages, phase and liquid proportions, phase and liquid compositions, phase-in/out boundaries, and compositions of clinopyroxene, ilmenite, orthopyroxene, plagioclase, and glass/melt/liquid.

The experimental study has some limitations relevant to this comparative study. For *Ar anhydrous*, Pertermann & Lundstrom (2006) report only melt fractions; compositional data is not provided for every phase in each assemblage. Consequently, comparisons of experimental results and thermodynamic modelling were made where the relevant data was available. Where no proportions were reported, an R Squared mixing routine was used to calculate proportions from compositional data, and also to assess the soundness of reported proportions. Phase modes were calculated at 1200 ºC , but due to the presence of augite, pigeonite, and amphibole at 1150 ºC and 1100 ºC, and the lack of compositional data for these phases, no modes could be calculated at these temperatures; these results are reported in Addendum B.

The experiments make use of Pt-capsules with graphite liners to minimise the uptake of Fe to the capsule. All of the experiments from Pertermann & Lundstrom (2006) were not intended to be volatile free, thus the authors do not describe strategies to avoid the absorption of H_2O in the capsules. Pertermann & Lundstrom (2006) state that the anhydrous experiments were not analysed for H_2O directly, but WDS analysis of these and other experiments allow a conclusion that the experiments were nominally anhydrous (microprobe totals near 100 wt.%). The authors also explain that, during analyses, monitored count rates at various beam spot sizes did not indicate the loss of alkalis, indicating a lack of detectable H_2O in the melts.

The thermodynamic modelling software packages utilised in the comparative study include rhyolite-MELTS (Gualda et al., 2012) (for intermediate compositions), and Rcrust (ultramafic to intermediate compositions). All modelling details follow that reported in the Methodology of Chapter 2. Pertermann & Lundstrom (2006) classified pyroxenes according to CaO content, reporting < 3 wt.% as orthopyroxene, 3–14 wt.% as pigeonite, and > 14 wt.% as augite. A similar approach was utilised for the pyroxenes predicted in Rcrust and rhyolite-MELTS in order to ensure coherence across the data sources. The outcomes for all comparisons have been recorded in Addendum B. Quantification of the results follow Q*asm*, percentage difference and relative difference, as defined in the Methodology of Chapter 2.

Stellenbosch University https://scholar.sun.ac.za

Results

Both the experiments and modelling agree in the presence of plagioclase, ilmenite, pigeonite, and melt, with a slightly higher BulkQ*asm* for Rcrust as shown in Table 2.3-2. Comparisons are limited to melt/glass/liquid and plagioclase abundance as a function of temperature at 0.5 GPa, as illustrated in Figure 2.3-1. The components of melt compositions of experiments compared to that of Rcrust and rhyolite-MELTS at 0.5 GPa is illustrated in Figure 2.3-2.

Assemblage: Q*asm*		
BulkQ*asm* in 6 experiments	Rcrust	rhyolite-MELTS
	68.42	65.00

Compositions: Sum of residuals^2						
0.5 GPa	1100 ºC		1150 ºC		1200 ºC	
	Rcrust	r-MELTS	Rcrust	r-MELTS	Rcrust	r-MELTS
Pig	-	-	115.95	113.60	-	90.24
Plag	-	-	82.27	13.70	59.69	0.71
Melt	65.27	118.38	75.24	36.42	7.06	4.71
0.5 GPa	1225 ºC		1250 ºC		1300 ºC	
	Rcrust	r-MELTS	Rcrust	r-MELTS	Rcrust	r-MELTS
Plag	40.38	0.54	36.44	1.30	-	-
Melt	3.10	6.21	7.18	2.43	1.31	1.06

Table 2.3-2. Scoring of the modelled assemblages (bulkQ*asm*) and compositions (sum of residuals^2) from rhyolite-MELTS (r-MELTS) and Rcrust in comparison with the experimental study on *Ar anhydrous* of Pertermann & Lundstrom (2006), where such data was available.

The experimental study reported the presence of amphibole in trace amounts at 1550 ºC, indicating that the experiments were not completely anhydrous, although it is stated as such. As discussed in Chapter 2, the presence of small amounts of H_2O could be due to a number of factors which should be considered when interpreting the comparisons of the experiments with thermodynamic calculations. Additionally, following the classification of the authors, neither modelling bundle predicts the presence of augite at 1100 ºC and 1150 ºC, and consequently no comparisons could be made with phase abundances or compositions.

In Figure 2.3-1, rhyolite-MELTS predicts lower abundances of melt from 1150–1225 ºC, displaying a difference of 15.35–41.33% from experimental proportions. However, the melt fraction increases rapidly when approaching liquidus temperatures, and thereafter show overestimations of melt (+19.22%). rhyolite-MELTS predicts the consumption of plagioclase, and thus the location of the liquidus, at least 10 ºC lower than the experiments, whilst Rcrust outputs match experimental assemblages when approaching the liquidus, but predicts

Stellenbosch University https://scholar.sun.ac.za

proportions of plagioclase much lower than the experiments. Comparing melt compositions predicted by Rcrust and rhyolite-MELTS with the experimental study (Figure 2.3-2) display very similar discrepancies. In general, most of the extreme outliers in Figure 2.3-2 are sourced from the comparisons at 1100 ºC and 1150 ºC, which show poor agreement with experimental values. At 1100 ºC, compared to experiments, the SiO_2 (-8% & -11%) values are underestimated by Rcrust and rhyolite-MELTS, but the CaO (+160% & +266%) and Rcrust FeO (+99%) values are overestimated. At 1150 ºC, the largest discrepancies are for SiO_2 (-10.78% & -7.45%) and Rcrust predicted MgO (+138.35%). From 1200 ºC upwards, the outputs from both modelling bundles display reasonable to good agreement with experimental melts.

Rcrust displays poor agreement with experimental plagioclase compositions, with discrepancies mainly due to the SiO_2 (-7% to 11%), Al_2O_3 (+10% to 17%) and CaO (+23% to 43%) values, whereas rhyolite-MELTS shows reasonable to good agreement, with discrepancies also mainly due to the SiO_2 (-4%) predicted value at 1150 ºC. Rcrust does not predict any pyroxene phases at 1200 ºC. Here, rhyolite-MELTS displays differences for FeO (+46.08%) and MgO (-24%) in pigeonite compared to the experimental study, with the increased FeO equating to a 6 wt.% drop for the calculated MgO value.

Discussion

In Figure 2.3-1, the melt abundance predicted by rhyolite-MELTS displays a greatly equivalent, sudden increase in melt fraction to that produced by pMELTS in Figures 2-2 and 2-5 in Chapter 2, with the plagioclase phase proportions reflecting this curve as it is consumed. Pigeonite, which is not displayed in Figure 2.3-1 due to lack of corresponding experimental data, mimics plagioclase consumption and is exhausted from the system at 1250 ºC. At 1225 ºC, the plagioclase proportion is not greatly dissimilar to what is observed experimentally, which subsequently shows mostly good agreement with experimental plagioclase. The melt phase proportions predicted by Rcrust are displaced to higher values than what is observed experimentally, but match well with experimental abundances at 1300 ºC. Both Rcrust and rhyolite-MELTS display the same proclivity of the plagioclase to drop in proportion at 1250 ºC, although this drop is less drastic in Rcrust outputs. Subsequently, rhyolite-MELTS predicts plagioclase to become exhausted at the point where the experiments only start to near the liquidus. As mentioned in the results above, rhyolite-MELTS also predicts the pigeonite phase at lower temperatures as is determined experimentally, with its decrease in proportion displaying its major involvement in the melting reaction. In Figure 2.3-2, variations of the predicted melt compositions compared to experiments are mostly at 1100 ºC and 1150 ºC.

Stellenbosch University https://scholar.sun.ac.za

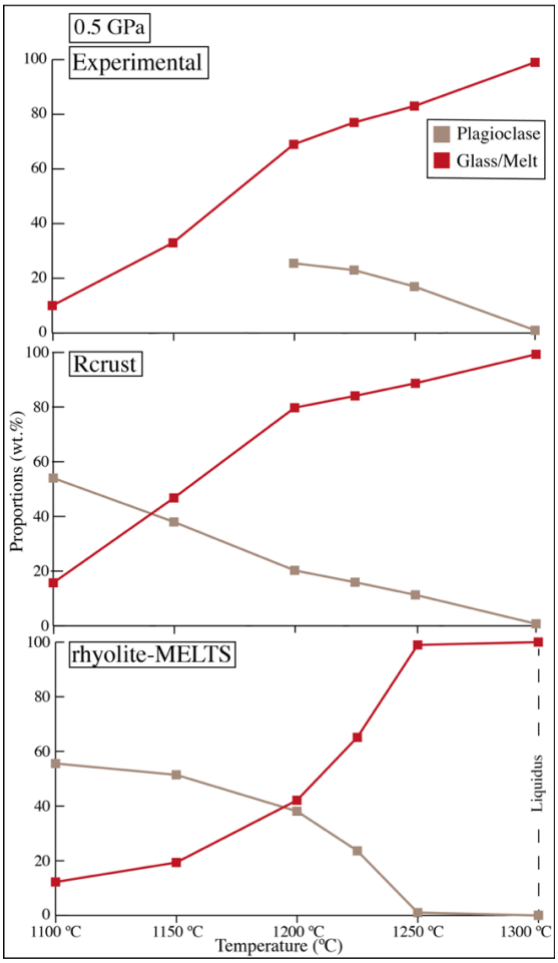

Figure 2.3-1. A comparison of melt (glass) and plagioclase at 0.5 GPa from the experimental study of *Ar anhydrous* of Pertermann & Lundstrom (2006), with the calculated values from rhyolite-MELTS and Rcrust as determined in this study. rhyolite-MELTS predicts the liquidus and plagioclase exhaustion at lower temperatures than the experiments, including melt proportions that vary from the experiments. Rcrust shows good agreement with the position of the solidus and the melt-curve. At temperatures below 1200 ºC, plagioclase proportions were not provided in the experimental study, but was predicted as discussed in the Methodology, and compared in the modelling outcomes. rhyolite-MELTS displays an overall greater proportion of plagioclase than Rcrust, apart from the initial values at 1100 ºC.

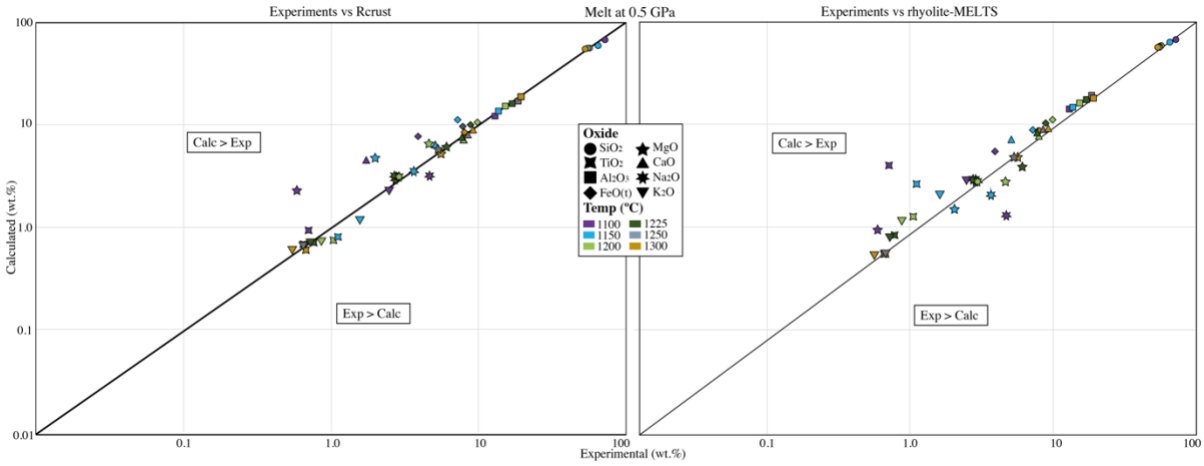

Figure 2.3-2. A comparison of oxides in melt (glass) compositions at 0.5 GPa from the experimental study on *Ar anhydrous* from Pertermann & Lundstrom (2006), with the calculated values from Rcrust and rhyolite-MELTS as determined in this study. Both Rcrust and rhyolite-MELTS show good agreement with the melt compositions from the experimental study above 1200 ºC, with the main differences in melt components discussed in-text.

Stellenbosch University https://scholar.sun.ac.za

The amphibole observed in the experimental assemblage as a result of unintended H_2O in the capsule would cause a displacement of the solidus to lower temperatures, and the liquidus to higher temperatures. Although the latter is observed, the trend of the experimental melt-curve suggests that the experiments would reach the solidus above 1300 ºC.

The large discrepancy between both modelling outputs and experimental results for melt compositions below 1200 ºC may thus be, in terms of experimental pitfalls, a combination of unintended H_2O in some of the experimental capsules, as well as analytical errors sourced from run product analyses in the experimental study. In terms of modelling pitfalls, rhyolite-MELTS predicts a slower increase in the melt fraction and thus consumption of the predicted mineral phases. It is peculiar that rhyolite-MELTS modelling continues to show reasonable to good results in terms of plagioclase and melt compositions above 1225 ºC, but both modelling bundles over- and underestimate the proportions of the phases. This is likely indicative of differences in *a-x* models and the thermodynamic datasets used by the modelling bundles, and may call for updates and/or additional experimental studies in the P-T-X region investigated here, in order to improve the thermodynamic datasets and calibrations.

Conclusion

This section of the experimental-modelling comparative study, conducted under upper crustal conditions, supports the same conclusions as the comparative study in Chapter 2, namely: 1) The use of thermodynamic modelling is a reasonable and time efficient alternative for analysing the phase assemblages, proportions, and compositions of basaltic and basaltic-intermediate rock compositions at upper crustal P-Ts, but should be seen as complementary to experimental work; 2) When compared with the experimental results, melt fractions and compositions predicted under upper crustal conditions compare reasonably with modelling outputs in Rcrust using Gibbs free energy minimisation inherited from Perple_X, the dataset of Holland & Powell (2011), and the *a-x* models of Cpx(TH) for clinopyroxene, Gt(TH) for garnet, Opx(TH) for orthopyroxene, Sp(TH) for spinel, and melt(TH) for melt (Tomlinson & Holland, 2021), O(HGP) for olivine (Holland et al., 2018), Fsp(C1) for feldspar (Holland & Powell, 2003), and Ilm(WPH) for ilmenite (White et al., 2000). The capability of Rcrust to allow the investigation of bulk compositional change makes the methodology presented here apt to study partial melting reactions in the upper mantle, followed by investigations of the effects of magma segregation and emplacement at upper crustal levels.

Stellenbosch University https://scholar.sun.ac.za

References

1. Gualda, G.A.R., Ghiorso, M.S., Lemons, R.V. and Carley, T.L. 2012. Rhyolite-MELTS: a Modified Calibration of MELTS Optimized for Silica-rich, Fluid-bearing Magmatic Systems. *Journal of Petrology*, 53(5):875–890.
2. Mayne, M., Moyen, J.-F., Stevens, G. and Kaislaniemi, L. 2016. Rcrust: a tool for calculating path-dependent open system processes and application to melt loss. *Journal of Metamorphic Petrology*, 34(7):663–682.
3. Pertermann, M. and Lundstrom, C.C. 2006. Phase equilibrium experiments at 0.5 GPa and 1100-1300ºC on a basaltic andesite from Arenal volcano, Costa Rica. *Journal of Volcanology and Geothermal Research*, 157:222–235.
4. Tomlinson, E.L. and Holland, T.J.B. 2021. A Thermodynamic model for the subsolidus evolution and melting of peridotite. *Journal of Petrology*, 62(1):egab012.

Stellenbosch University https://scholar.sun.ac.za

CHAPTER 3

PRESENTATION OF RESEARCH PAPER 2

PARTIAL MELTING IN THE MANTLE AND THE POTENTIAL OF PERITECTIC PHASE ENTRAINMENT TO SHAPE MANTLE MAGMA COMPOSITIONS: A PHASE EQULIBRIUM STUDY

This paper, first authored by Tahnee Otto, is in preparation for submission to *Earth and Planetary Science Letters*.

The following aspects of the research were done independently by Tahnee Otto while receiving standard supervision by her supervisors Professor Gary Stevens, Professor Jean-François Moyen, and Dr Matthew J Mayne: (i) conducting thermodynamic modelling; (ii) generation of the figures; (iii) writing of the manuscript.

Stellenbosch University https://scholar.sun.ac.za

Partial melting in the mantle and the potential of peritectic phase entrainment to shape mantle magma compositions: A phase equilibrium study.

Abstract

This study utilises phase equilibrium modelling to investigate partial melting reactions that occur in typical eclogite and peridotite under upper mantle pressure-temperature conditions. The aim of the study is to investigate the stoichiometry of the melting reactions as a function of pressure, temperature, and bulk compositional change due to melt loss. Additionally, the study aims to identify pressure-temperature regions where the partial melting reactions produce peritectic crystal phases that increase in abundance with melt and to investigate the effect of the entrainment of these crystals on the magma composition. The recognition of these areas of peritectic crystal production was achieved by identifying those sections of both isobaric heating and adiabatic decompression pressure-temperature paths that are characterised by an increase in abundance of a solid phase or phases that correspond with an increase in melt volume. The influence of the entrainment of such peritectic crystals on magma composition was investigated by comparing the chemistry of pure melt with that of corresponding magmas comprised of melt and peritectic phase/s. The results indicate a distinct shift in the composition of the extracted magmas with entrained crystals from that of pure melt extractions for both mantle sources, with eclogite partial melting producing up to ~1 wt.% (isobaric) and ~4.5 wt.% (adiabatic) peritectic garnet, clinopyroxene, and spinel, and peridotite partial melting producing peritectic orthopyroxene, olivine, spinel and clinopyroxene, with up to ~6 wt.% and ~13 wt.% peritectic crystals available for entrainment. The resulting magmas plot well within the range of global basalt compositions for the eclogite source and within the larger scatter for the peridotite source, but eclogite partial melts and crystal-bearing magmas display higher Na_2O contents, and peridotite extractions display generally higher MgO and lower Na_2O values, with prominently low Al_2O_3 values for extractions during isobaric heating. Olivine and/or clinopyroxene fractionation can, in some cases, drive the crystal-bearing magma compositions into the denser array of natural basalt compositions, however, this is more likely for melts/magmas derived from the eclogitic source, as extractions from the peridotite source would generally require extensive compositional evolution by some form of alteration process. By combining the trends produced via peritectic crystal entrainment and fractionation, the extent to which these primary melts/magmas can advance to compositionally diverse evolved melts/magmas can be characterised, and when the trends are collinear, the resultant magmas

Stellenbosch University https://scholar.sun.ac.za

are of nearly indistinguishable chemistries. These outcomes highlight how variation/s in the source can produce compositionally diverse primitive melts/magmas, where alteration processes such as fractionation merely amplify this diversity. Additionally, the process of peritectic crystal entrainment may be an important, principal mechanism for incorporating fertile phases to the melt upon segregation from the source that may not be distinguishable from crystal-free melts, considering the ambiguity associated with the extensive compositional range displayed by natural continental basaltic to intermediate rocks.

Keywords: partial melting, phase equilibrium modelling, thermodynamic modelling tools, mantle melt source components, peritectic entrainment

1. Introduction

Understanding how rocks melt and the potential magma compositions that are produced under different circumstances is central to understanding the geological evolution of Earth. In the continental crust, the understanding of partial melting processes and the conditions under which partial melting occurs has greatly benefited from three different lines of research: studies of migmatites that have undergone anatexis and often melt loss, experimental studies of partial melting, and phase equilibrium studies of partial melting (e.g. Cesare et al., 2015; Mayne et al., 2019a; Patiño Douce, 1999). Amongst other things, this collection of work has established the links between different types of source rocks and different types of granitic melts (e.g. Gao et al., 2016; Villaros et al., 2009a); the links between the fluid-state of anatexis, the temperature of partial melting and the chemistry of the magmas (e.g. Mayne et al., 2019a; Stevens & Clemens, 1993); and the importance of source peritectic assemblage entrainment in shaping granitic magma chemistry (e.g. Chappell et al., 1987; Clemens et al., 2011; García-Arias & Stevens, 2017; Stevens et al., 2007).

The partial melting of the mantle unfortunately occurs incognito, and its melt depleted source rocks are seldom well exposed at surface. Along mid-ocean ridges, melting of peridotite due to mantle convection driven decompression is conceptualised within a well-constrained physical and chemical framework (Kushiro, 2001 and references therein; Langmuir et al., 1977). Where mantle melting occurs in association with subduction zones and at within-plate settings, the details of the melting reactions and across what pressure-temperature (P-T) range melting takes place, is less well constrained (e.g. Long et al., 2019; Stern, 2002). The residua produced by melt extraction from the mantle and the source compositions available to undergo partial melting in the upper mantle can be studied by using the rare mantle xenoliths exhumed with mantle-derived magmas when they erupt (e.g. Jacob, 2004; Mathias et al., 1970).

Stellenbosch University https://scholar.sun.ac.za

Experimental investigations utilising these compositions provide insights into the partial melting reactions that occur in mantle sources, as well as the substantial range of mafic to intermediate magma compositions that are produced from partial melting processes. Partial melting experiments, however, are difficult to conduct at mantle P-Ts due to chemical interaction between the charge and PGE-bearing capsule materials (e.g. Brugier et al., 2015; Merrill & Wyllie, 1973), the difficulty of constraining volatile content of capsules that commonly contain a graphite liner (Médard et al., 2008; Merrill & Wyllie, 1973), and issues with quench crystallisation and identification of melt at low degrees of partial melting (e.g. Humphreys et al., 2006; Morgan & London, 1996).

Mafic to intermediate magmas that erupt onto or intrude the crust are principally generated by partial melting of the upper mantle in a variety of tectonic settings (e.g. Arculus, 1994; Grove & Kinzler, 1986; White & McKenzie, 1989, Yoder & Tilley, 1962). The major element chemistry of these primary magmas on leaving their sources must be dictated by the source rock composition, the degree of partial melting, and the mineral assemblage of the residuum. However, the magmas that erupt or intrude the continental crust must reflect both the primary magma compositions and the range of processes that modify the magma compositions after extraction from their sources, such as mixing with other magmas, assimilation of crust, and the removal of crystals (e.g. Langmuir et al., 1977; Reiners, 2002). The mafic to intermediate rocks that result from such magmatism show substantial ranges in major and trace element compositions, as is reflected by the large range of compositions for basaltic to intermediate rocks from continental tectonic environments displayed in Figure 3-1. Overlain by melts from a selection of relevant partial melting studies of eclogitic and peridotitic sources across 15–30 kbar, the plots in Figure 3-1 indicate that the compositions of partial melts determined experimentally are scattered across the global data, however, a number of the natural rock compositions display higher values of Al_2O_3, FeO_t, CaO, and K_2O compared to experimental melts, similarly observed for MgO at relatively high SiO_2. Evidently, experimentally determined partial melts may indicate links to natural rock data, but do not provide much detail regarding source dynamics or the processes of modification. The ultimate interpretation of how much of the compositional variation observed reflects variations in primary magma compositions, and how much reflects magma evolution after leaving the source, is problematic, because the amount of compositional variation that might be expected in the primary magmas is poorly constrained.

Discussed in detail in the following section, several mantle melting studies have identified the formation of small amounts of peritectic phases at a variety of melt fractions

Stellenbosch University https://scholar.sun.ac.za

during incongruent mantle melting processes, with the formation of such new crystals dependant on the P-T conditions and source composition. Considering the ability of mantle-derived melts to entrain solid xenoliths of mantle material, the production of new solid phases is likely to result in the entrainment of some or all of the peritectic crystals to the magma upon separation from the source. Additionally, in light of the established impact of the entrainment of source components in shaping magma compositions in the continental crust, it is reasonable to consider that the entrainment of peritectic phases to mantle-derived partial melts may also play a considerable role in the compositional variation observed for mafic to intermediate rocks. With recent advances in the available thermodynamic databases (e.g. Holland & Powell, 2011) and models for the behaviour of solid-solution and liquid-solution phases (e.g. Holland et al., 2018; Tomlinson & Holland, 2021), a greater range of phase equilibrium modelling approaches are available to study partial melting in the upper mantle, at least to pressures of approximately 60 kbar in volatile-free systems. Different databases and sets of activity-composition (*a*-*x*) models that define the variation in thermodynamic properties of the minerals are available to conduct such modelling. The Rcrust software of Mayne et al. (2016), which uses components of Perple_X (Connolly, 2005) to perform Gibbs free energy minimisation, uses built-in path dependence to deal with changing bulk compositions, and subsequently allows for extraction of melt and crystal phases with the possibility to trigger such extraction events by system characteristics such as melt proportion, or the fact that a phase has increased in abundance (Mayne et al., 2016, 2019b). This makes Rcrust ideally suited for studying the entrainment of peritectic phases to melts upon extraction and the effects of such entrainment on the resulting magma compositions.

This study utilises the Rcrust software and the Holland & Powell (2011) database to define the major element compositional variation that results from sequential melt extractions from eclogitic and peridotitic mantle source rocks undergoing partial melting under upper mantle P-T conditions. The study also identifies the portions of the open system melting P-T paths investigated where peritectic minerals are produced, and finally, constrains the magma (i.e. melt plus crystals) compositions that will be produced by the entrainment of the peritectic crystal fraction to the extracted magma batches. The range in major and trace element compositions produced by the entrainment of peritectic phases to extracted magmas provide important information on the role of mantle source dynamics in producing compositionally diverse primitive melts or magmas, how such diversity is interpreted considering magma alteration processes, and the importance peritectic phase entrainment may have in adding fertile

Stellenbosch University https://scholar.sun.ac.za

phases to magmas extracted from the mantle. Details of the modelling methodology are provided in the relevant section below.

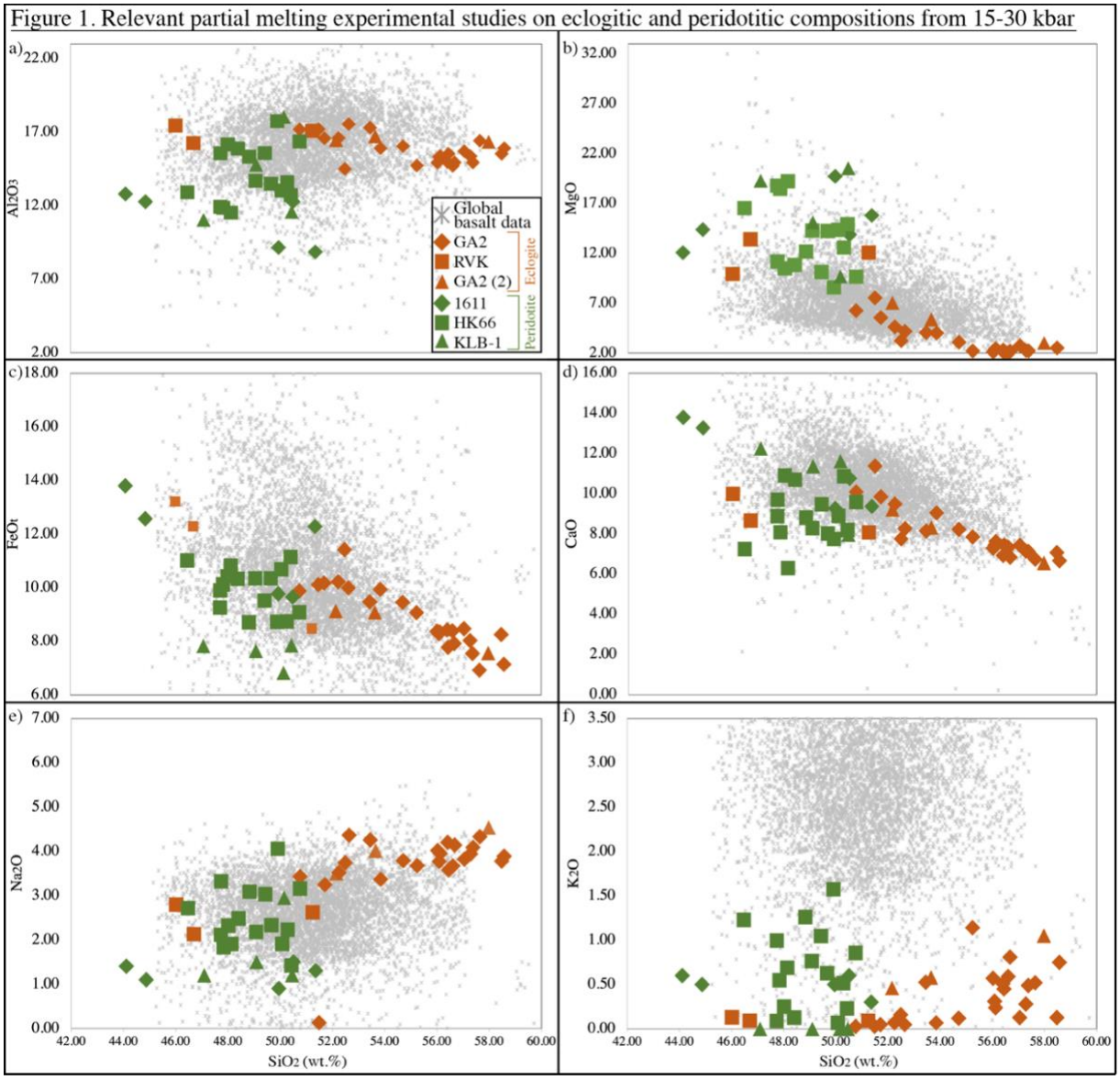

Figure 3-1. Harker diagrams displaying the compositions of quenched melts from relevant partial melting studies of three eclogitic starting compositions (orange) and three peridotitic starting compositions (green) across 15–30 kbar and 1240–1550 ºC, superimposed on a global basalt database compiled from various continental tectonic settings, displayed in grey. Details of the experimental studies and their starting compositions as well as the source and selection criteria of the global basalt database is available in Addendum C. The plots show that the experimental melt compositions are scattered across the global basalt data range. Melt compositions from eclogitic partial melting experiments display great variation in terms of SiO_2 values, but not much variation of other melt components, except for FeO_t. Conversely, melt compositions from peridotitic partial melting experiments do not show much variation in SiO_2 values, but a greater range in values for other components.

2. Partial melting in the shallow sub-continental lithospheric mantle

It is well accepted that the upper mantle is broadly peridotitic (Maaløe & Aoki, 1977, and references therein), and that partial melts that segregated from these ultramafic sources under various conditions produce the diverse compositional range of mafic to intermediate magmas

Stellenbosch University https://scholar.sun.ac.za

that emplace into or erupt on the continental crust. However, mantle xenolith suites from mafic and ultramafic eruptive rocks on many cratons indicate a significant diversity in potential mantle source compositions (e.g. Jacob, 2004; Mathias et al., 1970). Thus, it is perhaps reasonable to consider a wider range of source compositions, including eclogitic sources (e.g. Ito & Kennedy, 1974; Rosenthal et al., 2014). Additionally, it has become clear that in the case of magmas derived from the continental crust, where melting processes are well understood, that the entrainment of components of the source to the melt play a very important role in shaping magma compositions (Dorais & Spencer, 2014; García-Arias & Stevens, 2017). Results from experiments and phase equilibrium modelling studies on migmatites show that crustal melting is dependent on the abundance of high-temperature hydrous minerals in the source, principally biotite and hornblende (e.g. Clemens & Vielzeuf, 1984; Vielzeuf & Schmidt, 2001). The incongruent melting reactions are predominantly temperature dependent and the major additional reactants, quartz and plagioclase, are commonly amongst the most abundant minerals in the rock. In experimental studies, the ratio of H_2O:FeO+MgO is much higher in the melt than in the biotite or hornblende consumed by the reaction. Consequently, a peritectic ferromagnesian mineral or assemblage of minerals must be produced by the incongruent melting reaction, along with either ilmenite or rutile, produced due to the very low solubility of TiO_2 in the melt (e.g. Patiño Douce & Johnston, 1991; Stevens et al., 2007). The incorporation of variable amounts of this peritectic assemblage to granite magmas prior to or during their segregation from the source appears to exercise an important control on the chemistry of the magmas (Clemens et al., 2011; Stevens et al., 2007; Taylor & Stevens, 2010; Villaros et al., 2009a, 2009b), and thus the examination of such a mechanism in mantle melting processes is pertinent.

Experiments on partial melting in the mantle indicate that melting reactions in mantle rocks are less likely to produce large abundances of peritectic crystals relative to melt (e.g. Erdman et al., 2012; Walter, 1998). This reflects the fact that in mantle source rocks, fertility for melt production resides largely in the SiO_2-, Al_2O_3-, and CaO-rich phases (spinel, clinopyroxene, garnet, and orthopyroxene), and the realms of P-T space where a peritectic phase or assemblage will be produced cannot be simply predicted from general stoichiometric considerations, due to the range in mantle mineral phases stabilities across P-T space. For peridotitic sources, the main framework of the rock consists of olivine that may be relatively uninvolved in the partial melting reaction at low degrees of melting. This results in a melting process that preferentially consumes the fertile reactants in the rock, with partial melting mostly, but not certainly, producing a peritectic phase or phases (Figure 3-2), depending on the

Stellenbosch University https://scholar.sun.ac.za

details of the reaction stoichiometry, which is principally governed by the composition of the source as well as the P-T conditions (Niu, 1997, and references therein).

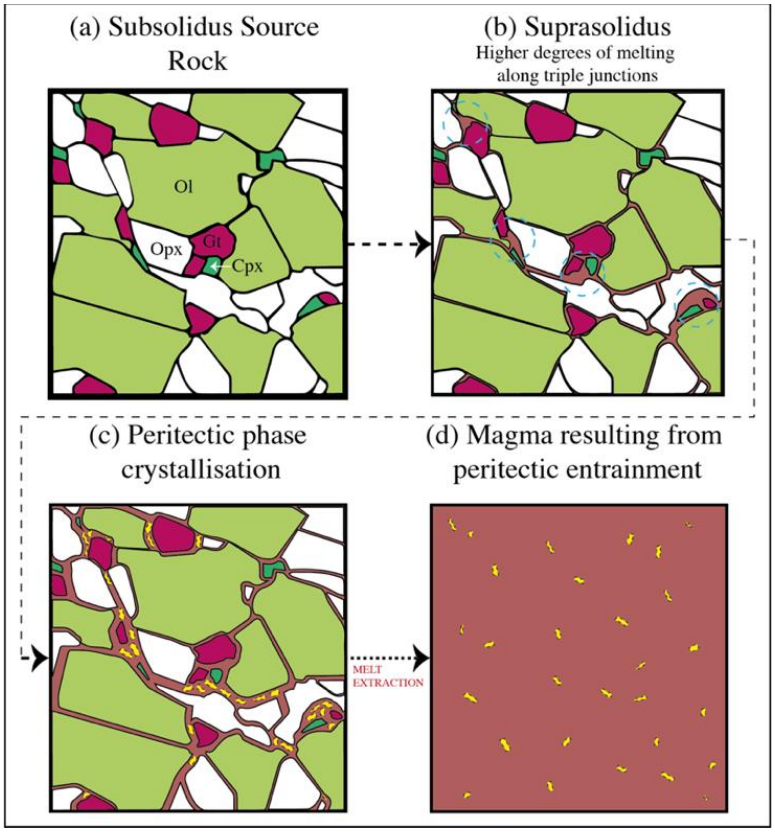

Figure 3-2. A general schematic depicting the sequence of events in the production and entrainment of peritectic phases to the melt during the partial melting of a peridotitic source, with magma extraction. Phases: Cpx: clinopyroxene; Gt: garnet; Ol: olivine; Opx: orthopyroxene. (a) Source rock at subsolidus conditions. (b) Once the solidus is reached, higher degrees of melting (red) occurs along crystal triple junctions where the principal reactants were in contact in the subsolidus rock (circled in dashed blue). (c) The incongruent melting of such reactants result in the formation of peritectic phases suspended within the melt, which may nucleate to form small crystals (yellow). (d) The peritectic crystals suspended within the melt are likely to form part of the magma, due to their small size and proximity to the melting site, on segregation from the source. This will create magmas with chemical compositions reflecting a combination of the mass of segregated melt and the composition and abundance of the entrained crystals (Figure 3-7). This does not only change the composition of the extracted magma, but must also change the composition of the residuum remaining after magma extraction, in turn affecting the future melting behaviour of the now more residual source.

The formation of peritectic phases during incongruent melting of the mantle has been identified by many studies (e.g. Kinzler, 1997; Niu, 1997; Presnall et al., 1978; Tomlinson & Kamber, 2021), and the production of new solid phases at a variety of melt fractions provide ample opportunity for entrainment of such solids to the magma on segregation from the source. During a melt extraction event, the entrainment of some or all of the peritectic crystals produced with the melt is likely for several reasons. Firstly, rapidly ascending mantle-derived melts demonstrably have the capacity to entrain and bring to the surface coherent xenoliths of mantle material (e.g. Jacob, 2004; Mathias et al., 1970). Clearly, such melts should be able to

Stellenbosch University https://scholar.sun.ac.za

entrain small crystals. Secondly, peritectic crystals are produced with melt and the fastest diffusion pathway within the partially molten source is likely through melt (Zhang et al., 2010), so peritectic crystals are likely to grow within the melt (Erdmann et al., 2012; Stevens et al., 2007). Additionally, metasomatism in peridotites is commonly focussed on veins and grain boundaries (Bell et al., 2005; Harte et al., 1993). Thus, fertility for melt (and peritectic crystal) production may commonly also have a spatial arrangement that focuses melt production into discrete zones of the source, favouring magma extraction. In order to investigate the P-T realms where peritectic phase entrainment to mantle melts produced from eclogitic and peridotitic sources is possible in the shallow sub-continental lithospheric mantle (SCLM), as well as the major element consequences of peritectic assemblage entrainment, this study seeks to constrain where in P-T space such phases and assemblages are produced, and to produce thermodynamically constrained models for the consequence of such entrainment on magma chemistry.

3. Modelling Methodology

This study utilised the Rcrust software version 2020-04-19 with the Holland & Powell (2011) dataset to investigate the partial melting of representative eclogitic and peridotitic source rocks (Addendum C), including the effects of compositional change on the stoichiometry of the melting reactions as melt is extracted from the source, as well as the magma compositions that result, particularly those influenced by peritectic mineral entrainment. Modelling runs were performed in the NKCFMASTCr (Na_2O-K_2O-CaO-FeO-MgO-Al_2O_3-SiO_2-TiO_2-Cr_2O_3), volatile-free, chemical system using the 2020 revised hp633ver.dat thermodynamic data file from Perple_X, and the *a-x* models from Holland et al. (2018) (details in Addendum C).

Partial melting investigations were conducted by mapping out phase abundance along isobaric heating paths and adiabatic decompression paths in a batch melting scenario, thereby covering the majority of possible permutations of mantle P-T trajectories. The generation of such plots provide simple, yet powerful tools that can be utilised to identify the reactant assemblage, rate and extent of melting, and the identification of peritectic phase formation. Isobaric heating paths were modelled at set pressures of 15, 20, 25, and 30 kbar, and the abundance of each phase predicted was plotted as a function of temperature with a 2 ºC resolution from the solidus to approximately 1800 ºC, or the liquidus if this was reached at a temperature lower than 1800 ºC. For adiabatic decompression paths, modelling was performed across 45–15 kbar with a 0.2 kbar pressure resolution; starting P-Ts are located below the solidus. To accommodate the heat of melting and subsequent departure of the temperature path

Stellenbosch University https://scholar.sun.ac.za

from the geotherm, the P-T path trajectories after crossing the solidus were modelled to follow a decreasing temperature path displaying the steadiest values of entropy for the bulk system during decompression. This yielded paths with potential temperatures (T_P as defined by Mckenzie & Bickle, 1988) of 1110 ºC for the eclogite, and 1260 ºC and 1450 ºC for the peridotite. For all isobaric and adiabatic paths, the abundance for each phase was plotted as a function of P-T, and any solid phase that increased in abundance above the solidus along the chosen P-T path was considered to be a peritectic phase produced by the incongruent melting reaction. Similarly, a reduction in the abundance of a phase was taken to reflect consumption of the phase by the melting reaction. It is important to note that these considerations are made in terms of the increase or decrease in abundance of the mineral phase/s as a consequence of the melting reaction, as described in Section 4.2., i.e. along decompression paths, phase changes due to pressure-induced mineral stability transitions (e.g. garnet to spinel) are not considered peritectic.

In order to model melt and magma extraction without the need to combine sets of closed system derived data (i.e. pseudosections), Rcrust was chosen as the appropriate software because of its ability to accommodate bulk compositional change due to the path-dependant nature of the Rcrust methodology. This has important implications for the phase diagrams produced and is noted here in order to prevent misinterpretation. In the case of the batch melting investigations, the bulk composition is constant across the entire P-T space of the phase diagrams (Figures 3-3 & 3-4). However, when using Rcrust to model melt segregation, path dependence becomes a feature of the phase diagram due to the open system change in bulk composition. In these diagrams (e.g. Figure 3-7), bulk composition varies with each melt segregation event. Consequently, the phase diagram is relevant only for the P-T path followed in generating the diagram.

To investigate the amount of peritectic phase/s produced along the different P-T paths investigated, the Rcrust ‘Delta’ function was utilised. The Delta function allows the positive change in abundance of a phase (absolute change in abundance in mol.%, vol.%, or wt.%) to be identified for each step along the modelled path. A detailed description of the Delta function can be found in Addendum C. The system was set to allow melt extraction whenever a melt threshold of 5 wt.% was exceeded, with 10% of the original melt content remaining un-extracted, approximating the amount of melt that may be retained on grain boundaries. For example, a P-T point along the isobaric heating path or adiabatic decompression path that registered 5.5 wt.% melt would have resulted in the extraction of 4.95 wt.% melt, with 0.55

Stellenbosch University https://scholar.sun.ac.za

wt.% melt remaining in the system as a grain boundary film. It is important to note that the amount of extracted material is relative to the size of the system at that point, and not the size of the initial starting system.

Peritectic phase entrainment to the melt was modelled in two different ways. Firstly, the software was set to extract only the positive delta of a peritectic phase produced in the previous step before a melt extraction event (for example, along isobaric paths, this would include only deltas produced in the previous 2 °C before the extraction). This is referred to as minimum entrainment magmas and simulates a scenario in which peritectic phases are only preferentially entrained if they are produced recently in the melting path, with subsequent melting reactions and peritectic crystal formation overwriting the crystals that were previously available for entrainment at the melting site. Secondly, the software was set to extract the positive delta of a peritectic phase produced between the current extract and the previous extract (or the solidus if there are no previous extracts). This is referred to as maximum entrainment magmas and simulates a scenario in which peritectic phases continue to be preferentially entrained to the melt long after their formation. In the case of the adiabatic paths, the proportion of peritectic phase that is entrained may be referencing a solidus position which is outside the upper boundary of the pressure interval (30–15 kbar) under investigation in this study.

4. Results

4.1. Application of thermodynamic modelling to analysing the nature of partial melting reactions in the upper mantle.

The data files with the full results of the closed system studies as well as the open system partial melting studies of an eclogite and peridotite using Rcrust thermodynamic modelling are available in Addendum C.

4.1.1. Eclogite

Figure 3-3 presents a P-T pseudosection (i.e. single composition phase diagram) for an average Premier eclogite under anhydrous conditions. The solidus is strongly pressure dependent, with the temperature of the solidus at 30 kbar being 190 ºC above that of the 15 kbar solidus. Low variance assemblage fields are observed close to and next to the solidus, with variance increasing when approaching the Cpx + Melt field at higher temperatures. The P-T window from the solidus to the liquidus is rather constant, displaying a largely uniform rate of melt production as a function of increasing temperature at low pressures. At higher pressures, the rate of melt increase with temperature is reasonably uniform until the Cpx + Gt + Melt field is

Stellenbosch University https://scholar.sun.ac.za

reached, where the melt fraction increases more strongly as a function of temperature towards the garnet-out phase boundary. Thereafter, a more uniform melt production rate is observed again at higher temperatures.

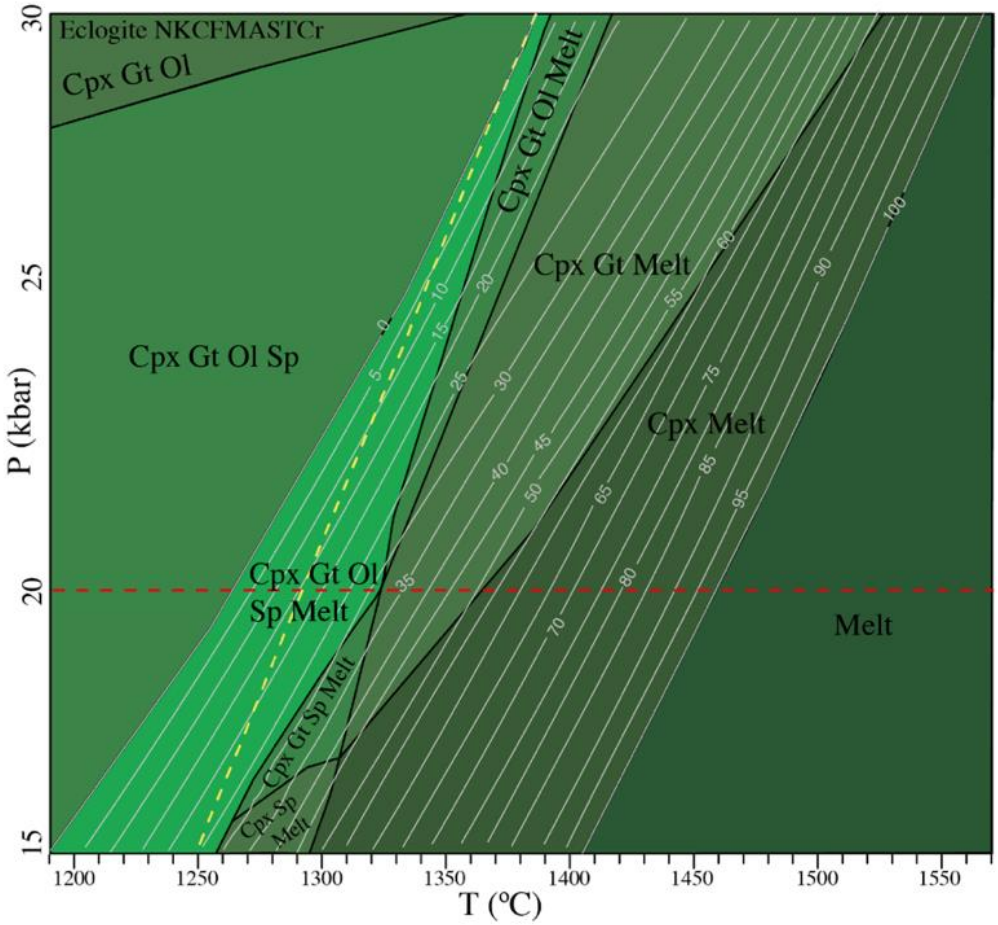

Figure 3-3. P-T pseudosection for an average Premier eclogite in the NKCFMASTCr system. Phases: Cpx, clinopyroxene; Gt, garnet; Melt, melt; Ol, olivine; Sp, spinel. Clinopyroxene is stable throughout all pressures and temperatures below the liquidus. The abundance of melt in wt.% is indicated as grey contours, with the solidus reached at 1190 ºC at 15 kbar, and 1380 ºC at 30 kbar. The liquidus is reached just below 1410 ºC at 15 kbar, and shortly before 1570 ºC at 30 kbar. The horizontal dashed line (red) at 20 kbar indicates an example of an isobaric heating path, and the oblique dashed line (yellow) indicates an example of an adiabatic decompression path. Analysis of such paths produced during the investigation of eclogite partial melting are reviewed in detail below.

4.1.2. Peridotite

Figure 3-4 presents a P-T pseudosection for a Premier peridotite under anhydrous conditions. It is important to note that the temperatures above 1590 ºC are displayed in Figure 3-4 to illustrate the production of a peritectic spinel phase at higher temperatures, however the attainment of such temperatures would require exceptional circumstances.

The stable phase assemblage before/at the solidus is strongly pressure dependant below 20 kbar, which has a distinct influence on the stoichiometry of the melting reaction along isobaric heating paths. Consequently, the solidus is also strongly pressure dependant, requiring a temperature increase of 200 ºC from the solidus temperature at 15.5 kbar before melting

Stellenbosch University https://scholar.sun.ac.za

commences at 30 kbar. The P-T window from the solidus to 75 wt.% melt is not constant across the pressure envelope; a large initial rise in temperature is required from the solidus to reach 5 wt.% melt, and thereafter the rate of melting changes depending on the stable phases and the pressure.

Several low variance fields are observed next to the solidus below 20 kbar, with higher variance from the Opx + Ol + Melt field to the Ol + Melt field present at higher temperatures. At low pressure, the presence of spinel stabilises several additional fields across a small temperature interval of approximately 100 ºC. Spinel re-enters the system at higher temperatures, stabilising two additional fields that span the entire pressure interval investigated. At low pressures, this Ol + Sp + Melt field is stable over a small temperature interval of < 30 ºC, whereas high pressure melting indicates a slightly larger temperature interval.

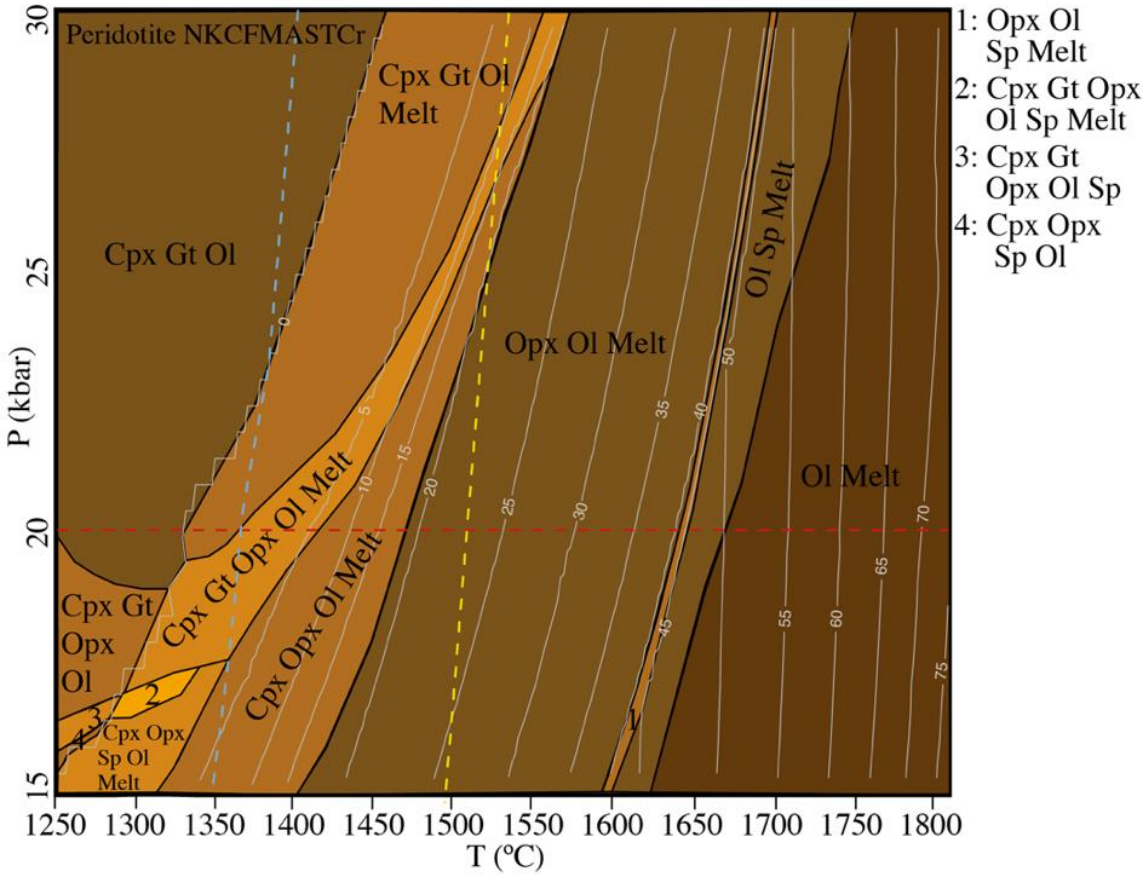

Figure 3-4. P-T pseudosection for a Premier peridotite in the NKCFMASTCr system. Phases: Cpx, clinopyroxene; Gt, garnet; Melt, melt; Ol, olivine; Opx, orthopyroxene; Sp, spinel. Olivine is stable throughout all P-Ts. The abundance of melt in wt.% is indicated as grey contours, with the solidus reached at 1250 ºC at 15.5 kbar, and 1450 ºC at 30 kbar. The liquidus is not reached in the entire pressure envelope investigated. Note the enhanced melt production as a function of increasing temperature as garnet and then clinopyroxene react out, followed in an even more marked fashion by orthopyroxene. The horizontal dashed line (red) at 20 kbar indicates an example of an isobaric heating path, and the oblique dashed lines (blue and yellow) indicate examples of adiabatic decompression paths. Analysis of such paths produced during the investigation of peridotite partial melting are reviewed in detail in the next section.

Stellenbosch University https://scholar.sun.ac.za

4.2. Interpretation of the melting reactions

Phase equilibrium modelling provides valuable information on the stoichiometry of the partial melting reactions in its simplest form, which can be read directly from plots of phase abundance along isobaric heating sections, and phase abundance along adiabatic decompression paths. Figure 3-5a displays an isobaric heating path for the eclogite source and Figure 3-6a to b for the peridotite source, both at a set pressure of 20 kbar; adiabatic decompression paths are displayed in Figure 3-5b for the eclogite source (T_P = 1110 ºC) and Figure 3-6c for the peridotite source (T_P = 1260 ºC).

4.2.1. Eclogite

Consider Figure 3-5a, where field (i) indicates the mineral proportion changes during subsolidus heating of the eclogite source. In field (ii), from the solidus, melting is strongly incongruent with clinopyroxene, minor olivine, and spinel being consumed, and peritectic garnet being produced. In field (iii), peritectic garnet production ceases, the rate of clinopyroxene consumption decreases as a function of increasing temperature, and garnet also starts to be consumed. Spinel and olivine are exhausted by the melting reaction in this field. The high temperature boundary of field (iii) is marked by a sharp jump in melt fraction with corresponding decreases in clinopyroxene and garnet. In field (iv), garnet is consumed at a greater rate than clinopyroxene until it is exhausted, and in field (v) the melting reaction consumes only clinopyroxene. The melting reactions for each identified section can thus be interpreted based on the consumption and production of phases from the solidus in Figure 3-5a: (ii) cpx + ol + sp = gt + melt; (iii) cpx + gt + ol + sp = melt; (iv) cpx + gt = melt; and (v) cpx = melt.

This analysis can also be performed along an adiabatic decompression path of the eclogite source, with phase abundance versus P-T decrease displayed in Figure 3-5b. Here, field (ii) indicates the consumption of garnet and olivine as the melt fraction increases, resulting in the formation of peritectic clinopyroxene (ii & iv) and peritectic spinel (ii-iv). Clinopyroxene is consumed in (iii), whereas garnet and olivine are exhausted by 15 kbar. Unlike the isobaric path, no peritectic garnet is formed, and the melting reactions from the solidus for each identified section in Figure 3-5b can be defined as follows: (ii) gt + ol = melt + cpx + sp; (iii) gt + ol + cpx = melt + sp, and; (iv) gt + ol = melt + cpx + sp.

Stellenbosch University https://scholar.sun.ac.za

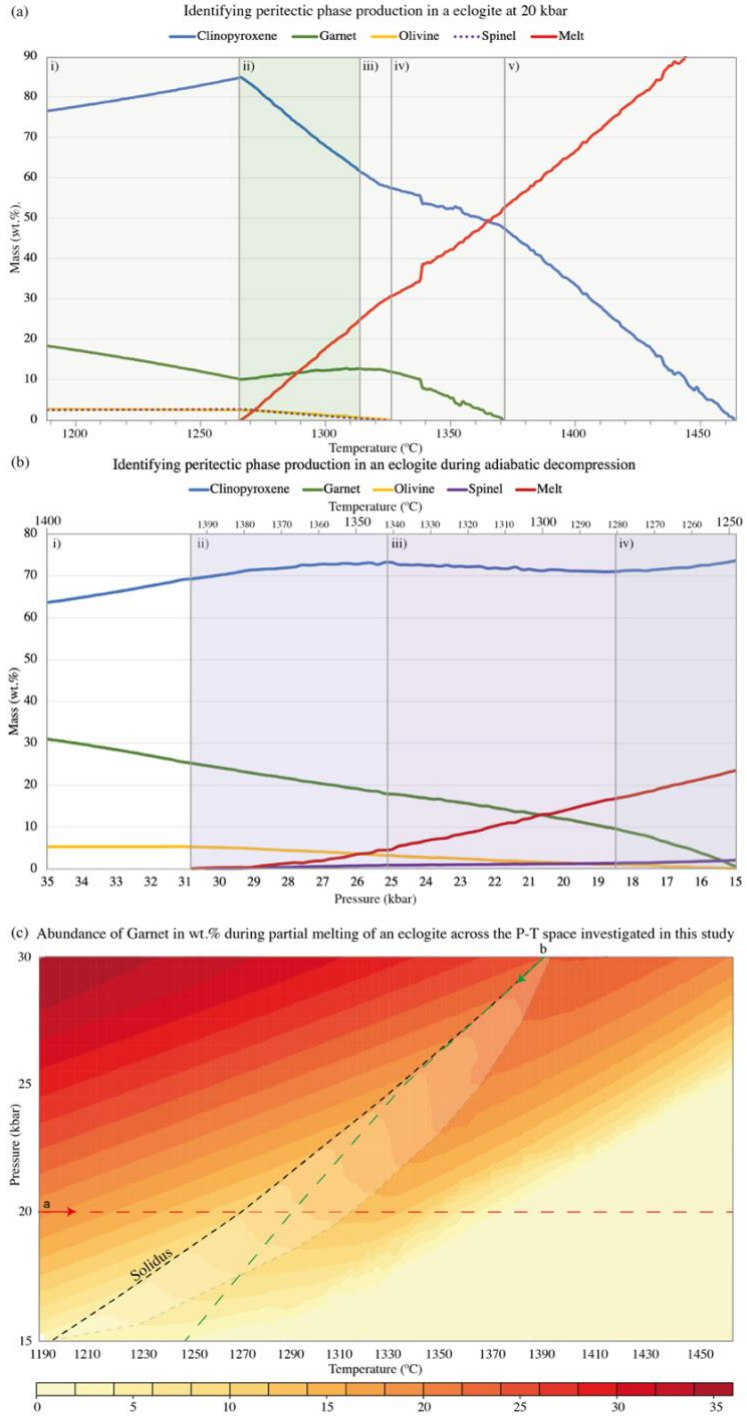

Figure 3-5. a) Isobaric heating path displaying phase abundances as a function of increasing temperature at 20 kbar for an eclogitic source. b) Adiabatic decompression path (T_P = 1110 ºC) displaying phase abundances as a function of P-T for an eclogitic source. Fields in a) and b) with roman numerals serve to distinguish P-T fields defined by consistent partial melting reaction stoichiometry, as discussed in-text, and coloured fields display areas of peritectic phase production. c) The abundance of garnet in wt.% over the P-T range investigated. The black dashed line indicates the solidus, and the transparent, shaded area extending up-temperature from the solidus displays the area of peritectic garnet production for paths that are dominated by temperature increase. The red dashed line at 20 kbar indicates the location of the isobaric heating path in a). Note that pressure, predictably, strongly controls the amount of garnet in the assemblage, but the solidus marks an increase in garnet abundance with heating at any pressure, and this increase represents the production of garnet as a peritectic product of the melting reaction for heating paths. The green dashed line indicates the location of the adiabatic decompression path in b). Here, no peritectic garnet is produced, as garnet mode decreases as melt fraction increases.

Stellenbosch University https://scholar.sun.ac.za

4.2.2. Peridotite

A similar analysis was again applied to the peridotitic source (Figure 3-6). The isobaric path (Figure 3-6a to b) displays the consumption of olivine and garnet from the solidus at 1345 ºC in field (ii). From 1365 ºC, orthopyroxene is produced as a peritectic phase and from approximately 1390 ºC, clinopyroxene begins to be consumed as the rate of melting increases (iii). At very low melt fractions, the abundance of peritectic orthopyroxene is almost negligible, but increases rapidly as garnet is exhausted, surpassing the amount of melt that is produced and increasing more rapidly as clinopyroxene is completely consumed (iv). Peritectic orthopyroxene formation reaches its peak at 1465 ºC, after which its abundance starts to decrease at a relatively uniform rate (v). Olivine is continuously consumed at a slow rate throughout the melting interval. Section (vi) displays several interactions in the system: (1) orthopyroxene is rapidly consumed, which leads to (2) a rapid increase in melt abundance, as well as the formation of (3) peritectic olivine and (4) a very small abundance of peritectic spinel (Figure 3-6b). Once orthopyroxene is exhausted, peritectic olivine and peritectic spinel formation ceases, and the phases are consumed. Note that the rate of melting decreases over the small temperature interval where olivine is once again consumed. As mentioned, the temperatures throughout fields (vi) to (vii) are only displayed as additional commentary on the incongruent partial melting reactions of the peridotite. The melting reactions from the solidus for each identified field in Figure 3-6a are as follows: (ii) ol + gt = melt; (iii) ol + cpx + gt = melt + opx; (iv) ol + cpx = melt + opx; (v) ol + opx = melt; (vi) opx = melt + ol + sp; and (vii) ol ± sp = melt.

Considering the adiabatic decompression path of the peridotite (Figure 3-6c), field (ii) displays the consumption of garnet after the solidus, with peritectic clinopyroxene forming. Olivine is consumed slowly, remaining relatively uninvolved in the reaction throughout the pressure range investigated. In fields (iii) to (iv), clinopyroxene is, for the most part, consumed with olivine and garnet (which is exhausted in (iii)), prompting the production of peritectic orthopyroxene at a greater rate than the generation of melt. The melting reactions from the solidus for each identified field in Figure 3-6c are as follows (ii) ol + gt = melt + cpx; (iii) ol + gt + cpx = melt + opx; and (iv) ol + cpx = melt + opx.

Stellenbosch University https://scholar.sun.ac.za

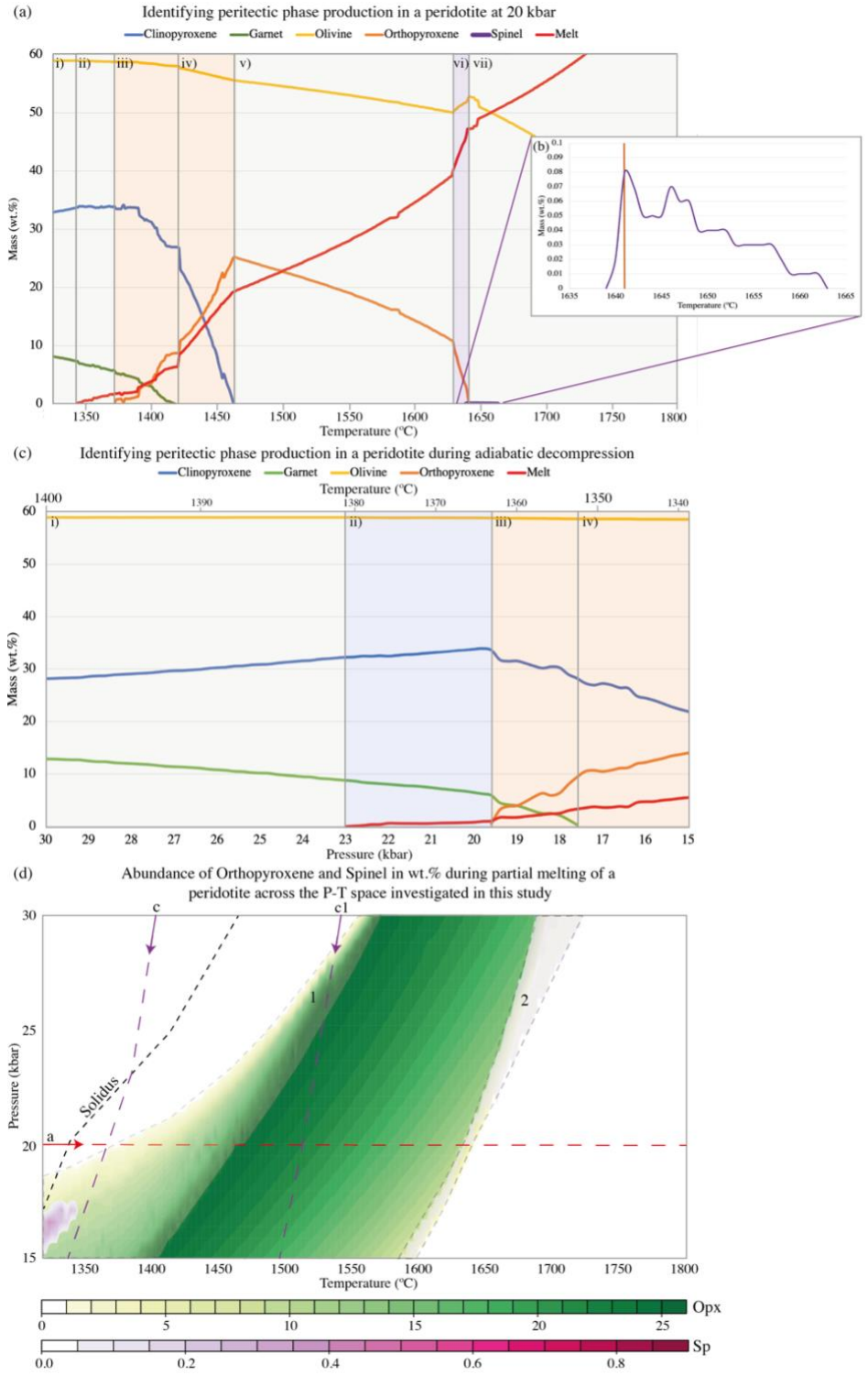

Figure 3-6. a) Isobaric path at 20 kbar through the peridotite pseudosection displaying phase abundances as a function of increasing temperature, with b) highlighting the change in abundance of spinel. c) Adiabatic decompression path (T_P = 1260 ºC) displaying phase abundances as a function of P-T for a peridotitic source. Fields in a) and b) labelled with roman numerals serve to distinguish P-T fields defined by consistent partial melting reaction stoichiometry, as discussed in-text, and coloured fields display peritectic phase production. d) The abundance of orthopyroxene (green) and spinel (pink) in wt.% across the P-T range investigated. The black dashed line indicates the solidus, and the transparent, shaded fields identify the areas of production of peritectic orthopyroxene (1) and peritectic spinel (2). Similar to the eclogite, pressure strongly controls the amount of orthopyroxene and spinel in the assemblage. As pressure increases, the solidus moves away from the peritectic orthopyroxene field low temperature boundary, indicating that some melting occurs before peritectic

Stellenbosch University https://scholar.sun.ac.za

orthopyroxene starts to form. The red dashed line at 20 kbar indicates the location of the isobaric heating path in a). Along this path, after some melting has occurred, an increase in orthopyroxene abundance is observed with heating, representing the production of orthopyroxene as a peritectic product of the melting reaction. A great amount of heating is required before an increase in spinel abundance is observed, and the production of small amounts of spinel as a peritectic product of the melting reaction accompanies a much higher degree of melting. The purple dashed lines indicate the locations of the adiabatic decompression paths, including the path in c), as well as one additional path, c1 (T_P = 1450 ºC). Both c and c1 cross the peritectic orthopyroxene field, and path c displays continuous peritectic orthopyroxene production below 20 kbar. Path c1 produces peritectic clinopyroxene with melt, with clinopyroxene consumption starting slightly before peritectic orthopyroxene starts to form just above 27 kbar. As displayed in d), orthopyroxene consumption starts from approximately 25 kbar.

By examining the phase abundance plots displayed in Figure 3-5a to b and Figure 3-6a to c, it is clear that interpreting phase abundance along isobaric heating paths and adiabatic decompression paths in combination with information from P-T sections provides an efficient way of broadly defining the stoichiometry of the melting reactions, and the areas of P-T space where the incongruency of the relevant melting reaction produces a peritectic phase or phases.

4.3. Interpretation of melt and magma extraction

Melt and magma extraction was achieved using the methodology defined in the introductory sections, and as examples, the 20 kbar isobaric heating paths are illustrated in the phase abundance plots displayed in Figure 3-7a and b. The differences in partial melting behaviour when compared to the batch melting exercises illustrated in Figure 3-5a and Figure 3-6a result from the change in source composition, occurring due to melt extraction from the source. In Figure 3-7, the superimposed stacked column plots display each extraction event in terms of the abundance of melt, and where applicable, the amount of the entrained peritectic phase. Figure 3-7a displays the extraction of melt or magma from an eclogitic source; extraction steps 1, 2, 4, 5 and 7 involve entrained peritectic crystals (in all cases garnet, except for step 7 where clinopyroxene is the peritectic phase). Extractions at temperatures above step 7 involve melt only. It is important to note that the consumption of garnet by the melting reaction from step 7 onwards occurs over a greater temperature interval than in a closed system. Thus, predictably, the melting interval involving garnet breakdown is increased by the loss of fertile components that would generally flux melting. Figure 3-7b displays the extraction of melt or magma from a peridotitic source; extraction steps 1 to 4 and 6 to 10 involve entrained peritectic crystals, with orthopyroxene entrained in steps 1–4, olivine in step 6, spinel in step 7, and a peritectic assemblage of olivine and spinel in steps 8–10. The extraction at step 5 involved melt only. Similarly to the eclogite, the consumption of orthopyroxene by the melting reaction at temperatures above the range of peritectic orthopyroxene production occurs over a greater temperature interval compared to the closed system.

Stellenbosch University https://scholar.sun.ac.za

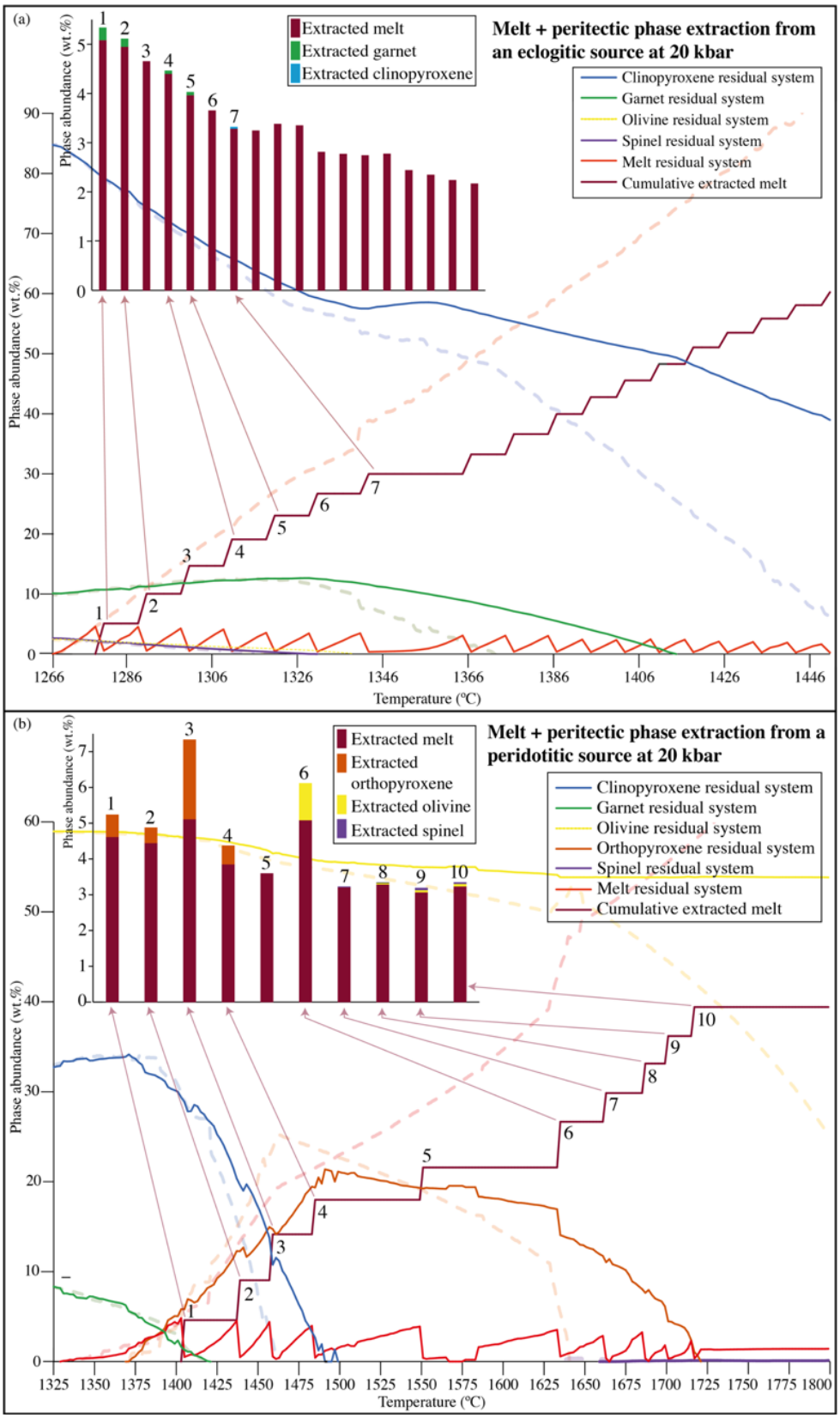

Figure 3-7. Isobaric heating paths showing phase abundance in the source and extracted melts and magmas as a function of temperature at 20 kbar, as a result of incremental extraction from the eclogitic (a) and peridotitic (b) sources. For comparison, the phase abundance changes from Figure 3-5a and Figure 3-6a are displayed as transparent, dashed lines. In these plots, the amount of peritectic material available for entrainment is considered to only be that which is produced in the 2 ºC temperature step preceding the extraction event, i.e. the minimum entrainment magmas discussed in the Methodology.

Stellenbosch University https://scholar.sun.ac.za

5. Discussion

Figures 3-8 to 3-11 display the range of melt and peritectic crystal-bearing magma compositions produced in this study, superimposed on the global basalt dataset as is first introduced in Figure 3-1. Crystal-bearing magma compositions plot along the tie-lines between melt only and phase only compositions, with their compositional range lying between the melt devoid of any crystals and the magma that would result from the entrainment of all of the available peritectic crystals (maximum entrainment magmas). Compositions of minimum entrainment magmas are also plotted, illustrating that the extent of the effects of phase entrainment on the resulting magma compositions are influenced by both the composition and amount of the entrained phase, i.e. the movement of magmas in compositional space as a function of the entrainment process. The amount of crystals that are entrained to the melt at any given point may be controlled by several factors, such as the P-T conditions, melt volume, the rate of melting, deformation during melting, etc. The results in this study show that, during partial melting of the eclogite, up to 0.85 wt.% (isobaric heating; Figure 3-8) and 4.47 wt.% (adiabatic decompression; Figure 3-10) peritectic crystals of either garnet, clinopyroxene or spinel, or a combination thereof, can be entrained to the melt. For the peridotite, a maximum of 6.25 wt.% (isobaric heating; Figure 3-9) and 12.94 wt.% (adiabatic decompression; Figure 3-11) peritectic crystals of either orthopyroxene, olivine, spinel or clinopyroxene, or a combination thereof, are available for entrainment to the melt.

Figures 3-12 and 3-13 serve as summary plots of Figures 3-8 to 3-11, displaying the maximum entrainment magma compositions as well as accompanying melts that did not entrain any peritectic crystals (individually indicated in Figures 3-8 to 3-11), and magma compositions extracted during a partial melting scenario where peritectic crystals are not considered, i.e. all extractions are pure melts. As compared to extractions of pure melts, it is clear that the entrainment of peritectic phase/s to the melt will affect the resulting magma chemistry, as well as the chemical evolution of the residual system (e.g. Figure 3-7). Importantly, the crystal-bearing magmas extracted from both sources at reasonable temperatures plot close to, and regularly within, the large range of values for basaltic rocks from continental tectonic environments, but their behaviour varies depending on the P-T path followed. The evolution of pure melt extractions along isobaric heating follow a discernible linear trend, as expected. For the eclogite, maximum entrainment magmas and accompanying crystal-devoid magmas mostly follow a similar evolution to that of the pure melts (Figure 3-12), likely as a result of the low amounts of peritectic crystals produced during the partial melting process, where phase

Stellenbosch University https://scholar.sun.ac.za

entrainment would not result in great compositional change. However, lower melt fractions plot compositions with higher values of Na_2O. For the peridotite, none of the extractions considering maximum entrainment are devoid of crystals, i.e. there are no extractions where peritectic phases are not produced during the decompression path. These maximum entrainment magmas evolve differently to the pure melt extractions from the peridotite source, remaining largely within the scattered area of global basalt compositions, although also increasing overall in SiO_2 character.

Along an adiabatic decompression path, pure melts extracted during partial melting of the eclogitic source also follow a linear trend (Figure 3-13), plotting within the denser cloud of global basalt compositions, and again displaying higher Na_2O values. For maximum entrainment magmas, an increase in SiO_2 is displayed, consequently evolving the compositions into the denser basalt array. Pure melts extracted during partial melting of the peridotite source do not evolve linearly, with the higher P-T extractions plotting within the denser array of the global basalt data and evolving to more ultramafic compositions as the P-T decreases. Maximum entrainment magmas extracted from the peridotite at higher P-Ts are more ultramafic in nature, becoming more SiO_2-rich at lower P-Ts; this is the opposite behaviour of that observed for pure melt extractions. For both the eclogitic source and peridotitic source, none of the extractions along adiabatic decompression paths that consider a maximum entrainment scenario are devoid of crystals. From the above, it is clear that variability in the amount of the entrained phases introduce great amounts of magma compositional heterogeneity whilst being derived from the same individual source rocks, even if these sources are generally considered homogenous.

Stellenbosch University https://scholar.sun.ac.za

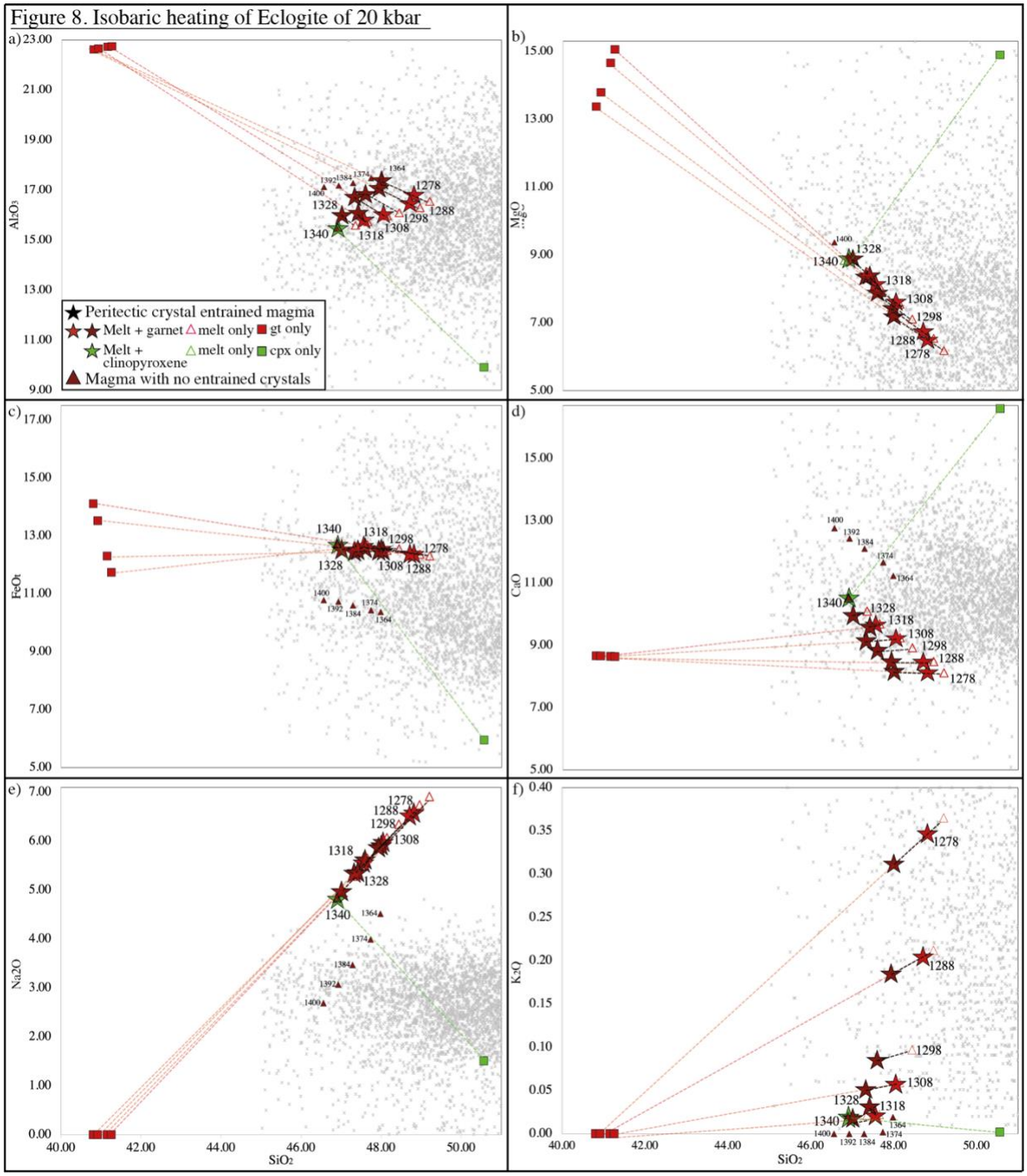

Figure 3-8. Harker diagrams showing the compositions of the magmas derived from the modelled extraction events during partial melting of an eclogite at 20 kbar along an isobaric path, superimposed on a global basalt database. Minimum entrainment magma compositions are displayed in threefold, connected by a dotted line: the bulk composition of melt and peritectic phase is displayed using red (garnet entrainment) and green (clinopyroxene entrainment) stars; the compositions of the associated melt only is displayed using triangles; the compositions of the peritectic phases only are displayed using squares. Maximum entrainment magma extractions are displayed as magma compositions only (maroon stars for garnet). The temperature of each extraction is listed alongside the melt marker. Extraction steps where no peritectic phase has been entrained are displayed as maroon triangles. All oxides display similar patterns, with magma evolution along decreasing SiO_2. The plots for MgO and FeO display a more pronounced variation in the composition of the entrained garnet phase, but for Al_2O_3, CaO, Na_2O, and K_2O, these compositions vary mainly in SiO_2 content. The evolution of the residual system when the maximum amount of the available peritectic phase is entrained results in two additional garnet entrained magma extractions at 1298 ºC and 1328 ºC, as well as several crystal-devoid extractions as indicated.

Stellenbosch University https://scholar.sun.ac.za

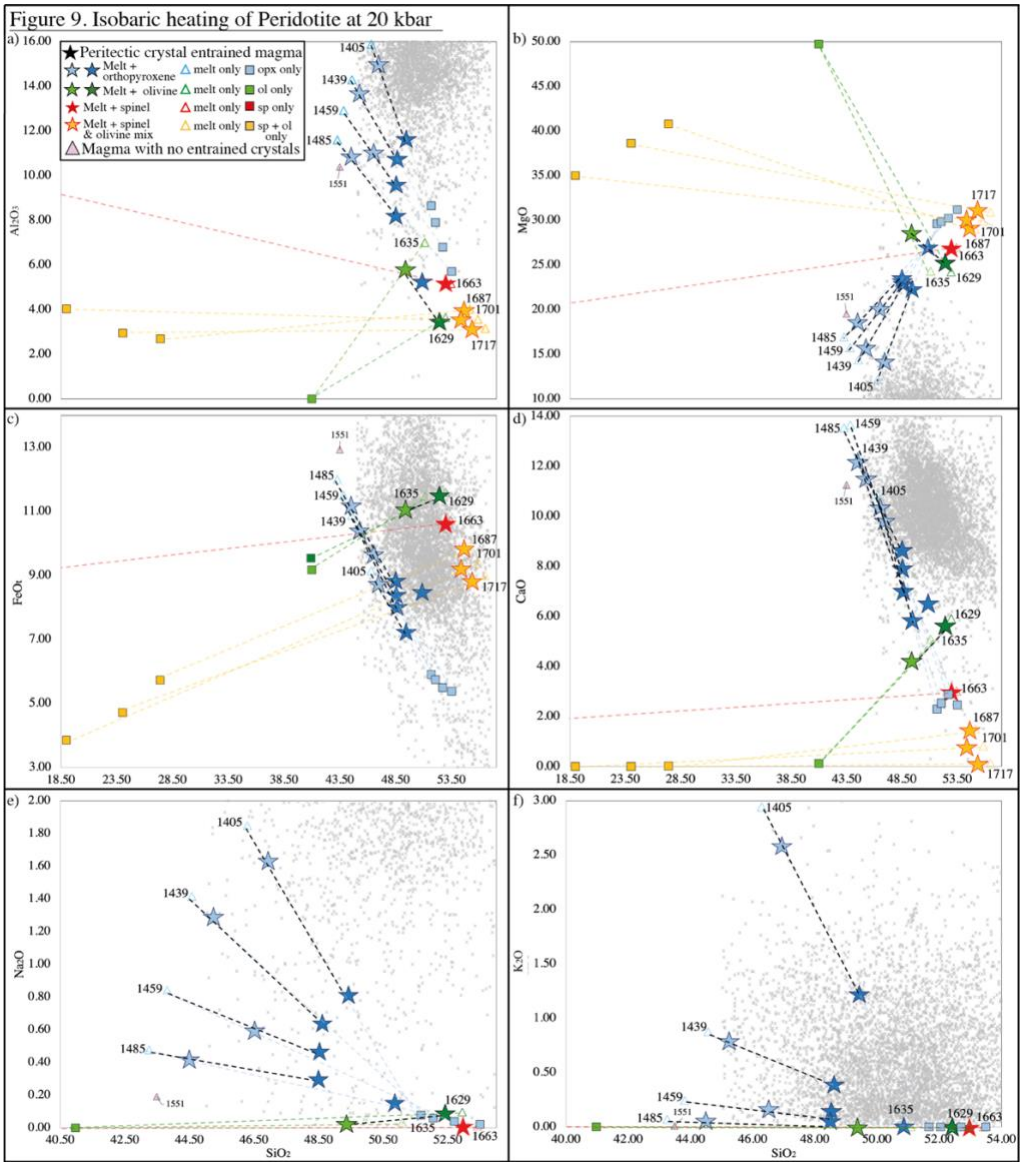

Figure 3-9. Harker diagrams showing the compositions of the magmas derived from the modelled extraction events during partial melting of a peridotite at 20 kbar along an isobaric path, superimposed on a global basalt database. Minimum entrainment magma compositions are displayed in threefold, connected by a dotted line: the bulk composition of melt and peritectic phase is displayed using blue (orthopyroxene entrainment), green (olivine entrainment), red (spinel) and yellow (spinel and olivine mix) stars; the compositions of the associated melt only is displayed using triangles; the compositions of the peritectic phases only are displayed using squares. Maximum entrainment magma extractions are displayed as stars of magma compositions only (dark blue for orthopyroxene; dark green for olivine). The temperature of each extraction is listed alongside the melt marker. Extraction steps where no peritectic phase has been entrained are displayed as pink triangles. Extractions at 1687 ºC, 1701 ºC and 1717 ºC for Na_2O and K_2O have not been displayed, as the values cluster at zero and display very small increases in SiO_2. The plots show systematic evolution of the extracted magma compositions, with the SiO_2 content of the compositions displaying variable intervals of increase and decrease, after which SiO_2 continuously increases for all extraction events that follow. Both FeO and CaO follow the same pattern for their evolution, initially increasing during early extractions followed by a constant decrease; MgO displays the opposite of FeO, increasing throughout all extraction events. In turn, Al_2O_3 displays the opposite of MgO. Generally minor variations are displayed in orthopyroxene-only phase compositions (except for Al_2O_3), but great variation is displayed in the compositions of the magma extractions entraining the minimum or the maximum amount of peritectic orthopyroxene from their melt only counterparts. Later extractions with minor amounts of a peritectic spinel and olivine mixture display more extensive phase compositional variations, but a less pronounced effect on the bulk compositional variation of the magma.

Stellenbosch University https://scholar.sun.ac.za

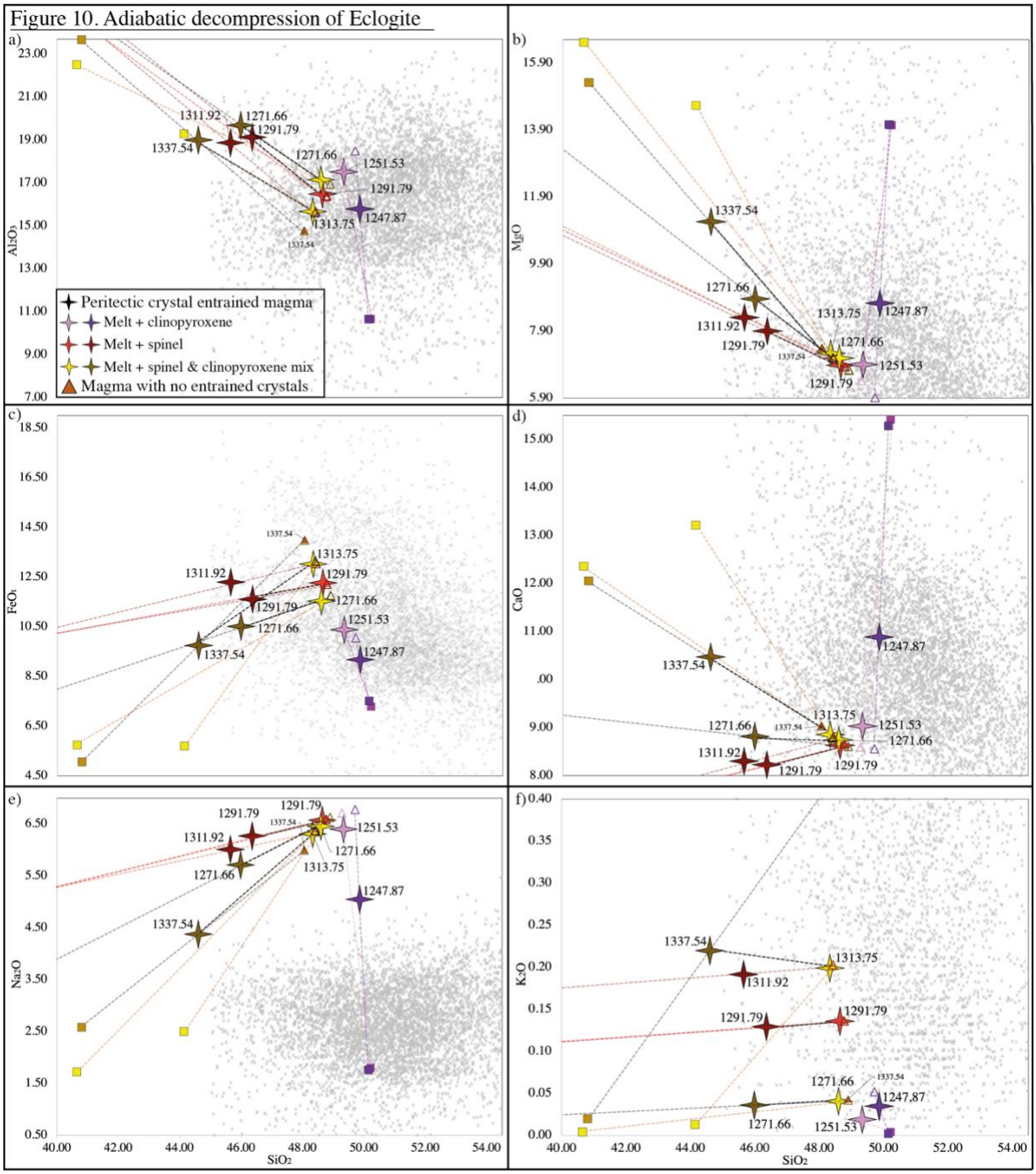

Figure 3-10. Harker diagrams showing the compositions of the magmas derived from the modelled extraction events during partial melting of a eclogite during adiabatic decompression, superimposed on a global basalt database. Minimum entrainment magma compositions are displayed in threefold, connected by a dotted line: i) the bulk composition of melt and peritectic phase is displayed using pink and purple (clinopyroxene entrainment), red and maroon (spinel entrainment) and yellow and brown (clinopyroxene and spinel entrainment) compass stars, with the darker colours representing maximum entrainment magmas; ii) the compositions of the associated melt only is displayed using triangles, and; iii) the compositions of the peritectic phases only are displayed using squares. The temperature of each extraction is listed alongside the melt marker. Extraction steps where no peritectic phase has been entrained is displayed as orange triangles. Magma evolution is different from that in Figure 3-8, with minimum entrainment magmas evolving along increasing SiO_2, however phase entrainment evolves the system to lower SiO_2 values. Evolution of the residual system when the maximum available amount of the peritectic phase is entrained results in an additional spinel entrained magma extraction at 1311.92 ºC, indicated as a lone compass star.

Stellenbosch University https://scholar.sun.ac.za

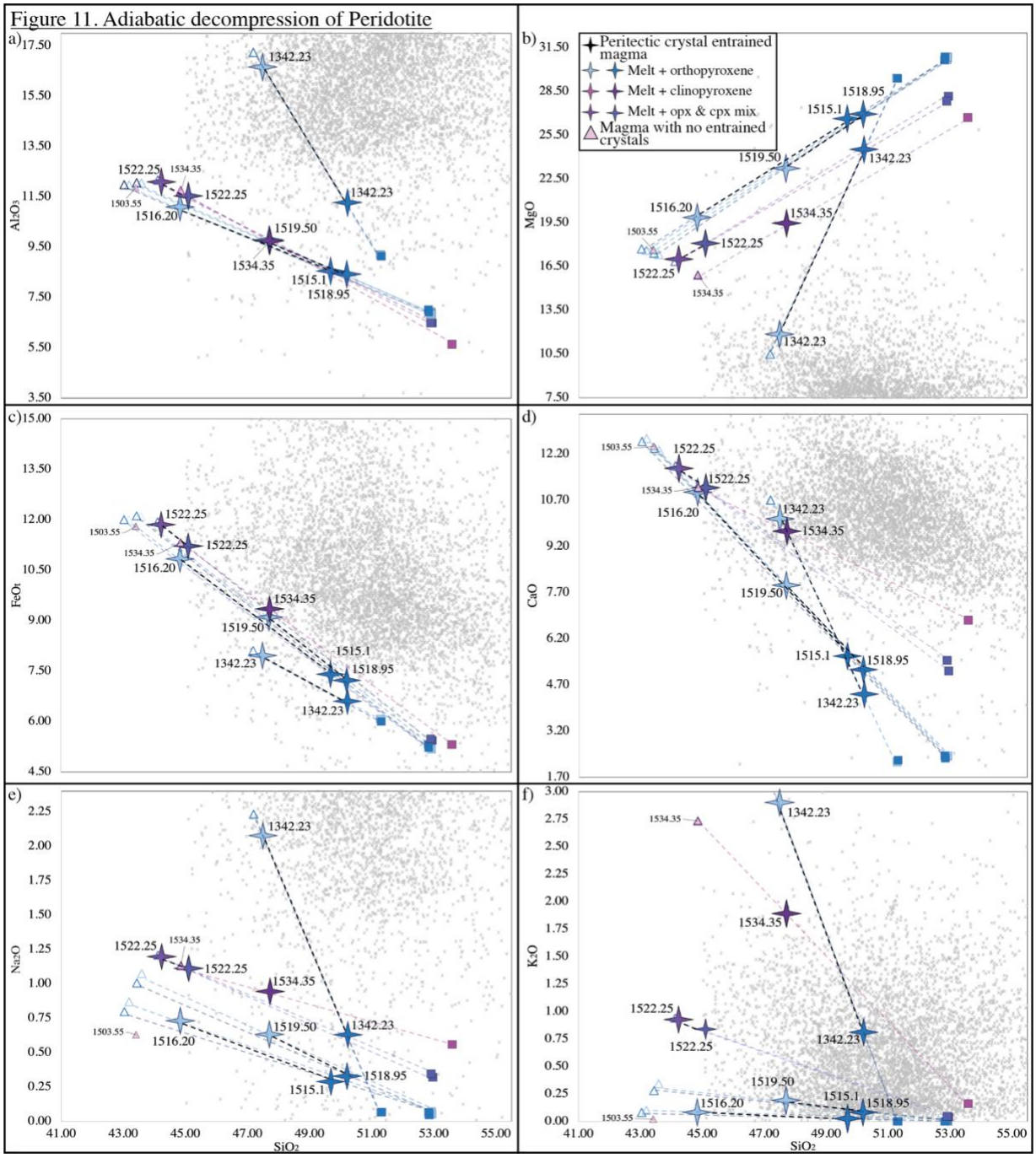

Figure 3-11. Harker diagrams showing the compositions of the magmas derived from the modelled extraction events during partial melting of a peridotite during adiabatic decompression, superimposed on a global basalt database. Magma compositions are displayed in threefold, connected by a dotted line: i) the bulk composition of melt and peritectic phase is displayed using light blue and dark blue (orthopyroxene entrainment), mauve (clinopyroxene entrainment), and light purple and dark purple (orthopyroxene and clinopyroxene mix) compass stars, with the lighter colours representing minimum entrainment magmas and the darker colours representing maximum entrainment magmas; ii) the compositions of the associated melt only is displayed using triangles and; iii) the compositions of the peritectic phases only are displayed using squares. The temperature of each extraction is listed alongside the melt marker. Extraction steps where no peritectic phase has been entrained is displayed as pink triangles. The plots display systematic evolution of the melt only compositions, evolving along decreasing SiO_2. Minimum and maximum entrainment extractions evolve all magmas to higher SiO_2 values.

Stellenbosch University https://scholar.sun.ac.za

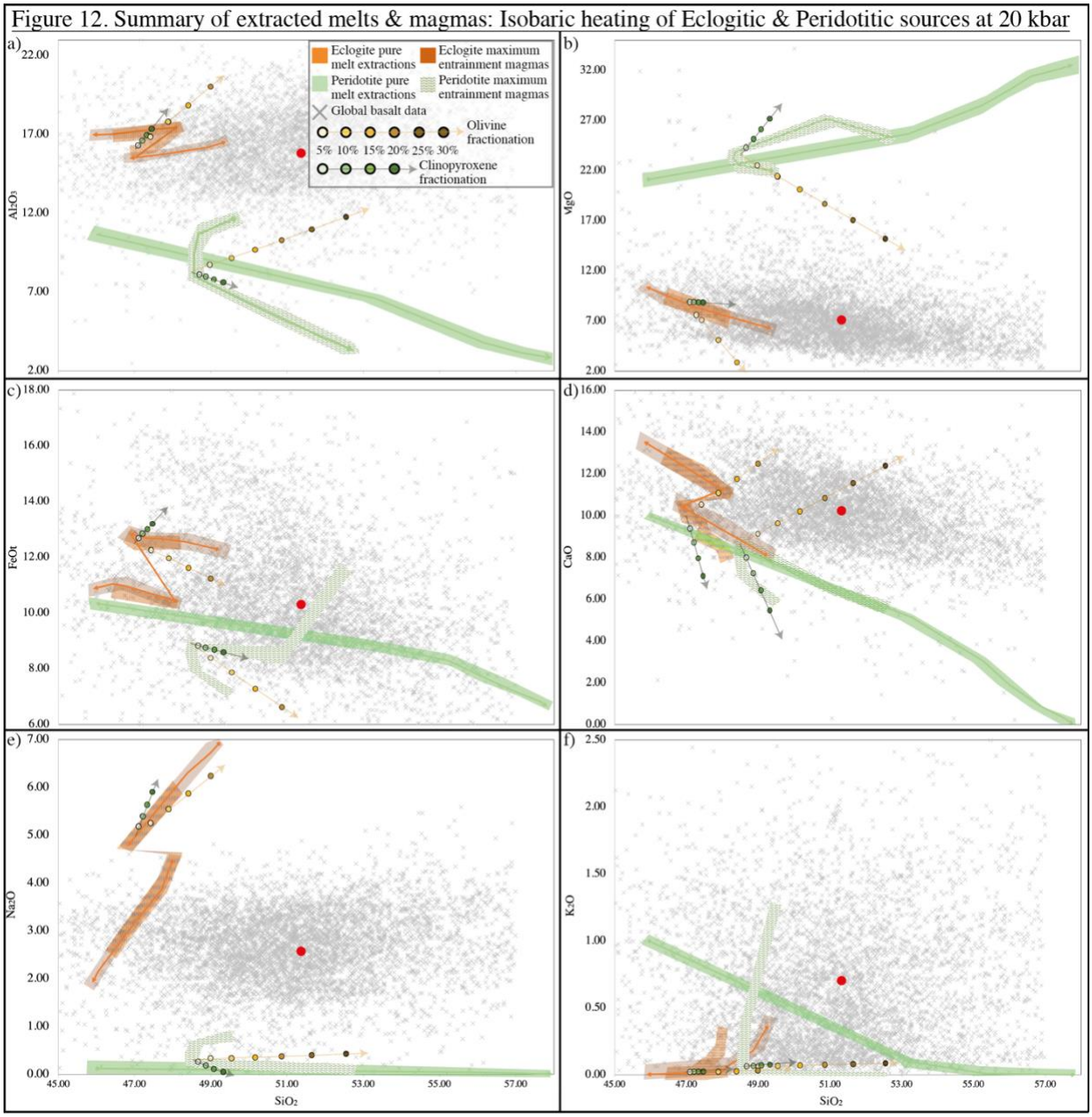

Figure 3-12. Harker diagrams showing a summary of the compositions of magmas derived from the modelled extraction events during partial melting of an eclogite and peridotite at 20 kbar along an isobaric path, superimposed on a global basalt database; the red circle indicates average basalt. The compositions included in the summary are all magmas separated from the residual system during a maximum entrainment extraction routine, including magmas with no entrained crystals (orange and green patterned clouds), as well as magma compositions constituting pure melt extractions, i.e. no peritectic entrainment was involved (orange and green coloured clouds). Compositions of pure melt extractions from the eclogitic source display overall SiO_2 reduction, despite a sudden reversal to higher SiO_2 values, and display increases in Al_2O_3, MgO and CaO, whilst decreasing in FeO_t, Na_2O and K_2O. Pure melts extracted from the peridotite display a continued increase in SiO_2, decreasing for all oxides except MgO. Maximum entrainment and crystal devoid magmas extracted during partial melting of the eclogitic source follow a mostly similar evolution to the pure melt extractions, becoming less SiO_2-rich in character, increasing in Al_2O_3, MgO and CaO, and decreasing in FeO_t, Na_2O and K_2O. Maximum entrainment magmas extracted during partial melting of the peridotitic source follow a different evolution to pure melt extractions, initially decreasing in SiO_2 followed by an increase, and displays an overall decrease in Al_2O_3, CaO, Na_2O and K_2O, and an increase in MgO and FeO_t. The transparent yellow and green arrows follow olivine (yellow circles) and clinopyroxene (green circles) fractionation trends.

Stellenbosch University https://scholar.sun.ac.za

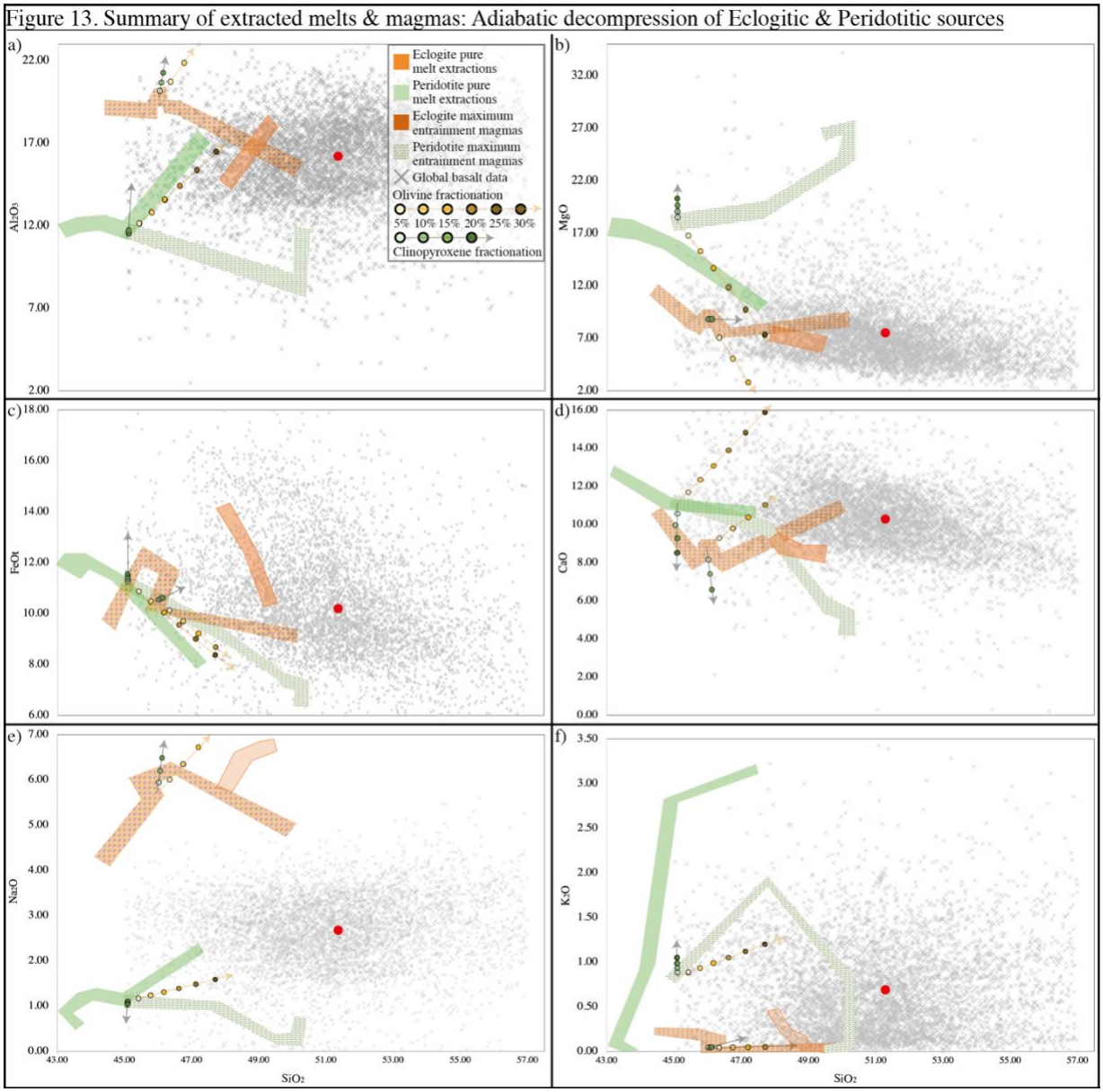

Figure 3-13. Harker diagrams showing a summary of the compositions of magmas derived from the modelled extraction events during partial melting of an eclogite and peridotite during adiabatic decompression, superimposed on a global basalt database; the red circle indicates average basalt. The compositions included in the summary are all magmas separated from the residual system during a maximum entrainment extraction routine, including magmas with no entrained crystals (orange and green patterned clouds) as well as magma compositions constituting pure melt extractions, i.e. no peritectic entrainment was involved (orange and green coloured clouds). Pure melts extracted during partial melting of the eclogitic source follow a linear trend, increasing in SiO_2 whilst MgO, FeO_t, CaO and K_2O decrease, and Al_2O_3 and Na_2O increase. Maximum entrainment magmas extracted during eclogite partial melting also increase in SiO_2, with increases and decreases in different orders seen for all oxides, and mostly evolving into the denser array of basalt data, apart from Na_2O. Pure melts extracted from partial melting of the peridotite source show an initial decrease in SiO_2, followed by an increase in the composition of the last extraction. This is accompanied by different oxide trends, displaying initial increases followed by a decrease in MgO, FeO, and CaO, decreases in Na_2O and K_2O, and a more complicated trend of increasing and decreasing Al_2O_3 values. Maximum entrainment magmas extracted during peridotite partial melting are more ultramafic in nature at higher P-Ts, and become more SiO_2-rich in character at lower P-Ts. The transparent yellow and green arrows follow olivine (yellow circles) and clinopyroxene (green circles) fractionation trends.

Stellenbosch University https://scholar.sun.ac.za

Studying the extent of mantle-derived compositional diversity in natural rocks remains a challenge, because none of the natural compositions of global mafic and intermediate rocks may reflect the primitive melts or magmas which left their source rocks (O'Hara, 1968). Long-standing observations indicate that the majority of basalts have undergone some compositional modifications when transferred to the continental crust, meaning that erupted basalts may be more or less compositionally diverse than the primary magmas from which they have evolved (Neave et al., 2021). Such evolution of primitive magmas to their final compositions are dependent on several processes considered important in shaping basalt compositions, such as fractionation, crustal assimilation, magma mixing, etc (e.g. Cribb & Barton, 1996; Neave et al., 2021; Reiners et al., 1995). These processes would, in theory, yield distinct evolution trends within the large scatter observed for the basalt population (Moyen et al., 2021); for example, the alteration of primitive magmas by crustal assimilation would produce observable trends of incompatible and trace element compositional data, because of the wide variation between such data for mantle-derived partial melts and continental crustal rocks. Unfortunately, it is nearly impossible to indisputably identify all alteration processes and their effects on the chemical composition of the rocks, particularly using major element-based plots, which display similar trends for fractionation, melting, and mixing (Moyen, 2020), and the variation related to such processes are minor in comparison to the scatter of natural rock compositions. In other words, the uniform observation of trends associated with alteration processes cannot be tracked on a planetary scale, because common lines of magmatic evolution will connect the resulting basalt compositions through any alteration process involved (Moyen et al., 2021). Therefore, no one such process can be assumed as a primary driver in the formation of all evolved magmas, due to the broad similarity of the petrologic and geochemical features of the resulting igneous rocks from all petrogenetic scenarios (Moyen et al., 2021).

Although it is clear that the process of peritectic crystal entrainment has the potential to produce a large range of primitive magma compositions, considering this in the context of the above is complicated. Processes such as magma mixing or crustal assimilation are dependent on additions of new material (i.e. not directly related to the particular melt/magma extraction), further complicating the interpretation of the variations in melt or magma chemistry that might be produced in the source. In comparison, the effects of an alteration process such as fractionation would be dependent on, and thus strongly correlated, to the compositional diversity of the primitive magmas. Because performing such calculations for all the magma compositions produced in this study would be exhaustive, modelling was

Stellenbosch University https://scholar.sun.ac.za

performed on selected crystal-bearing magmas (Figures 3-12 & 3-13) in order to examine the effects of fractionation on the evolution of the extracted magma chemistries.

The outcomes for eclogite-derived melt compositions show that, for all major elements except Na_2O, the melt and peritectic crystal entrained magma compositions could conceivably evolve into the field of common basalt compositions through up to 20% olivine and/or clinopyroxene fractionation (Figures 3-12 & 3-13), as both decompression and isobaric heating partial melting scenarios plot towards the low-SiO_2 side of the range of basalt compositions. Conceivably, the high Na_2O content of the modelled melts/magmas produced during adiabatic decompression (Figure 3-10e) precludes the partial melting of eclogitic source rocks of group I subdivision (Addendum C) from being involved in the production of common basalts from continental environments. For the peridotite source, lower temperature melts produced during isobaric heating partial melting scenarios may evolve to overlap with the broader range of common basalt compositions through up to 25% olivine fractionation and 20% pyroxene fractionation, similarly observed with up to 25% olivine fractionation of peritectic crystal entrained magmas that arise from relatively low temperatures (Figure 3-12). In decompression heating partial melting scenarios, up to 25% olivine (and in some cases, pyroxene) fractionation may evolve both the compositions of melt and peritectic crystal entrained magmas even more into the range of basalt compositions (Figure 3-13), however, the compositional range of the melts and magmas for which this holds true is limited by high MgO contents, particularly along isobaric heating paths (Figure 3-11b). Ultimately, crystal-bearing magmas and pure melts extracted from a deformed garnet lherzolite (extensively recrystallised; Addendum C) cannot evolve into the denser cloud of basalt compositions without substantive compositional change.

An important implication of examining possible trends of fractionation is how the coalescence of the peritectic entrainment trends and possible fractionation trends delineate the outer bounds of that can be occupied by the crystal-bearing magma chemistry in compositional space. Examining these trends provide three major observations: Firstly, although the combination of peritectic crystal entrainment and the fractionation of the resulting magmas may not cover the entire range of natural basaltic compositions, when the trends are colinear, magma compositions that result from phase entrainment and fractionation processes are (nearly) indistinguishable. Considering the ambiguity in petrological evidence discussed above, it is evident that variations in basalt compositions that may have been interpreted to be due to fractionation, may also be as a result of the mantle source entrainment process, or both. Secondly, when the trends of entrainment and fractionation are not colinear, this provides an indication of the possible extent of the diversity of magmas that can be generated. This

Stellenbosch University https://scholar.sun.ac.za

highlights the role of source dynamics in determining the compositional character of primitive melts and magmas, indicated by many of the primitive compositions determined in this study that already plot within the global array of basaltic data, without changing via of any process of alteration. Fractionation can evolve these magmas either into the denser part of the global array, or produce a greater scatter; a conclusion that can applied to other alteration processes in a similar manner. It thus remains imperative to see these alteration processes as ancillary to the variations in basalt global data – the scatter observed for continental basalts are, ultimately, a source characteristic, with any modifications merely amplifying the chemistries produced during partial melting reactions in the mantle, which may or may not include the entrainment of peritectic phases to the melt. Lastly, even at low degrees of partial melting, the melts and magmas produced by the peridotite utilised in this study are not poor enough in MgO to overlap the denser array of global basaltic database, unless significant olivine fractionation occurs or some magma mixing is involved. Basaltic to intermediate rocks from continental environments thus most likely represent magmas derived from an eclogitic material with less elevated Na_2O contents, or a peridotite metasomatised by a significant component of eclogite, or mixed with a high-SiO_2 andesitic composition.

6. Conclusions

The compositions produced in this thermodynamic modelling study illustrate how variation/s in the source can produce compositionally diverse primitive melts or magmas, which can evolve by fractionation to be a compositionally diverse array of evolved melts or magmas. Three important conclusions can be drawn: Firstly, although fractionation is possibly one of the main process that evolves primitive melt or magma compositions to those of the basalts found in the continental crust, it is not the process of fractionation that causes the extensive variation displayed by the basalt data. The observed compositional variation is a source characteristic, i.e. it is produced by processes acting in the source, with fractionation merely mirroring the compositional diversity displayed by the primitive melts or magmas. The process of peritectic crystal entrainment may thus be considered a viable mechanism for producing large-scale compositional variation in basalts found in the continental crust. Secondly, as a result of the above, peritectic crystal entrainment to the melt could possibly be a fundamental process easily overlooked due to the large range of values observed for basalt compositions, displaying no obvious evidence for its occurrence. Thirdly, although there are multiple potential sources for primitive magmas that result in continental basalts, it appears that isobaric heating of type 1 eclogites produce melts and magmas that are too sodic to produce basalts,

Stellenbosch University https://scholar.sun.ac.za

and that decompression melting of deformed garnet lherzolites produce many melt and magma compositions too magnesian to produce continental basalts, even after fractionation has occurred, thus limiting the possibility of the source compositions and conditions examined in this study to produce the compositions observed for continental basalts.

Addenda

Addendum C

Acknowledgements

Funding by the South African National Research Foundation (NRF) through the South African Research Chairs Initiative (SARChI) to G. Stevens is gratefully acknowledged. Additionally, J.-F. Moyen acknowledges the co-funding of the BuCoMO International Research Project (IRP) by the French Centre for Scientific Research (CNRS) and the NRF. T Otto thanks D. Nel at the Centre for Statistical Consultation for his assistance.

Stellenbosch University https://scholar.sun.ac.za

References

1. Arculus, R.J. 1994. Aspects of magma genesis in arcs. *Lithos*, 33(1–3):189–208.
2. Bell, D.R., Grégoire, M., Grove, T.L., Chatterjee, N., Carlson, R.W. and Buseck, P.R. 2005. Silica and volatile-element metasomatism of Archean mantle: a xenolith-scale example from the Kaapvaal Craton. *Contributions to Mineralogy and Petrology*, 150:251–167.
3. Brugier, Y.-A., Alletti, M. and Pichavant, M. 2015. Fe pre-enrichment: A new method to counteract iron loss in experiments on basaltic melts. *American Mineralogist*, 100:2106–2111.
4. Cesare, B., Acosta-Vigil, A., Bartoli, O. and Ferrero, S. 2015. What can we learn from melt inclusions in migmatites and granulites? *Lithos*, 239:186–216.
5. Chappell, B.W., White, A.J.R. and Wyborn, D. 1987. The importance of residual source material in granite petrogenesis. *Journal of Petrology*, 28:1111–1138.
6. Clemens, J.D., Stevens, G. and Farina, F. 2011. The enigmatic sources of I-type granites: the peritectic connexion. *Lithos*, 126:174–181.
7. Clemens, J.D. and Veilzeuf, D. 1987. Constraints on melting and magma production in the crust. *Earth and Planetary Science Letters*, 86(2–4):286–304.
8. Connolly, J.A.D. 2005. Computation of phase equilibria by linear programming: A tool for geodynamic modeling and its application to subduction zone decarbonation. *Earth and Planetary Science Letters*, 236:524–541.
9. Cribb, J.W. and Barton, M. 1996. Geochemical effects of decoupled fractional crystallization and crustal assimilation. *Lithos*, 37(4):293–307.
10. Dorais, M.J. and Spencer, C.J. 2014. Revisiting the importance of residual source material (restite) in granite petrogenesis: The Cardigan Pluton, New Hampshire. *Lithos*, 202:237–249.
11. Erdmann, S., Scaillet, B. and Kellett, D.A. 2012. Textures of Peritectic Crystals as Guides to Reactive Minerals in Magmatic Systems: New Insights from Melting Experiments. *Journal of Petrology*, 53(11):2231–2258.
12. Gao, P., Zheng, Y.-F. and Zhao, Z.-F. 2016. Distinction between S-type and peraluminous I-type granites: Zircon versus whole-rock geochemistry. *Lithos*, 258–259:77–91.

Stellenbosch University https://scholar.sun.ac.za

13. García-Arias, M. and Stevens, G. 2017. Phase equilibrium modelling of granite magma petrogenesis: A. An evaluation of the magma compositions produced by crystal entrainment in the source. *Lithos*, 277:131–153.
14. Grove, T.L. and Kinzler, R.J. 1986. Petrogenesis of andesites. *Annual Review of Earth and Planetary Sciences*, 14(1):417–454.
15. Harte, B., Hunter, R.H. and Kinny, P.D. 1993. Melt geometry, movement and crystallization, in relation to mantle dykes, veins and metasomatism. *Philosophical Transactions of the Royal Society of London. Series A: Physical and Engineering Sciences*, 342(1663):1–21.
16. Holland, T.J.B. and Powell, R. 2003. Activity-composition relations for phases in petrological calculations: an asymmetric multicomponent formulation. *Contributions to Mineralogy and Petrology*, 145:492–501.
17. Holland, T.J.B. and Powell, R. 2011. An improved and extended internally-consistent thermodynamic dataset for phases of petrological interest, involving a new equation of state for solids. *Journal of Metamorphic Geology*, 29:333–383.
18. Holland, T.J.B., Green, E.C.R. and Powell, R. 2018. Melting of peridotites through to granites: A simple thermodynamic model in the system KNCFMASHTOCr. *Journal of Petrology*, 59:881–900.
19. Humphreys, M.C.S., Kearns, S.L. and Blundy, J.D. 2006. SIMS investigation of electron-beam damage to hydrous, rhyolitic glasses: Implications for melt inclusion analysis. *American Mineralogist*, 91:667–679.
20. Ito, K. and Kennedy, G.C. 1974. The Composition of Liquids Formed by Partial Melting of Eclogites at High Temperatures and Pressures. *The Journal of Geology*, 82(3)
21. Jacob, D.E. 2004. Nature and origin of eclogite xenoliths from kimberlites. *Lithos*, 77:295–316.
22. Kinzler, R. J. 1997. Melting of mantle peridotite at pressures approaching the spinel to garnet transition: Application to mid-ocean ridge basalt petrogenesis. *Journal of Geophysical Research*, 102(B1):853–874.
23. Kushiro, I. 2001. Partial Melting Experiments on Peridotite and Origin of Mid-Ocean Ridge Basalt. *Annual Review of Earth and Planetary Sciences*, 29(1):71–107.
24. Langmuir, C.H., Bender, J.F., Bence, A.E., Hanson, G.N. and Taylor, S.R. 1977. Petrogenesis of basalts from the FAMOUS area: Mid-Atlantic Ridge. *Earth and Planetary Science Letters*, 36(1):133–156.

Stellenbosch University https://scholar.sun.ac.za

25. Long, X., Ballmer, M.D., Córdoba, A.M.-C. and Li, C.-F. 2019. Mantle Melting and Intraplate Volcanism Due to Self-Buoyant Hydrous Upwellings From the Stagnant Slab That Are Conveyed by Small-Scale Convection. *Geochemistry, Geophysics, Geosystems*, 20(11):4972–4997.

26. Maaløe, S. and Aoki, K. 1977. The major element composition of the upper mantle estimated from the composition of lherzolites. *Contributions to Mineralogy and Petrology*, 63(2):161–173.

27. Mathias, M., Siebert, J.C. and Rickwood, P.C. 1970. Some aspects of the mineralogy and petrology of ultramafic xenoliths in kimberlite. *Contributions to Mineralogy and Petrology*, 26:75–123.

28. Mayne, M., Moyen, J.-F., Stevens, G. and Kaislaniemi, L. 2016. Rcrust: a tool for calculating path-dependent open system processes and application to melt loss. *Journal of Metamorphic Petrology*, 34(7):663–682.

29. Mayne, M., Stevens, G. and Moyen, J.-F. 2019a. A phase equilibrium investigation of selected source controls on the composition of melt batches generated by sequential melting of an average metapelite, in V. Janoušek, B. Bonin, W.J. Collins, F. Farina and P. Bowden (eds.). *Post-Archean Granitic Rocks: Petrogenetic Processes and Tectonic Environments.* Bath: Geological Society of London Special Publications 491.

30. Mayne, M., Stevens, G., Moyen, J.-F. and Johnson, T. 2019b. Performing process-oriented investigations involving mass transfer using Rcrust: a new phase equilibrium modelling tool, in V. Janoušek, B. Bonin, W.J. Collins, F. Farina and P. Bowden (eds.). *Post-Archean Granitic Rocks: Petrogenetic Processes and Tectonic Environments.* Bath: Geological Society of London Special Publications 491.

31. McKenzie, D. and Bickle, M.J. 1988. The Volume and Composition of Melt Generated by Extension of the Lithosphere. *Journal of Petrology*, 29(3):625–679.

32. Médard, E., McCammon, C.A., Barr, J.A. and Grove, T.L. 2008. Oxygen fugacity, temperature reproducibility, and H_2O contents of nominally anhydrous piston-cylinder experiments using graphite capsules. *American Mineralogist*, 93:1838–1844.

33. Merrill, R.B. and Wyllie, P.J. 1973. Absorption of iron by platinum capsules in high pressure rock melting experiments. *American Mineralogist*, 58:16–20.

34. Morgan, G.B.IV. and London, D. 1996. Optimizing the electron microprobe analysis of hydrous alkali aluminosilicate glasses. *American Mineralogist*, 81:1176–1185.

35. Moyen, J.-F. 2020. Granites and crustal heat budget, in V. Janoušek, B. Bonin, W.J. Collins, F. Farina, P. Bowden (Eds.), Post-Archean

Stellenbosch University https://scholar.sun.ac.za

Granitic Rocks: Contrasting Petrogenetic Processes and Tectonic Environments, Geological Society, London, Special Publications, 491:77–100.

36. Moyen, J.-F., Janoušek, V., Laurent, O., Bachmann, O., Jacob, J-B., Farina, F., Fiannacca, A. and Villaros, A. 2021. Crustal melting vs. fractionation of basaltic magmas: Part 1, granites and paradigms. *Lithos*, 402–403:106291.
37. Neave, D.A., Beckmann, P., Behrens, H. and Holtz, F. 2021. Mixing between chemically variable primitive basalts creates and modifies crystal cargoes. *Nature Communications*, 12:5495.
38. Niu, Y. 1997. Mantle Melting and Melt Extraction Processes beneath Ocean Ridges: Evidence from Abyssal Peridotites. *Journal of Petrology*, 38(8):1047–1074.
39. O'Hara, M.J. 1968. Are Ocean Floor Basalts Primary Magma? *Nature*, 220:683-686.
40. Patiño Douce, A.E. 1999. What do experiments tell us about the relative contributions of crust and mantle to the origin of granitic magmas? in: A. Castro, C. Fernandez and J.L. Vigneresse, (eds.). *Understanding granites: integrating new and classical techniques.* Geological Society, London, Special Publications, 168:55–75.
41. Patiño Douce, A.E. and Johnston, A.D. 1991. Phase equilibria and melt productivity in the pelitic system: implications for the origin of peraluminous granitoids and aluminous granulites. *Contributions to Mineralogy and Petrology*, 107:202–218.
42. Presnall, D.C., Dixon, J.R., O'Donnell, T.H. and Dixon, S.A. 1978. Generation of Mid-ocean Ridge Tholeiites. *Journal of Petrology*, 20:3–35.
43. Reiners, P.W. 2002. Temporal-compositional trends in intraplate basalt eruptions: Implications for mantle heterogeneity and melting processes. *Geochemistry, Geophysics, Geosystems*, 3(2):1-30.
44. Reiners, P.W., Nelson, B.K. and Ghiorso, M.S. 1995. Assimilation of felsic crust by basaltic magma: Thermal limits and extents of crustal contamination of mantle-derived magmas. *Geology*, 23(6): 563–566.
45. Rosenthal, A., Yaxley, G.M., Green, D.H., Hermann, J., Kovács, I. and Spandler, C. 2014. Continuous eclogite melting and variable refertilisation in upwelling heterogeneous mantle. *Scientific Reports*, 4:6099.
46. Stern, R.J. 2002. Subduction Zones. *Reviews of Geophysics*, 40(4): 3–1–3–38.
47. Stevens, G. and Clemens, J.D. 1993. Fluid-absent melting and the roles of fluids in the lithosphere: a slanted summary? *Chemical Geology*, 108(1–4):1–17.
48. Stevens, G., Villaros, A. and Moyen, J.-F. 2007. Selective peritectic garnet entertainment as the origin of geochemical diversity in S-type granites. *Geology*, 35:9–12.

Stellenbosch University https://scholar.sun.ac.za

49. Taylor, J. and Stevens, G. 2010. Selective entrainment of peritectic garnet into S-type granitic magmas: Evidence from Archaean mid-crustal anatectites. *Lithos*, 120(3–4):277–292.

50. Tomlinson, E.L. and Holland, T.J.B. 2021. A Thermodynamic model for the subsolidus evolution and melting of peridotite. *Journal of Petrology*, 62(1):egab012.

51. Tomlinson, E.L. and Kamber, B.S. 2021. Depth-dependent peridotite-melt interaction and the origin of variable silica in the cratonic mantle. *Nature Communications*, 12:1082.

52. Vielzeuf, D. and Schmidt, M.W. 2001. Melting relations in hydrous systems revisited: application to metapelites, metagreywackes and metabasalts. *Contributions to Mineralogy and Petrology*, 141:251–267.

53. Villaros, A., Stevens, G. and Buick, I.S. 2009a. Tracking S-type granite from source to emplacement: clues from garnet in the Cape Granite Suite. *Lithos*, 112:217–235.

54. Villaros, A., Stevens, G., Moyen, J.-F. and Buick, I.S. 2009b. The trace element compositions of S-type granites: evidence for disequilibrium melting and accessory phase entrainment in the source. *Contributions to Mineralogy and Petrology*, 158:543–561.

55. Walter, M.J. 1998. Melting of Garnet Peridotite and the Origin of Komatiite and Depleted Lithosphere. *Journal of Petrology*, 39(1):29–60.

56. White, R.S. and McKenzie, D. 1989. Magmatism at Rift Zones the Generation of Volcanic Continental Margins and Flood Basalts. *Journal of Geophysical Research*, 94:7685–7730.

57. White, R.W., Powell, R., Holland, T.J.B. and Worley, B.A. 2000. The effect of TiO_2 and Fe_2O_3 on metapelitic assemblages at greenschist and amphibolite facies conditions: mineral equilibria calculations in the system K_2O-FeO-MgO-Al_2O_3-SiO_2-H_2O-TiO_2-Fe_2O_3. *Journal of Metamorphic Geology*, 18(5):497–512.

58. Yoder, H.S. and Tilley, C.E. 1962. Origin of Basalt Magmas: An Experimental Study of Natural and Synthetic Rock Systems. *Journal of Petrology*, 3(3):342–532.

59. Zhang, Y., Ni, H. and Chen, Y. 2010. Diffusion Data in Silicate Melts. *Reviews in Mineralogy & Geochemistry*, 72:311–408.

Stellenbosch University https://scholar.sun.ac.za

CHAPTER 4

PRESENTATION OF RESEARCH PAPER 3

SOURCE PERITECTIC CRYSTAL ENTRAINMENT TO MANTLE MAGMAS SOLVES THE CR-PARADOX IN LAYERED MAFIC INTRUSIONS

This paper, first authored by Tahnee Otto, is currently under peer review for publication in *Communications Earth and Environment*.

The following aspects of the research were done independently by Tahnee Otto while receiving standard supervision by her supervisors Professor Gary Stevens, Professor Jean-François Moyen, and Dr Matthew J Mayne: (i) conducting thermodynamic modelling; (ii) generation of the figures; (iii) writing of the manuscript.

Stellenbosch University https://scholar.sun.ac.za

Source peritectic crystal entrainment to mantle magmas solves the Cr-paradox in Layered Mafic Intrusions

Tahnee Otto, Gary Stevens, Jean-François Moyen, Matthew M. Mayne, John D. Clemens

Abstract

The presence of chromitite seams and average bulk rock Cr_2O_3 contents well above mantle values in some layered mafic intrusions, such as the Bushveld Complex, which represents the largest mineable chromium reserve on Earth, is at odds with the low solubility of chromium in mantle-derived melts. Using thermodynamic modelling, we show that under appropriate upper mantle conditions, partial melting reactions in peridotite produce Cr-rich peritectic orthopyroxene together with melt. These crystals are available for entrainment to the magma during extraction from the source because they are produced with the melt, and this dramatically increases the chromium content of the magma. The orthopyroxene breaks down during magma ascent and forms olivine and chromite. Thus, the injection of mantle-derived magma, that in their sources contained entrained peritectic orthopyroxene, into crustal magma chambers can produce chromitite layers by crystal settling that represent > 1% of the volume of the magma batch.

1. Introduction

The Rustenburg Layered Suite of the Bushveld Complex of South Africa[1-3] is uniquely enriched in chromium (Fig. 4-1), and this remains a challenge to explain[4-17]. Chromium is poorly soluble in mafic melts[18], yet widely accepted models for the formation of chromitite layers within the suite have assumed that the chromite crystals that produced the layers formed by chromite saturation of the silicate melts that formed the complex[4-10]. Thus, the 'chrome paradox'[11,18-20], refers to the great volume of melt that would be required to form the chromitite seams[4-17,21] by crystallisation from melt, but is not observed in the relevant rock record. This study used phase-equilibrium thermodynamic modelling[22] to investigate the stoichiometry of partial melting reactions in peridotitic source rocks in the upper mantle, with particular reference to the formation of layered mafic intrusions. In mantle source rocks, melting is incongruent; the melt has a composition different to the sum of the reactants. Under some circumstances, this results in the formation of a new, peritectic, crystalline phase or phases[23-25]. Our modelling has defined a pressure-temperature domain within the upper subcratonic mantle where peritectic, chromium-bearing orthopyroxene crystals are produced by partial melting of peridotite. As the peritectic crystals are produced at the site of melting, and as

Stellenbosch University https://scholar.sun.ac.za

pyroxene is known from experiments to nucleate easily and abundantly[26], these form small crystals suspended in the melt[27], and are likely to be entrained during melt extraction. Upon segregation and magma (i.e. melt plus crystals) ascent from this source domain, melt volume in the magma batch grows due to decompression, and the entrained orthopyroxene reacts to form peritectic olivine and chromite. Thus, such magmas arrive in crustal magma chambers as mixtures of melt, olivine and chromite, and if emplaced as sills, will produce chromitite and dunite layers by density sorting directly from the crystal cargo present at the time of intrusion. Such sills will contain chromitite layers that may constitute in excess of 1% of the volume of the original magma batch, assuming no magma drainage occurs. However, magma drainage from such structures may occur at any time in their formation, potentially leaving only chromitite layers as evidence of their existence. Thus, the formation of chromitite layers, and the substantial enrichment of chromium in the Rustenburg Layered Suite and other similar layered complexes, can be explained by peritectic orthopyroxene entrainment to the magma in the mantle source and density segregation of the resultant crystal load directly on emplacement, without the need to invoke complex phase equilibrium considerations in staging chambers or at the site of emplacement.

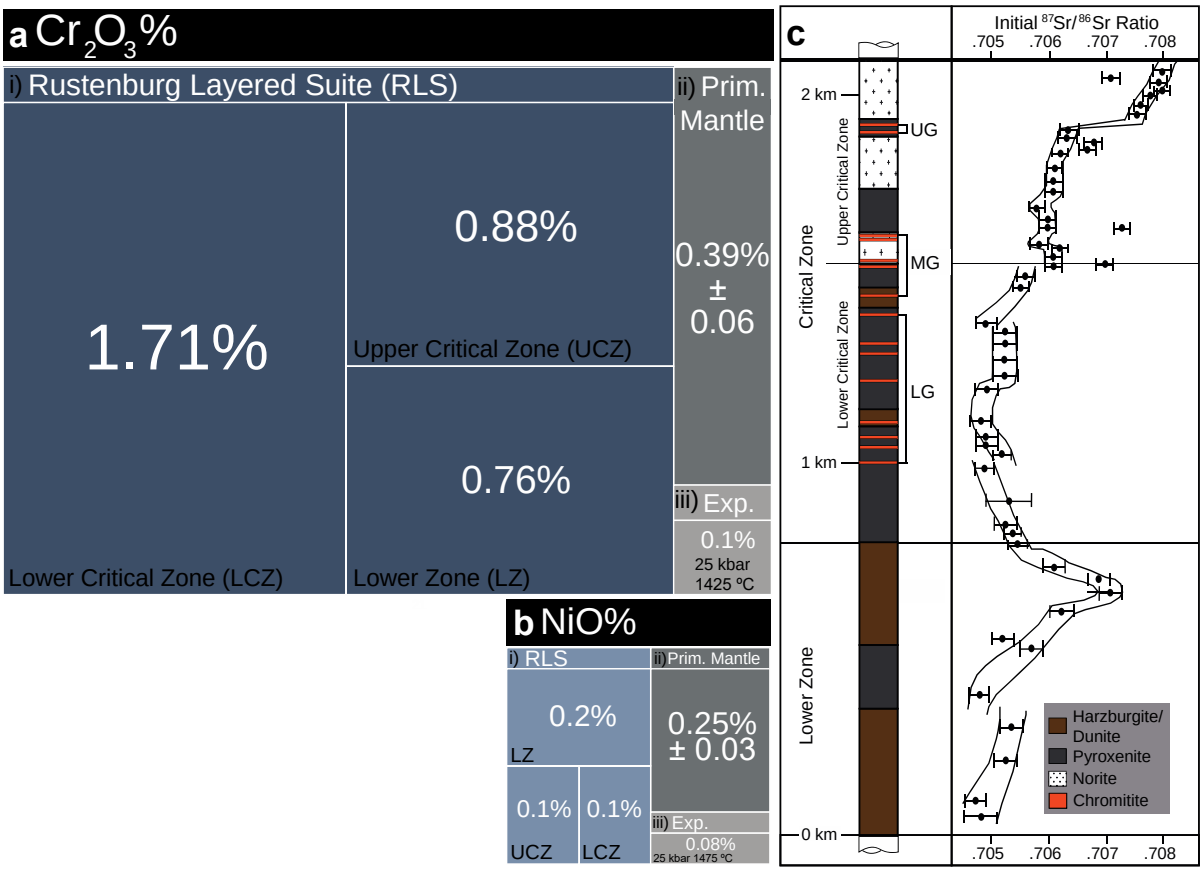

Fig. 4-1 Quantitative visualisation of the 'chrome paradox'. **a** The amount of Cr_2O_3 (%) in the Lower and Critical Zones of the Rustenburg Layered Suite[11] (RLS) **(i)**, is significantly higher than primitive mantle values[28] **(ii)**, and

Stellenbosch University https://scholar.sun.ac.za

is also at least an order of magnitude in excess of the solubility of chromium (Cr) in relevant mantle-derived mafic melts[29] **(iii)**. Thus, if all the Cr_2O_3 in the RLS was accommodated within melt, the observed abundance of Cr would require a volume of magma to form the cumulates that is not evident in the rock record. **b** A similar diagram is presented for NiO[21,28,30]. **c** Generalised stratigraphic column of the RLS[15] with a plot of $^{87}Sr/^{86}Sr$ initial ratios of the Lower Zone and Critical Zone[31]. In summary, the diagram demonstrates that magmas with variable Sr isotopic compositions formed the rocks of the RLS, and concentrated Cr beyond primitive mantle values, but did not similarly concentrate Ni. LG: Lower Group chromitites; MG: Middle Group chromitites; UG: Upper Group chromitites.

2. Results

2.1. Modelling Overview

There are several steps involved in the modelling method designed to investigate the details of melting reactions in mantle source rocks, the magma compositions that would result, and the crystallisation of these magmas in the upper crust. All modelling used the Rcrust software[32] and the Holland and Powell[33] thermodynamic dataset, with appropriately selected solution models (details in Methods). First, we investigated the stoichiometry of the partial melting reactions in a representative peridotitic mantle source in a relevant area of pressure-temperature (P-T) space, in a constant composition system without magma extraction. This allowed the peritectic crystals that increase in abundance with melt to be identified. Second, we investigated magma extraction events that may occur, and the magma compositions produced along two different adiabatic melting paths. Magma extraction was set to occur when melt volume exceeded 5 wt.%[34], with peritectic crystal entrainment set to occur when these crystals were produced with the melt. Last, we modelled the results of fractional crystallisation of selected magma batches emplaced as sills into the crystal mush at the base of a hypothetical 3 kbar magma chamber in the crust, over the cooling interval to ~1000 ºC. Details of each step are described in the following sections.

2.2. Identifying peritectic phases

The partial melting behaviour of a representative volatile-free garnet peridotite[35] (Table 4-1) was modelled between 1300 and 1600 ºC and 30 to 15 kbar. The volatile-free system was modelled because the peridotite solidus is lowered by both H_2O and CO_2, however available phase equilibrium modelling routines cannot deal with carbonate in the mantle source. A consequence of this is that our modelling maps out behaviour in the highest possible temperature range. Introduction of volatiles would lower the solidus temperature and increase the peritectic crystal yield. The volatile-free solidus is located at 1300 ºC at ~17 kbar and at ~1470 ºC at 30 kbar (Fig. 4-2). To identify areas of peritectic crystal production with high probability of crystal entrainment in the magma, phase abundance was mapped above the solidus. These were defined as areas where the melting reactions result in an increase in the

Stellenbosch University https://scholar.sun.ac.za

abundance of crystalline phase. In the P-T region of interest, both spinel and orthopyroxene were identified as peritectic products of partial melting that increased in abundance, with peritectic spinel being present in two small areas at low pressure, and peritectic orthopyroxene present in a wedge-shaped band that narrows with increasing pressure. With increasing degrees of melting, both spinel and orthopyroxene become reactants in the partial melting reactions.

Table 4-1 Composition of the peridotitic source used for Rcrust modelling along a pressure range of 30 to 15 kbar

Composition	SiO_2	TiO_2	Al_2O_3	Cr_2O_3	FeO_t	MgO	CaO	Na_2O	K_2O	Total
Garnet Peridotite	44.69	0.32	4.04	0.39	9.0	37.93	3.21	0.22	0.19	100.00

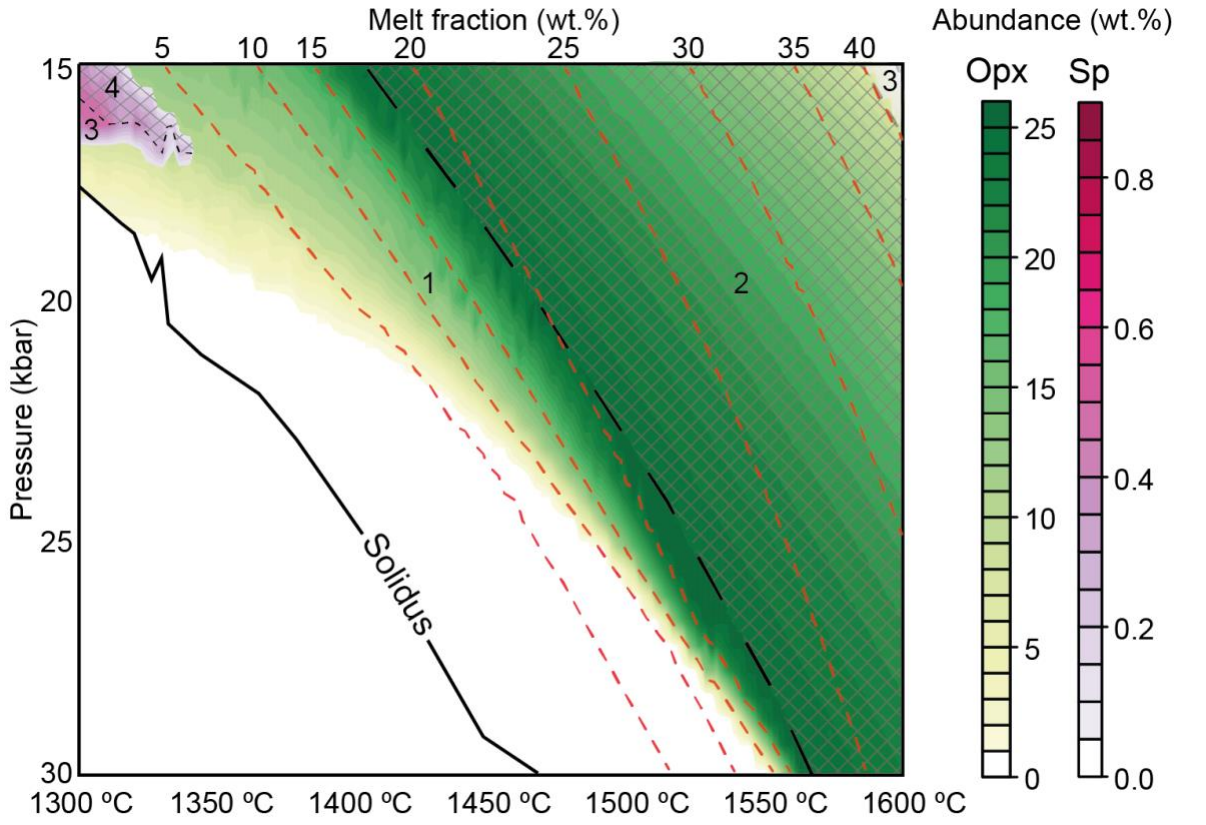

Fig. 4-2 A constant-composition P-T section showing the abundance of orthopyroxene (green, fields 1 and 2) and spinel (pink, fields 3 and 4) across the P-T range investigated. The yellow to green field (1) to the left of the heavy black dashed line represents the area of peritectic orthopyroxene production, where orthopyroxene abundance increases with melt volume. In this area, orthopyroxene abundance increases from 0 to > 25 wt.% (colour change from white to dark green). The cross-hatched, green to yellow field (2) to the right of the black dashed line indicates the area where orthopyroxene is consumed by melting, as is evident by the orthopyroxene abundance change from 25 to < 10 wt.% (colour change from dark green to yellow). Areas indicated in 3 represent the two small areas of P-T space, superimposed on the orthopyroxene fields, where peritectic spinel forms and is then consumed (4; cross-hatched) at higher temperature and/or lower pressure. Thus, the production of peritectic crystals, the nature of these crystals, and their abundance is strongly controlled by pressure, temperature, and the degree of melting. Within the modelled area there are two broad regions where melting of the peridotite produces no new mineral phases and the proportion of all crystal phases in the source decreases as a function of increasing melt volume. The first is the white area above the solidus and the second is area 2. These areas hold no potential for the entrainment of peritectic crystals. Opx: orthopyroxene; Sp: spinel.

Stellenbosch University https://scholar.sun.ac.za

2.3. Magma extraction events

The information provided in Fig. 4-2 is useful for understanding the details of partial melting of a single rock composition within a P-T space. However, magma extraction changes the composition of the source. Thus, to investigate magma extraction, with the possibility of peritectic phase entrainment, we investigated partial melting and magma extraction for rocks undergoing adiabatic decompression from 30 to 15 kbar. Lower temperature ($T^{30\ kbar}$ = 1400 ºC) and higher temperature ($T^{30\ kbar}$ = 1530.5 ºC) adiabatic decompression paths were investigated (paths 1 and 2 respectively in Fig. 4-3a). Where peritectic phase production was identified, the amounts of peritectic phase/s were quantified by calculating the increase in abundance for each P-T step along the path. Magma extraction events were triggered whenever melt exceeded 5 wt.% in the source. To approximate a degree of melt retention on grain boundaries, an amount of 10% of the original melt content was left un-extracted. Two different methods were used to model peritectic phase entrainment. In the first, most conservative method (Routine A), only the peritectic crystals produced in the preceding step along the P-T path were entrained into the extracted magma, with peritectic crystals produced in previous steps prior to the most recent past extraction being assumed to have recrystallised into structures too large for entrainment. As the temperature steps used in this modelling were small (0.5 & 1 ºC), this represents a minimum estimate of the amount of peritectic material that may be entrained. The second method (Routine B) involves the entrainment of all peritectic phase/s produced since encountering the solidus or since the most recent past magma extraction event. If no peritectic phases were produced in either routine, only melt was extracted. The conditions of the resulting extractions along the two adiabatic paths are displayed in Fig. 4-3a, numbered from A1 to 6 and B1 to 5 for reference. The weight fractions of melt and peritectic phase/s entrained are displayed in Fig. 4-3b, for each routine. The entrained phases are not considered to have a profound effect on the viscosity of the magma[36] and its rate of transfer during adiabatic ascent. Note that, due to reaction between the entrained peritectic crystals and melt as the magma ascends adiabatically, melt proportion grows relative to the crystal fraction.

Stellenbosch University https://scholar.sun.ac.za

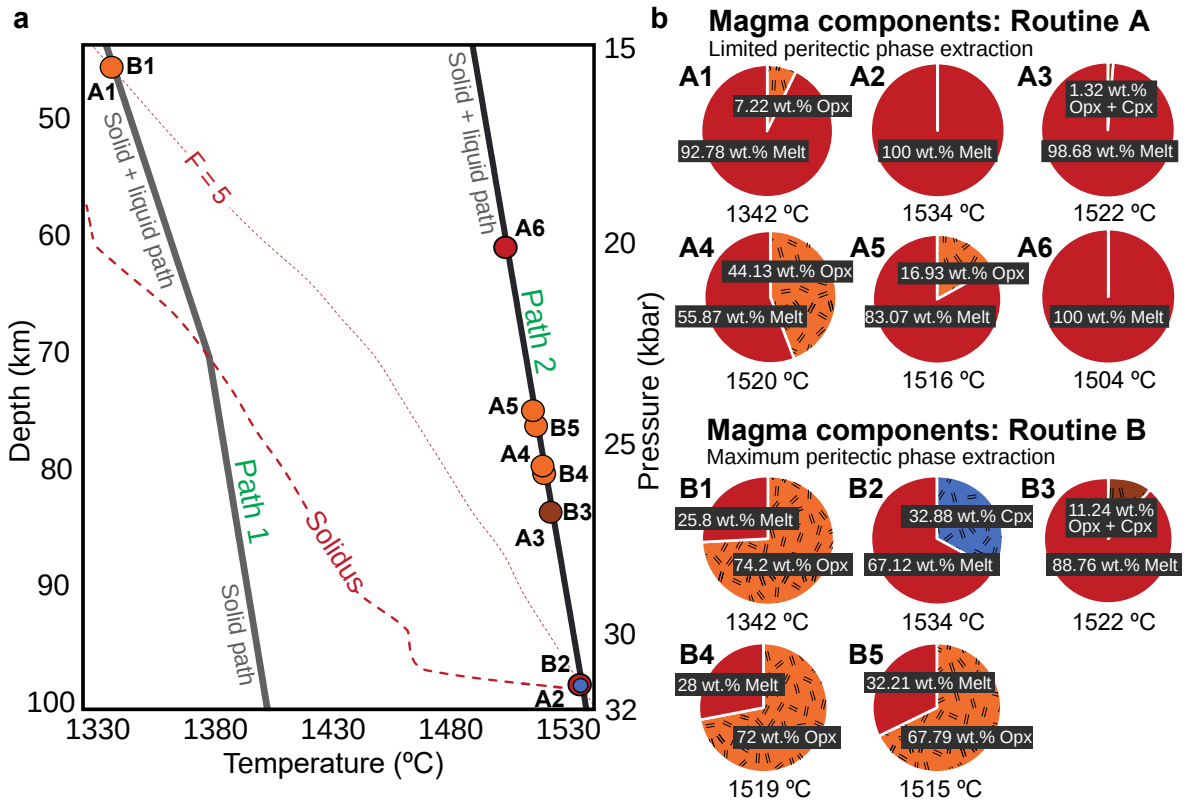

Fig. 4-3 The results of thermodynamic modelling of the melting reactions and magma extraction events in a representative garnet peridotite during adiabatic ascent from 30 to 15 kbar. **a** The P-T conditions of the magma extraction events along the two adiabatic decompression. Melt production along the cold path was sufficient only to trigger one extraction event for each entrainment routine. **b** The components of the magma batches on extraction from the source. The different peritectic entrainment routines discussed in-text produce significantly different outcomes. Routine A, the most conservative peritectic assemblage entrainment model, produces two extraction events where the magma leaving the source is crystal free. In general, peritectic crystal to melt ratios are lower, but despite this, extraction event A4 produces a crystal-rich magma, with > 40% entrained peritectic orthopyroxene. Routine B, which models the most favourable peritectic crystal entrainment scenario, produces three extraction events in which the magmas are crystal rich (> 65%). F: melt fraction in wt.%; Opx: orthopyroxene; Cpx: clinopyroxene.

2.4. Emplacement and crystallisation

To investigate the crystallisation of the individual magma batches after emplacement into a shallow-level crustal magma chamber, the magma bulk compositions determined from the extraction modelling were set to follow isobaric cooling paths at 3 kbar, starting at a temperature determined by their relevant adiabatic ascent path. Solid phases that existed in the magma at emplacement were modelled as undergoing immediate density separation on intrusion as a sill. Ferromagnesian silicate and oxide minerals that crystallised together, as a function of cooling in the sill, were not modelled as undergoing density segregation from one another, but were regarded as separating from the near-neutral-buoyancy plagioclase by this mechanism (Fig. 4-4). It is likely that melt could be removed from a plagioclase-rich crystal mush by filter pressing due to compaction[37] from layers deposited by overlying sills or other deformation processes.

Stellenbosch University https://scholar.sun.ac.za

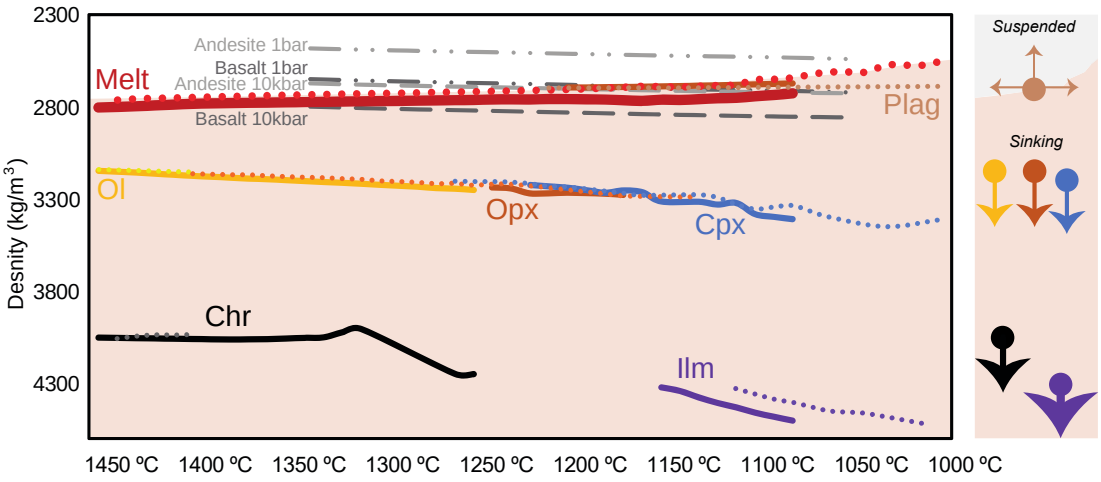

Fig. 4-4 Plot of the presence of phases in the magma during fractional crystallisation and the thermodynamically determined density values as a function of temperature along the 3 kbar isobaric crystallisation paths. The above examples represent the magma produced by extraction events A4 (solid lines) and B4 (dotted lines), as numbered in Fig 4-3a. Density data for typical basaltic (dark grey) and andesitic magmas (light grey) at 1 bar and 10 kbar[38] are displayed as a reference for comparison with the modelled density values for the melt phase. Vectors on the right indicate the effects of the density differences between the phases and the melt. Cpx: clinopyroxene; Chr: chromite; Ilm: ilmenite; Ol: olivine; Opx: orthopyroxene; Plag: plagioclase.

Assuming that melt and crystal separation occur, the crystallisation products produced by individual magma batches extracted from the source can be analysed by phase-equilibrium modelling. Fig. 4-5 displays the resulting variation in phase abundances as a function of decreasing temperature, and the igneous stratigraphy that would be produced by selected magma batches from entrainment routines A and B, if intruded as sills. The amounts of melt remaining in the sill at the end of the cooling temperature interval are also displayed.

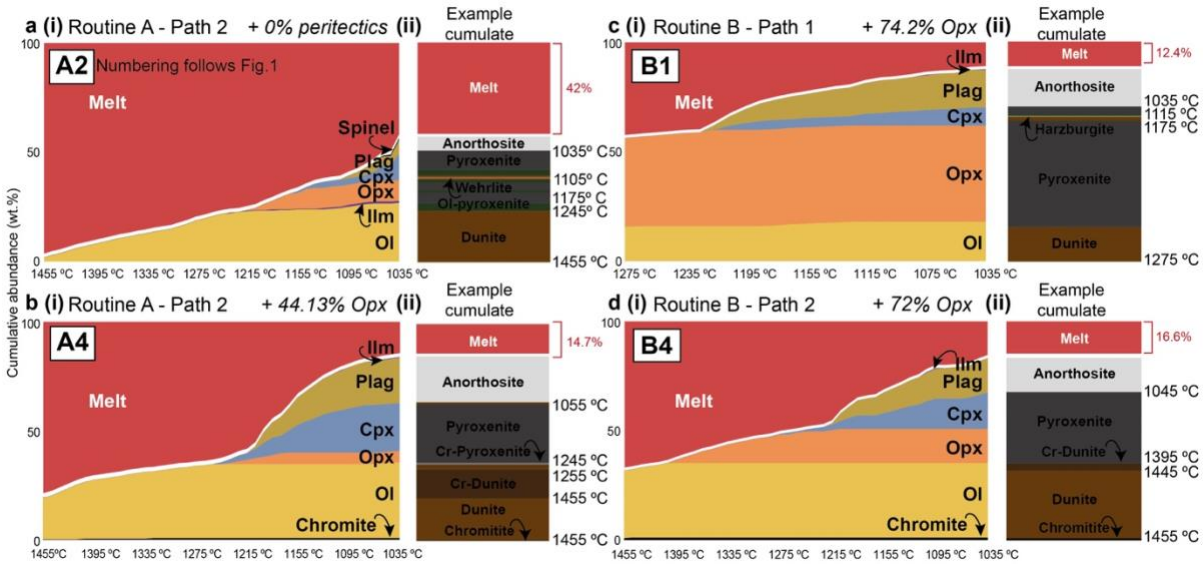

Fig. 4-5 Plots of cumulative phase abundance and the igneous stratigraphy that would be produced upon cooling from emplacement temperature to 1035 °C, assuming that the crystals present at emplacement undergo perfect density-driven segregation. Magma with no crystal entrainment (**a**), and magma batches with peritectic orthopyroxene (**b, c, d**) were modelled at 3 kbar. The plots are labelled according to the extraction event (Fig. 4-3) that produced the model magma. The crystallisation behaviour of magma A2, which involves no peritectic

Stellenbosch University https://scholar.sun.ac.za

phase entrainment, shows the formation of less cumulate along the crystallisation path and no chromite (**a(i)**). As displayed in **b(i)** and **d(i)**, emplacement of magmas with entrained peritectic orthopyroxene (extraction events A4 and B4, respectively) results in the formation of a chromitite layer; in both cases the magmas intrude as chromite- and olivine-bearing slurries. Crystallisation due to cooling in the sill produces pyroxenite and then norite or, as illustrated, if plagioclase segregates by density, an anorthosite layer will result following loss of the residual melt. Note that the removal of orthopyroxene on the ascent path is important to chromite formation. As a result of the lower intrusion temperature in **c**, the magma produced by extraction event B1 is predicted to intrude the crustal magma chamber as an orthopyroxene- and olivine-bearing slurry. The magma is Cr_2O_3-bearing, but this Cr is contained in orthopyroxene and therefore cannot undergo density segregation from the silicate minerals. Cpx: clinopyroxene; Ilm: ilmenite; Ol: olivine; Opx: orthopyroxene; Plag: Plagioclase.

3. Discussion

A key finding of this study is that during the partial melting of mantle rocks, the production of peritectic crystal phases that increase in abundance with the degree of melting varies as a function of pressure, temperature, and melt extraction. Where production and entrainment of peritectic orthopyroxene occur, this has profound consequences for the Cr content of the magma and for how layering in crustal mafic magma chambers is produced. Large magma systems are now known to be constructed by a multitude of magma batches[3,20,39-40]. When magma batches intrude as sills within melt-crystal mush, the formation of igneous layering may result[41-42]. In the case of the RLS, the Sr isotopic and Mg# stratigraphy strongly supports multi-batch assembly and the intrusion of magma batches as sills, and the documented out of sequence formation of layers[17] demands this for these specific layers. In our modelling, magma batches that leave their sources as melt only (e.g. extraction event A2) produce significantly less high-temperature crystallisation products, reaching a total abundance of less than 58%, with the remainder representing melt still present in the sill after cooling to ~1000 °C. In contrast, crystallisation paths of extracted magmas that included peritectic phase/s display a much greater potential for high-temperature crystallisation and the production of layering, due to the fact that the magmas intrude the crustal magma chamber as melt-crystal mixtures containing crystals of markedly different density. For example, the magma extracted in event B4 will, on intrusion, form a chromitite layer at the base of its sill, which will be overlain by a dunite layer, a pyroxenite layer and an anorthosite (or norite) layer. At the end of the modelled crystallisation sequence, only ~17% melt remained in the sill. As Fig. 4-3b illustrates, the peritectic phase most abundantly entrained into magmas derived from a garnet peridotite source undergoing partial melting in the upper mantle is likely to be orthopyroxene, and to a lesser degree, clinopyroxene. From Fig. 4-6, it is clear these peritectic crystals are not stable in the magma at high temperature under crustal pressures and continuously react will melt to reequilibrate during magma ascent. Their initial entrainment to the magma, however, results in the formation of a significant fraction of olivine in the magma at high temperature (Fig. 4-5b,d

Stellenbosch University https://scholar.sun.ac.za

and Fig. 4-6b). Importantly, the peritectic pyroxene crystals contain substantial amounts of Cr_2O_3 when entrained to the magma in the source. During ascent, breakdown of this peritectic orthopyroxene due to magma decompression results in the crystallisation of chromite (Fig. 4-6). Therefore, where these requirements are met, the magma batch contains chromite on arrival in the crustal magma chamber, and the density contrast between these crystals, the ferromagnesian silicates, and melt, should result in effective density segregation, at least on the scale of meters, and thus the likely formation of a chromitite layer at the base of the sill. Further cooling of the magma can produce layers of dunite, pyroxenite, norite, and possibly anorthosite, unless interrupted by melt drainage, in which case potentially only a chromitite, or a chromitite and a dunite layer would mark the site of intrusion. If effective crystal separation does not occur on intrusion of the sill, layers of dunite, gabbro and norite with interstitial chromite can be formed. Note that if the composition of the magma batch and the temperature path of magma ascent are such that, after magma ascent, a significant quantity of pyroxene is present in the magma, this may result in the available Cr_2O_3 being accommodated within pyroxene; chromite will not form in such cases (e.g. Fig. 4-5c). We can therefore conclude that the results are strongly weighted in favour of even relatively small sills produced from magmas that included peritectic pyroxene from the source being able to explain the formation of chromitite layers in the lower part of the RLS, as well as potentially producing a range of ferromagnesian and anorthositic layered silicate rocks that fit well with the general layers from high- and low temperature magmas (Fig. 4-5b to d). Where the peritectic phase can accommodate relatively high amounts of Cr, it massively enhances the potential of high-temperature magma batches to produce chromite (Fig. 4-5b,d). In contrast, extraction events in which no phases are entrained to the magma are incapable of producing the chromitite layers observed in such layered mafic intrusions (Fig. 4-5a).

The melt Cr-solubility problems associated with the formation of chromitite layers in the lower portions of the Bushveld Complex have been seemingly insurmountable due to a lack of evidence for the enormous volume of magma that would be needed to produce the chromitite layers in the Critical Zone of the RLS. An additional problem is the physical challenge of needing to, at moments in time, effectively fractionate only crystals of chromite or only crystals involved in the silicate layering out of such a large column of magma. Our results provide a chemically and thermodynamically constrained model that strongly aligns with a simple alternative for the formation of the chromitite layers of the RLS, one of Earth's largest high-temperature mineral deposits, as a consequence of peritectic crystal entrainment.

Stellenbosch University https://scholar.sun.ac.za

The strength of the novel hypothesis presented here lies in its basis in fundamental melting reaction dynamics. Silicate rock melting is an incongruent process under almost all geologically relevant conditions, and in the case of the mantle peridotite we have studied, this means that peritectic orthopyroxene will be the most common and abundant crystalline phase produced with melt in the subcratonic upper mantle. Orthopyroxene has a natural crystal chemical affinity for Cr_2O_3, and thus, the entrainment of peritectic orthopyroxene, which must be produced in the source of the magma, fundamentally changes the magma chemistry to be enriched in Cr_2O_3 and able to crystallise chromite on ascent. The fact that peritectic orthopyroxene is the entrained component and not a representative sample of all the residual minerals that coexist with melt in the source prior to magma segregation is demonstrated by the fact that Cr (strongly partitioned into pyroxene by substituting for Al[43]) is concentrated in the RLS to well above primitive mantle values, whereas Ni (strongly partitioned into olivine) is not (Fig. 4-1).

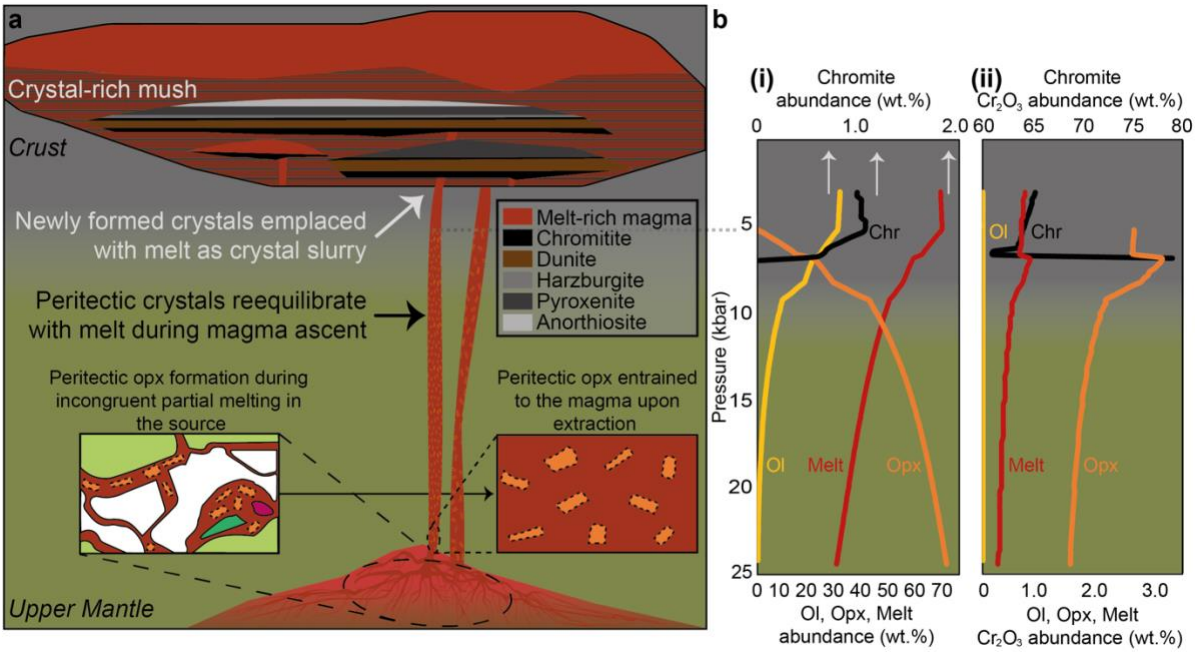

Fig. 4-6 A physical model for the generation of chromitite and silicate layering from the entrainment of peritectic crystals in the upper mantle source during magma extraction. **a** Under specific upper mantle conditions, incongruent partial melting reactions result in the production of new peritectic crystals at the sites of melting. A proportion of these peritectic crystals are entrained into the melt upon segregation from the source. Changing P-T conditions during adiabatic ascent consume the entrained peritectic phases, and recrystallisation at mid- to shallow crustal conditions produces a melt-dominated magma with new crystal phases in suspension. Emplacement of sills within or below magma chambers of this crystal-mush can produce layering similar to that found in the lower portions of the RLS, assuming effective density separation of crystals in the magma chamber as the magma cools. The upward migration of the remaining melt is achieved by filter pressing due to compaction, or due to the decreasing density of melt as crystalline phases settle out. **b** The consumption of the entrained peritectic orthopyroxene during magma ascent is displayed by its decrease in abundance as the magma travels along the adiabat. **(i)** As soon as the magma is extracted, the reaction of the chromium-rich orthopyroxene with the melt results in the consumption of the orthopyroxene, resulting in an increase in the melt fraction, the

Stellenbosch University https://scholar.sun.ac.za

crystallisation of peritectic olivine, and ultimately, the formation of peritectic chromite at low pressure, after which the orthopyroxene is exhausted. **(ii)** The first peritectic chromite phase to form during the reaction of orthopyroxene with melt is magnesiochromite, which evolves towards chromite over a short interval along the decompression path. The olivine- and chromite-bearing magma is emplaced into the crystal mush of the magma chamber, forming chromitite and dunite layers by density segregation. Fractional crystallisation at the site of intrusion produces further magmatic layering, as is displayed in Fig. 4-5. Chr: chromite; Ol: olivine; Opx: orthopyroxene.

4. Methods

4.1. Thermodynamic Modelling Details

Thermodynamic calculations were carried out using the Rcrust software[32] version 2020-04-19 with the Holland and Powell[33] thermodynamic dataset and the 2020 revised hp633ver.dat thermodynamic data file from Perple_X in the NKCFMASTCr (Na_2O-K_2O-CaO-FeO-MgO-Al_2O_3-SiO_2-TiO_2-Cr_2O_3) chemical system. The following phase solution models were used: Cpx(HGP) for clinopyroxene[22], Fsp(C1) for plagioclase and potassium-feldspar[44], Gt(HGP) for garnet[22], Ilm(WPH) for ilmenite[45], O(HGP) for olivine[22], Opx(HGP) for orthopyroxene[22], Sp(HGP) for spinel[22], and melt(HGP) for melt[22].

4.2. Modelling magma segregation

Melt formation and entrainment of peritectic phases to the melt on segregation from the source will create magmas with a chemical composition reflecting a combination of the mass of segregated melt and the composition and abundance of the entrained crystals. When such magmas leave the source, the bulk composition of the reactive system is altered, which affects the subsequent melting behaviour. Extractions in this study were set to occur when 5 wt.% melt is reached.

4.3. Quantifying peritectic phase production

Quantification of the proportion of peritectic phases produced, if any, was calculated using the Rcrust 'Delta' function. Since peritectic phases are produced as products of incongruent melting reactions, they must therefore increase in abundance during melting. The Delta function allows the user to specify only the portion of a predicted phase that increased in abundance during melting to be quantified and included in extraction simulations. In other words, the Delta function calculates the incremental difference observed for a predicted phase between the point of extraction (point *b*) and a specified previous point (point *a*), such that the change in the phase mode from point *a* to point *b* can be added to the extraction simulation. The Delta function can be expressed as:

$$delta\{phase; x_a; y_a; unit\} \quad (1)$$

Stellenbosch University https://scholar.sun.ac.za

where $phase$ is the phase intended for extraction, x_a and y_a describe the location of point a, and $unit$ can be measured in mol.%, vol.% or wt.%. Point a can specified in two manners: i) 'prev_ext_X', where X can be any phase of choice from which the delta change must be calculated, or ii) 'prev_ext', where the name of the extracting phase is the default choice for the delta calculation.

4.4. Entrainment Routine A and Routine B

An upper and lower estimate on the behaviour of peritectic entrainment was considered as Routine A and Routine B. Routine A was modelled using the 'prev_ext' specification of the Delta function, with the delta change in wt.% of the peritectic phase/s to be entrained is calculated from the point of extraction to one P-T point (which is dependent on the adiabat) before the extraction. Routine B was modelled using the command of 'prev_ext_Melt', where the delta change in wt.% of the peritectic phase/s to be entrained is calculated from point of extraction to the solidus if it is the first extraction, or from the subsequent point of extraction to the previous point of extraction.

4.5. Fractional crystallisation

The crystallisation of emplaced magma batches were modelled assuming immediate density separation of the phases at each cooling step. To simulate this segregation of the crystals from the magma, the 'any_phase' expression was utilised in Rcrust, which allows generic arguments for all phases that may be predicted to be set, given that the phase does not have a phase extraction proportion already specified. Subsequently, for each P-T point along the cooling path, the melt phase extraction proportion was specified as 0%, and for all other predicted phases (any_phase), the extraction proportion was set to 100%. This results in a scenario where the continued crystallisation of the evolving magma can be simulated, with already crystallised phases 'leaving' the magma system as they settle onto the chamber floor, immediately excluding these phases from contributing to the reactive bulk composition of future steps. The abundance and density (amongst numerous other data) of the crystallising phases for each P-T step can thus be gathered and quantified in a thermodynamically evolving system, allowing predictions of the possible cumulates that could form as a result of gravity settling.

Data Availability

The datasets generated during the current study are available in Addendum D.

Stellenbosch University https://scholar.sun.ac.za

Acknowledgements

The research was supported by the South African National Research Foundation (NRF) through the South African Research Chairs Initiative awarded to G.S, and the BuCoMO International Research Project by the French Centre for Scientific Research and the NRF.

Stellenbosch University https://scholar.sun.ac.za

References

1. Wager, L. R. & Brown, G. M. *Layered Igneous Rocks.* 588 (Oliver & Boyd, Edinburgh & London, 1968).
2. Eales, H. V. *et al.* The mafic rocks of the Bushveld Complex: a review. *J. Afr. Earth Sci.* **16**, 121–142 (1993).
3. Eales, H. V. & Cawthorn, R. G. in *Layered Intrusions* (ed. Cawthorn, R.G.) 181–229 (Elsevier Science, Amsterdam, 1996).
4. Cameron, E. N. Evolution of the lower critical zone, central sector, eastern Bushveld Complex. *Econ. Geol.* **75**, 845–871 (1980).
5. Irvine, T. N. & Sharpe, M. R. in *Metallogeny of Basic and Ultrabasic Rocks* (eds. Gallagher, M. J., Ixer, R. A., Neary, C. R. & Pritchard, H. M.) 183–198 (Instit. Mining Metallurgy, London, 1986).
6. Nicholson, D. M. & Mathez, E. A. Petrogenesis of the Merensky Reef in the Rustenburg section of the Bushveld Complex. *Contrib. Mineral. Petrol.* **107**, 293–309 (1991).
7. Cawthorn, R. G. Pressure fluctuations and the formation of the PGE-rich Merensky and chromitite reefs, Bushveld Complex. *Miner. Depos.* **40**, 231–235 (2005).
8. Naldrett, A. J., Kinnaird, J., Wilson, A., Yudovskaya, M. & Chunnett, G. The origin of chromitites and related PGE mineralization in the Bushveld Complex: new mineralogical and petrological constraints. *Miner. Depos.* **47**, 209–232 (2012).
9. Latypov, R., Chistyakova, S. and Mukherjee, R. A. 2017. A novel hypothesis for origin of massive chromitites in the Bushveld Igneous Complex. *J. Petrol* **58**, 1899–1940 (2017).
10. Latypov, R. *et al.* Platinum-bearing chromite layers are caused by pressure reduction during magma ascent. *Nat. Commun.* **9**, 462 (2018).
11. Eales, H. V. Implications of the chromium budget of the Western Limb of the Bushveld Complex. *S. Afr. J. Geol.* **103,** 141–150 (2000).
12. Mondal, S. K. & Mathez, E. A. Origin of the UG2 chromitite layer, Bushveld Complex. *J. Petrol.* **48**, 495–510 (2007).
13. Maier, W. D. & Barnes, S. -J. Platinum-group elements in the UG1 and UG2 chromitites, and the Bastard Reef, at Impala platinum mine, western Bushveld Complex, South Africa: evidence for late magmatic cumulate instability and reef constitution. *S. Afr. J. Geol.* **111**, 159–176 (2008).

Stellenbosch University https://scholar.sun.ac.za

14. Voordouw, R., Gutzmer, J. & Beukes, N. J. Intrusive origin for upper group (UG1, UG2) stratiform chromitite seams in the Dwars River area, Bushveld Complex, South Africa. *Mineral. Petrol.* **97**, 75–94 (2009).
15. Maier, W. D., Barnes, S. -J. & Groves, D. L. The Bushveld Complex, South Africa: formation of platinum-palladium, chrome- and vanadium-rich layers via hydrodynamic sorting of a mobilized cumulate slurry in a large, relatively slowly cooling, subsiding magma chamber. *Miner. Depos.* **48**, 1–56 (2012).
16. Eales, H. V. & Costin, G. Crustally contaminated komatiite: primary source of the chromitites and Marginal, Lower, and Critical Zone magmas in a staging chamber beneath the Bushveld Complex. *Econ. Geol.* **107**, 645–665 (2012).
17. Mungall, J. E., Kamo, S. L. & McQuade, S. U–Pb geochronology documents out-of-sequence emplacement of ultramafic layers in the Bushveld Igneous Complex of South Africa. *Nat. Commun.* **7**, 13385 (2016).
18. Roeder, P. L. & Reynolds, I. Crystallization of chromite and chromium solubility in basaltic melts. *J. Petrol.* **32**, 909–934 (1991).
19. Ulmer, G. C. Experimental investigations of chromite spinels. *Econ. Geol. Monogr.* **4**, 114–131 (1969).
20. Kruger, F. J. Filling the Bushveld Complex magma chamber: lateral expansion, roof and floor interaction, magmatic unconformities, and the formation of giant chromitite, PGE and Ti-V-magnetitite deposits. *Mineral. Depos.* **40**, 451–472 (2005).
21. Teigler, B. Mineralogy, petrology and geochemistry of the Lower and Lower Critical zones, northwestern Bushveld Complex. (Rhodes University, 1990).
22. Holland, T. J. B., Green, E. C. R. & Powell, R. Melting of peridotites through to granites: A simple thermodynamic model in the system KNCFMASHTOCr. *J. Petrol.* **9**, 881–900 (2018).
23. Kinzler, R. J. Melting of mantle peridotite at pressures approaching the spinel to garnet transition: Application to mid-ocean ridge basalt petrogenesis. *J. Geophyst. Res.* **102(B1)**, 853–874 (1997).
24. Presnall, D. C., Dixon, J. R., O'Donnell, T. H. & Dixon, S. A. Generation of Mid-ocean Ridge Tholeiites. *J. Petrol.* **20**, 3–35 (1978).
25. Tomlinson, E. L. & Kamber, B. S. Depth-dependent peridotite-melt interaction and the origin of variable silica in the cratonic mantle. *Nat. Commun.* **12**, 1082 (2021).

Stellenbosch University https://scholar.sun.ac.za

26. Stevens, G., Clemens, J. D. & Droop, G. T. R. Migmatites, granites and granulites: The data from experiments on "primitive" metasedimentary protoliths. *Contrib. Mineral. Petrol.* **128**, 352–370 (1997).

27. Erdmann, S., Scaillet, B. & Kellett, D. A. Textures of Peritectic Crystals as Guides to Reactive Minerals in Magmatic Systems: New Insights from Melting Experiments. *J. Petrol*. **53(11)**, 2231–2258 (2012).

28. Lyubetskaya, T. & Korenaga, J. Chemical composition of Earth's primitive mantle and its variance: 1. Method and results. *J. Geophys. Res.* **112(B3)** (2007).

29. Takahashi, E. & Kushiro, I. Melting of a dry peridotite at high pressures and basalt magma genesis. *Amer. Mineral.* **68**, 859–879 (1983).

30. Matzen, A. K., Baker, M. B., Beckett, J. R., Wood, B. J. & Stolper, E. M. The effect of liquid composition on the partitioning of Ni between olivine and silicate melt. *Contrib. Mineral. Petrol.* **172**, 3 (2017).

31. Kruger, F. J. The Sr-isotopic stratigraphy of the western Bushveld Complex. *S. Afr. J. Geol.* **97**, 393–398 (1994).

32. Mayne, M., Moyen, J. -F., Stevens, G. & Kaislaniemi, L. Rcrust: a tool for calculating path-dependent open system processes and application to melt loss. *J. Metamorph. Petrol.* **34(7)**, 663–682 (2016).

33. Holland, T. J. B. & Powell, R. An improved and extended internally-consistent thermodynamic dataset for phases of petrological interest, involving a new equation of state for solids. *J. Metamorph. Geol.* **29**, 333–383 (2011).

34. Winter, J. D. N. *Principles of Igneous and Metamorphic Petrology*. 203–204 (New York Prentice Hall, 2010).

35. Danchin, R. V. in *The Mantle Sample: Inclusions in Kimberlites and Other Volcanics. Proceedings of the Second International Kimberlite Conference* (eds. Boyd, F. R. & Meyer, H. O. A.) 104–126 (American Geophysical Union, Washington, 1979).

36. Costa, A., Caricchi, L. & Bagdassarov, N. A model for the rheology of particle-bearing suspensions and partially molten rocks. *Geochem. Geophyst. Geosyst.* **10(3)** (2009).

37. Connolly, J. A. D. & Schmidt, M. W. Viscosity of Crystal-Mushes and Implications for Compaction-Driven Fluid Flow. *J. Geophys. Res. Solid Earth* **127(9)**, e2022JB024743 (2022).

38. Lesher, C. E. & Spera, F. J. in *The Encyclopaedia of Volcanoes* (eds. Sigurdsson, H., Houghton, B., Rymer, H., Stix, J. & McNutt, S.). 118 (Academic Press, 2015).

Stellenbosch University https://scholar.sun.ac.za

39. Annen, C., Blundy, J. D., Leuthold, J. & Sparks, R. S. J. Construction and evolution of igneous bodies: towards an integrated perspective of crustal magmatism. *Lithos* **230**, 206–221 (2015).

40. Sparks, R. S. J., Annen, C., Blundy, J. D., Cashman, K. V. Rust, A. C. & Jackson M. D. Formation and dynamics of magma chambers. *Philos. Trans. R. Soc. A.* **377,** 20180019 (2019).

41. Yao, Z., Mungall, J. E. & Jenkins, M. C. The Rustenburg Layered Suite formed as a stack of mush with transient magma chambers. *Nat. Commun.* **12**, 505 (2021).

42. Nebel O., Sossi P. A., Ivanic T. J., Benard A., Gardiner N. J., Langford R. L. & Arculus R. J. Incremental Growth of Layered Mafic-Ultramafic Intrusions Through Melt Replenishment Into a Crystal Mush Zone Traced by Fe-Hf Isotope Systematics. *Front. Earth Sci.* **8**, 2 (2020).

43. Jean, M. M. & Shervais, J. W. The distribution of fluid mobile and other incompatible trace elements in orthopyroxene from mantle wedge peridotites. *Chem. Geol.* **457**, 118–130 (2017).

44. Holland, T. J. B. & Powell, R. Activity-composition relations for phases in petrological calculations: an asymmetric multicomponent formulation. *Contrib. Mineral. Petrol.* **145**, 492–501 (2003).

45. White, R. W., Powell, R., Holland, T. J. B. & Worley, B. A. The effect of TiO_2 and Fe_2O_3 on metapelitic assemblages at greenschist and amphibolite facies conditions: mineral equilibria calculations in the system K_2O–FeO–MgO–Al_2O_3–SiO_2–H_2O–TiO_2–Fe_2O_3. *J. Metamorph. Geol.* **18(5)**, 497–512 (2000).

Stellenbosch University https://scholar.sun.ac.za

CHAPTER 5

Conclusions

This study has used a thermodynamically constrained phase equilibrium modelling approach to investigate the details of how Earth's upper sub-cratonic mantle melts, how the partial melting reactions may control the composition of magmas through the production of entrainable peritectic crystals, as well as the consequences of this for the formation of layered ultramafic cumulates in the continental crust and the chromium deposits they host.

Phase equilibrium modelling of upper mantle partial melting

In investigating the applicability of using thermodynamic modelling to study partial melting in the upper mantle, this work has shown that thermodynamic modelling, if carefully applied, can represent a reasonable alternative to performing experimental investigations in order to understand how rock systems behave over a range of Pressure-Temperature-Composition (P-T-X) conditions. The constant evolution of phase equilibrium modelling has developed the methodology to be possibly even more desirable than conducting experiments due to several factors, such as greater P-T resolution, the ability to select bulk composition at will, control of volatiles and their fugacities, and more, all in a much shorter timeframe. In particular, thermodynamic modelling front-ends, such as Rcrust (Mayne et al., 2016), allow investigation into the roles of processes that result in bulk compositional change, including melt and magma extractions, and the consequences thereof for the downstream evolution of the source and the resulting bulk composition of the segregated liquid. Attempting to address such complexities via experiments is possible, but it is exceedingly time consuming to synthesise multiple compositions, locating the solidus is not straightforward, and at low melt fractions, finding analysable volumes of quenched melt is problematic, even when utilising melt traps, which come with their own problems.

Evidently, experimental design factors must introduce some degree of uncertainty into the experimental results produced during partial melting investigations. Although several previous studies that have compared thermodynamic modelling outputs with experimental results (e.g. García-Arias, 2020; Gervais & Trapy, 2021; Hernández-Uribe et al., 2022; Tropper & Hauzenberger, 2015; Tomlinson & Holland, 2021) do discuss such uncertainties, no attempt has been made to constrain them. The overarching conclusion that can be drawn from an analysis of uncertainties in experimental studies focussed on partial melting of mantle rocks, is that there is a significant likelihood that the actual effective bulk compositions depart from the reported bulk compositions in terms of H_2O content, CO_2 content, and FeO content,

Stellenbosch University https://scholar.sun.ac.za

depending on the details of the experimental design. This has been investigated in a realist manner in Chapter 2, by using thermodynamic modelling to systematically model an envelope of uncertainty that these factors introduce. In investigating the effects of the incorporation of small amounts of H_2O or CO_2 in the capsule, or the effects of Fe loss, the results show that the match between experimental data and modelling outputs show improvement, particularly due to the incorporation of a tiny amount of H_2O, which results in notable effects on the location of the solidi that lowers the percentage difference between modelled and experimental results (Figure 2-7). However, a reasonable mismatch still exists between the two forms of investigation, in general. In essence, experimental and modelling matches may never correlate perfectly, even by factoring in experimental and modelling uncertainties that may be inherent to the results (Table 5-1). Regardless, thermodynamic modelling as a reasonable alternative to performing experiments in establishing the behaviour of systems across large ranges of P-T-X space is tenable. Importantly, however, thermodynamic modelling cannot be considered to represent the absolute truth of the behaviour of any given chemical system at a particular P-T point; in such cases, experimental investigations produce more desirable outcomes due to the fact that the full system can be investigated, including the effects of kinetics (e.g. García-Arias, 2020), if the experiments are designed appropriately.

Experiments	**Thermodynamic modelling**
1) Pt or AgPd capsules: - Uptake of Fe	1) Thermodynamic datasets and *a-x* models: - The understanding of thermodynamic properties of minerals and melts are limited to experimentally determined data
2) Graphite-liners to avoid uptake of Fe: - Results in higher fH_2O and fCO_2 in the capsule - Experiments inevitably buffered to C-CO	2) Internal consistency: - Dependant on input data: thermodynamic datasets and their interactions with *a-x* models - Limits use of the various *a-x* models to predetermined sets
3) Temperature and Pressure: - Deviations of reported values due to friction or temperature control	3) Chemical system: - Omission of chemical components: Phases do not stabilise and show lowered or limited appearances - Elemental partitioning overestimation: Incorrect prediction of phase stability

Stellenbosch University https://scholar.sun.ac.za

4) Temperature gradients: - Disequilibrium	4) Kinetics: - Modelling cannot consider the effects of grain sizes, diffusion, heat slopes, etc
5) Diamond aggregates or carbon spheres: - Low pressure in diamond void spaces separate liquids that are in disequilibrium with the system - Carbon spheres require longer calibration runs which may increase Fe loss - Inclusion of some C-bearing gas species in both methods	5) Use of input data across software/front-ends: - Potential for inaccuracies during formatting, or delays
6) Phase compositions: - The analyses of silicate glasses have an effect on reported compositions - More prominent for glasses that are hydrous or have higher alkali contents - Hard to identify low melt fractions due to crystallisation upon quenching	6) Correct use of software/front-end: - User does not implement parameters inherent to the calculation strategy: e.g. resolution is too low or tie-lines not identified

Table 5-1. Summary list of common experimental uncertainties and thermodynamical modelling uncertainties, as discussed in Chapter 2.

As is discussed in detail in Chapter 2, thermodynamic modelling relies on thermodynamic datasets as well as activity-composition (*a-x*) models, and several options of modelling software utilise particular calculation strategies, which may vary depending on their intended use. During the investigation of thermodynamic modelling compared to experiments under upper mantle conditions in this study, two of the most commonly used datasets (Berman, 1988; Holland & Powell, 2011) were considered. The dataset of Berman (1988), as well as a range of *a-x* models, are embedded in the MELTS family of software (Asimow & Ghiorso, 1998; Ghiorso & Sack, 1995; Ghiorso et al., 2002), which is reported as using Gibbs free energy minimisation in calculations involving P-T inputs. Importantly, this embedded nature of MELTS input files limits the extent to which the behaviour of the combination of input data and the software's calculation strategy can be investigated. In contrast, the dataset of Holland & Powell (2011) and the sets of *a-x* models originally developed for the THERMOCALC software can be used across a range of other thermodynamic software and applications when suitably adapted, and where access to the input files allows the user to investigate the details

Stellenbosch University https://scholar.sun.ac.za

of the behaviour of mineral and melt species, and how calculation strategies may affect the outputs.

Such transparency is important in considering the differences in the behaviour of outputs produced using the same thermodynamic dataset and calculation strategy, but different *a-x* models. Thermodynamic calculations were performed in this study using Rcrust, which performs Gibbs free energy minimisation using Perple_X, with the Holland & Powell (2011) thermodynamic dataset, firstly using the *a-x* models from Holland et al. (2018) and secondly using the *a-x* models from Tomlinson & Holland (2021). The latter model (further referred to as TH) is intended to address some of the issues observed in the former (further referred to as HGP); a number of the known issues as applicable to different thermodynamic modelling applications for upper mantle conditions are discussed in more detail in Chapter 2. Although substantial improvements are shown for assemblage and proportion predictions using TH (comparing Addendums A and E), predictions of melt compositions appear to improve or worsen, depending on the component of the melt (Figure 5-1), and whether results are considered in terms of melt fraction (a-j) or temperature (k-t). For any given user, the perceived accuracy may vary depending on what they regard as the more important factor. In other words, because melt abundance increases with temperature, the variations in the increase in melt abundance may result in predicted melt components that are either more accurate for the given melt fraction, or more accurate for the given temperature, compared to experimental studies - either of which may be preferred by the user. Thus, although the TH models in Figure 5-1 display improvement for SiO_2 (a, f, k, p) and Na_2O (c, j, o, t) in terms of melt fraction and temperature, components such as FeO (c, h, m, r) and CaO (d, i, n, s) may improve in terms of melt fraction, but appear to worsen in terms of temperature. A user that is to draw important conclusions from specific components of melt or mineral phases may decide to utilise either- or set of igneous *a-x* models, depending on the accuracy of the match they require for a specific component at particular P-T conditions. A secondary conclusion of the essential first step of this work is thus that 'improvements' for sets of *a-x* models may better some aspects of modelling, but may result in other shortfalls. Following the investigation conducted in this thesis, the author is inclined to favour the use of HGP *a-x* models over that of TH, more so because the HGP melt model allows investigations of bulk compositions that include H_2O, and recently, CO_2 (HGPH; Heinrich & Connolly, 2022), whereas at present, the TH melt model does not have this capability.

Stellenbosch University https://scholar.sun.ac.za

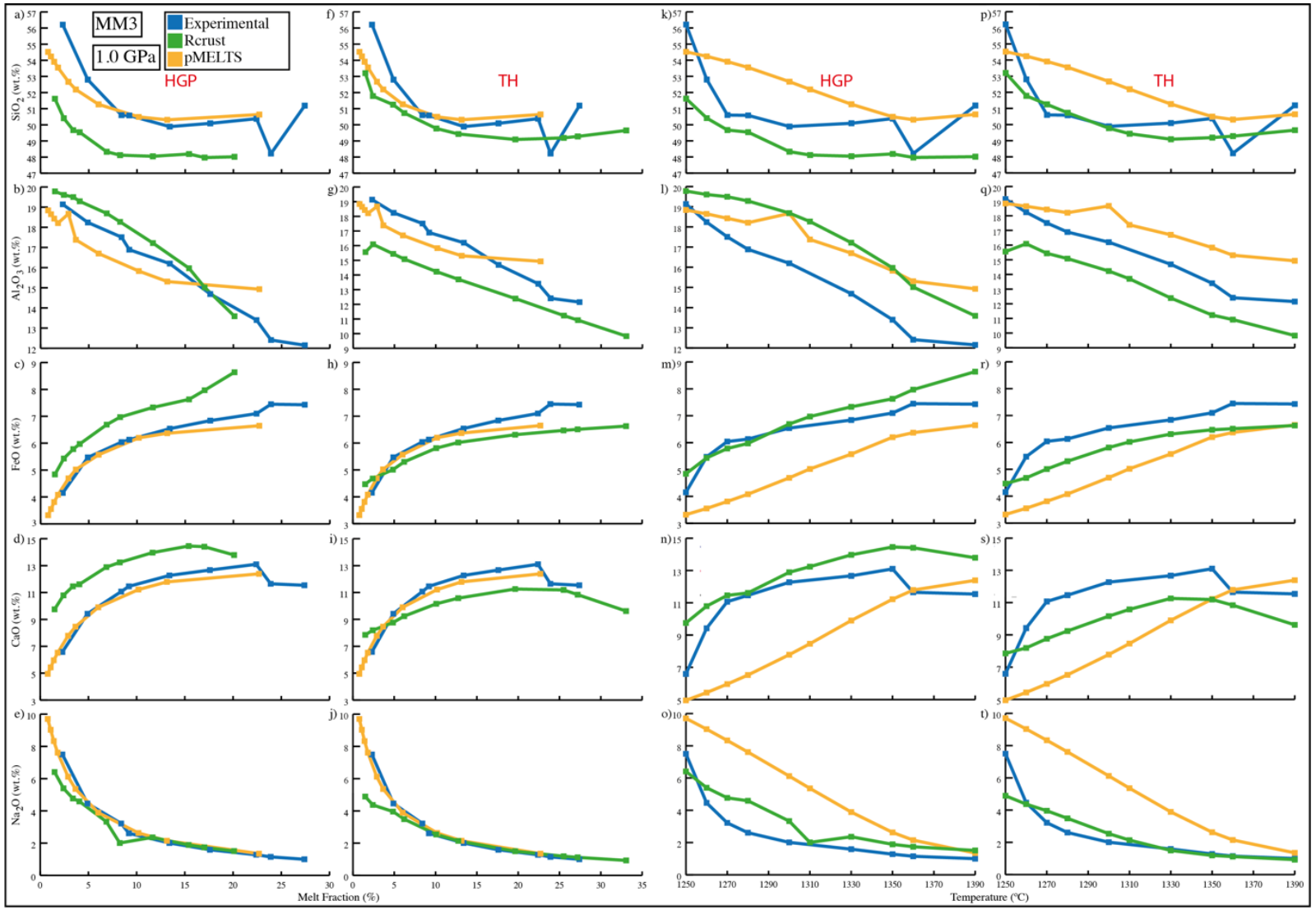

Figure 5-1. A comparison of selected components of melt compositions as the melt fraction (a-e; k-o) increases and as the temperature (f-j; p-t) increases at 1.0 GPa from the experimental study on MM3 of Baker & Stolper (1994) and Hirschmann et al. (1998), with the calculated values from pMELTS and Rcrust as determined in this study. The results from Rcrust include outputs using the Holland et al. (2018) *a-x* models (HGP) as well as the Tomlinson & Holland (2021) *a-x* models (TH).

Stellenbosch University https://scholar.sun.ac.za

The ability of users to familiarise themselves with the details associated with sets of *a-x* models beyond what is specified on a superficial level, is crucial in selecting the best combination of input files during thermodynamic investigation across a chosen P-T-X space. It is this capability that renders limitations for the use of the MELTS family of software, considering the embedded nature of its input files. Figure 5-2 displays melt fraction curves from the experimental-modelling comparative investigations presented in Chapter 2 and Subchapter 2.2 for pMELTS and rhyolite-MELTS, as well as Rcrust. These investigations involve two mantle sources, and a basaltic andesite. What is particularly apparent in Figure 5-2a is that although both modelling bundles are reported as following the same calculation strategy, the melt curves produced by pMELTS/rhyolite-MELTS appear extremely similar in that, after a single inflection point soon after reaching the solidus, a linear increase is observed.

This is not noticeable for Rcrust outputs (Figure 5-2b), where no distinct melt curve behaviour is observed. Although such variation in the outputs produced by the modelling bundles are likely attributed to differences in the thermodynamic datasets and *a-x* models, the fact that the user cannot investigate the interaction between the MELTS family input files, and how these interact with the calculation strategy, makes it impossible to truly determine how the outputs are generated. Additionally, as made clear in Figure 5-1, the chosen set of *a-x* models can have a notable effect on the outputs of the modelling, and the ability to inspect the details of these models beyond what is publicised are of profound importance. It is this lack of transparency, together with the results displayed in Chapter 2 and Subchapter 2.2 for experimental-modelling comparisons of phase assemblages, proportions, and compositions, that bring the author to the conclusion that the Holland & Powell (2011) dataset, in combination with the igneous *a-x* models of either Holland et al. (2018) or those extended by Tomlinson & Holland (2021), are preferred for conducting thermodynamic modelling investigations under upper mantle conditions and at crustal emplacement conditions.

The consequences of entrainment of components of the source

As is discussed in detail in Chapter 3, advances in the understanding of partial melting processes and the conditions under which partial melting occurs in the continental crust have aided enormously in establishing the connection between various types of source rocks, the P-T conditions of partial melting, and the composition of the magmas, and importantly, how the entrainment of the source peritectic assemblage plays a major role in shaping granitic magma chemistry (e.g. Chappell et al., 1987; Clemens et al., 2011; Stevens et al., 2007). Conversely, because partial melting of the mantle cannot be observed directly, and access to mantle source

Stellenbosch University https://scholar.sun.ac.za

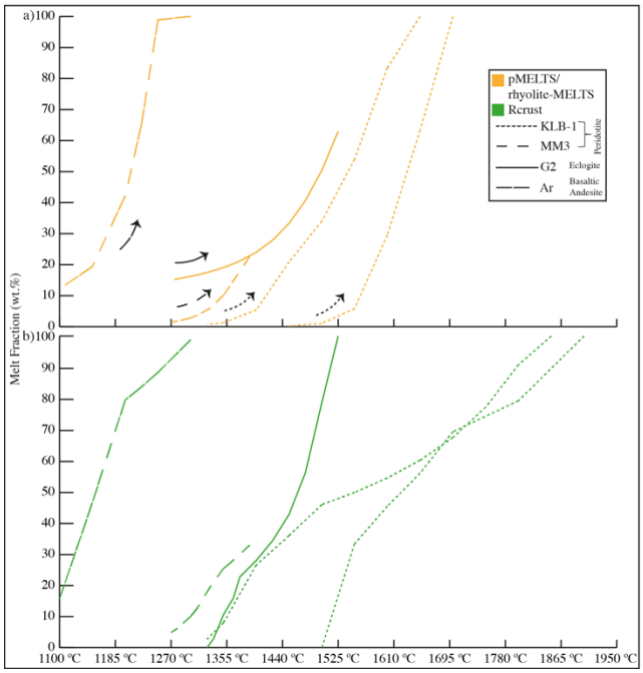

Figure 5-2. Modelled melt fractions from pMELTS and Rcrust as determined in this study for the compositions of KLB-1 of Takahashi et al. (1993) at 1.0 and 1.5 GPa, MM3 of Baker & Stolper (1994) and Hirschmann et al. (1998) at 1.0 GPa, G2 from Pertermann & Hirschmann (2003a, 2003b) at 3.0 GPa, and *Ar anhydrous* of Pertermann & Lundstrom (2006) at 0.5 GPa.

rocks that have undergone partial melting are limited, constraining the P-T range within which mantle partial melting occurs and the details of the melting reactions are more complex, relying heavily on experimental studies for insights into mantle melting reactions. Several of these experimental works have identified the formation of peritectic phases during incongruent melting of the mantle across a range of melt fractions (e.g. Kinzler, 1997; Niu, 1997; Presnall et al., 1978; Tomlinson & Kamber, 2021), and although these new crystals form in and are thus are suspended in the melt, the concept of entraining some or all of the peritectic assemblage to the melt upon segregation from the mantle source has not previously been considered.

By utilising the Rcrust software (details outlined in Chapter 3), this work has developed a set of methodologies that have identified peritectic phase production during partial melting reactions in the upper mantle. Considering the general consensus that the upper mantle is broadly peridotitic due to the diversity of potential mantle source compositions observed from erupted mafic and ultramafic rock xenolith suites (e.g. Jacob, 2004; Mathias et al., 1970), these methodologies have been applied to differing compositions of known mantle sources. By investigating an eclogitic and peridotitic mantle source and the stoichiometry of their melting reactions across upper mantle P-Ts, insights into the variation in the behaviours of these different mantle sources during partial melting, and areas where solid phases increase in abundance after the solidus, could be identified (Figure 5-3). Importantly, by using Rcrust to model melt and magma (i.e. melt plus crystals) extractions along different P-T paths of isobaric

Stellenbosch University https://scholar.sun.ac.za

and adiabatic nature, the resultant compositional range of mafic to intermediate melts or magmas that may segregate from these ultramafic sources under various conditions could be explored, and the consequences of the entrainment of peritectic phases on the bulk compositions of the magmas could be quantified (Figure 5-4).

The results from this second step of the work support the paramount conclusion that the heterogeneity observed in magmas that are produced from partial melting of peridotitic and eclogitic mantle sources are not only a function of the heterogeneity of said mantle source, but may also depend on the entrainment of peritectic phases to the melt, as well as the nature and quantity of the peritectic crystals incorporated into the magma. As displayed in Figure 5-4, the compositions observed for successive extractions of pure melts display more linear trends, whereas magmas that have entrained the maximum amount of peritectic phase/s available upon segregation show a much greater compositional diversity, with fractional crystallisation of either melt or magma amplifying the range of compositions observed for both scenarios. These results open up a range of new vectors that may explain why mafic magmas from continental environments can show substantial variability, considering the enormously scattered range of basalt compositions observed worldwide. Importantly, however, even at low degrees of partial melting, the melts/magmas produced by the garnet lherzolite utilised in this study are not poor

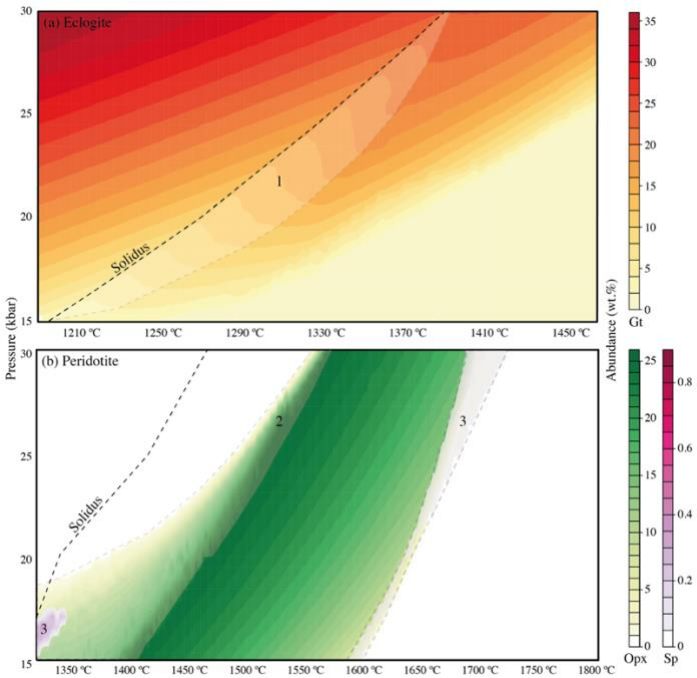

Figure 5-3. Using thermodynamic modelling techniques to identify peritectic phase formation during partial melting of two upper mantle source rocks. The black dashed line indicates the solidus. a) The abundance of garnet in wt.% over the P-T range investigated for the eclogitic composition. The transparent shaded area extending up-temperature from the solidus displays the area of peritectic garnet production (1) for paths that are dominated by temperature increase. b) The abundance of orthopyroxene (green) and spinel (pink) in wt.% across the P-T range investigated for the peridotitic composition. The transparent, shaded fields identify the areas of production of peritectic orthopyroxene (2) and peritectic spinel (3).

Stellenbosch University https://scholar.sun.ac.za

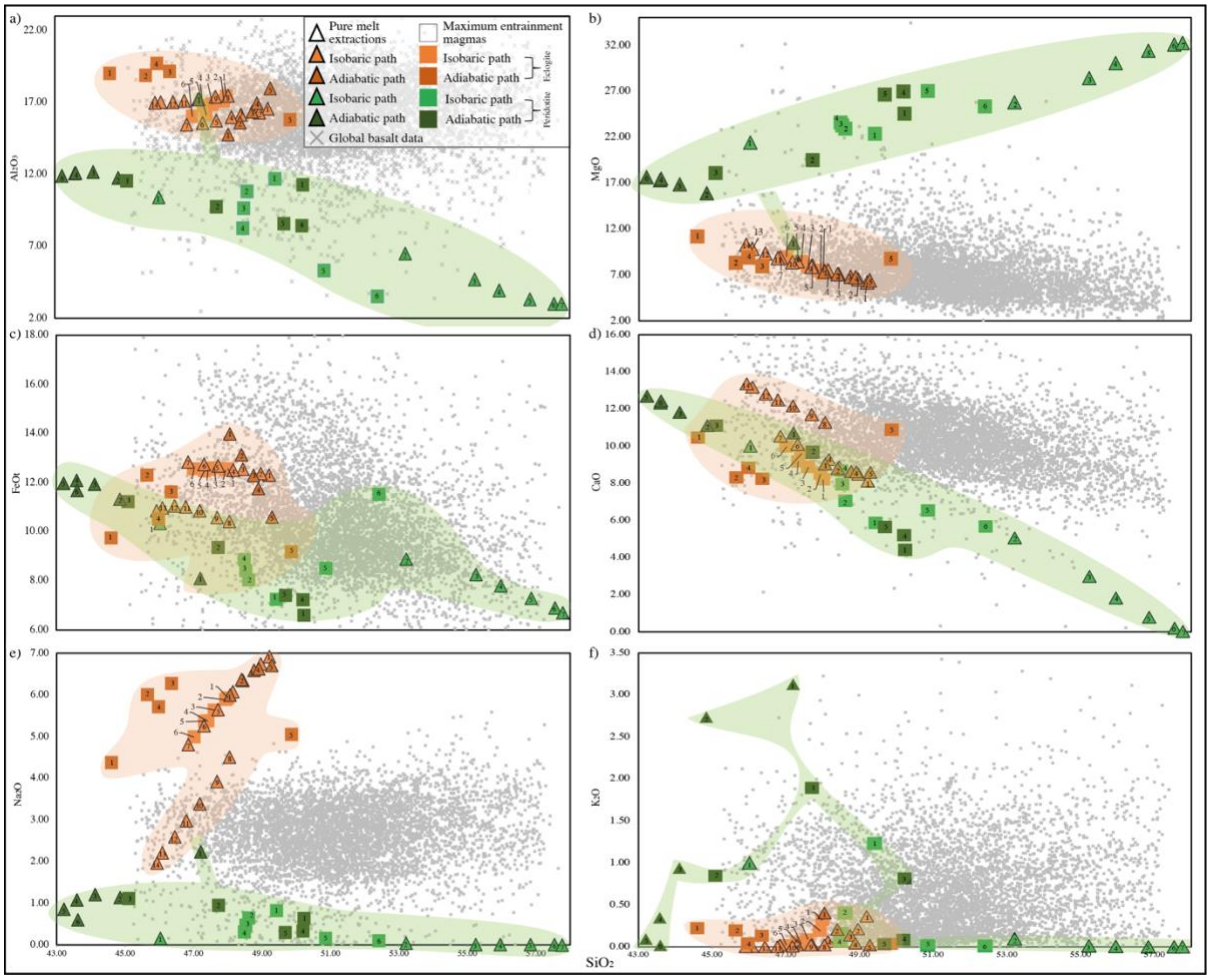

Figure 5-4. Harker diagrams displaying a summary of the compositions of melts and magmas derived from the modelled extraction events in Chapter 3, during partial melting of an eclogite and peridotite as a result of isobaric heating or adiabatic decompression. These outputs are superimposed on a global basalt database compiled from various continental tectonic settings, displayed in grey. Details of the source and selection criteria of the global basalt database is available in Addendum C. The compositions included in the summary are all magmas separated from the residual system during a maximum entrainment extraction routine, including melts with no entrained crystals (except for the eclogite isobaric heating path), as well as compositions constituting pure melt extractions, i.e. no peritectic entrainment was involved. Each set of magmas are numbered in order of their extraction.

of global basalt compositions, unless significant olivine fractionation occurs or magma mixing is involved. Basaltic to intermediate rocks from continental environments thus most likely represent magmas derived from an eclogitic source with lower Na_2O contents, or a peridotite metasomatised by a significant component of eclogite, or mixed with a high-SiO_2 andesitic composition.

Other key conclusions from this section of the work are, firstly, that the compositional variation observed in basalt compositions should be considered a source characteristic, with fractionation merely reflecting the diversity of the primitive melt or magma. Secondly, although source heterogeneity is known to have a fundamental control on *melt* compositions, source entrainment processes may exert a fundamental control on the large-scale diversity of *magma* compositions that may be produced and emplaced into the continental crust.

Stellenbosch University https://scholar.sun.ac.za

The role of peritectic phase entrainment in the petrogenesis of chromitite and the formation of ferromagnesian layers

Recognising the fundamental role that peritectic phase entrainment can play in shaping the chemistry of mafic magmas has important implications when considering the ambiguity surrounding the parental melts of the Rustenburg Layered Suite (RLS) of the Bushveld Complex (BC) in South Africa, particularly the transport of Cr from the mantle to the crust in quantities large enough to produce the chromitites as present in Layered Mafic Intrusions (LMIs) found in the upper crust. The latter has remained a major question in igneous petrology communities and from an economic geology perspective.

Although a great number of models and estimations have been put forward by various authors on both fronts (chromitite formation in Table 1-1 and RLS parental melts in Table 1-2), the fundamental limitation of all remains the limited solubility of Cr in basaltic melts (Figures 1-5 & 5-5). Regardless of whether the melt becomes saturated in chromite before or after intruding into the magma chamber, as is generally the major focus of many of the models proposed for chromitite formation, vast amounts of source liquid would be required in either case to produce the chromitites and silicate layering observed in the igneous stratigraphy of the lower parts of the RLS, where such quantities of material are not observed in the rock record.

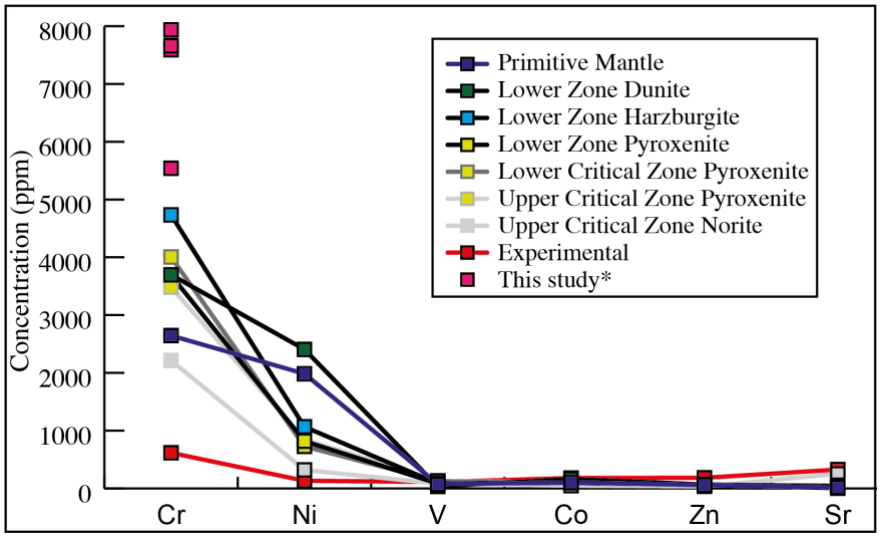

Figure 5-5. Spidergram showing selected trace element concentrations (ppm) of proposed Primitive Mantle (Lyubetskaya & Korenega, 2006), the Lower Zone and Critical Zone of the RLS (Maier et al., 2012), and experimentally determined values of basaltic partial melts (Klemme et al., 2002; Spandler et al., 2017; Takahashi, 1986). Cr ppm data is also presented for the magmas modelled in this study. There is a clear difference between the low abundance of Cr in the proposed Primitive Mantle composition and in experimental basaltic partial melts, compared to the Cr in the lower portions of the RLS. In comparison, other trace elements, such as Nickel (Ni), do not show the same extreme discrepancy, with almost no difference observed for Vanadium (V), Cobalt (Co), Zinc (Zn), and Strontium (Sr). The bulk compositions of the magmas modelled in this study are made up of melt as well as peritectic pyroxene crystals, which increases the available Cr in the magma to concentrations much higher than is observed for experimental partial melts, eliminating the issue of the 'chrome-paradox'. *Values presented here include the modelled magmas with the highest Cr_2O_3 contents.

Stellenbosch University https://scholar.sun.ac.za

This study has developed a completely new hypothesis, which is entirely based on first principles of fundamental melting reaction dynamics, for the formation of chromitite layers in LMIs, such as the RLS. Investigations into the partial melting reactions of mantle peridotite displayed peritectic pyroxene formation with melt (Figure 3-6), and the peritectic pyroxene crystals contain substantial amounts of Cr_2O_3 (Figures 5-5 & 5-6). It is clear from Figure 5-6 that garnet is the major reactant host of the Cr_2O_3, followed by clinopyroxene. As these phases are consumed during the melting reaction and the melt cannot accommodate the increasing abundance of Cr_2O_3, the remaining Cr_2O_3 substitutes into the newly formed orthopyroxene phase (Figure 5-6), which increases the available Cr in the magma by several orders of magnitude.

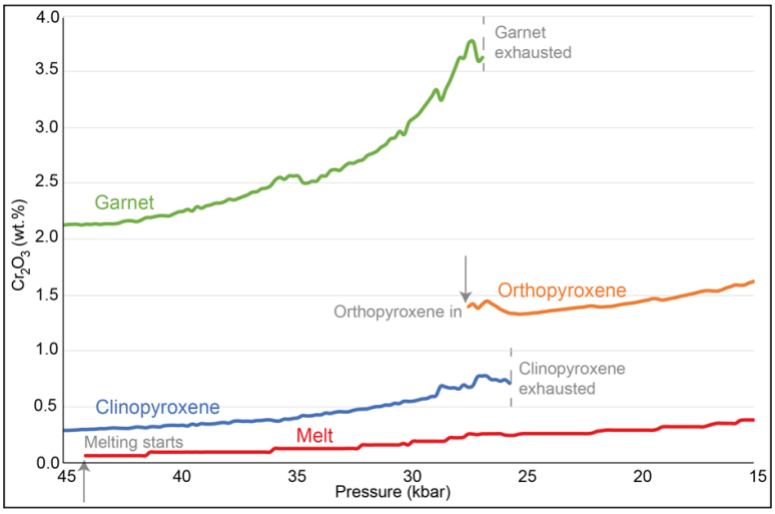

Figure 5-6. Plot showing the Cr_2O_3 abundance of the chromium-bearing phases of the investigated garnet peridotite (Table 4-1) during the partial melting reaction along an adiabatic decompression path. Garnet is the reactant phase that is the major host of the chromium, followed by clinopyroxene. As the melting reaction continues and these phases are consumed, Cr_2O_3 substitutes into melt and the newly forming peritectic orthopyroxene phase.

Importantly, the peritectic orthopyroxene is the first orthopyroxene crystal to appear. This favours its formation as a discrete peritectic crystal in melt (Zellmer et al., 2016). Experiments using glass starting materials have demonstrated the formation of peritectic orthopyroxene during mantle melting (Grove et al., 2013) and experiments on crustal compositions that have used mineral mixtures as starting materials (Stevens et al., 1997) commonly show that orthopyroxene nucleates easily and forms many small crystals suspended in the melt. In addition, rates of mantle melting in the plume settings that likely apply to the formation of large igneous provinces in cratonic environments are high (White, 1993). Thus, it is likely that melt segregation from the source would carry peritectic orthopyroxene crystals with it on magma segregation.

Stellenbosch University https://scholar.sun.ac.za

For high temperature melt extractions, the re-equilibration of the entrained orthopyroxene with melt during magma ascent allows the liberation of Cr from this orthopyroxene phase, and forces crystallisation of olivine and chromite crystals, producing a melt-dominated crystal slurry that is emplaced into the magma chamber in the continental crust (Figure 4-6). Here, density segregation allows the separation of the olivine and chromite crystals, forming a layer of chromitite upon emplacement into the magma chamber. It is notable that if the temperature path of magma ascent and the composition of the magma batch are such that a significant quantity of pyroxene remains in the magma after magma ascent, the available Cr_2O_3 may remain accommodated within pyroxene, and chromitite layers will not form (Fig. 4-5c). In either scenario, cooling of the magma can produce layers of dunite, harzburgite, pyroxenite, and anorthosite (or norite), depending on the extent of the cooling before the expulsion of melt from the chamber. These results broadly mimic the igneous stratigraphy as is observed in the lower parts of the RLS of the BC.

The proposed model can also be applied to other LMIs, such as the Stillwater Complex in Montana, USA, or the Skaergård Intrusion in Greenland, both discussed here briefly. The Ultramafic Series of the Stillwater Complex is subdivided into a Peridotite Zone and Orthopyroxene Zone (Winter, 2010). The lower Peridotite Zone is made up of 20 cycles of macrorhythmic layering with a distinct lithological sequence, starting with dunite and chromitite, then harzburgite, and then orthopyroxenite (e.g. Jackson, 1961). This typical basaltic crystallisation sequence is similar to that observed in the RLS, and considering Figures 4-4 and 4-5, peritectic orthopyroxene entrainment can broadly explain the lithologies of the Peridotite Zone of the Stillwater Complex, if magmas are emplaced as a series of sills where the crystallising phases undergo gravity settling. The Skaergård Intrusion is a small LMI subdivided into a Layered Series, Upper Border Series, and Marginal Border Series (Winter, 2010). The Layered Series displays cumulates of olivine and plagioclase (set in interstitial augite), followed by augite, pigeonite, and magnetite as cumulate phases. It is clear that, during emplacement, an orthopyroxene entraining magma is likely not able to produce a crystallisation sequence that would satisfy the igneous stratigraphy observed in the Layered Series. However, the entrainment of approximately 35 wt.% peritectic clinopyroxene produced during the partial melting of an eclogite source can result in the simultaneous crystallisation of the majority of the phases observed (Figure 5-7). Although other mechanisms may be at play that denotes a simple gravity settling scenario, the results shown in Figure 5-7 suggest that the igneous stratigraphy observed in the Layered Series of the Skaergård Intrusion can be broadly mimicked by the phases produced during peritectic crystal entrained magma emplacement and

Stellenbosch University https://scholar.sun.ac.za

cooling at crustal pressures, proving that the model proposed in this study can be applied to the formation of LMIs in a general sense. It is thus clear that the range of available mantle source rocks, their melting reaction stoichiometries under different P-T conditions, and consequently, the various peritectic phases available for entrainment to the segregating magmas, can produce a large number of outcomes at the level of emplacement.

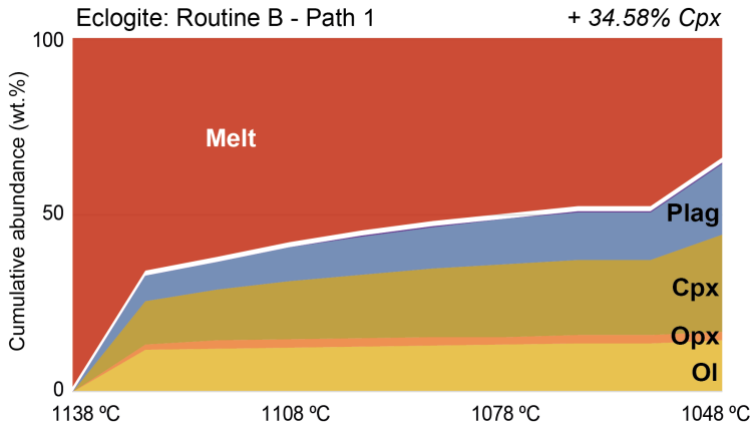

Figure 5-7. Plot showing cumulative phase abundance produced upon magma extracted from an eclogitic source being emplaced at 3 kbar and undergoing cooling from emplacement temperature to 1048 °C. Investigating the melting reactions in a representative bimineralic eclogite (Addendum C, Table 2) during adiabatic ascent from 30–15 kbar showed the production of different peritectic phases as the melting reaction continues. After magma extraction, the simulation of the emplacement of a peritectic clinopyroxene entraining magma yielded results that show similar crystallising phases as is observed in the Layered Series of the Skaergård Intrusion in eastern Greenland.

From the above, it is apparent how the entrainment of peritectic phases to melts produced during partial melting in the mantle is an important, previously overlooked mechanism that has proven pertinent to the understanding of LMIs. By providing a simple and elegant explanation for the formation of the RLS in Chapter 4, the volumetric problems implicit in other theories of chromitite formation or suggested parental melts is overcome. The solubility problems associated with LMIs that contain layers of chromitites are insurmountable unless other mechanisms for including Cr into the magma as a crystal phase is considered. This work has solved this ‘chrome-paradox’ by showing how the identification of Cr-rich peritectic crystals and their probable entrainment to mantle melts are the key to a simple and effective alternative explanation for the formation of chromitite layers in LMIs, particularly the RLS. Not only does this render intensive and complicated models moot, but paves the way for a new perspective on the investigation of mantle melting, the fundamental mechanisms that might be at play, and the roles these mechanisms may have in the formation of magmatic deposits.

Stellenbosch University https://scholar.sun.ac.za

References

1. Asimow, P.D. and Ghiorso, M.S. 1998. Algorithmic modifications extending MELTS to calculate subsolidus phase relations. *American Mineralogist*, 83:1127–1132.
2. Berman, R.G. 1988. Internally-consistent thermodynamic data for minerals in the system Na_2O-K_2O-CaO-MgO-FeO-Fe_2O_3-Al_2O_3-SiO_2-TiO_2-H_2O-CO_2. *Journal of Petrology* 29(2):445–522.
3. Chappell, B.W., White, A.J.R. and Wyborn, D. 1987. The importance of residual source material in granite petrogenesis. *Journal of Petrology*, 28:1111–1138.
4. Clemens, J.D., Stevens, G. and Farina, F. 2011. The enigmatic sources of I-type granites: the peritectic connexion. *Lithos*, 126:174–181.
5. García-Arias, M. 2020. Consistency of the activity–composition models of Holland, Green, and Powell (2018) with experiments on natural and synthetic compositions: a comparative study. *Journal of Metamorphic Geology*, 38(9):993–1010.
6. Gervais, F. and Trapy, P.-H. 2021. Testing solution models for phase equilibrium (forward) modeling of partial melting experiments. *Contributions to Mineralogy and Petrology*, 167(4).
7. Ghiorso, M.S. and Sack, R.O. 1995. Chemical mass transfer in magmatic processes, IV. A revised and internally consistent thermodynamic model for the interpolation and extrapolation of liquid-solid equilibria in magmatic systems at elevated temperatures and pressures. *Contributions to Mineralogy and Petrology*, 119:197–212.
8. Ghiorso, M.S., Hirschmann, M.M., Reiners, P.W. and Kress, V.C.III. 2002. The pMELTS: A revision of MELTS for improved calculation of phase relations and major element partitioning related to partial melting of the mantle to 3 GPa. *Geochemistry Geophysics Geosystems*, 3(5).
9. Grove, T.L., Holbig, E.S., Barr, J.A., Till, C.B., and Krawczynski, M.J. 2013. Melts of garnet lherzolite: experiments, models and comparison to melts of pyroxenite and carbonated lherzolite. *Contributions to Mineralogy and Petrology*, 166:887–910.
10. Heinrich, C.A. and Connolly, J.A.D. 2022. Physical transport of magmatic sulfides promotes copper enrichment in hydrothermal ore fluids. *Geology*, 50:1101–1105.
11. Hernández-Uribe, D., Spera, F.J., Bohrson, W.A. and Heinonen, J.S. 2022. A comparative study of two-phase equilibria modeling tools: MORB equilibrium states at variable pressure and H_2O concentrations. *American Mineralogist*, 107:1789–1806.

Stellenbosch University https://scholar.sun.ac.za

12. Holland, T.J.B. and Powell, R. 2011. An improved and extended internally consistent thermodynamic dataset for phases of petrological interest, involving a new equation of state for solids. *Journal of Metamorphic Geology*, 29:333–383.
13. Holland, T.J.B., Green, E.C.R. and Powell, R. 2018. Melting of peridotites through to granites: A simple thermodynamic model in the system KNCFMASHTOCr. *Journal of Petrology*, 59:881–900.
14. Jackson, E.D. 1961. Primary textures and mineral associations in the ultramafic zone of the Stillwater complex, Montana. *Geological Survey Professional Paper 358*, https://doi.org/10.3133/pp358.
15. Jacob, D.E. 2004. Nature and origin of eclogite xenoliths from kimberlites. *Lithos*, 77:295–316.
16. Kinzler, R.J. 1997. Melting of mantle peridotite at pressures approaching the spinel to garnet transition: Application to mid-ocean ridge basalt petrogenesis. *Journal of Geophysical Research*, 102(B1):853–874.
17. Klemme, S., Blundy, J.D. and Wood, B.J. 2002. Experimental constraints on major and trace element partitioning during partial melting of eclogite. *Geochimica et Cosmochimica Acta* 66(17):3109–3123.
18. Long, X., Ballmer, M.D., Córdoba, A.M.-C. and Li, C.-F. 2019. Mantle Melting and Intraplate Volcanism Due to Self-Buoyant Hydrous Upwellings From the Stagnant Slab That Are Conveyed by Small-Scale Convection. *Geochemistry, Geophysics, Geosystems*, 20(11):4972–4997.
19. Lyubetskaya, T. and Korenaga, J. 2007 Chemical composition of Earth's primitive mantle and its variance: 1. Method and results. *Journal of Geophysical Research*, 112(B3).
20. Maier, W.D., Barnes, S-J. and Groves, D.L. 2012. The Bushveld Complex, South Africa: formation of platinum-palladium, chrome- and vanadium-rich layers via hydrodynamic sorting of a mobilized cumulate slurry in a large, relatively slowly cooling, subsiding magma chamber. *Mineralium Deposita*, 48:1–56.
21. Mathias, M., Siebert, J.C. and Rickwood, P.C. 1970. Some aspects of the mineralogy and petrology of ultramafic xenoliths in kimberlite. *Contributions to Mineralogy and Petrology*, 26:75–123.
22. Mayne, M., Moyen, J.-F., Stevens, G. and Kaislaniemi, L. 2016. Rcrust: a tool for calculating path-dependent open system processes and application to melt loss. *Journal of Metamorphic Petrology*, 34(7):663–682.

Stellenbosch University https://scholar.sun.ac.za

23. Niu, Y. 1997. Mantle Melting and Melt Extraction Processes beneath Ocean Ridges: Evidence from Abyssal Peridotites. *Journal of Petrology*, 38(8):1047–1074.
24. Presnall, D.C., Dixon, J.R., O'Donnell, T.H. and Dixon, S.A. 1978. Generation of Mid-ocean Ridge Tholeiites. *Journal of Petrology,* 20:3–35.
25. Spandler, C. Hammerli, J. and Yaxley, G.M. 2017. An experimental study of rare element distribution during partial melting of mantle heterogeneities. *Chemical Geology,* 462:74–87.
26. Stern, R.J. 2002. Subduction Zones. *Reviews of Geophysics,* 40(4): 3–1–3–38.
27. Stevens, G., Clemens, J.D. and Droop, G.T.R. 1997. Migmatites, granites and granulites: The data from experiments on "primitive" metasedimentary protoliths. *Contributions to Mineralogy and Petrology,* 128:352–370
28. Stevens, G., Villaros, A. and Moyen, J.-F. 2007. Selective peritectic garnet entertainment as the origin of geochemical diversity in S-type granites. *Geology*, 35:9–12.
29. Tomlinson, E.L. and Holland, T.J.B. 2021. A Thermodynamic model for the subsolidus evolution and melting of peridotite. *Journal of Petrology,* 62(1):egab012.
30. Tomlinson, E.L. and Kamber, B.S. 2021. Depth-dependent peridotite-melt interaction and the origin of variable silica in the cratonic mantle. *Nature Communications,* 12:1082.
31. Tropper, P. and Hauzenberger, C. 2015. How well do pseudosection calculations reproduce simple experiments using natural rocks: an example from high-P high-T granulites of the Bohemian Massif. *Austrian Journal of Earth Sciences,* 108(1):123–138.
32. van Wijk, J.W., Huismans, R.S., ter Voorde, M. and Cloetingh, S.A.P.L. 2001. Melty generation at Volcanic Continental Margins: no Need for a Mantle Plume? *Geophysical Research Letters,* 28(20):3995–3998.
33. White, R.S. 1993. Melt production rates in mantle plumes. *Philosophical Transactions of the Royal Society of London A,* 342:137–153.
34. Winter, J.D.N. 2010. *Principles of Igneous and Metamorphic Petrology.* New York: Prentice Hall. 228–232.
35. Zellmer, G.F., Sakamoto, N., Matsuda, N., Iizuka, Y., Moebis, A. and Yurimoto, H. 2016. On progress and rate of the peritectic reaction Fo + SiO_2 → En in natural andesitic arc magmas. *Geochimica et Cosmochimica Acta,* 185:383–393.

Stellenbosch University https://scholar.sun.ac.za

ADDENDA

ADDENDUM A

SUPPLEMENTARY DATA FOR RESEARCH PAPER 1 (CHAPTER 2)

The results from the comparisons of Rcrust (**using the TH activity-composition models**) and pMELTS predictions with the experimental study of KLB-1 (Takahashi, 1986; Takahashi et al., 1993), MM3 (Baker & Stolper, 1994; Hirschmann et al., 1998), and G2 (Pertermann & Hirschmann, 2003a, 2003b), as well as the outputs produced in establishing an envelope of uncertainty surrounding experimental results using thermodynamic modelling (**using the HGP activity-composition models and HGPH melt model**), is available upon request.

Stellenbosch University https://scholar.sun.ac.za

ADDENDUM B

SUPPLEMENTARY DATA FOR SUBCHAPTER 2.3

The results from the comparisons of Rcrust (**using the TH activity-composition models**) and rhyolite-MELTS predictions with the experimental study of *Ar Anhydrous* by Pertermann & Lundstrom (2006) is available upon request.

Stellenbosch University https://scholar.sun.ac.za

ADDENDUM C

SUPPLEMENTARY DATA FOR RESEARCH PAPER 2 (CHAPTER 3)

This Addendum is comprised of several files. Addendum C1 is recorded below. The modelled data associated with the eclogite (Addenda C2 & C4) and peridotite (Addenda C3 & C5) is available upon request.

Addendum C1

1. Introduction

1.1. Partial melting experimental studies starting compositions

	1611[1]	HK66[2]	KLB-1[3]	GA2[4]	RVK[5]	GA2 (2)[6]
SiO_2	44.54	48.35	44.65	50.15	46.67	50.03
TiO_2	0.25	0.22	0.16	1.97	0.40	1.83
Al_2O_3	2.80	4.91	3.60	15.79	16.50	17.06
Cr_2O_3	0.29	0.25	0.31	-	-	0.08
FeO_t	10.24	9.97	8.13	9.37	12.15	9.78
MgO	37.93	32.57	39.37	7.92	14.26	8.14
CaO	3.32	2.99	3.45	11.76	8.02	9.34
Na_2O	0.34	0.66	0.30	3.05	1.90	3.36
K_2O	0.14	0.07	0.02	0.03	0.09	0.37
Sum	100.00	100.00	100.00	100.00	100.00	100.00

Table 1. Bulk compositions of plotted eclogite and peridotite compositions. (-) indicates unreported values. Compositions were recalculated to 100% NiO, P_2O_5, MnO, and H_2O free; these oxides are not considered due to an incomplete set of solution models defining the compositional space, and only anhydrous and volatile-free experiments were included.

[1] Garnet peridotite nodule from Mysen & Kushiro (1977).

[2] Spinel lherzolite from Takahashi & Kushiro (1983).

[3] Lherzolite from Takahashi (1986).

[4] Quartz eclogite composition from Pertermann & Hirschmann (2003).

[5] Roberts Victor kimberlite eclogite nodule from Ito & Kennedy (1973).

[6] Synthetic mid-ocean ridge basalt from Spandler et al. (2007).

2. Methodology

2.1. Source Compositions

The eclogite composition used in the partial melting study was sourced from Dludla et al. (2006) and represents an average, group I bimineralic (clinopyroxene and garnet) eclogite composition calculated using mineral mode and mineral composition data from a suite of xenoliths from the Premier Mine kimberlite, South Africa. The composition of the peridotite was sourced from Danchin (1979), representing a deformed garnet lherzolite xenolith, also from the Premier Mine kimberlite.

Stellenbosch University https://scholar.sun.ac.za

	Average Premier Eclogite[1]	Premier Garnet Lherzolite (502)[2]
SiO_2	48.74	44.69
TiO_2	0.39	0.32
Al_2O_3	13.33	4.04
Cr_2O_3	0.14	0.39
FeO_t	8.55	9.0
MgO	12.74	37.93
CaO	13.37	3.21
Na_2O	2.71	0.22
K_2O	0.04	0.19
Sum	100.00	100.00
Mg#	72.43	88.14

Table 2. Modelled eclogite and peridotite compositions. Compositions were recalculated to 100% NiO, P_2O_5 and MnO free; these oxides are not considered due to an incomplete set of solution models defining the compositional space.

[1] Average Premier Mine kimberlite bi-mineralic eclogite from Dludla et al. (2006).

[2] Deformed garnet lherzolite from the Premier Mine kimberlite (Danchin, 1979).

2.2. Modelling Details

Modelling runs were performed in the NKCFMASTCr (Na_2O-K_2O-CaO-FeO-MgO-Al_2O_3-SiO_2-TiO_2-Cr_2O_3) volatile-free chemical system using the 2020 revised hp633ver.dat thermodynamic data file from Perple_X, and the following activity-composition models: Cpx(HGP) for clinopyroxene, Gt(HGP) for garnet, O(HGP) for olivine, Opx(HGP) for orthopyroxene, Sp(HGP) for spinel, and melt(HGP) for melt (Holland et al., 2018), Fsp(C1) for plagioclase and potassium-feldspar (Holland & Powell, 2003), and Ilm(WPH) for ilmenite (White et al., 2000).

2.3. Delta function

The entrainment of peritectic phases to the melt on segregation from the source will create magmas with a chemical composition reflecting a combination of the mass of segregated melt and the composition and abundance of the entrained crystals. When such magmas segregate, the bulk composition of the reactive system is also altered. Rcrust functionality allowed the modelling of this behaviour by extracting proportions of the peritectic phases when melt loss was triggered. This was achieved using the 'Delta' function, which allows the user to specify the portion of a predicted phase that increased in mass during melting to be included in the extraction, i.e. the incremental difference observed for a predicted phase between the point of extraction (point b) and a specified previous point (point a), such that the change in the phase mode from point *a* to point *b* is added to the extraction. This Delta function can be expressed as

$$delta\{phase; x_a; y_a; unit\} \quad (1)$$

Stellenbosch University https://scholar.sun.ac.za

where $phase$ is the phase intended for extraction, x_a and y_a describe the location of point a, and $unit$ specifies the measure of the delta value as phase mass (mol.%, vol.%, or wt.%). Point a can specified in two manners: i) 'prev_ext_X', where X can be any phase of choice from which the delta change must be calculated, or ii) 'prev_ext', where the name of the extracting phase is the default choice for the delta calculation. In this way, four sets of melt only data, and four sets of melt plus peritectic entrainment data was generated for the eclogite composition and for the peridotite composition, separately.

3. Sources of analytical data for global basalt database and data filtering

Data for basaltic rocks were collected through the EarthChem portal (http://www.earthchem.org/portal), compiling analyses from the GEOROC and NAVDAT databases. The primary criteria for data selection were that the analysis is complete for all major and minor oxides, that all Fe is expressed as FeO_t, and that the rock composition plots between basaltic and basaltic andesite. Secondary chemical data filtering inspected sample compositions to remove any alkaline or ultrapotassic rocks. Final data filtering was carried out by filtering of the source publication titles to exclude all rocks from oceanic environments, including ocean islands. This was done to ensure that the database represents compositions associated with continental tectonic environments. The final database includes 5896 analyses of volcanic rocks (basalts, basaltic andesites, tholeiites, adakites).

Stellenbosch University https://scholar.sun.ac.za

References

1. Danchin, R.V. 1979. Mineral and bulk chemistry of garnet lherzolite and garnet harzburgite xenoliths from the Premier mine, South Africa. In: Boyd, F. R. and Meyer, H. O. A. (eds.). *The Mantle Sample: Inclusions in Kimberlites and Other Volcanics. Proceedings of the Second International Kimberlite Conference.* Washington, DC, American Geophysical Union, 104–126.
2. Dludla, S., le Roex, A.P. and Gurney, J.J. 2006. Eclogite xenoliths from the Premier kimberlite, South Africa: geochemical evidence for a subduction origin. *South African Journal of Geology*, 109(3):353–368.
3. Ito, K. and Kennedy, G.C. 1973. The composition of liquids formed by partial melting of eclogites at high temperatures and pressures. *Journal of Geology*, 82:383–392.
4. Mysen, B.O. and Kushiro, I. 1977. Compositional variations of coexisting phases with degree of melting of peridotite in the upper mantle. *American Mineralogist*, 62:843–865.
5. Pertermann, M. and Hirschmann, M.M. 2003. Anhydrous Partial Melting Experiments on MORB-like Eclogite: Phase Relations, Phase Compositions and Mineral - Melt Partitioning of Major Elements at 2-3 GPa. *Journal of Petrology*, 44(12):2173–2201.
6. Spandler, C., Yaxley, G., Green, D.H. and Rosenthal, A. 2008. Phase Relations and Melting of Anhydrous K-bearing Eclogite from 1200 to 1600 ºC and 3 to 5 GPa. *Journal of Petrology*, 49(4):771–795.
7. Takahashi, E. 1986. Melting of a Dry Peridotite KLB-1 up to 14 GPa: Implications on the Origin of Peridotitic Upper Mantle. *Journal of Geophysical Research*, 91(B9):9367–9382.
8. Takahashi, E. and Kusiro, I. 1983. Melting of a dry peridotite at high pressures and basalt magma genesis. *American Mineralogist*, 68:859–879.
9. Takahashi, E., Shimazaki, T., Tsuzaki, Y. and Yoshida, H. 1993. Melting study of peridotite KLB-1 to 6.5 GPa, and the origin of basaltic magmas. *Philosophical Transactions: Physical Sciences and Engineering*, 342:105–120.

Stellenbosch University https://scholar.sun.ac.za

ADDENDUM D

SUPPLEMENTARY DATA FOR RESEARCH PAPER 3 (CHAPTER 4)

Supplementary Table 1, which provides data from Routines A and B applied to the lower temperature and higher temperature adiabats, as well as phase abundance along temperature of the emplacement runs of magma extractions A2, A4, B1, and B4, is available upon request.

Stellenbosch University https://scholar.sun.ac.za

ADDENDUM E

SUPPLEMENTARY DATA FOR CONCLUSION (CHAPTER 5)

The results from the comparisons of Rcrust (**using the HGP activity-composition models)** and pMELTS predictions with the experimental study of KLB-1 (Takahashi, 1986; Takahashi et al., 1993), MM3 (Baker & Stolper, 1994; Hirschmann et al., 1998), and G2 (Pertermann & Hirschmann, 2003a, 2003b), as well as the outputs produced in establishing an envelope of uncertainty surrounding experimental results using thermodynamic modelling (**using the HGP activity-composition models**), is available upon request.